

# Investigation of the Kinetics and Mechanism of RAFT Polymerization via EPR Spectroscopy

Dissertation

zur Erlangung des mathematisch-naturwissenschaftlichen Doktorgrades  
„Doctor rerum naturalium“  
der Georg-August-Universität Göttingen

vorgelegt von  
**Wibke Meiser**  
aus Berlin

Göttingen 2012

**Referent:** Prof. Dr. Michael Buback

**Korreferent:** Prof. Dr. Philipp Vana

**Tag der mündlichen Prüfung:** 4. Juli 2012

*Meiner Familie*



# Table of Contents

<b>Abstract</b>	<b>1</b>
<b>Zusammenfassung</b>	<b>3</b>
<b>Resumen</b>	<b>5</b>
<b>1 Introduction</b>	<b>7</b>
<b>2 Mechanism and kinetics of RAFT polymerization</b>	<b>11</b>
2.1 The ideal RAFT mechanism . . . . .	11
2.2 Features of the RAFT agent . . . . .	13
2.3 Kinetic anomalies in dithiobenzoate-mediated polymerizations . . . . .	15
2.3.1 Intermediate radical termination . . . . .	17
2.3.2 Slow fragmentation . . . . .	19
2.3.3 “Missing step” reactions . . . . .	20
2.3.4 Intermediate radical termination with short chains only . . . . .	21
<b>3 Choice of the methods of investigation</b>	<b>23</b>
3.1 Experiments based on polymerization behavior . . . . .	23
3.2 Quasi-stationary EPR experiments . . . . .	24
3.3 Time-resolved EPR experiments . . . . .	25
3.4 Product analysis by NMR spectroscopy and mass spectrometry . . . . .	27
3.5 Selection of experimental conditions . . . . .	27
<b>4 EPR with macromolecular systems</b>	<b>31</b>
4.1 Xanthate-mediated <i>n</i> -butyl acrylate polymerization . . . . .	31
4.1.1 Quasi-stationary EPR experiments . . . . .	33
4.1.2 Time-resolved EPR experiments . . . . .	36
4.1.3 Comparison of both approaches . . . . .	41

## Table of Contents

---

4.2	Trithiocarbonate-mediated <i>n</i> -butyl acrylate polymerization . . . . .	43
4.2.1	Quasi-stationary EPR experiments . . . . .	43
4.2.2	Time-resolved EPR experiments . . . . .	48
4.2.3	Comparison of both approaches . . . . .	53
4.3	Dithiobenzoate-mediated <i>n</i> -butyl acrylate polymerization . . . . .	54
4.3.1	Quasi-stationary EPR experiments . . . . .	58
4.3.2	Time-resolved EPR experiments . . . . .	62
4.3.3	Comparison of both approaches . . . . .	66
4.4	Discussion . . . . .	67
<b>5</b>	<b>EPR with monomer-free model systems</b>	<b>71</b>
5.1	<i>tert</i> -Butyl/ <i>tert</i> -butyl dithiobenzoate . . . . .	71
5.1.1	Choice of the initiator . . . . .	73
5.1.2	Determination of the equilibrium constant . . . . .	74
5.2	Cyano- <i>iso</i> -propyl/2-(2'-cyanopropyl)-dithiobenzoate . . . . .	78
5.3	Phenylethyl/1-phenylethyl dithiobenzoate . . . . .	91
5.3.1	Investigation of initiator kinetics . . . . .	91
5.3.2	Determination of the equilibrium constant . . . . .	96
5.4	Discussion . . . . .	106
<b>6</b>	<b>Closing Remarks</b>	<b>111</b>
<b>7</b>	<b>Experimental</b>	<b>115</b>
7.1	Chemicals . . . . .	115
7.1.1	Transfer agents . . . . .	115
7.1.2	Initiators . . . . .	121
7.1.3	Miscellaneous . . . . .	123
7.2	Instrumentation . . . . .	123
7.2.1	Electron paramagnetic resonance spectroscopy . . . . .	123
7.2.2	Size-exclusion chromatography . . . . .	125
7.2.3	UV Spectroscopy . . . . .	125
7.2.4	NMR Spectroscopy . . . . .	125
7.3	Procedures . . . . .	125
7.3.1	Sample preparation for EPR experiments . . . . .	125
7.3.2	Calibration of the EPR setup . . . . .	126
7.3.3	Deconvolution of EPR spectra . . . . .	127
7.3.4	Identification of side products in the model systems cyano- <i>iso</i> - propyl/2-(2'-cyanopropyl)-dithiobenzoate . . . . .	128
7.3.5	Identification of PEDA decomposition products . . . . .	130
7.3.6	Identification of side products in the model system phenylethyl/ 1-phenylethyl dithiobenzoate . . . . .	132

<b>8 Development of PREDICI models</b>	<b>135</b>
8.1 Implementation of the 2D RAFT mechanism into PREDICI . . . . .	136
8.2 Implementation of the 3D RAFT mechanism into PREDICI . . . . .	142
<b>Appendix</b>	<b>155</b>
A Abbreviations . . . . .	155
B Matlab Code . . . . .	160
<b>Bibliography</b>	<b>167</b>





# Abstract

This thesis provides new insights into the mechanism and kinetics of reversible addition-fragmentation chain transfer (RAFT) polymerizations. Electron paramagnetic resonance (EPR) spectroscopy experiments to determine the rate coefficients governing the RAFT equilibrium were developed. The equilibrium constant,  $K_{\text{eq}}$ , is deduced from the concentration ratio of the intermediate species, INT, and propagating radicals, P, via an EPR spectrum taken during stationary RAFT polymerization. Another approach uses highly time-resolved EPR spectroscopy to trace INT and P concentrations in single-pulse laser-initiated RAFT polymerizations (SP-PLP-EPR-RAFT). PREDICI<sup>®</sup> simulations of the experimental data result in rate coefficients for addition,  $k_{\text{ad}}$ , fragmentation,  $k_{\beta}$ , and cross-termination,  $k_{\text{t}}^{\text{cross}}$ .

Both methods have been applied to xanthate-, trithiocarbonate- and dithiobenzoate-mediated RAFT polymerizations of butyl acrylate at  $-40\text{ }^{\circ}\text{C}$ . The equilibrium constants,  $K_{\text{eq}} = k_{\text{ad}}/k_{\beta}$ , obtained from the stationary approach are in excellent agreement with the ones from SP-PLP-EPR-RAFT, indicating that both experimental approaches provide access to reliable data for RAFT kinetics. Fast fragmentation of INT has been observed in all polymerizations under investigation. The values for the fragmentation rate coefficient,  $k_{\beta}$ , are  $2.3 \times 10^3\text{ s}^{-1}$  for the xanthate,  $1.4 \times 10^2\text{ s}^{-1}$  and  $4.5 \times 10^1\text{ s}^{-1}$  for the trithiocarbonates, and  $4.7\text{ s}^{-1}$  for the dithiobenzoate. The corresponding equilibrium constants are  $12\text{ L} \cdot \text{mol}^{-1}$ ,  $2.6 \times 10^4\text{ L} \cdot \text{mol}^{-1}$ ,  $8 \times 10^4\text{ L} \cdot \text{mol}^{-1}$ , and  $3 \times 10^5\text{ L} \cdot \text{mol}^{-1}$ , respectively.  $K_{\text{eq}}$  is highest for the dithiobenzoate and lowest for the xanthate, which is consistent with the better control of dithiobenzoate-mediated acrylate polymerization as compared with the xanthate. Cross-termination plays a minor role when xanthates or trithiocarbonates are used as the RAFT agent, but is an important reaction step when dithiobenzoates are employed. In the latter case, adopting a chain-length dependent  $k_{\text{t}}^{\text{cross}}$  is necessary to explain the experimental data.

To gain further insight into the rate retardation phenomenon observed in some dithiobenzoate-mediated polymerizations and to evaluate the accuracy of *ab initio* calculated  $K_{\text{eq}}$  values reported by Coote *et al.*, the EPR experiments were carried out on monomer-free model systems. These systems were composed of a radical,

generated by decomposition of an appropriate initiator, and a dithiobenzoate-type RAFT agent bearing a leaving group, which was identical to the initiator-derived radical, i. e., a *tert*-butyl, a cyano-*iso*-propyl or a phenylethyl group. The corresponding equilibrium constants at 20 °C are between  $10^5$  and  $10^8$  L · mol<sup>-1</sup>, 53 L · mol<sup>-1</sup> and  $2.2 \times 10^3$  L · mol<sup>-1</sup>, respectively.

The trends in  $K_{\text{eq}}$  for the different model systems correlate with the stability of the intermediate radical and the stabilization energy of the radical which adds to the thiocarbonyl bond of the RAFT agent. The theoretical values show the same trends but are up to six orders of magnitude above the experimentally obtained equilibrium constants. In addition, *ab initio* calculations predict a pronounced chain-length dependence of  $K_{\text{eq}}$ , which was tested using macromolecular RAFT agents for stationary EPR experiments and by comparing the macromolecular systems with monomer-free model systems. Only a minor influence of the chain length was observed. The experimental results thus question *ab initio* calculations predicting slow fragmentation of INT and a pronounced chain-length dependence of  $K_{\text{eq}}$ .

In addition, the product mixtures of the model systems were analyzed by nuclear magnetic resonance (NMR) spectroscopy. The results of EPR and NMR measurements show that cross-termination with subsequent “missing step” reactions of unstable cross-termination products are responsible for the rate retardation observed in dithiobenzoate-mediated polymerizations.

# Zusammenfassung

Die vorliegende Doktorarbeit eröffnet neue Einblicke in den Mechanismus und die Kinetik von Reversiblen Additions-Fragmentierungs Kettenübertragungs (RAFT)-Polymerisationen. Es wurden Elektronenspinresonanz (ESR)-spektroskopische Untersuchungsmethoden zur Bestimmung der Geschwindigkeitskoeffizienten des RAFT-Gleichgewichts entwickelt. Die Gleichgewichtskonstante,  $K_{\text{eq}}$ , wird aus dem Konzentrationsverhältnis der Intermediatspezies, INT, und wachsenden Radikale, P, erhalten. Dieses Verhältnis lässt sich aus dem ESR-Spektrum einer stationären RAFT-Polymerisation berechnen. Zudem wird hoch-zeitaufgelöste ESR-Spektroskopie verwendet, um die INT- und P-Konzentrationen in Laser-Einzelpuls-initiierten RAFT-Polymerisationen (SP-PLP-EPR-RAFT) zu verfolgen. Die Geschwindigkeitskoeffizienten der Addition,  $k_{\text{ad}}$ , der Fragmentierung,  $k_{\beta}$ , und der Kreuzterminierung,  $k_{\text{t}}^{\text{cross}}$ , wurden durch PREDICI<sup>®</sup>-Simulationen der experimentellen Daten erhalten.

Beide ESR-Methoden wurden zur Untersuchung von Xanthat-, Trithiocarbonat- und Dithiobenzoat-vermittelten Butylacrylat-Polymerisationen bei  $-40\text{ }^{\circ}\text{C}$  verwendet. Die Gleichgewichtskonstanten,  $K_{\text{eq}} = k_{\text{ad}}/k_{\beta}$ , der untersuchten Systeme, die mit Hilfe der stationären Methode erhalten wurden, stimmen gut mit den Werten aus den SP-PLP-EPR-RAFT-Experimenten überein. Mit beiden experimentellen Untersuchungsmethoden können daher zuverlässige kinetische Daten für RAFT-Polymerisationen bestimmt werden. In allen Polymerisationen war eine schnelle Fragmentierung des Intermediats zu beobachten. Die Werte für die Fragmentierungsgeschwindigkeitskoeffizienten,  $k_{\beta}$ , sind  $2.3 \times 10^3\text{ s}^{-1}$  für das Xanthat,  $1.4 \times 10^2\text{ s}^{-1}$  und  $4.5 \times 10^1\text{ s}^{-1}$  für die Trithiocarbonate und  $4.7\text{ s}^{-1}$  für das Dithiobenzoat. Die entsprechenden Gleichgewichtskonstanten sind  $12\text{ L} \cdot \text{mol}^{-1}$ ,  $2.6 \times 10^4\text{ L} \cdot \text{mol}^{-1}$ ,  $8 \times 10^4\text{ L} \cdot \text{mol}^{-1}$  und  $3 \times 10^5\text{ L} \cdot \text{mol}^{-1}$ . Die größte Gleichgewichtskonstante wurde dementsprechend für das Dithiobenzoat gefunden und die niedrigste für das Xanthat. Dies ist im Einklang mit der experimentellen Beobachtung, dass Dithiobenzoate Acrylat-Polymerisationen besser kontrollieren als Xanthate. Wenn Xanthate oder Trithiocarbonate als RAFT-Agenzien verwendet werden, spielt die Kreuzterminierung nur eine untergeordnete Rolle. Werden hingegen Dithiobenzoate eingesetzt, kann dieser Reaktionsschritt nicht vernachlässigt werden.

In diesem Fall ist die Anpassung der experimentellen Daten nur mit Hilfe eines kettenlängenabhängigen  $k_t^{\text{cross}}$  möglich.

Um die Ursachen der Retardierung der Polymerisationsgeschwindigkeit in Dithiobenzoat-vermittelten Polymerisationen zu ergründen und die Genauigkeit der mittels *ab initio*-Methoden berechneten Gleichgewichtskonstanten abzuschätzen, wurden zusätzliche ESR-Untersuchungen an monomerfreien Modellsystemen durchgeführt. Diese Systeme bestanden aus einem durch Initiatorzerfall gebildeten Radikal und einem Dithiobenzoat mit einer Abgangsgruppe, die identisch war mit dem vom Initiator stammenden Radikal, d. h. *tert*-Butyl, Cyano-*iso*-propyl oder Phenylethyl. Die entsprechenden Gleichgewichtskonstanten bei 20 °C sind  $10^5 - 10^8 \text{ L} \cdot \text{mol}^{-1}$ ,  $53 \text{ L} \cdot \text{mol}^{-1}$  und  $2.2 \times 10^3 \text{ L} \cdot \text{mol}^{-1}$ .

Der Trend, der für die  $K_{\text{eq}}$ -Werte zu beobachten ist, korreliert mit der Stabilität des Intermediat-Radikals und der Stabilisierungsenergie des Radikals, das an die C=S-Doppelbindung des RAFT-Agens addiert. Die von Coote *et al.* berechneten Gleichgewichtskonstanten folgen dem gleichen Trend, liegen aber um bis zu sechs Größenordnungen über den experimentell ermittelten Werten. Außerdem sagen die *ab initio*-Berechnungen eine starke Kettenlängenabhängigkeit für  $K_{\text{eq}}$  voraus. Das wurde experimentell überprüft indem polymere RAFT-Agenzien für die stationären ESR-Untersuchungen verwendet wurden und die polymeren mit den monomerfreien Modellsystemen verglichen wurden. Es wurde nur eine sehr schwache Kettenlängenabhängigkeit beobachtet. Die experimentellen Befunde widerlegen somit die *ab initio*-Berechnungen, die eine langsame Fragmentierung von INT und eine deutliche Kettenlängenabhängigkeit für  $K_{\text{eq}}$  voraussagen.

Desweiteren wurden die Produktgemische der Modellsysteme mittels Kernspinresonanzspektroskopie (NMR) analysiert. Die Ergebnisse der ESR- und NMR-Messungen zeigen, dass Kreuzterminierung mit anschließenden „Missing Step“-Reaktionen der instabilen Kreuzterminierungsprodukte für die Retardierung der Polymerisationsgeschwindigkeit in Dithiobenzoat-vermittelten Polymerisationen verantwortlich sind.

# Resumen

La tesis proporciona nueva información acerca del mecanismo y de la cinética de las polimerizaciones de transferencia de cadena por adición-fragmentación reversible (RAFT). Para determinar los coeficientes cinéticos que gobiernan el equilibrio RAFT se desarrollaron experimentos realizados con resonancia paramagnética electrónica (EPR). La constante de equilibrio,  $K_{\text{eq}}$ , se obtiene de la proporción de las concentraciones del radical intermedio, INT, y de los radicales propagadores, P. Ésta proporción se calcula de un espectro EPR durante la polimerización RAFT estacionaria. El otro método utiliza la espectroscopía EPR con alta resolución temporal para seguir las concentraciones de INT y P en polimerizaciones iniciadas por un pulso de láser (SP-PLP-EPR-RAFT). Simulaciones de los datos experimentales dan como resultado las constantes de velocidad de adición,  $k_{\text{ad}}$ , de fragmentación,  $k_{\beta}$ , y de terminación entre el radical intermedio y radicales propagadores,  $k_{\text{t}}^{\text{cross}}$ .

Los dos métodos se han aplicado a las polimerizaciones RAFT de acrilato de butilo mediadas por xantato, tritiocarbonato y ditiobenzoato. Las constantes de equilibrio,  $K_{\text{eq}} = k_{\text{ad}}/k_{\beta}$ , de los sistemas investigados obtenidas con el enfoque estacionario son iguales a las del método SP-PLP-EPR-RAFT, indicando que las dos estrategias experimentales proporcionan valores fiables para la cinética de RAFT. La rápida fragmentación de INT ha sido observada en todas las polimerizaciones. Los valores de los coeficientes de fragmentación,  $k_{\beta}$ , son  $2.3 \times 10^3 \text{ s}^{-1}$  para el xantato,  $1.4 \times 10^2 \text{ s}^{-1}$  y  $4.5 \times 10^1 \text{ s}^{-1}$  para los tritiocarbonatos y  $4.7 \text{ s}^{-1}$  para el ditiobenzoato. Las constantes de equilibrio correspondientes son  $12 \text{ L} \cdot \text{mol}^{-1}$ ,  $2.6 \times 10^4 \text{ L} \cdot \text{mol}^{-1}$ ,  $8 \times 10^4 \text{ L} \cdot \text{mol}^{-1}$  y  $3 \times 10^5 \text{ L} \cdot \text{mol}^{-1}$ . Por lo tanto, la constante de equilibrio más alta se ha encontrado en el caso del ditiobenzoato y la más baja en el caso del xantato. Esto es consistente con la observación experimental que muestra que las polimerizaciones mediadas por ditiobenzoatos están mejor controladas que las mediadas por xantatos. La terminación entre el radical intermedio y radicales propagadores desempeña un papel menor en las polimerizaciones en las cuales tritiocarbonatos o xantatos están usados, pero es una reacción muy importante si se emplean ditiobenzoatos. En este caso, un  $k_{\text{t}}^{\text{cross}}$  dependiente de la longitud de cadena es necesario para poder explicar los datos experimentales.

Para examinar los orígenes del efecto de retardación en polimerizaciones mediadas por ditiobenzoatos y para evaluar la exactitud de las constantes de equilibrio calculadas por Coote *et al.* con el método *ab initio*, se llevaron a cabo investigaciones EPR con sistemas de modelo libre de monómero. Estos sistemas estuvieron formados por un radical, generado por descomposición de un iniciador apropiado, y un ditiobenzoato con un grupo saliente R, que es idéntico al radical procedente del iniciador, o sea *tert*-butilo, ciano-*iso*-propilo o feniletilo. Las constantes de equilibrio correspondientes a 20 °C son  $10^5 - 10^8 \text{ L} \cdot \text{mol}^{-1}$ ,  $53 \text{ L} \cdot \text{mol}^{-1}$  y  $2.2 \times 10^3 \text{ L} \cdot \text{mol}^{-1}$ .

La tendencia de los valores de  $K_{\text{eq}}$  observada corresponde con la estabilidad del radical intermedio y con la energía de estabilización del radical, que adiciona al enlace doble C=S del agente RAFT. Las constantes de equilibrio teóricas siguen la misma tendencia, pero están hasta seis ordenes de magnitud encima de los valores experimentales. Además, los cálculos *ab initio* pronostican una gran dependencia de la longitud de cadena para  $K_{\text{eq}}$ . Esto se revisó experimentalmente usando agentes RAFT poliméricos para la investigación estacionaria y comparando los sistemas poliméricos con los sistemas de modelo libre de monómero. Se observó solamente una dependencia de la longitud de cadena muy leve. Por lo tanto, los resultados experimentales refuten los cálculos *ab initio* que predicen una fragmentación lenta y una dependencia clara de la longitud de cadena.

Además, se analizó con espectroscopia de resonancia magnética nuclear (RMN) la mezcla de productos de los sistemas de modelo. Los resultados de las mediciones EPR y RMN demuestran, que la terminación de INT con radicales propagadores seguida de unas reacciones llamadas “Missing Step” de los productos de terminación inestables es responsable de la retardación de la velocidad en las polimerizaciones mediadas por ditiobenzoatos.

# 1

## Introduction

A polymer is a large molecule built up by the repetition of small monomer-derived units. Biopolymers such as the genetic information carrier deoxyribonucleic acid (DNA), proteins, and polysaccharides are the building blocks of life. Natural polymers, for example wood, wool, silk, starch, and rubber, are used by mankind since many centuries as construction material, for clothing or as thickener.<sup>[1]</sup>

Since the invention of the first man-made synthetic plastic by Baekeland<sup>[2]</sup> in 1907 and the investigations of Staudinger<sup>[3]</sup> in the 1920's that form the basis for modern macromolecular science, synthetic polymers have revolutionized our way of life. Applications range from packaging, sports and outdoor equipment, paints, coatings, electronics, automobiles to the aircraft and space industry.<sup>[4]</sup> In many of these applications, plastics replaced other materials because of their beneficial properties like low weight, chemical resistance, shape flexibility, durability, as well as thermal, acoustic and electrical insulation properties.

Over the past two decades plastics production grew almost 5 % per year. In 2010, 265 million tons were produced worldwide – thereof approximately 50 % by radical polymerization (RP).<sup>[5,6]</sup> The success of radical polymerization can be attributed to the large range of monomers, which can be homo- and co-polymerized under convenient reaction conditions, and the insensitivity to impurities.<sup>[6]</sup> However, conventional radical polymerization produces non-biodegradable polymeric chains. This is a major problem considering that, in Europe alone, 10.4 million tons of plastic waste were disposed of in landfill in 2010.<sup>[5]</sup> While the world is gradually running out of fossil fuel, the conventional radical polymerization process depends on petroleum resources as the raw material.<sup>[7]</sup> The need of modern society for highly functional polymeric

materials is increasing, but conventional radical polymerization does not provide control over the microstructure of the polymer.

The most promising candidates for minimizing the environmental impact and producing materials with well-defined properties at the same time are the controlled/living radical polymerization techniques (CLRP) developed since the early 1990s. The concept of living polymerization was first discovered by Szwarc<sup>[8,9]</sup> in 1956 and describes polymerization processes in which chain transfer and chain termination are absent – a major key for tailoring macromolecular architecture.<sup>[10]</sup> Applying the concept of livingness to radical polymerizations affords techniques which combine the advantages of both approaches. Of particular scientific interest are currently nitroxide-mediated polymerization (NMP),<sup>[11]</sup> atom transfer radical polymerization (ATRP),<sup>[12,13]</sup> reversible addition-fragmentation chain transfer polymerization (RAFT),<sup>[14]</sup> and reversible chain transfer catalyzed polymerization (RTCP).<sup>[15–17]</sup>

All CLRP systems are based on a dynamic equilibrium between propagating radicals and a dormant species,<sup>[18]</sup> which suppresses termination reactions. In this way, the lifetime of growing chains can be extended from approximately one second in free-radical polymerization to hours or days in CLRP. This leads to polymers of uniform chain length that is pre-determined by monomer conversion and initiator concentration. The International Union of Pure and Applied Chemistry (IUPAC) encourages the use of the term “reversible-deactivation radical polymerization” for polymerizations exhibiting these characteristics.<sup>[19]</sup>

The increasing attention that particularly RAFT polymerization has attracted since its invention in 1998,<sup>[14]</sup> is partly due to the fact that it allows for the sustainable production of highly functionalized plastics. Environmentally friendly solvents like water and supercritical carbon dioxide may be employed,<sup>[20,21]</sup> polymerization can be carried out at room temperature,<sup>[22]</sup> renewable monomers can be polymerized,<sup>[23]</sup> and biodegradable polymers can be produced.<sup>[24]</sup> In addition, RAFT enables the formation of a large variety of macromolecular architectures such as block copolymers,<sup>[25–27]</sup> star-like polymers,<sup>[28,29]</sup> comb-like structures,<sup>[30]</sup> hyperbranched polymers, dendritic structures, and polymer networks.<sup>[31]</sup> These novel structures are valuable for surface and particle modification,<sup>[31]</sup> drug delivery,<sup>[32,33]</sup> nano- and microporous materials,<sup>[30,34,35]</sup> and microelectronics.<sup>[6]</sup>

The RAFT process operates on the principle of reversible chain transfer (also termed degenerative chain transfer),<sup>[18]</sup> with the pre- and main equilibrium being superimposed on a conventional radical polymerization scheme. The equilibria are decisive for the control of polymerization and, consequently, for polymer properties. The rate coefficients governing the equilibria are the addition and fragmentation rates,  $k_{ad}$  and  $k_{\beta}$ , respectively. Precise determination of these rate coefficients is therefore essential. The rate coefficients  $k_{ad}$  and  $k_{\beta}$  are, however, not easily accessible, as the RAFT equilibria do only cause a minimal perturbation to the conventional radical polymerization kinetics. The rate of polymerization remains unaffected, which poses



---

a challenge with respect to the determination of  $k_{\text{ad}}$  and  $k_{\beta}$ , as rate measurements are one of the key techniques for gaining insight into a mechanistic process.

Due to these difficulties most of the literature values for  $k_{\text{ad}}$  and  $k_{\beta}$  were derived from *ab initio* quantum-chemical calculations.<sup>[36–42]</sup> Experimentally obtained rate coefficients depend strongly on the assumed kinetic scheme and, in some cases, differ by up to six orders of magnitude for the same polymerization system.<sup>[43–46]</sup> The biggest controversy concerns the addition and fragmentation rate coefficients in dithiobenzoate-mediated polymerizations, because with some dithiobenzoates the polymerization rate is decreasing with increasing RAFT agent concentration. This phenomenon, called rate retardation, has given rise to an ongoing debate on the origin of this effect. The proposed models include slow fragmentation (SF) of the intermediate radical,<sup>[47]</sup> intermediate radical termination (IRT)<sup>[48]</sup> and IRT with subsequent “missing step” reactions of unstable cross-termination products.<sup>[49]</sup> Whereas *ab initio* calculations carried out so far support the slow fragmentation model,<sup>[42]</sup> electron paramagnetic resonance (EPR) measurements, nuclear magnetic resonance (NMR) spectroscopy and size-exclusion chromatography (SEC) studies point to the IRT model.<sup>[50]</sup> In addition, *ab initio* calculations predict a strong chain-length dependence for  $k_{\text{ad}}$  and  $k_{\beta}$ , which needs to be experimentally verified.<sup>[39]</sup>

The aims of this thesis are to develop direct experimental methods for the determination of the rate coefficients relevant to the RAFT equilibria and to test whether these rate coefficients are chain-length dependent. In this way, the evaluation of the accuracy of theoretical calculations becomes possible. Additionally, the work intends to shed light on the reasons behind the rate retardation observed in some dithiobenzoate-mediated polymerizations. The design of an appropriate kinetic model and the accurate measurement of the kinetic parameters is needed, as the molecular structure is determined by the individual reaction steps that occur during polymerization. The microscopic structure, in turn, governs the macroscopic material properties. Knowledge of the entire kinetic scheme and the rate coefficients involved therefore serves as the basis for further development and optimization of the RAFT process.



# 2

## Mechanism and kinetics of RAFT polymerization

This chapter provides the theoretical background for the thesis. It introduces the reader to the mechanism of the RAFT process, the key features of a RAFT agent and the associated rate coefficients. The kinetic anomalies which occur with some RAFT agents are illustrated and an overview of the models proposed to describe the reasons behind the observed behavior is given.

### 2.1 The ideal RAFT mechanism

The basic kinetic scheme of the RAFT process is illustrated in Scheme 2.1. The pre- and main equilibrium (II and V, respectively) are superimposed on a conventional radical polymerization scheme with the elementary steps,<sup>[51]</sup> i. e. initiation (I), propagation (IV), and termination (VI), being unaffected. The mechanism and kinetics of conventional radical polymerization are detailed in literature.<sup>[6]</sup>

In the first reaction step, radical formation is induced either by thermal, chemical or photochemical excitation of an initiator (Ia). The initiator-derived radicals,  $I^{\bullet}$ , subsequently initiate polymerization by adding to a monomer molecule (Ib).

In the pre-equilibrium (II), macroradicals,  $P_i^{\bullet}$ , add to the C=S double bond of the RAFT agent forming an intermediate radical, INT1, which can either react back to the educts or proceed to release the leaving group,  $R^{\bullet}$ , and form a polymeric RAFT agent, polyRAFT. The leaving group radical may either react with the polymeric RAFT agent, forming INT1, or with the initial RAFT agent to yield an intermediate

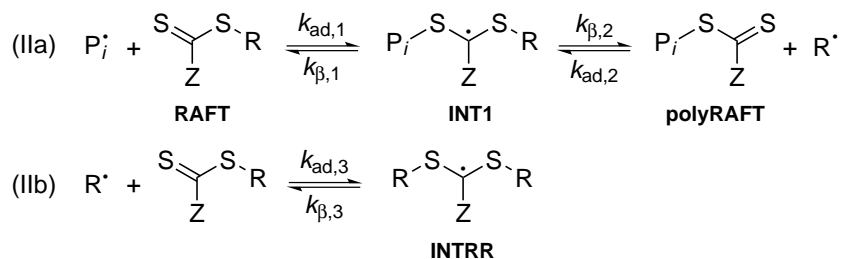
## 2 Mechanism and kinetics of RAFT polymerization

---

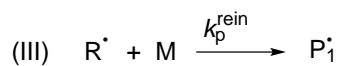
### I. INITIATION



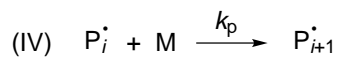
### II. PRE-EQUILIBRIUM



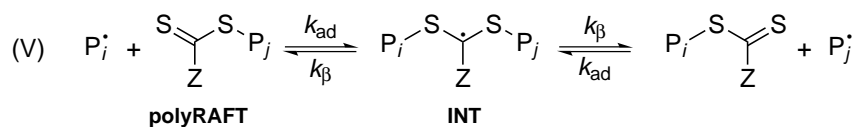
### III. REINITIATION



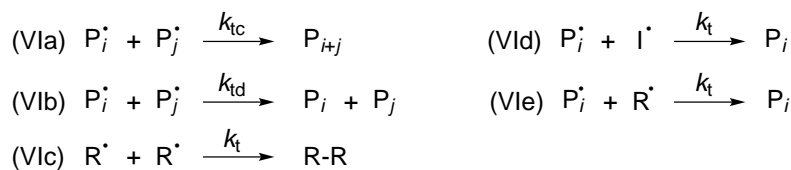
### IV. PROPAGATION



### V. MAIN EQUILIBRIUM



### VI. TERMINATION



Scheme 2.1. Basic RAFT mechanism.

radical bearing two leaving groups, INTRR. The pre-equilibrium is governed by three addition and fragmentation rate coefficients ( $k_{\text{ad},1}$ ,  $k_{\text{ad},2}$ ,  $k_{\text{ad},3}$ ,  $k_{\beta,1}$ ,  $k_{\beta,2}$  and  $k_{\beta,3}$ ).

The next sequence of reaction steps are the reinitiation (III) and propagation (IV), which are proceeding with the rate coefficients  $k_{\text{p}}$  and  $k_{\text{p}}^{\text{rein}}$ , respectively. In the propagation step (IV), the radicals grow by adding monomer molecules.

The reinitiation step shifts the pre-equilibrium to the side of the polyRAFT species and the initial RAFT agent is consumed. After complete consumption the polymerization is governed by the main equilibrium (V), which constitutes the core of the RAFT process. Rapid equilibration between the active propagating radicals,  $\text{P}_i^\bullet$  and  $\text{P}_j^\bullet$ , and the dormant polymeric thiocarbonylthio compounds, polyRAFT, provides equal probability for all chains to grow and allows for the production of narrow-dispersity polymers. The addition reaction proceeds with the rate coefficient  $k_{\text{ad}}$ , whereas the formed intermediate radical, INT, fragments with the rate coefficient  $k_{\beta}$ . The  $k_{\text{ad}}$  and  $k_{\beta}$  values are different from those of the pre-equilibrium. The presence of intermediate radicals in the pre- and main equilibrium (given in reaction step IIa, IIb and V, respectively) has been evidenced by electron paramagnetic resonance (EPR) spectroscopy.<sup>[50,52–58]</sup> The main equilibrium is usually described by the equilibrium constant  $K_{\text{eq}}$ , which indicates the stability of the intermediate radical and is defined by

$$K_{\text{eq}} = \frac{k_{\text{ad}}}{k_{\beta}} \quad (2.1)$$

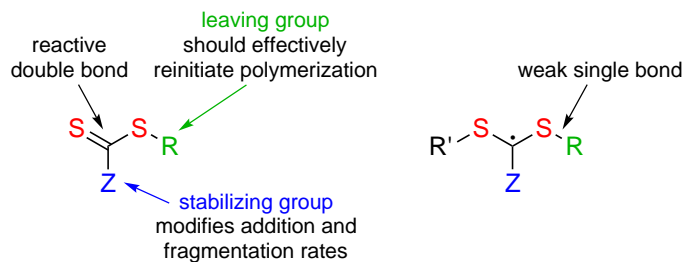
Finally, reaction steps VI consider radical-radical termination, which is not fully suppressed by the RAFT process. As in conventional radical polymerization, termination occurs either by disproportionation, in which a hydrogen atom is transferred from one radical to another, or by combination, which is mostly a simple head-to-head coupling of two radicals.<sup>[59]</sup> The termination rate coefficient,  $k_{\text{t}}$ , is the sum of the individual rate coefficients for disproportionation,  $k_{\text{td}}$ , and combination,  $k_{\text{tc}}$ . The termination reaction, in which “dead” polymer is formed, is preceded by translational diffusion of the two radicals and the segmental diffusion to make contact between their radical sites.<sup>[60–62]</sup>

## 2.2 Features of the RAFT agent

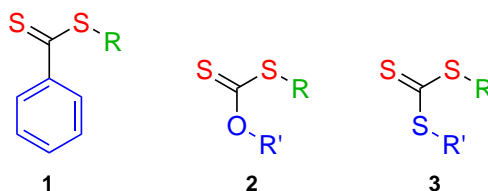
The mediating compounds employed in RAFT polymerizations are thiocarbonylthio compounds, the structural features of which are illustrated in Scheme 2.2. The effectiveness of RAFT agents strongly depends on the nature of the stabilizing Z group and the leaving group R, the monomer, and the polymerization conditions.<sup>[25,47,63–75]</sup> The group Z can be chosen to activate or deactivate the thiocarbonyl double bond of the RAFT agent and modifies the stability of the intermediate radicals, INT1, INTRR

## 2 Mechanism and kinetics of RAFT polymerization

and INT. As a result, RAFT agents vary in their suitability for different monomers. The main classes of RAFT agents – which are distinguished by their different Z groups – are dithioesters,<sup>[14]</sup> dithiocarbamates,<sup>[63,67]</sup> trithiocarbonates,<sup>[76]</sup> and xanthates.<sup>[77]</sup> The structures of the RAFT classes used in this work are illustrated in Scheme 2.3.



**Scheme 2.2.** Structural features of the RAFT agent and the intermediate formed on radical addition.<sup>[78]</sup>



**Scheme 2.3.** Overview of the RAFT classes investigated in this work: (1) dithiobenzoates belonging to the group of dithioesters, (2) xanthates, and (3) trithiocarbonates.

The features of a RAFT agent which efficiently controls polymerization and the requirements for the corresponding rate coefficients can be summarized as follows:<sup>[78,79]</sup>

- The initial and the polymeric RAFT agent should have a reactive C=S double bond, allowing for a high  $k_{ad}$ .
- The intermediate radicals, INT1, INTRR and INT, should fragment rapidly and undergo no side reactions. Therefore, the S–R bond of the intermediate should be weak to assure a high  $k_{\beta}$ .
- The intermediate radical INT1 should partition in favor of products, i. e.  $k_{\beta,2} > k_{\beta,1}$ .
- The expelled radicals,  $R^{\bullet}$ , must efficiently reinitiate the polymerization, i. e.  $k_p^{rein} > k_p$ .

## 2.3 Kinetic anomalies in dithiobenzoate-mediated polymerizations

In case the RAFT process depicted in Scheme 2.1 proceeds ideally, that is the chain-transfer process is fast and the RAFT intermediate is short-lived, the propagating radical concentration is not altered. The rate of polymerization should therefore be similar to the one found for conventional radical polymerization. However, some polymerization systems employing dithiobenzoates (compound 1 in Scheme 2.3) as mediating agents deviate from the ideal behavior in showing extended induction periods and a significant deceleration in polymerization rate – termed rate retardation – with increasing RAFT agent concentration. The two phenomena are illustrated in Figure 2.1 taking the 2-(2'-cyanopropyl)-dithiobenzoate-mediated polymerization of *n*-butyl acrylate as an example.

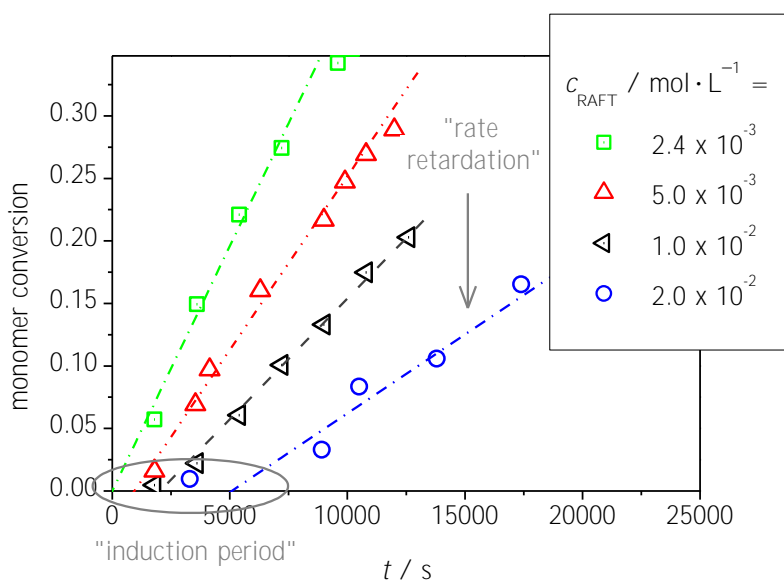


**Figure 2.1.** Illustration of induction period and rate retardation using the example of 2-(2'-cyanopropyl)-dithiobenzoate-mediated polymerization of *n*-butyl acrylate at 65 °C with 2,2'-azobis(2-methylpropionitrile) ( $1.5 \times 10^{-3} \text{ mol} \cdot \text{L}^{-1}$ ) as the initiator.

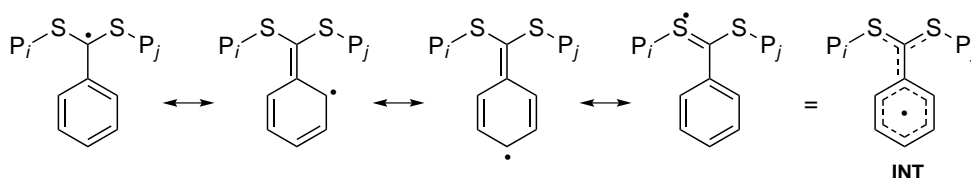
There are several potential explanations for the induction period. Inhibition may be induced by slow reinitiation by the leaving group of the RAFT agent, the selective conversion of the original RAFT agent into a single monomer adduct,<sup>[80–84]</sup> slow fragmentation of the leaving group,<sup>[85]</sup> or termination reactions of the intermediate

radicals INT1 and INTRR.<sup>[58]</sup> When performing RAFT polymerizations using a polymeric RAFT agent, i. e., effectively skipping the pre-equilibrium, no induction period can be observed, whereas rate retardation still occurs. The induction period can hence be attributed to the pre-equilibrium.<sup>[86]</sup> Since pre-equilibrium characteristics do not seem to be the cause of rate retardation during main-equilibrium conditions, both phenomena should be investigated separately.

This work will focus on the origin of rate retardation. The different explanations put forward for rate retardation are

- intermediate radical termination (Section 2.3.1)
- slow fragmentation of the RAFT intermediate (Section 2.3.2)
- intermediate radical termination followed by “missing step” reactions (Section 2.3.3)
- intermediate radical termination with short chains only (Section 2.3.4).

The proposed models have in common that they attribute rate retardation to the higher stability of the intermediate radical during the main equilibrium in polymerizations mediated by dithiobenzoate as compared to the ones mediated by other RAFT agents. The high stability of the intermediate radical is assigned to the delocalization of the radical into the phenyl ring, which is illustrated in Scheme 2.4.



**Scheme 2.4.** Resonance structures of the intermediate radical in dithiobenzoate-mediated polymerizations.

For example, almost no retardation is observed in cumyl phenyldithioacetate-mediated styrene or methyl acrylate polymerization, whereas the cumyl dithiobenzoate mediated polymerization shows significant retardation.<sup>[22,64]</sup> The rate retardation phenomenon has caused a lively debate in the scientific community leading to the formation of the IUPAC task group “*Towards a Holistic Mechanistic Model for RAFT Polymerizations: Dithiobenzoates as Mediating Agents*” in 2005. There are several articles reviewing the current situation.<sup>[78,84,86,87]</sup>

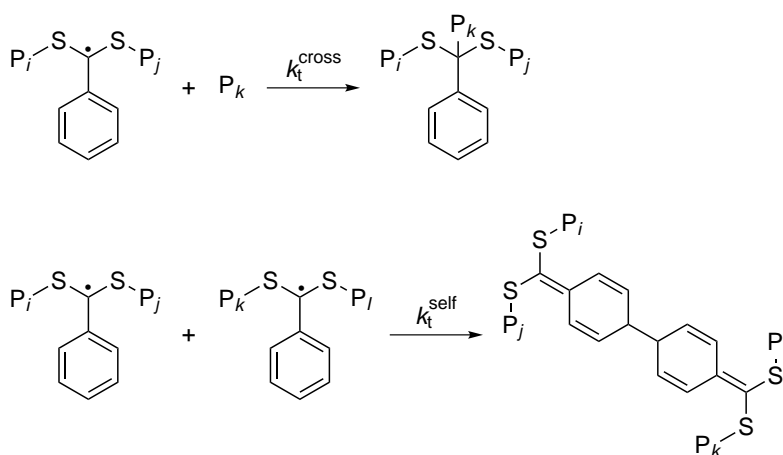
Note that all RAFT agents induce retardation when they are employed in very high concentrations, since chain length decreases with increasing RAFT content which



leads to higher termination rates.<sup>[88]</sup> This apparent retardation, which is due to a significant enhancement of termination rate upon lowering radical size, is not covered in the following.

### 2.3.1 Intermediate radical termination

Monteiro and de Brouwer<sup>[48]</sup> proposed that rate retardation is caused by termination reactions of the intermediate radical, which may either terminate with a propagating radical (cross-termination) or with another intermediate radical (self-termination). This so-called intermediated radical termination model (IRT) is illustrated in Scheme 2.5. As the radical center of the dithiobenzoate intermediate is delocalized into the aromatic ring and may be shifted to more exposed sites (see Scheme 2.4), such reactions may suffer less steric hindrance than is the case with other RAFT intermediates where the radical functionality is localized between the sulfur atoms. When steric hindrance is introduced at the *para* position of the Z group – making this position less prone to radical attack – a significant reduction of the rate retardation effect has been observed.<sup>[89]</sup> It is therefore reasonable to assume that intermediate radical termination is favored by the delocalization of the radical functionality.



**Scheme 2.5.** Illustration of the cross-termination reaction between a propagating radical and an intermediate radical (upper part) and the self-termination reaction of two intermediate radicals (lower part). Only one possible reaction pathway for each termination reaction is shown. Both termination reactions may occur with all resonance structures depicted in Scheme 2.4.

Evidence for this model mainly comes from electron spin resonance (EPR) spectroscopy. Using this technique, Kwak *et al.*<sup>[50,90]</sup> studied the polymerization of styrene

mediated by a polystyryl dithiobenzoate. A relatively low concentration of intermediate radicals (of the order of  $10^{-7} \text{ mol} \cdot \text{L}^{-1}$ ) was produced by the addition of the polystyryl radical to the RAFT agent. From the rate of polymerization the concentration of the growing radical was estimated. The ratio of radical concentrations yields a  $K_{\text{eq}}$  value of  $55 \text{ L} \cdot \text{mol}^{-1}$  at  $60 \text{ }^\circ\text{C}$  (see Equation 3.3) and it was shown that fragmentation of the intermediate radical is a fast process with a relevant rate constant of the order of  $k_{\beta} = 10^4 \text{ s}^{-1}$ . In addition, cross-termination with the polystyryl radical led to the formation of a stable 3-arm star, which causes rate retardation. Thus, Kwak *et al.* proposed to calculate  $K_{\text{eq}}$  from the observed rates of polymerization,  $R_{\text{p}}$ , at different RAFT agent concentrations,  $c_{\text{RAFT}}$ , via the equations<sup>[50,90]</sup>

$$R_{\text{p}} = \frac{R_{\text{p}}^0}{\sqrt{1 + \frac{2 \cdot k_{\text{t}}^{\text{cross}}}{k_{\text{t}}} \cdot K_{\text{eq}} \cdot c_{\text{RAFT}}}} \quad (2.2)$$

and

$$R_{\text{p}} = \frac{R_{\text{p}}^0}{\sqrt{1 + \frac{k_{\text{t}}^{\text{self}}}{k_{\text{t}}} \cdot K_{\text{eq}}^2 \cdot c_{\text{RAFT}}^2}} \quad (2.3)$$

where  $R_{\text{p}}^0$  denotes the rate of the RAFT-free polymerization,  $c_{\text{RAFT}}$  the initial RAFT agent concentration and  $k_{\text{t}}$ ,  $k_{\text{t}}^{\text{cross}}$  and  $k_{\text{t}}^{\text{self}}$  the chain-length averaged termination, cross-termination and self-termination rate coefficient, respectively.

Tonge *et al.*<sup>[91]</sup> used EPR spectroscopy to directly detect both propagating and intermediate radicals during dithiobenzoate-mediated polymerizations of styrene and methyl acrylate. From the RAFT agent concentrations used and the fact that both species are seen, i. e., that they occur at similar concentrations, one can conclude that  $K_{\text{eq}} < 100 \text{ L} \cdot \text{mol}^{-1}$ . Unfortunately, not all concentrations are given so that no quantitative estimate of  $K_{\text{eq}}$  can be made.

The identification of IRT products is challenging as only a few percent of dead chains with broad molecular mass distribution are formed during the process. However, some studies prove the occurrence of cross- and self-termination products: Calitz *et al.*<sup>[58]</sup> investigated the reactions of short-chain species during the initial periods of cumyl dithiobenzoate-mediated polymerizations of styrene at  $84 \text{ }^\circ\text{C}$  using  $^{13}\text{C}$  NMR spectroscopy and found species resulting from termination of intermediate radicals. Venkatesh *et al.*<sup>[92]</sup> showed on the basis of model experiments that the formation of long-arm star-shaped polymers through IRT is possible using a combination of size-exclusion chromatography (SEC) and matrix-assisted laser desorption ionization time-of-flight mass spectrometry (MALDI-TOF-MS). Geleen and Klumperman used the same method to identify IRT products formed during a “normal” RAFT-mediated BA polymerization.<sup>[93]</sup> They employed a dithiobenzoate with a chromophore in the leaving group and found that cross- and self-termination products of the intermediate

species are being formed from the early stages of polymerization on and remain unchanged throughout.

Wang and Zhu successfully fitted molar mass, polydispersity index (*PDI*) and monomer conversion versus reaction time data of the polystyryl dithiobenzoate-mediated styrene polymerization with the IRT model using the method of moments.<sup>[45,46]</sup> Monte Carlo simulations of cumyl dithiobenzoate mediated methyl acrylate polymerization also suggest that cross-termination occurs.<sup>[55]</sup> Both simulations were able to predict intermediate radical concentrations correctly.

Further evidence for the IRT model comes from miniemulsion polymerization. Lou *et al.*<sup>[94]</sup> investigated the RAFT miniemulsion polymerization of styrene with a dithioacetate and a dithiobenzoate as mediating agents. The  $K_{\text{eq}}$  values are estimated to be  $22 \text{ L} \cdot \text{mol}^{-1}$  and  $314 \text{ L} \cdot \text{mol}^{-1}$  for the dithioacetate and dithiobenzoate, respectively. Monomer conversion versus time traces were fitted to a kinetic model yielding fragmentation rate coefficients of about  $10^4$  to  $10^5 \text{ s}^{-1}$ . Suzuki *et al.*<sup>[95,96]</sup> carried out styrene polymerization using dithiobenzoate as the RAFT agent in both bulk and miniemulsion systems with the same rates of radical generation and the same RAFT agent concentrations. Polymerization in miniemulsion was by far faster than in bulk and the obtained rate of polymerization agreed with the calculated results assuming cross-termination between the propagating radical and intermediate radical.

### 2.3.2 Slow fragmentation

Moad *et al.*<sup>[47]</sup> proposed that resonance stability of the intermediate radical by itself leads to slow fragmentation, that is a very low  $k_{\beta}$  and a high  $K_{\text{eq}}$  value. Support for this so-called slow fragmentation (SF) model comes from *ab initio* calculations by Coote and co-workers.<sup>[36–42]</sup> Most of these calculations focus on the pre-equilibrium situation, i. e., small model compounds, and predict  $K_{\text{eq}}$  values in the order of  $10^7 \text{ L} \cdot \text{mol}^{-1}$  at  $60 \text{ }^{\circ}\text{C}$ . This SF value exceeds the  $K_{\text{eq}}$  value from the IRT model by six orders of magnitude.

Quantum-chemical studies of dithiobenzoates and oligomeric species are available for the 2-(2'-cyanopropyl)-dithiobenzoate-mediated styrene polymerization up to the trimer stage of the attacking radical<sup>[39,97]</sup> and for *tert*-butyl dithiobenzoate-mediated MMA polymerization.<sup>[98]</sup> For the styrene system  $K_{\text{eq}}$  increases by about three orders of magnitude going from the unimer to trimer stage. For the MMA system an increase by one order of magnitude is predicted. Hence, a chain-length dependence of  $K_{\text{eq}}$  alone can not account for the huge discrepancy between SF and IRT model.

Experimental evidence for slow fragmentation is scarce. Barner-Kowollik *et al.*<sup>[43,44]</sup> successfully modeled the evolution of molar mass, *PDI* and monomer conversion versus reaction time in polystyryl dithiobenzoate-mediated styrene polymerization with PREDICI<sup>®</sup> using  $k_{\beta} = 3 \times 10^{-2} \text{ s}^{-1}$  and  $K_{\text{eq}} = 1.6 \times 10^7 \text{ L} \cdot \text{mol}^{-1}$ . Yet, with these

coefficients intermediate radical concentrations of about  $10^{-4}$  mol · L<sup>-1</sup> should occur,<sup>1</sup> which contradicts EPR measurements. In another experiment, Barner-Kowollik *et al.* subjected a mixture of CDB and styrene to  $\gamma$ -irradiation. From the results they suggested that a stable intermediate product is formed.<sup>[99]</sup> However, the influence of  $\gamma$ -irradiation on RAFT polymerization is not yet fully understood.<sup>[84]</sup>

The only direct observation of slow fragmentation comes from Chernikova *et al.* for the model system *tert*-butyl/*tert*-butyl dithiobenzoate (TB/TBDB) using a spin trap method (see Section 5.1).<sup>[100]</sup> The observed slow fragmentation rate is in line with the high intermediate radical concentrations, which were detected with EPR spectroscopy by the same group in the initial period of *n*-butyl acrylate polymerizations in the presence of *tert*-butyl dithiobenzoate.<sup>[56]</sup> However, the intermediate radical concentration then slowly decreased and it was concluded that retardation in the initial stages was caused by slow fragmentation, but retardation afterwards was due to IRT. This model system does not prove slow fragmentation, as it is not generally valid.

The supporters of the SF model further argue that high amounts of cross- and self-termination products should be found in dithiobenzoate-mediated polymerizations, which is however not the case in acrylate polymerizations.<sup>[101–103]</sup> Barner-Kowollik and Junkers also compared acrylate midchain radicals with RAFT intermediate radicals and concluded that both species should be associated with a low fragmentation rate coefficient.<sup>[104]</sup>

### 2.3.3 “Missing step” reactions

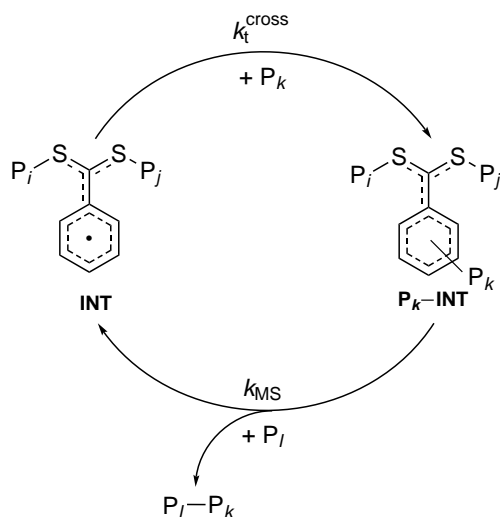
Neither the intermediate radical termination model nor the slow fragmentation model are capable of explaining the entire body of experimental observations. The high concentrations of cross- and self-termination products predicted by the IRT model were not found under polymerization conditions. Slow fragmentation should lead to high intermediate radical concentrations, which is incompatible with EPR data. Therefore, Buback and Vana proposed to include an additional reaction – termed “missing step” – into the kinetic scheme.<sup>[49]</sup> As illustrated in Scheme 2.6, the “missing step” occurs subsequent to cross-termination and transforms a highly reactive propagating radical and a not overly stable three-arm star species into the resonance-stabilized RAFT intermediate radical and a very stable polymer molecule. DFT estimates suggest that these reactions should be rather fast.<sup>[105]</sup>

PREDICI<sup>®</sup> simulations show that these steps neither influence polymerization rate nor intermediate radical concentration but provide a way to resolve the controversy about the low concentrations of IRT products. Thus, an extended kinetic scheme including IRT and “missing step” reactions represents all essential observations made

---

<sup>1</sup>The concentration of intermediate radicals was simulated with PREDICI<sup>®</sup> using the rate coefficients given by Barner-Kowollik *et al.*<sup>[43]</sup>

for the main-equilibrium period of dithiobenzoate-mediated RAFT polymerizations. Indication for the occurrence of a “missing step” reaction has been provided by Moad *et al.* by monitoring AIBN-initiated benzyl dithiobenzoate-mediated styrene polymerization via real-time  $^{13}\text{C}$  NMR. They found an NMR resonance signal which could correspond to a ring-substituted benzyl dithiobenzoate formed by a “missing step” process.<sup>[106]</sup>



**Scheme 2.6.** Illustration of the “missing reaction step” by Buback and Vana.<sup>[49]</sup>

### 2.3.4 Intermediate radical termination with short chains only

Intermediate radical termination in conjunction with the “missing step” process allows for adequate representation of the entire body of kinetic characteristics of dithiobenzoate-mediated polymerization, but clear experimental evidence for the latter reaction steps is still pending (see above). Therefore, the debate has not yet come to an end. The supporters of the SF model claim that the *ab initio* calculations are correct, whereas the results from experiments are model-dependent and differences in experimental and calculated  $K_{\text{eq}}$  may be due to effects of chain-length dependence and/or of solvent interactions.<sup>[98,107]</sup> As some kind of a compromise, the supporters of the SF model by now accept a model which assumes cross-termination of RAFT intermediates with propagating radicals up to a chain length of  $i = 3$  and very slow cross-termination of larger species.<sup>[108–110]</sup>

This model, as introduced by Konkolewicz *et al.*,<sup>[109,110]</sup> accounts for the absence of 3-armed stars predicted by IRT with radicals of arbitrary chain length, since the short

radical makes a negligible difference to the overall molecular mass. The predicted rate coefficients are consistent with slow fragmentation of the RAFT intermediate, and the overall concentration of radicals is consistent with ESR experiments.

As in the case of the “missing step” process, there is currently no unambiguous proof for this proposition. A study of Ting *et al.*<sup>[111]</sup> certainly indicates that cross-termination becomes negligibly small at longer chain lengths. In this study, all short radicals were eliminated from the polymerization system by employing a macro-azo-initiator and a polymeric RAFT agent based on cumyl dithiobenzoate. The results show – in agreement with the model proposed by Konkolewicz *et al.* – that there is very little retardation in dithiobenzoate-mediated RAFT polymerization of styrene in the absence of short radicals, but it must be stressed that initial chain lengths of around 50 were used. Thus, this experiment does not provide any information about the influence of cross-termination in the chain length range of 3 to 50. In addition, Geelen and Klumperman found indications for 3- and 4-arm stars consisting of long chain arms in dithiobenzoate-mediated butyl acrylate polymerizations.<sup>[93]</sup>

That intermediate radicals exclusively terminate with propagating radicals of very short chain length is also in conflict with results from Monte Carlo simulations, where the contact probability between radical chain ends and several positions along the arms of star-branched chains with up to six arms was investigated.<sup>[112]</sup> For a two-arm star, a reduction of the contact probability with radical size according to a power law with an exponent of  $-0.27$  has been found, which number is only slightly above the exponent of  $-0.16$  for the contact probability of the radical chain ends of two linear chains. Thus, the contact probability is not reduced to such an extent as to impede the production of larger star-shaped species. The result from theory is in full agreement with the observed control of RAFT synthesis of star polymers, which requires efficient chain transfer at the center of the star-shaped polymer.<sup>[113]</sup> For cross-termination between an intermediate radical and a growing chain, the same shielding effects as for chain transfer processes should operate.

The IRT process and the associated termination rate coefficients can also be discussed using the mean field theory<sup>[114]</sup> or the theory of irreversible intermolecular reactions of polymeric species in dilute polymer solutions.<sup>[115]</sup> The power law exponents are close to the ones from Monte Carlo simulations, which suggests that the rate coefficient for a 100-meric radical is still about 27 % that of a monomeric radical.<sup>[84]</sup> Therefore, restricting termination of INT species to reaction with very small radicals would be associated with a highly unusual chain-length dependence of this process, for which no physical reason is seen.

# 3

## Choice of the methods of investigation

This chapter focuses on the appropriate design of experiments to determine addition and fragmentation rate coefficients of the RAFT equilibrium and to clarify the kinetics of dithiobenzoate-mediated polymerizations. The requirements of discrimination between the models presented in Chapter 2 are discussed. Quasi-stationary EPR experiments for the determination of the RAFT equilibrium constant and time-resolved EPR experiments for measuring the individual rate coefficients for addition and fragmentation are outlined. In addition, the considerations made for selecting the appropriate reaction conditions are given.

### 3.1 Experiments based on polymerization behavior

Measuring the rate of radical polymerization constitutes one of the main techniques for gaining insight into a mechanistic process. However, since the RAFT equilibria do – in principle – not change the concentration of propagating radicals, the rate coefficients associated with the equilibria are difficult to obtain. Only the addition rate coefficient,  $k_{\text{ad}}$ , may be calculated from the transfer constant, which is obtained using the Mayo equation or by analyzing the dependence of the monomer conversion on RAFT conversion.<sup>[43,47,64,66,73,74,116,117]</sup> The equilibrium constant,  $K_{\text{eq}}$ , and the fragmentation rate coefficient,  $k_{\beta}$ , can not be obtained from the polymerization behavior.

If the polymerization rate is retarded Kwak *et al.*<sup>[50]</sup> proposed to derive  $K_{\text{eq}}$  from the observed rates of polymerization at different RAFT agent concentrations via

### 3 Choice of the methods of investigation

---

Equation 2.2 and 2.3. However, this procedure is only applicable to a restricted extent, since

- determination of  $K_{\text{eq}}$  is limited to RAFT agents which retard polymerization rate,
- determination of  $K_{\text{eq}}$  is model-dependent (assumption of chain-length averaged  $k_t^{\text{cross}}$  and  $k_t^{\text{self}}$ ), and
- rate retardation may not be only a consequence of intermediate radical termination, but also of a combination of various effects (see Section 2.3).

One may thus conclude that Equations 2.2 and 2.3 provide only limited access to an accurate RAFT equilibrium constant.

Measuring the polymerization rate, the *PDI* or the molar mass distribution during RAFT polymerization also does not allow for discrimination between the intermediate radical termination and the slow fragmentation model. Since only a small fraction of intermediate radicals undergoes termination, the loss of RAFT species is only by a few percent. Hence, there is little or no effect on the molecular mass distribution and controlled polymer architecture with low polydispersity will be maintained. A method which focuses on the RAFT equilibrium and directly traces the species which are being part of it should be developed preferentially.

### 3.2 Quasi-stationary EPR experiments

Since two of the three species involved in the RAFT equilibrium are of radical nature, electron paramagnetic resonance (EPR) spectroscopy should be the method of choice. First attempts to determine the rate coefficients associated with the RAFT equilibrium via EPR spectroscopy were undertaken by Kwak *et al.*<sup>[50]</sup> They assumed that with the polymerization system illustrated in Scheme 2.1 and 2.5 being in a stationary state for observation over a relatively short time scale, the following equation should hold with respect to the intermediate-radical concentration:

$$0 = \frac{dc_{\text{INT}}}{dt} = k_{\text{ad}} \times c_{\text{P}} \times c_{\text{RAFT}} - k_{\beta} \times c_{\text{INT}} - k_t^{\text{cross}} \times c_{\text{P}} \times c_{\text{INT}} - k_t^{\text{self}} \times c_{\text{INT}}^2 \quad (3.1)$$

If the rates of cross- and self-termination reactions are negligibly small compared to those of addition and fragmentation, Equation 3.1 may be rewritten as:

$$k_{\text{ad}} \times c_{\text{P}} \times c_{\text{RAFT}} = k_{\beta} \times c_{\text{INT}} \quad (3.2)$$

Combining Equation 3.2 and the definition for the RAFT equilibrium constant (Equation 2.1) one obtains the relation:

$$\frac{c_{\text{INT}}}{c_{\text{P}}} = \frac{k_{\text{ad}}}{k_{\beta}} \times c_{\text{RAFT}} = K_{\text{eq}} \times c_{\text{RAFT}} \quad (3.3)$$



Hence, the radical concentration ratio allows evaluation of the RAFT equilibrium constant by way of a plot of  $c_{\text{INT}}/c_{\text{P}}$  against initial RAFT agent concentration,  $c_{\text{RAFT}}$ . The slope of the so-obtained straight line yields  $K_{\text{eq}}$ .

Kwak *et al.*<sup>[50]</sup> derived the intermediate-radical concentration,  $c_{\text{INT}}$ , during dithio-benzoate-mediated styrene bulk polymerization at 60 °C via EPR spectroscopy. In addition, the rate of polymerization was monitored to deduce the concentration of propagating radicals,  $c_{\text{P}}$ . The ratio of  $c_{\text{INT}}$  to  $c_{\text{P}}$  gave the equilibrium constant,  $K_{\text{eq}}$ . Apart from the assumption that cross- and self-termination occur at negligible rates as compared to addition and fragmentation – which has to be verified by additional experiments – this approach is model-free.

In the present thesis, the accuracy of  $K_{\text{eq}}$  determination based on Equation 3.3 has been improved by measuring the ratio of  $c_{\text{INT}}$  and  $c_{\text{P}}$  in one EPR experiment, which eliminates the necessity of calibrating the EPR setup and thus greatly facilitates the experiment.<sup>[118]</sup> The two types of radicals may be spectroscopically distinguished due to their individual hyperfine splitting. The individual radical fractions can be determined by the deconvolution procedure described in Section 7.3.3. This constitutes an enormous advantage over methods for  $K_{\text{eq}}$  determination,<sup>[50]</sup> where absolute radical concentrations have to be measured. For determination of the INT to P ratio with the lowest possible experimental error the two types of radicals have to occur at similar concentrations, which – according to Equation 3.3 – is the case, when  $c_{\text{RAFT}}$  is close to the inverse of  $K_{\text{eq}}$ . Therefore, the RAFT agent concentrations has to be adjusted to  $K_{\text{eq}}$ .

In systems where significant cross-termination between intermediate and propagating or initiator-derived radicals occurs, the RAFT agent concentration decreases with reaction time. In this case, the  $c_{\text{INT}}/c_{\text{P}}$  ratios were determined from successive EPR scans and extrapolated to  $t = 0$ . The extrapolated value refers to the initial concentration of RAFT agent.

### 3.3 Time-resolved EPR experiments

The individual rate coefficients  $k_{\text{ad}}$  and  $k_{\beta}$  can not be derived via the stationary approach illustrated in Section 3.2, but require measurement of the concentrations of both INT and P species by time-resolved EPR spectroscopy after pulse laser initiation (SP-PLP-EPR-RAFT). Such EPR measurements of two types of radicals have already been used to study the intramolecular chain transfer (backbiting) kinetics of *n*-butyl acrylate where secondary chain-end radicals may react via 1,5 H-shift to tertiary midchain radicals.<sup>[119]</sup>

During RAFT polymerization, the time evolutions of INT and P concentrations are monitored and  $k_{\text{ad}}$  and  $k_{\beta}$  are deduced from fitting the associated concentration versus time profiles via the software package PREDICI<sup>®</sup> (see Chapter 8). Chain-length

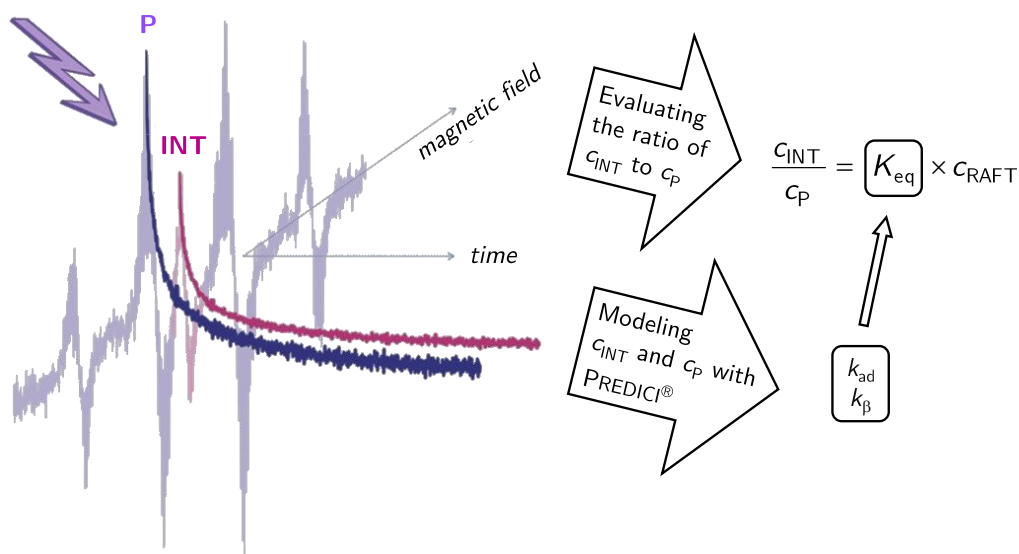


**Figure 3.1.** Illustration of the quasi-stationary  $K_{eq}$  determination and the SP-PLP-EPR-RAFT method using the example of a trithiocarbonate-mediated *n*-butyl acrylate polymerization.

dependent rate coefficients for termination and cross-termination reactions were implemented into the model as obtained from SP-PLP-EPR from the associated RAFT-free system. This procedure constitutes a considerable improvement over the previously described approach where only the concentration versus time trace of the intermediate radical has been measured.<sup>[120]</sup>

As shown in Figure 3.1, the equilibrium constant,  $K_{eq}$ , obtained from this single-pulse approach can be compared directly with  $K_{eq}$  determined via the quasi-stationary approach. Since the accuracy of  $k_{ad}$  and  $k_{\beta}$  determination depends on the application of the correct kinetic scheme, the comparison of the results obtained by the two independent methods is valuable to ensure the applicability of the model implemented into PREDICI®.

In addition,  $k_t^{cross}$  may be estimated and – in conjunction with  $k_{ad}$  and  $k_{\beta}$  – the assumption made for the stationary determination of  $K_{eq}$ , i.e., that the rates of cross-termination and self-termination are negligibly small as compared to the rates of addition and fragmentation, can be verified.

### 3.4 Product analysis by NMR spectroscopy and mass spectrometry

The EPR experiments are valuable for deducing the rate coefficients relevant for the RAFT equilibrium. Especially the magnitude of the fragmentation rate coefficient allows to distinguish between the competing models put forward to describe rate retardation in dithiobenzoate-mediated polymerizations, i. e., intermediate radical termination and slow fragmentation in particular. Most studies using NMR spectroscopy and mass spectrometry focus on the detection of cross- and self-termination products. To check, however, whether cross-termination products undergo follow-up reactions, the identification of all side product which form during the process is required.

In most of the previous studies described in Section 2.3.1 high initial RAFT agent concentrations were used, which resulted in a very long pre-equilibrium period and only oligomeric material was formed. The products were monitored online. The 3-arm star oligomeric products, which have been found, may result from cross-termination, but also from the “missing step” process. The exact structures have not been identified, because the separation of all products is not possible under conditions where oligomer or polymer is formed.

In the present work, the product compositions of model systems without monomer were analyzed. Studying model systems provides the advantage of having reactants and products showing significant differences in their chemical structure, which enables their individual spectroscopic monitoring. All products can be isolated and characterized individually. The products of the model systems (Chapter 5) were therefore separated by column chromatography and their structures subsequently identified via mass spectrometry, 1D ( $^1\text{H}$ ,  $^{13}\text{C}$ ) and 2D (COSY, HSQC, HMBC) NMR spectroscopy. The fractions of side products were determined from  $^1\text{H}$  NMR spectroscopy. In this way, the impact of side reactions on the RAFT kinetics may be evaluated.

### 3.5 Selection of experimental conditions

For the experiments described in the previous sections (I) RAFT agent, (II) initiator, (III) solvent, (IV) monomer and (V) reaction conditions have to be chosen carefully in order to avoid side reactions and reduce the complexity of the kinetic scheme.

(I) The leaving group of the RAFT agent should have the same chemical structure as the propagating radical for the experiments with macromolecular systems (Chapter 4) and as the initiator-derived radical for the model systems (Chapter 5). This assures the applicability of Equation 3.3 and reduces the number of fitting parameters for PREDICI<sup>®</sup> simulations.

For the experiments with photoinitiation, the RAFT agent should show only weak absorption in the spectral range of the 500 W mercury UV lamp or at the laser line (351 nm) and should be stable towards laser and UV irradiation. To check for this conditions, UV spectra were recorded after irradiation of the investigated RAFT agents with UV light. The RAFT agents used in this work, which had to be checked for their UV stability, are the xanthate ethyl 2-[1-diethoxyphosphoryl-2,2,2-trifluoroethoxythio carbonylsulfanyl] propionate (EDTCP), the trithiocarbonates *S*-ethyl propan-2-ylonate-*S'*-propyl trithiocarbonate (EPPT) and *S'*-bis(methyl-propion-2-ylate) trithiocarbonate (BMPT), as well as the dithiobenzoate ethyl *S*-thiobenzoyl-2-thiopropionate (ETTP). The decay of EDTCP, EPPT and ETTP concentration with UV irradiation are illustrated in Figure 3.2. The decay of BMPT is not shown, as it is identical to the one of EPPT. For all RAFT agents, the decrease in concentration is less than 1 % after 75 s UV irradiation, whereas the maximum UV irradiation in the experiments is about 60s. No influence of laser pulsing at 351 nm on the RAFT agent concentrations has been observed.

The concentration of the RAFT agent has to be chosen in such a way that intermediate and propagating or initiator-derived radical, respectively, occur at similar concentrations to reduce the experimental error. In addition, high concentrations of RAFT agents induce high UV absorbance, which reduces the overall concentration of radicals – when polymerization is started with a photoinitiator – and leads to inhomogeneities in the EPR sample tube.

(II) For the experiments with photoinitiation (see Chapter 4), the initiator should decompose efficiently upon irradiation with the excimer laser and the mercury UV lamp. The decomposition must be fast as compared to propagation. For the SP-PLP-EPR-RAFT experiments the two initiator-derived radical fragments should be capable of rapidly initiating chain growth at similar rate. In this work, 2-methyl-1-[4-(methylthio)phenyl]-2-morpholin-4-ylpropan-1-one (MMMP) was used, the decomposition mechanism of which is shown in Scheme 3.1.<sup>[121]</sup>

For the experiments with thermal initiation (see Chapter 5), the initiator should decompose into radicals which have the same structure as the RAFT leaving group and exhibit no side reactions with the RAFT agent or the initiator itself.

(III) The solvent should be inert to transfer reactions to avoid an influence on radical concentration, should have a wide liquid range and show no significant UV absorbance. In the present work, toluene was used between  $-40\text{ }^{\circ}\text{C}$  to  $110\text{ }^{\circ}\text{C}$  and naphthalene at temperatures above  $110\text{ }^{\circ}\text{C}$ .

(IV) The monomer needs to be chosen in such a way that the termination rate of the propagating radicals is not too high, since the steady state concentration of propagating radicals has to be above the limit of detection of EPR. If possible, no side

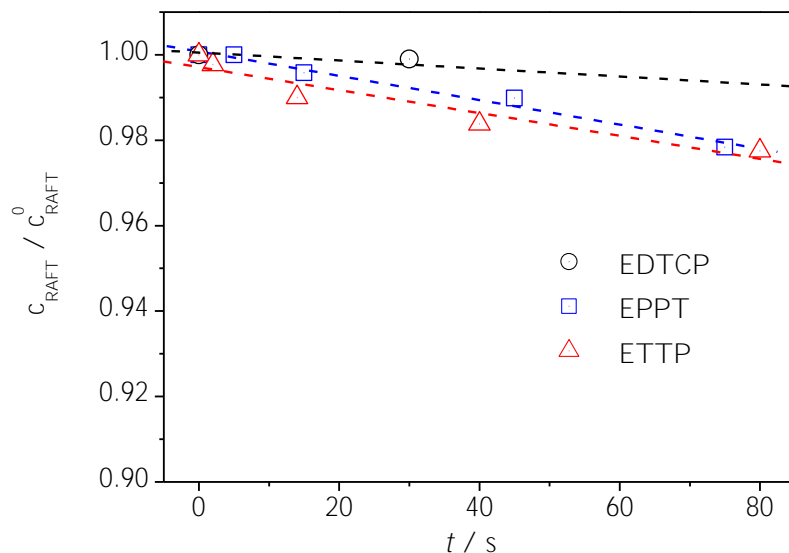
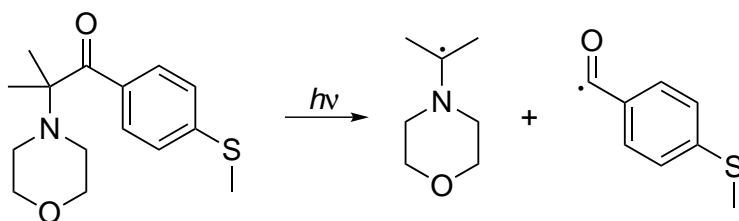


**Figure 3.2.** Decrease of RAFT agent concentrations in toluene after irradiation with a 500 W mercury UV lamp for ethyl 2-[1-diethoxyphosphoryl-2,2,2-trifluoroethoxythio carbonylsulfanyl] propionate (EDTCP), *S*-ethyl propan-2-ylonate-*S*'-propyl trithiocarbonate (EPPT) and ethyl *S*-thiobenzoyl-2-thiopropionate (ETTP).



**Scheme 3.1.** Decomposition reaction of the photoinitiator used in this thesis, 2-methyl-1-[4-(methylthio)phenyl]-2-morpholin-4-ylpropan-1-one (MMMP).

### 3 Choice of the methods of investigation

---

reactions (backbiting, transfer to solvent) should occur. In addition, the monomer should not absorb light in the UV range. As *n*-butyl acrylate has already been thoroughly investigated by EPR spectroscopy, it was chosen as the monomer for this work.

(V) For the macromolecular systems (Chapter 4), the polymerization temperature of  $-40\text{ }^{\circ}\text{C}$  was chosen in order to avoid significant backbiting of the secondary propagating radicals. The presence of three types of radicals – secondary chain-end ones, tertiary midchain ones, and RAFT intermediate ones – turns EPR analysis more difficult but should pose no principal problem toward the applicability of the EPR procedures described in the above sections. For the SP-PLP-EPR-RAFT experiments several radical concentration versus time traces were co-added in order to enhance signal-to-noise ratio.

For the model systems (Chapter 5) the temperature range was varied to ensure sufficiently fast decomposition of the initiator and thus a detectable radical concentration.

To avoid side reactions, all solutions have to be completely deoxygenated prior to the EPR measurements.

# 4

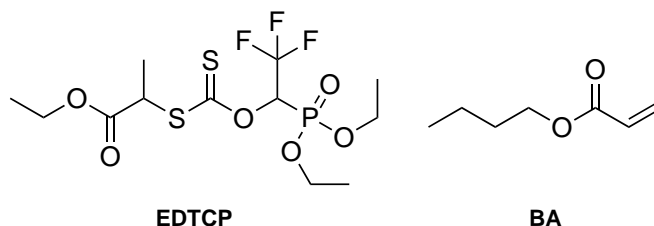
## EPR with macromolecular systems

This chapter covers the RAFT-mediated polymerization of *n*-butyl acrylate. Different types of RAFT agents, i. e. a xanthate, a symmetric and a non-symmetric trithio-carbonate and a dithiobenzoate, were used to investigate the influence of the stabilizing Z group on the rate coefficients associated with the RAFT equilibrium. To allow for direct comparison of the results, the same acrylate-type leaving group was used for all RAFT agents. The quasi-stationary approach was chosen to measure the equilibrium constant and the SP-PLP-EPR-RAFT experiment to determine independently the addition, fragmentation and cross-termination rate coefficients.

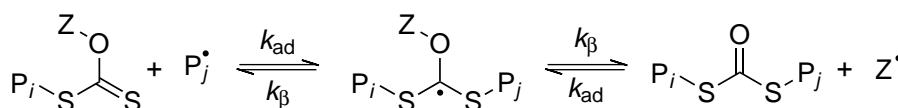
### 4.1 Xanthate-mediated *n*-butyl acrylate polymerization

Ethyl 2-[1-diethoxyphosphoryl-2,2,2-trifluoroethoxythio carbonylsulfanyl] propionate, EDTCP, was chosen as the first RAFT agent to be studied.<sup>[122]</sup> EDTCP belongs to the xanthate chain transfer agents where Z = O-alkyl. The structure of the investigated RAFT agent and the monomer are depicted in Scheme 4.1. RAFT polymerizations involving xanthates are also referred to as MADIX for MAcromolecular Design via the Interchange of Xanthates.<sup>[123]</sup>

Both processes essentially follow the same mechanism, but in the MADIX process fragmentation of the intermediate radical potentially occurs via two pathways, which are illustrated in Scheme 4.2: In addition to normal  $\beta$ -scission, the alkoxy group may fragment. If this additional fragmentation step can be excluded, determination of the RAFT-related rate coefficients via the procedures outlined in Chapter 3 becomes possible. In order to check for  $\beta$ -scission of the Z-group, product samples were



**Scheme 4.1.** The RAFT agent ethyl 2-[1-(diethoxyphosphoryl)-2,2,2-trifluoroethoxythio carbonylsulfanyl] propionate and the monomer *n*-butyl acrylate, which are used in this study.



**Scheme 4.2.** Normal  $\beta$ -scission (l. h. s.) versus alkoxy  $\beta$ -scission (r. h. s.).

collected after the EPR experiments and subjected to end-group analysis by mass spectrometry.<sup>[124,125]</sup> The results prove that alkoxy  $\beta$ -scission of the O-Z bond may be ignored, since no oligomer from reinitiation by the Z-group could be found.

Xanthates are normally used for vinyl monomers and only poor control is observed with acrylates.<sup>[126,127]</sup> The reactivity of the carbon-sulfur double bond against radical attack is reduced because of conjugation with the free electron pair on the oxygen atom. Better transfer may be achieved by introducing an electron-withdrawing group, i. e., phosphor or fluorine as with EDTCP, which disfavors such conjugation and enhances the reactivity.<sup>[128]</sup> Furthermore, EDTCP carries a leaving group, which is similar to the growing radical. Thus, the addition and fragmentation rate coefficients for the primary EDTCP-derived radical and for propagating radicals may be assumed to be identical.

The polymerization temperature of  $-40\text{ }^\circ\text{C}$  was chosen in order to avoid significant backbiting of the secondary propagating radicals.<sup>[129]</sup> EPR spectra measured at higher temperature clearly show midchain radicals. The presence of three types of radicals – secondary chain-end ones, tertiary midchain ones, and RAFT intermediate ones – turns EPR analysis more difficult but poses no principal problem toward the applicability of the procedures described in Chapter 3. Determination of  $K_{\text{eq}}$  from the ratio of EPR intensities via the stationary approach is detailed in the following section. Afterwards, time-resolved monitoring of  $c_{\text{INT}}$  and  $c_{\text{P}}$  is used to investigate the individual rate coefficients.



### 4.1.1 Quasi-stationary EPR experiments

As  $K_{\text{eq}}$  is expected to be rather low, relatively large MADIX concentrations,  $c_{\text{MADIX}} \approx 10^{-2} \text{ mol} \cdot \text{L}^{-1}$  were used to obtain similar INT and P concentrations under quasi-stationary conditions (see Equation 3.3). Since two types of radicals, INT and P, are monitored, the molar fractions of the individual radical species need to be known. This information may be obtained by deconvolution of the spectra (detailed in Section 7.3.3). The individual spectra are simulated on the basis of the coupling constants and line widths determined from EPR measurements under conditions where either the propagating radical or the intermediate radical is dominant. The EPR splitting schemes of the INT and P components shown in Figure 4.1a and b may be adequately described by the hyperfine coupling constants listed in Table 4.1.

The EPR spectrum of the intermediate radical is characterized by the coupling of the carbon-centered radical with the phosphor and fluorine atoms in  $\gamma$  and  $\delta$  position, respectively. The spectrum actually consists of 8 lines but reduces to a 7-line spectrum due to line broadening. Fitting of the measured EPR spectrum by the individual INT and P spectra yields the fractions of both species,  $x_{\text{INT}}$  and  $x_{\text{P}}$ , respectively. Experimental and simulated spectra for a MADIX polymerization of BA at  $-40 \text{ }^\circ\text{C}$  using an EDTCP concentration of  $2.1 \times 10^{-2} \text{ mol} \cdot \text{L}^{-1}$  are compared in Figure 4.1c.

EPR spectra of different MADIX agent concentrations were taken during pulsed-laser-initiated polymerization. A pulse repetition rate of 20 Hz was chosen to generate quasi-stationary concentrations of INT and P.<sup>[59]</sup> In Figure 4.2, the measured ratios of  $c_{\text{INT}}/c_{\text{P}}$  are plotted for BA polymerizations carried out at different initial EDTCP concentrations. According to Equation 3.3, the slope of the straight line passing through the origin yields  $K_{\text{eq}} = (12.0 \pm 0.2) \text{ L} \cdot \text{mol}^{-1}$ . The low  $K_{\text{eq}}$  value is consistent with the poor control observed in xanthate-mediated acrylate polymerization. To examine, whether this  $K_{\text{eq}}$  value refers to pre-equilibrium or main-equilibrium conditions, product samples were collected after irradiation and analyzed via SEC. The molecular mass increases from  $\overline{M}_n = 1.3 \times 10^3 \text{ g} \cdot \text{mol}^{-1}$  at  $c_{\text{EDTCP}} = 4.3 \times 10^{-2} \text{ mol} \cdot \text{L}^{-1}$  to  $\overline{M}_n = 1.2 \times 10^4 \text{ g} \cdot \text{mol}^{-1}$  at  $c_{\text{EDTCP}} = 3.5 \times 10^{-3} \text{ mol} \cdot \text{L}^{-1}$ . These results are indicative of a main-equilibrium situation.

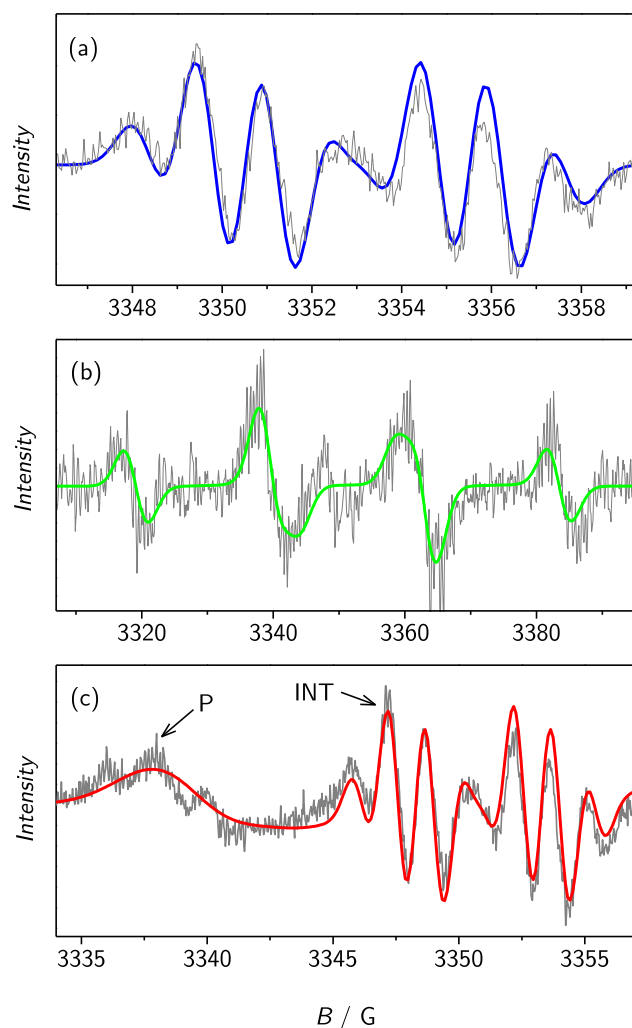


**Figure 4.1.** (a) Simulated (blue line) and experimental (gray line) EPR spectra of the EDTCP intermediate radical, INT. (b) Simulated (green line) and experimental (gray line) EPR spectra of the propagating radical, P. (c) Section of the EPR spectrum used for determining  $c_{\text{INT}}/c_{\text{P}}$ . Gray line: EPR spectrum recorded during laser-initiated polymerization of BA ( $1.5 \text{ mol} \cdot \text{L}^{-1}$  in toluene) in the presence of EDTCP at  $-40 \text{ }^\circ\text{C}$ ;  $c_{\text{EDTCP}} = 2.1 \times 10^{-2} \text{ mol} \cdot \text{L}^{-1}$ ,  $c_{\text{MMMP}} = 1.0 \times 10^{-2} \text{ mol} \cdot \text{L}^{-1}$ . Pulse repetition rate: 20 Hz; sweep time: 42 s; modulation amplitude: 1 G; microwave power: 10 mW. Red line: Simulated EPR spectrum; the field positions for monitoring INT and P individually as a function of time after laser initiation are indicated by the arrows.

**Table 4.1.** Coupling constants deduced from experimental spectra of intermediate radical, INT, and propagating radical, P, in EDTCP-mediated *n*-butyl acrylate polymerization.

radical	coupling constants / G	
INT	$a_{P,\gamma}$	$a_{F,\delta}$
	0.5	1.4
P	$a_{H,\alpha}$	$a_{H,\beta}$
	24.3	21.0

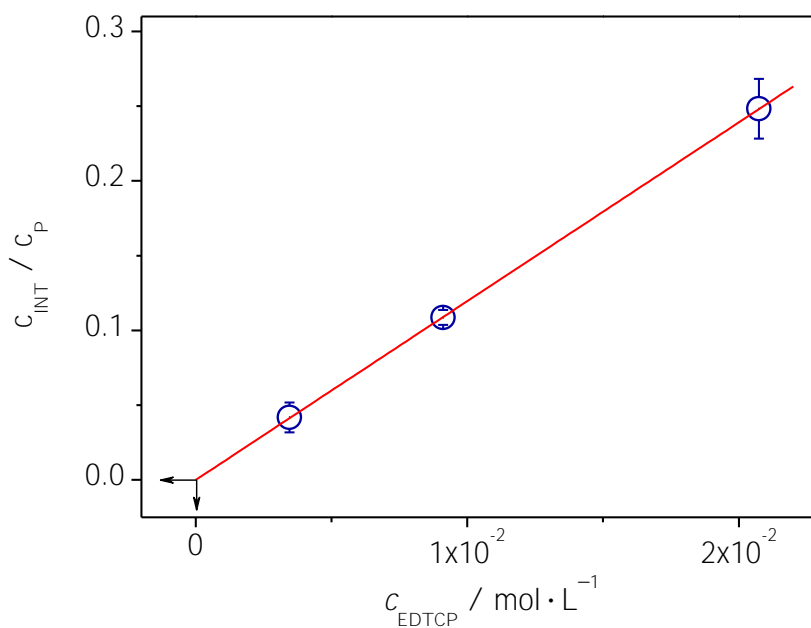


**Figure 4.2.**  $c_{\text{INT}}/c_{\text{P}}$  ratio at different RAFT agent concentrations during BA ( $1.5 \text{ mol} \cdot \text{L}^{-1}$  in toluene) polymerization at  $-40 \text{ }^\circ\text{C}$  using MMMP ( $1.0 \times 10^{-2} \text{ mol} \cdot \text{L}^{-1}$ ) as the photoinitiator. The slope of the linear fit yields the equilibrium constant,  $K_{\text{eq}}$ . Each data point refers to an average value from at least three independent experiments at the same EDTCP concentration.

### 4.1.2 Time-resolved EPR experiments

For deducing the individual rate coefficients,  $k_{\text{ad}}$  and  $k_{\beta}$ , both the intermediate and propagating radical concentrations,  $c_{\text{INT}}$  and  $c_{\text{P}}$ , were separately measured via time-resolved EPR spectroscopy after single laser pulse initiation. In order to enhance signal-to-noise ratio, up to 20 INT and up to 200 P concentration-versus-time traces were co-added. The absolute concentration of the intermediate radical,  $c_{\text{INT}}$ , and the propagating radical,  $c_{\text{P}}$ , were determined via the three-step calibration procedure described in Section 7.3.2. The field positions used for monitoring the individual radical concentrations are indicated by the arrows in Figure 4.1.

Illustrated in Figure 4.3 is the time evolution of the concentration of the intermediate radical and of the propagating radical after firing the laser pulse at  $t = 0$ . The lines in each figure refer to different RAFT agent concentrations. The concentration has been varied to assure that the obtained rate coefficients are independent of  $c_{\text{EDTCP}}$ . The data in Figure 4.3 demonstrate that, towards lower  $c_{\text{EDTCP}}$ ,  $c_{\text{P}}$  increases whereas  $c_{\text{INT}}$  decreases.

The experimental traces were fitted to the kinetic Scheme 8.1 given in Section 8.1, which encompasses initiation, propagation, chain-length dependent termination, the individual RAFT pre- and main equilibrium reaction steps as well as cross-termination of the intermediate radical. The alkoxy  $\beta$ -scission reaction has not been considered because of the experimental findings presented above. Backbiting of the propagating radical was ignored at  $-40$  °C.<sup>[129]</sup>

Radical chain length increases linearly with time  $t$  after applying a laser pulse at  $t = 0$ . It is known that the impact of a chain-length dependence of  $k_{\text{t}}$  is pronounced in PLP experiments where relatively large amounts of small radicals undergo termination. Chain-length dependent termination, considering both the chain lengths of propagating radicals and of the “arms” of the INT species was thus implemented into PREDICI<sup>®</sup>. The “arms” of the intermediate radical bear two chains which, in principle, requires a two-dimensional (2D) treatment of chain-length dependence. As the solution of the 2D problem is associated with extensive numerical effort, reactions involving a two-armed intermediate radical had to be translated into a one-dimensional problem. The derivation and implementation of the kinetic scheme into PREDICI<sup>®</sup> are detailed in Section 8.1.

The rate coefficients for the homo-termination of propagating radical,  $k_{\text{t}}^{i,i}$ , as well as for cross-termination,  $k_{\text{t}}^{\text{cross}} = 0.5 \times k_{\text{t}}^{i,i}$ , were taken from literature.<sup>[119]</sup> It should be noted that the chain-length dependent approach used for modeling the experimental radical concentration-versus-time traces is based entirely on experimental data from previous studies and thus does not afford for any fitting.

Although *ab initio* calculations predict a chain-length dependence of  $k_{\text{ad}}$  and  $k_{\beta}$ , no experimental evidence was presented so far.<sup>[39,41]</sup> Therefore, these coefficients have not been implemented into the model as chain-length dependent quantities. This would

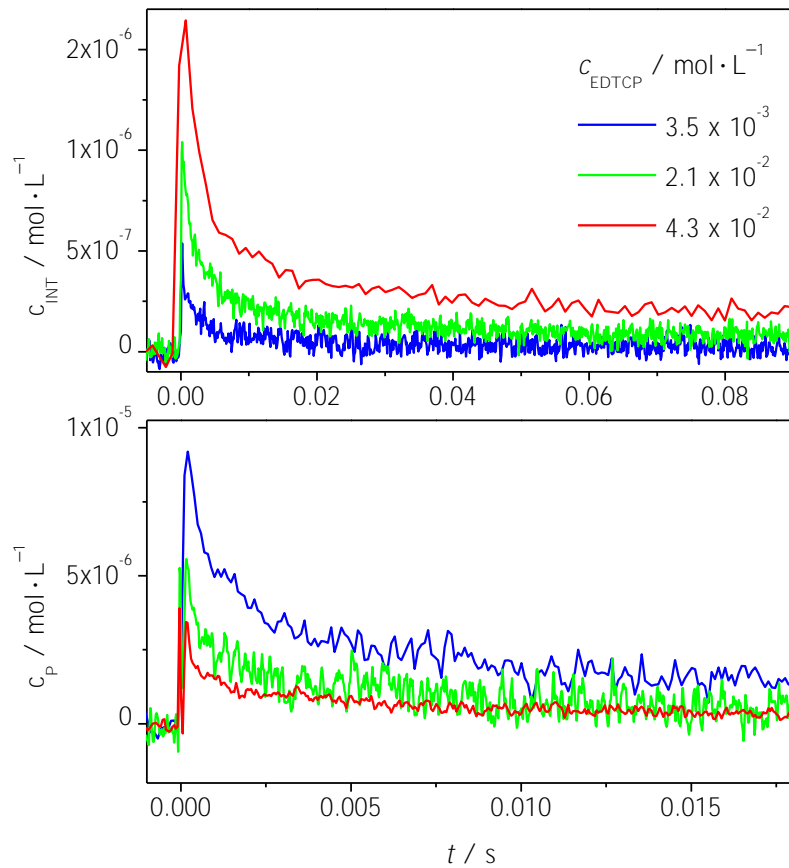


**Figure 4.3.** Intermediate radical and propagating radical concentration-versus-time profiles obtained by EPR spectroscopy in single laser pulse induced polymerization of BA ( $1.5 \text{ mol} \cdot \text{L}^{-1}$  in toluene) at  $-40 \text{ }^\circ\text{C}$  with EDTCP being the MADIX agent and MMMP ( $1.0 \times 10^{-2} \text{ mol} \cdot \text{L}^{-1}$ ) the photoinitiator.

require the fitting of additional parameters and the reliability of such an approach is questionable. Thus, the addition and fragmentation rate coefficients obtained are chain-length averaged values. Since the experimental radical concentration-versus-time traces are fitted over an extended chain-length regime, the first polymerization steps do not influence the fitted parameters significantly.

Simulation of the concentration-time profiles yields the addition rate coefficient,  $k_{\text{ad}}$ , the fragmentation rate coefficient,  $k_{\beta}$ , the primary concentration of initiator-derived radicals produced by the laser pulse,  $c_{\text{R}}^0$ , and the addition rate coefficient of the initiator-derived radical to the MADIX species,  $k_{\text{ad}}^{\text{I}}$ . It is assumed that, due to chemical similarity, the addition and the fragmentation rate coefficients of radical species containing the EDTCP-derived moiety do not differ from the associated coefficients for growing radicals of arbitrary size. Furthermore, the leaving group is assumed to add to a monomer molecule, and thus reinitiate, at the same rate as the propagating radical, i. e.,  $k_{\text{p}}^{\text{rein}} = k_{\text{p}}$ . The propagation rate coefficient,  $k_{\text{p}}$ ,<sup>[130]</sup> the chain-length dependent termination rate coefficient,  $k_{\text{t}}^{i,i}$ ,<sup>[119]</sup> and the initiation rate coefficient,  $k_{\text{i}}$ ,<sup>[131]</sup> were taken from literature. A chain-length dependent propagation rate coefficient may be implemented into the simulation as soon as such data is available. As will be shown further below, the cross-termination rate coefficient,  $k_{\text{t}}^{\text{cross}}$ , was varied to check for its impact on the radical concentration-versus-time profiles.

Figure 4.4 compares the simulated and experimental concentration-versus-time traces of the intermediate radical and the propagating radical for an EDTCP-mediated BA polymerization ( $c_{\text{EDTCP}} = 2.1 \times 10^{-2} \text{ mol} \cdot \text{L}^{-1}$ ) at  $-40 \text{ }^{\circ}\text{C}$ . The experimental traces are remarkably well fitted by the kinetic model, as are the traces for the polymerizations at other RAFT agent concentrations employed in the present study. The best fits were obtained for  $k_{\text{t}}^{\text{cross}} = 0.5 \times k_{\text{t}}$  and for assuming an identical chain-length dependence of cross-termination between INT and P and of termination between two P species.

The results of the PREDICI<sup>®</sup> simulations as listed in Table 4.2 can be summarized as follows:

1. Towards increasing EDTCP concentration, the amount of initiator-derived radicals produced by a single laser pulse,  $c_{\text{R}}^0$ , decreases, which is assigned to laser light absorption by EDTCP. The absorbance at higher EDTCP content may affect the homogeneity, in particular of radical production, in the polymerizing solution and thus may reduce the reliability of data obtained at the highest EDTCP concentration. As a consequence, the data for  $c_{\text{EDTCP}} = 4.3 \times 10^{-2} \text{ mol} \cdot \text{L}^{-1}$  is given in italics. In what follows, only the results from the EPR experiments at the two lower EDTCP concentrations will be considered.
2. The rate coefficient for addition of an initiator fragment to EDTCP,  $k_{\text{ad}}^{\text{I}}$ , was found to be  $(2.2 \pm 0.3) \times 10^5 \text{ L} \cdot \text{mol}^{-1} \cdot \text{s}^{-1}$ . Thus, the rate coefficient for addition

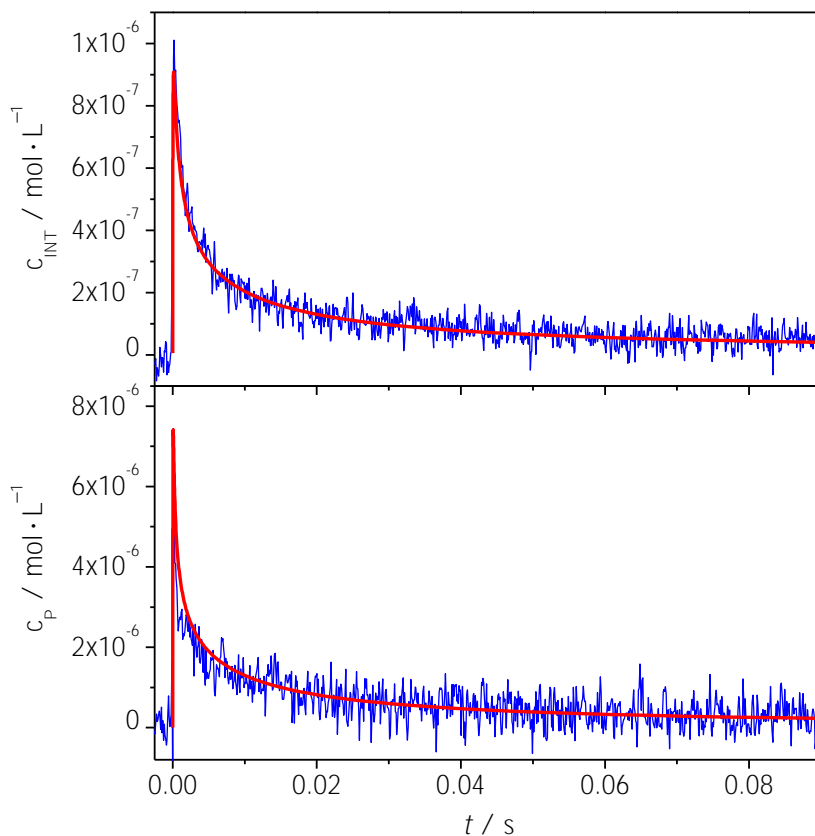


**Figure 4.4.** Comparison of simulated and experimental concentration-versus-time profiles for propagating and intermediate radicals in BA polymerization ( $1.5 \text{ mol} \cdot \text{L}^{-1}$  in toluene) at  $-40 \text{ }^\circ\text{C}$  with EDTCP being the RAFT agent ( $2.1 \times 10^{-2} \text{ mol} \cdot \text{L}^{-1}$ ) and MMMP the photoinitiator ( $1.0 \times 10^{-2} \text{ mol} \cdot \text{L}^{-1}$ ).

**Table 4.2.** Rate coefficients, equilibrium constants, and primary radical concentrations for EDTCP-mediated BA polymerization at  $-40$  °C. The following input parameters have been used in the fitting procedure:  $k_p = 2.27 \times 10^3 \text{ L} \cdot \text{mol}^{-1} \cdot \text{s}^{-1}$ ,  $k_i = 2.27 \times 10^4 \text{ L} \cdot \text{mol}^{-1} \cdot \text{s}^{-1}$ ,  $k_t^{1,1} = 1.65 \times 10^8 \text{ L} \cdot \text{mol}^{-1} \cdot \text{s}^{-1}$ ,  $\alpha_s = 0.85$ ,  $\alpha_1 = 0.22$ ,  $i_c = 30$ ,  $k_t^{\text{cross}} = 0.5 \times k_t$ .

$c_{\text{EDTCP}} / \text{mol} \cdot \text{L}^{-1}$	$3.5 \times 10^{-3}$	$2.1 \times 10^{-2}$	$4.3 \times 10^{-2}$
$c_{\text{R}}^0 / \text{mol} \cdot \text{L}^{-1}$	$2.79 \times 10^{-5}$	$8.80 \times 10^{-6}$	$5.80 \times 10^{-6}$
$k_{\text{ad}}^{\text{I}} / \text{L} \cdot \text{mol}^{-1} \cdot \text{s}^{-1}$	$2.00 \times 10^5$	$2.42 \times 10^5$	$1.78 \times 10^5$
$k_{\text{ad}} / \text{L} \cdot \text{mol}^{-1} \cdot \text{s}^{-1}$	$2.40 \times 10^4$	$2.59 \times 10^4$	$7.38 \times 10^4$
$k_{\beta} / \text{s}^{-1}$	$2.00 \times 10^3$	$2.51 \times 10^3$	$4.56 \times 10^3$
$K_{\text{eq}} / \text{mol} \cdot \text{L}^{-1}$	12.0	10.3	16.2

to the RAFT agent is by about a factor of 10 above the rate coefficient for addition of the initiator fragment to a BA molecule,  $k_i = 2.27 \times 10^4 \text{ L} \cdot \text{mol}^{-1} \cdot \text{s}^{-1}$ . Such a difference of about one order of magnitude has also been found between the addition rate coefficients of a propagating radical to EDTCP and to BA,  $k_{\text{ad}}$  and  $k_p$ , respectively. This observation indicates that the reactivity for addition of the initiator fragment and of the propagating radical is higher by about the same factor for addition to the carbon-sulfur double bond of the MADIX agent than for addition to the BA carbon-carbon double bond.

3. The arithmetic mean values of the addition and fragmentation rate coefficients obtained from the two experiments at lower EDTCP concentration are:  $k_{\text{ad}} = (2.5 \pm 0.1) \times 10^4 \text{ L} \cdot \text{mol}^{-1} \cdot \text{s}^{-1}$  and  $k_{\beta} = (2.3 \pm 0.3) \times 10^3 \text{ s}^{-1}$ .
4. The addition rate coefficient is in good agreement with the *ab initio* value of ( $k_{\text{ad}} = 10^4 \text{ L} \cdot \text{mol}^{-1} \cdot \text{s}^{-1}$ ) reported by Coote *et al.*<sup>[40]</sup> The comparison between the two  $k_{\text{ad}}$  values referring to different temperatures can be made, as the addition reaction, according to the *ab initio* estimates, should be associated with a small activation energy. No such information is available for the activation energy of  $k_{\beta}$ . It should however be noted that the obtained fragmentation rate coefficient is not too far off the value of  $k_{\beta} = 10^2$  to  $10^3 \text{ s}^{-1}$  that has been reported by Coote *et al.*<sup>[40]</sup>

To obtain information on macroradical size after applying a very few laser pulses, molar mass distributions were determined via SEC. Depending on MADIX concentration, average chain lengths between 20 and 90 have been obtained, which are close to the values determined from the above-mentioned stationary experiments. The



obtained rate coefficients thus also refer to main-equilibrium conditions.

The fitting has been carried out assuming  $k_t^{\text{cross}} = 0.5 \times k_t$ . To check, whether and to which extent this assumption affects  $k_\beta$ , the time-resolved EPR trace measured for the BA polymerization at the lowest RAFT content,  $c_{\text{EDTCP}} = 3.5 \times 10^{-3} \text{ mol} \cdot \text{L}^{-1}$ , has additionally been fitted for  $k_t^{\text{cross}} = k_t$  and for  $k_t^{\text{cross}} = 0$ . In Figure 4.5, the initial phase of the polymerization is illustrated, where the magnitude of cross-termination shows the strongest effects. Approximately 0.1 s after application of the single laser pulse all simulated concentration traces coincide irrespective of the size of considered  $k_t^{\text{cross}}$ . The resulting change in  $k_\beta$  is by less than a factor of two. The concentration decay measured for both types of radicals is thus not sensitive enough to decide whether there is any significant contribution from cross-termination. The insensitivity is due to the low intermediate radical concentration and the high addition and fragmentation rates.

### 4.1.3 Comparison of both approaches

From the individual  $k_{\text{ad}}$  and  $k_\beta$  values obtained via the SP-PLP-EPR-RAFT method, the equilibrium constant for  $-40 \text{ }^\circ\text{C}$  is found to be  $K_{\text{eq}} = (11.1 \pm 1.2) \text{ L} \cdot \text{mol}^{-1}$ , in close agreement with  $K_{\text{eq}} = (12.0 \pm 0.2) \text{ L} \cdot \text{mol}^{-1}$  deduced from the above-described method in which the ratio of intermediate and propagating radical concentrations is measured. Thus, both EPR-based methods are suitable for accurate measurement of RAFT equilibrium constants. The stationary method, which rests on measuring a ratio of radical concentrations, does not require calibration, which constitutes a major advantage. The time-resolved method, which requires calibrated EPR data is, on the other hand, far more powerful because the individual rate coefficients  $k_{\text{ad}}$  and  $k_\beta$  are accessible and because the assumption  $r_t^{\text{cross}} \ll r_{\text{ad}}, r_\beta$  needs not to be fulfilled.

The resulting  $k_{\text{ad}}$  and  $k_\beta$  may be used to check, whether the reaction conditions of the stationary experiments were adequate for estimating  $K_{\text{eq}}$  via Equation 3.3, i. e., whether rate of cross-termination is negligible as compared to the addition and fragmentation rates. The absolute concentrations of INT and P were determined by calibration of the EPR spectra. The maximum value of  $r_t^{\text{cross}}$  was estimated by adopting  $k_t^{\text{cross}} = k_t^{1,1}$ , whereas the lowest rates of addition and fragmentation were calculated for lowest  $c_{\text{EDTCP}}$ . Under these limiting conditions of our study,  $r_t^{\text{cross}}$  is still by about one order of magnitude below the addition and fragmentation rates, thus verifying the validity of using Equation 3.3 for the RAFT concentration range selected for our experiments.

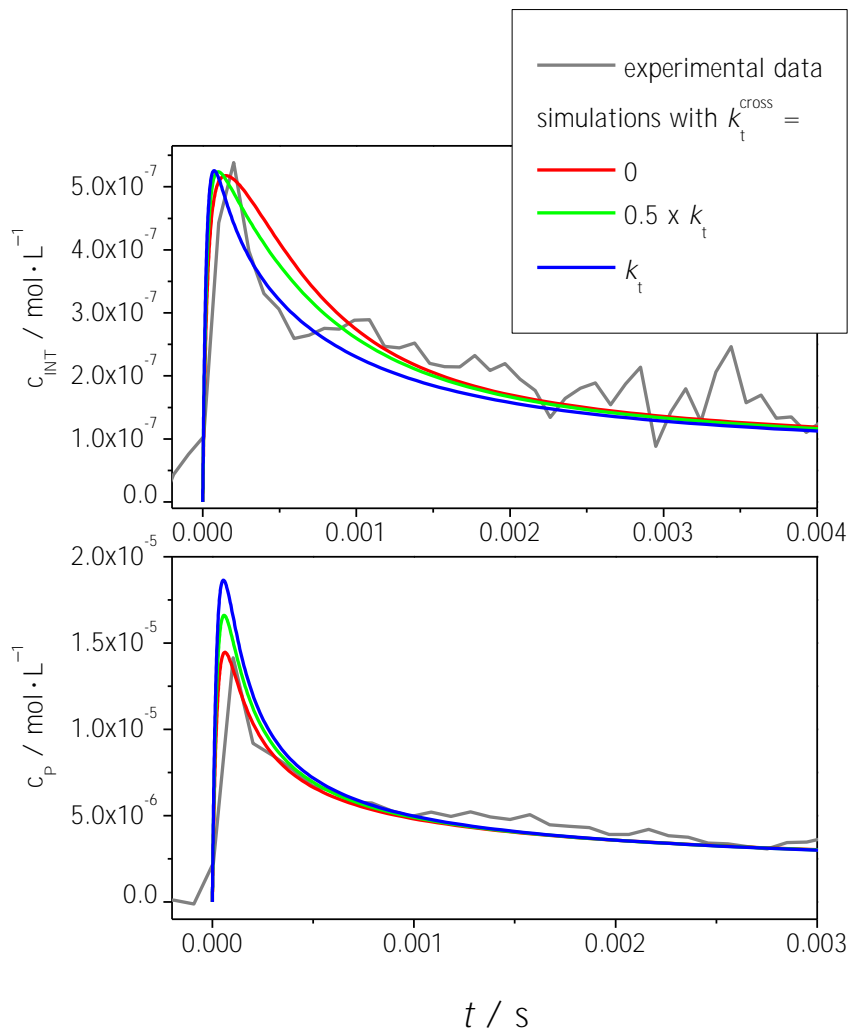
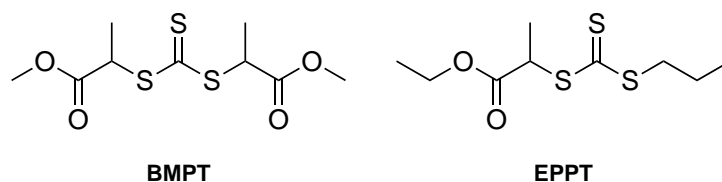


**Figure 4.5.** PREDICI<sup>®</sup> fitting of the experimental intermediate and propagating radical concentrations as a function of time after applying a laser pulse at  $t = 0$  for BA polymerization ( $1.5 \text{ mol} \cdot \text{L}^{-1}$  in toluene) at  $-40 \text{ }^\circ\text{C}$  in the presence of EDTCP ( $3.5 \times 10^{-3} \text{ mol} \cdot \text{L}^{-1}$ ) and with MMMP ( $1.0 \times 10^{-2} \text{ mol} \cdot \text{L}^{-1}$ ) as the photoinitiator. The fitting was carried out for different cross-termination rate coefficients:  $k_t^{\text{cross}} = k_t$ ,  $k_t^{\text{cross}} = 0.5 \times k_t$ , and  $k_t^{\text{cross}} = 0$ , where  $k_t$  refers to the chain-length dependent termination rate coefficient of BA radicals.

## 4.2 Trithiocarbonate-mediated *n*-butyl acrylate polymerization

As the second type of RAFT agent, two trithiocarbonates were investigated: *S*-ethyl propan-2-ylonate-*S'*-propyl trithiocarbonate (EPPT), which transforms into an intermediate radical bearing two growing chains, and *S,S'*-bis(methyl-propion-2-ylate) trithiocarbonate (BMPT), which gives rise to an intermediate radical with three growing chains. The structures of the trithiocarbonates are illustrated in Scheme 4.3. BMPT was studied previously, monitoring the build-up and subsequent decay in intermediate radical concentration after laser single pulse initiation.<sup>[120]</sup> A simple kinetic scheme was used to deduce  $k_{\text{ad}}$  and  $k_{\beta}$ , in which neither termination was considered as chain-length dependent nor the propagating radical concentration monitored. A relatively high BMPT concentration was chosen ( $4 \times 10^{-3} \text{ mol} \cdot \text{L}^{-1}$ ), which might be considered as a problem because of light absorbance of the RAFT agent. This can lead to inhomogeneities in the sample tube. To avoid this, lower concentrations (around  $10^{-5} \text{ mol} \cdot \text{L}^{-1}$ ) were used in the following study and the RAFT agent concentration was varied.



**Scheme 4.3.** RAFT agents under investigation: *S,S'*-bis(methyl-propion-2-ylate) trithiocarbonate (BMPT) and *S*-ethyl propan-2-ylonate-*S'*-propyl trithiocarbonate (EPPT).

### 4.2.1 Quasi-stationary EPR experiments

The EPR spectrum of the intermediate radical in BMPT-mediated BA polymerization is presented in Figure 4.6a. It appears as a singlet signal and is identical to the INT peak observed in EPPT- and benzyl propyl trithiocarbonate (BPT)-mediated BA polymerizations.<sup>[118]</sup> The EPR spectrum of the propagating BA radical is shown in Figure 4.1b. The experimental spectrum for a BA polymerization at  $-40 \text{ }^{\circ}\text{C}$  using a BMPT concentration of  $c_{\text{BMPT}} = 2.3 \times 10^{-5} \text{ mol} \cdot \text{L}^{-1}$  is depicted in Figure 4.6b. It is in excellent agreement with the simulated one, which is a summation of the individual radical spectra of INT and P. The spectra of the investigated trithiocarbonate-mediated BA polymerizations are identical, so that the EPPT spectrum is not shown separately.

Fitting of the measured EPR spectrum by the individual INT and P spectra yields the fractions of both species. The measured  $c_{\text{INT}}/c_{\text{P}}$  ratios are plotted versus BMPT concentration in Figure 4.7. According to Equation 3.3 the slope of the straight

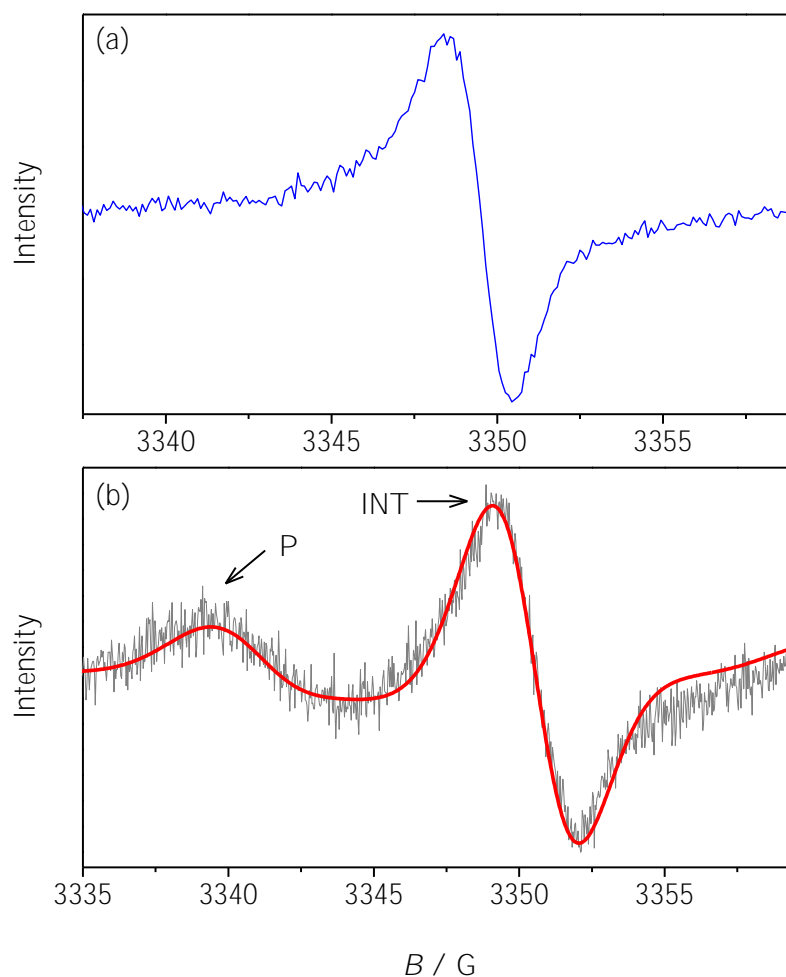


**Figure 4.6.** EPR spectrum of the intermediate radical recorded during a BMPT-mediated polymerization of BA with MMMP as the photoinitiator at  $-40\text{ }^{\circ}\text{C}$ . (a) Pseudo-stationary conditions apply with laser pulsing at a repetition rate of 20 Hz; modulation amplitude: 3 G, microwave power: 10 mW,  $c_{\text{BMPT}} = 1 \times 10^{-4}\text{ mol}\cdot\text{L}^{-1}$ . (b) EPR spectrum recorded in a 2.6 s field sweep during a stationary BA polymerization ( $c_{\text{BMPT}} = 2.3 \times 10^{-5}\text{ mol}\cdot\text{L}^{-1}$ ) with continuous UV initiation under otherwise identical experimental conditions. The red line indicates the best fit of overall EPR contour by summation of the individually simulated EPR spectra for INT and P. The P component is more pronounced in (b) because of the lower BMPT concentration. Note, that the same spectra are observed in EPPT-mediated polymerizations of BA.

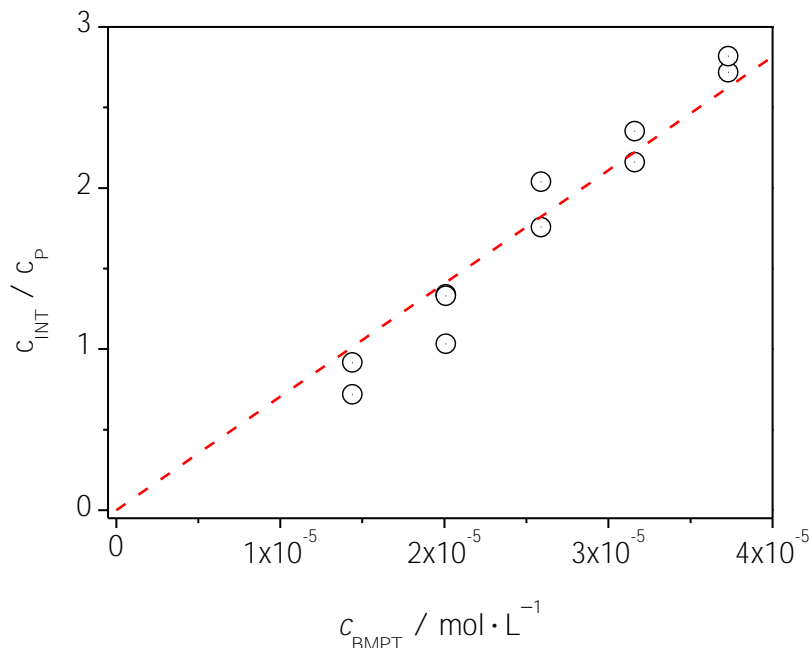


**Figure 4.7.** Ratio of intermediate radical and propagating radical concentrations,  $c_{\text{INT}}/c_{\text{P}}$ , plotted versus BMPT concentration for BA polymerizations ( $1.5 \text{ mol} \cdot \text{L}^{-1}$  in toluene) at  $-40 \text{ }^\circ\text{C}$  using MMMP ( $1.0 \times 10^{-2} \text{ mol} \cdot \text{L}^{-1}$ ) as the photoinitiator. The slope of the straight-line fit yields the equilibrium constant,  $K_{\text{eq}} = (7.0 \pm 0.2) \times 10^4 \text{ L} \cdot \text{mol}^{-1}$ .

line passing through the origin yields  $K_{\text{eq}} = (7.0 \pm 0.2) \times 10^4 \text{ L} \cdot \text{mol}^{-1}$ . The values obtained in the previous study of BMPT-mediated BA polymerization at  $-30 \text{ }^\circ\text{C}$  are  $9.5 \times 10^2 \text{ L} \cdot \text{mol}^{-1}$  assuming that intermediate radicals do not undergo cross-termination reactions and  $2.5 \times 10^4 \text{ L} \cdot \text{mol}^{-1}$  assuming  $k_{\text{t}}^{\text{cross}} = 0.5 \times k_{\text{t}}$ .<sup>[120]</sup> The previously applied model-dependent approach, which requires calibration of the EPR setup, thus yields slightly lower  $K_{\text{eq}}$  values.

In order to check for a possible chain-length dependence of  $K_{\text{eq}}$  the stationary EPR experiments for the second trithiocarbonate EPPT were not only carried out with monomeric but also with pre-polymerized RAFT agent, i. e. with initial RAFT chain lengths of 1, 17 and 38, respectively. For the synthesis of low polydispersity macroEPPT with defined chain length, high initial RAFT agent concentrations were used. The measured  $c_{\text{INT}}/c_{\text{P}}$  ratios for the monomeric and macromolecular RAFT agent are plotted versus EPPT concentration in Figure 4.8. The resulting equilibrium constant,  $K_{\text{eq}} = (2.6 \pm 0.1) \times 10^4 \text{ L} \cdot \text{mol}^{-1}$ , does not vary with initial chain length, which indicates that either  $K_{\text{eq}}$  is not chain-length dependent or the main equilibrium situation is reached rapidly with monomeric EPPT.

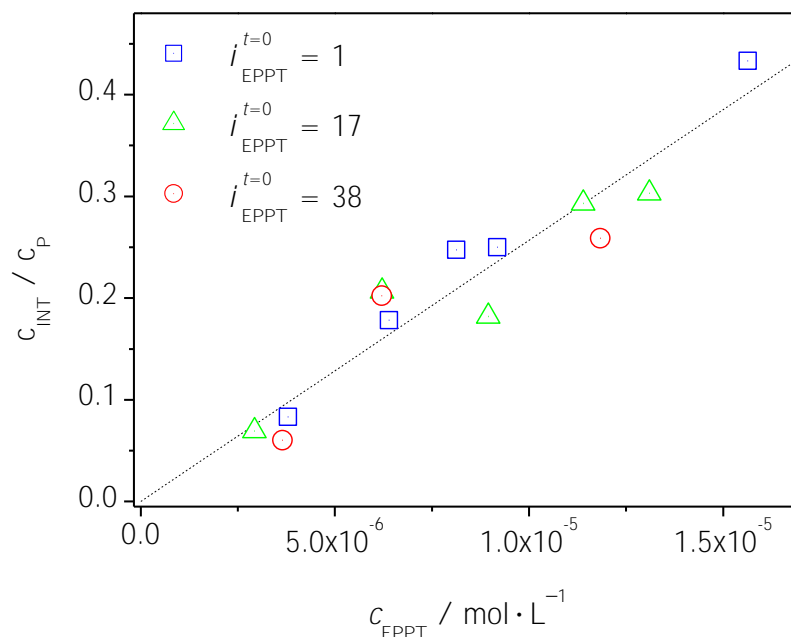


**Figure 4.8.** Ratio of intermediate radical and propagating radical concentrations,  $c_{\text{INT}}/c_{\text{P}}$ , plotted versus EPPT concentration for BA polymerizations ( $1.5 \text{ mol} \cdot \text{L}^{-1}$  in toluene) at  $-40 \text{ }^\circ\text{C}$  using MMMP ( $1.0 \times 10^{-2} \text{ mol} \cdot \text{L}^{-1}$ ) as the photoinitiator. The EPR experiments under stationary conditions were carried out with monomeric ( $i_{\text{EPPT}}^{t=0} = 1$ ) and macromolecular ( $i_{\text{EPPT}}^{t=0} = 17$ ,  $i_{\text{EPPT}}^{t=0} = 38$ ) RAFT agent. The slope of the straight-line fit yields the equilibrium constant,  $K_{\text{eq}} = (2.6 \pm 0.1) \times 10^4 \text{ L} \cdot \text{mol}^{-1}$ .

In comparison, the equilibrium constant of the previously studied BA polymerization mediated by BPT is  $(1.0 \pm 0.1) \times 10^4 \text{ L} \cdot \text{mol}^{-1}$ .<sup>[118]</sup> Apart from the leaving group, the trithiocarbonates BPT and EPPT possess the same structure. Under main-equilibrium conditions, macromolecular BPT and macromolecular EPPT are therefore identical and their equilibrium constants should be the same. However, BPT bears a benzyl leaving group instead of an acrylate-type leaving group, which is part of the same monomer family as the propagating radical. The resonance stabilization of the benzyl radical may enhance fragmentation and slow down addition, resulting in a lower equilibrium constant for the pre-equilibrium. The value of  $(1.0 \pm 0.1) \times 10^4 \text{ L} \cdot \text{mol}^{-1}$  obtained in the previous study thus refers to a combined pre- and main equilibrium constant.<sup>[118]</sup> Since it is not possible to separate both  $K_{\text{eq}}$  values, it is important to choose a RAFT agent with an adequate leaving group. One can conclude, that the equilibrium constant is different for the pre- and main equilibrium when the stability of the leaving group significantly differs from the one of the propagating radical. The chain-length dependence of RAFT agents bearing a leaving group which resembles

the propagating species cannot be excluded finally since the degree of polymerization is not well controlled when very low concentrations of the RAFT agent are used, as is the case in the present study. The samples which were subjected to SEC analysis after EPR measurements show very broad molecular mass distributions.

Thus, the kinetic studies presented here were obviously not carried out under conditions of good control. As the novel method, however, focuses on the determination of accurate rate coefficients, it is of primary importance that the concentrations of both the intermediate and propagating radicals are not too dissimilar and thus may precisely be determined by EPR. The so-obtained rate coefficients are physically reasonable quantities and thus, although being determined under conditions of poor control, should be well suited for estimating and designing polymerization conditions with excellent control by the particular RAFT agent.

The equilibrium constants for the trithiocarbonates are around 3 orders of magnitude above the one for the xanthate, which is probably due to faster addition to the trithiocarbonate and slower fragmentation of the resulting intermediate species. The equilibrium constant for BMPT is higher than for EPPT. This may be explained by a slightly slower fragmentation of the intermediate radical bearing three growing chains as compared to the one bearing only two growing chains. The 3-arm species is most likely more stable than the 2-arm radical. To check these assumptions, the individual rate coefficients,  $k_{ad}$  and  $k_{\beta}$ , are determined in Section 4.2.2.

To investigate the temperature dependence of  $K_{eq}$  the stationary EPR experiments for EPPT were additionally carried out at  $-20$ ,  $0$  and  $20$  °C. At a polymerization temperature of  $-40$  °C midchain radical (MCR) formation is negligible and the EPR spectra only show peaks resulting from the intermediate radical, INT, and the secondary propagating radical, SPR. At higher temperatures, midchain radicals can be observed by EPR spectroscopy. Figure 4.9 compares the spectra of a RAFT-free BA polymerization at  $0$  °C with the same polymerization in the presence of  $1.4 \times 10^{-3}$  mol · L<sup>-1</sup> EPPT. The characteristic peaks of the individual radical species are indicated by symbols. The EPR spectrum of the EPPT-mediated BA polymerization only differs from the RAFT-free system due to the occurrence of an additional EPR signal in the center of the spectrum, which belongs to the INT species. It seems that the addition of RAFT agent does not significantly alter the MCR/SPR ratio and  $K_{eq}$  may therefore be estimated from Equation 4.1:

$$\frac{c_{INT}}{(c_{SPR} + c_{MCR})} = K_{eq} \times c_{RAFT} \quad (4.1)$$

The  $c_{INT}/(c_{SPR}+c_{MCR})$  ratios were determined from the EPR spectra taken at different temperatures and the resulting equilibrium constants are listed in Table 4.3. The fraction of intermediate radicals and consequently the equilibrium constant sharply decreases with increasing temperature. The  $K_{eq}$  values at temperatures above  $-40$  °C

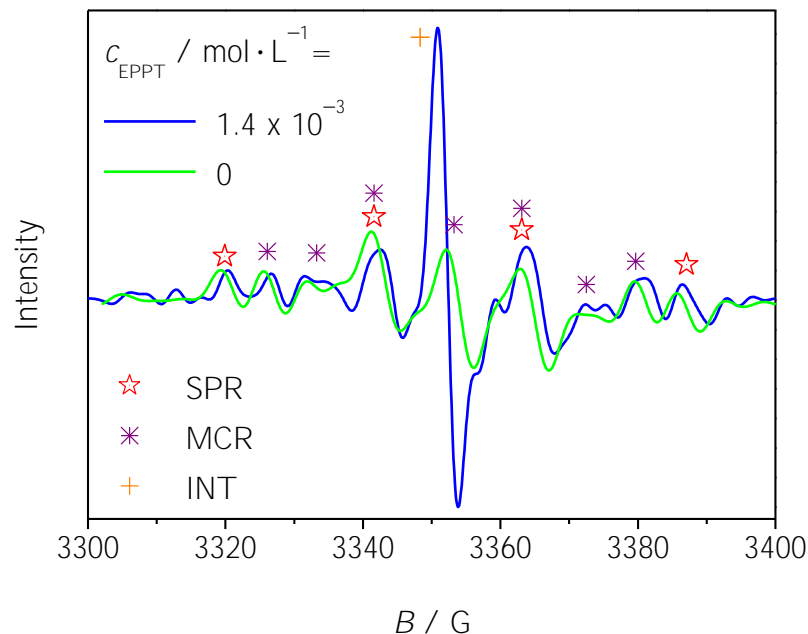


**Figure 4.9.** EPR spectra recorded during BA polymerization with and without EPPT at 0 °C. The symbols indicate the characteristic EPR signals of the secondary propagating radical, SPR, the midchain radical, MCR, and the intermediate radical, INT.

represent apparent equilibrium constants since both SPRs and MCRs take part in the addition-fragmentation equilibrium.

In Figure 4.10 the EPR-derived equilibrium constants are plotted in an Arrhenius form. The resulting slope of the straight-line fit yields an activation energy of  $E_a = -67 \text{ kJ} \cdot \text{mol}^{-1}$ . Since *ab initio* calculations predict an activation energy close to zero for the addition reaction,<sup>[38]</sup> the fragmentation reaction is associated with a high activation energy and fragmentation becomes faster at higher temperatures.

#### 4.2.2 Time-resolved EPR experiments

EPPT- and BMPT-mediated BA polymerizations at  $-40 \text{ °C}$  were investigated via the SP-PLP-EPR-RAFT approach. The intermediate and propagating radical concentrations,  $c_{\text{INT}}$  and  $c_{\text{P}}$ , were separately measured after single laser pulse initiation. In order to enhance signal-to-noise ratio, up to 10 INT and up to 20 P concentration-versus-time traces were co-added. The absolute concentration of the intermediate radical,  $c_{\text{INT}}$ , and the propagating radical,  $c_{\text{P}}$ , were determined via the three-step calibration procedure described in Section 7.3.2. The field positions used for monitoring the individual radical concentrations are indicated by the arrows in Figure 4.6.



**Table 4.3.** Equilibrium constants for EPPT-mediated BA polymerizations at temperatures between  $-20$  and  $20$  °C using  $1.4 \times 10^{-3}$  mol · L $^{-1}$  EPPT.

$T / \text{°C}$	$c_{\text{INT}}/(c_{\text{SPR}}+c_{\text{MCR}})$	$K_{\text{eq}} / \text{L} \cdot \text{mol}^{-1}$
20	$\approx 0$	$\approx 0$
0	0.23	165
-20	1.78	1270

The experimental INT and P traces during EPPT-mediated BA polymerization at  $-40$  °C, after initiation with a single laser pulse at  $t = 0$ , are shown in Figure 4.11. In comparison with the xanthate-containing polymerization, the INT lifetime is extended from 0.05 s to around 0.5 s. The concentration-versus-time profiles were fitted to the kinetic Scheme 8.1 given in Section 8.1, which has already been used for simulating the xanthate-mediated BA polymerization (see Section 4.1.2). To reduce the number of fitting parameters the same assumptions as in the xanthate case have been made, i. e.  $k_{\text{p}}^{\text{rein}} = k_{\text{p}}$ ,  $k_{\text{i}} = 10 \times k_{\text{p}}$ ,  $k_{\text{t}}^{\text{cross}}$  displays the same chain-length dependence as  $k_{\text{t}}^{i,i}$ , and  $k_{\text{ad}}$  and  $k_{\beta}$  are equal for the leaving group and the propagating radicals, respectively. The propagation rate coefficient,  $k_{\text{p}}$ ,<sup>[130]</sup> and the chain-length dependent termination rate coefficient,  $k_{\text{t}}^{i,i}$ ,<sup>[119]</sup> were taken from literature. The remaining rate coefficients, which need to be estimated by fitting the experimental data to the kinetic scheme, are the rate coefficients for addition,  $k_{\text{ad}}$ , fragmentation,  $k_{\beta}$ , and addition of an initiator-derived radical to the RAFT agent,  $k_{\text{ad}}^{\text{I}}$ , as well as the initial concentration of initiator radicals produced by the laser pulse,  $c_{\text{R}}^0$ .

Figure 4.11 compares the experimental and simulated time traces of the BA polymerization in the presence of EPPT. The influence of the cross-termination reaction between an intermediate species and a propagating radical is examined by varying the  $k_{\text{t}}^{\text{cross}}$  value between  $k_{\text{t}}^{\text{cross}} = 0$  and  $k_{\text{t}}^{\text{cross}} = k_{\text{t}}^{i,i}$ . Best fits for three different cross-termination coefficients are shown in Figure 4.11. The concentration of propagating radicals decreases more rapidly assuming a higher  $k_{\text{t}}^{\text{cross}}$ , which leads to a better fit of the experimental data at later stages of the polymerization. However, the variation of  $k_{\text{t}}^{\text{cross}}$  has only a negligibly small influence on the decay of the intermediate and propagating radical concentration.

The SP-PLP-EPR-RAFT approach yields the rate coefficients and equilibrium constants listed in Table 4.4. Addition and fragmentation are fast for all assumed  $k_{\text{t}}^{\text{cross}}$  values. The average numbers obtained are  $(3.4 \pm 0.3) \times 10^6$  L · mol $^{-1}$  · s $^{-1}$  for the addition rate coefficient,  $(1.4 \pm 0.4) \times 10^2$  s $^{-1}$  for the fragmentation rate coefficient,

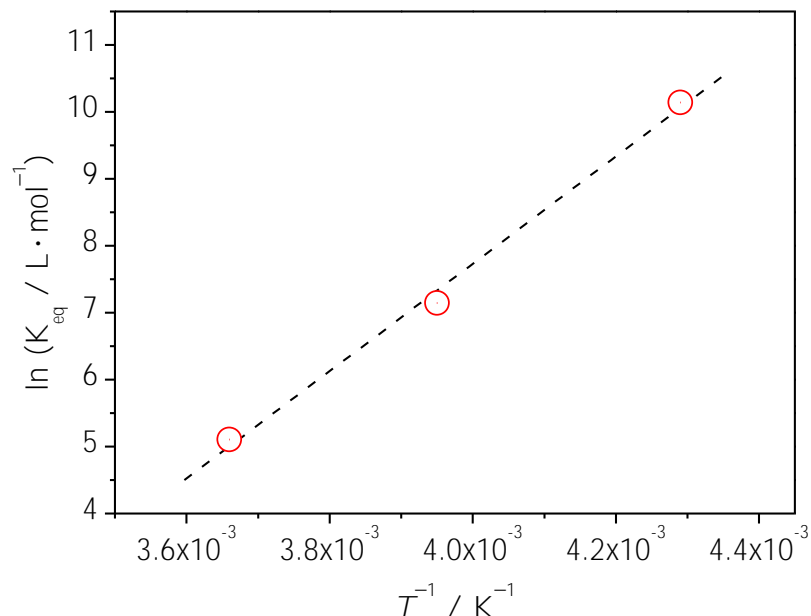


**Figure 4.10.** Arrhenius plot of the (apparent) equilibrium constants obtained in stationary EPPT-mediated BA polymerizations at  $-40$ ,  $-20$  and  $0$  °C. The slope of the straight-line fit yields an apparent activation energy of  $E_a = -(67 \pm 4) \text{ kJ} \cdot \text{mol}^{-1}$ .

and  $(2.6 \pm 0.8) \times 10^4 \text{ L} \cdot \text{mol}^{-1}$  for the equilibrium constant.

The experimental INT and P traces during BMPT-mediated BA polymerization at  $-40$  °C after initiation with a single laser pulse at  $t = 0$  are shown in Figure 4.12. The lifetime of the “3-arm” intermediate radical formed when BMPT is employed as the RAFT agent is 3 s, which is significantly longer than the lifetime of around 0.5 s in the case of the “2-arm” intermediate radical formed during EPPT-mediated polymerization (see Figure 4.11). Since the BMPT-derived intermediate radical bears three chains a three-dimensional (3D) treatment of the kinetic scheme is required, which is associated with extensive numerical effort. Therefore, the reactions involving a three-armed intermediate radical were translated into a one-dimensional problem. The derivation and implementation of the kinetic scheme into PREDICI<sup>®</sup> are detailed in Section 8.2. To reduce the number of fitting parameters, the same assumptions as in the EPPT-mediated polymerization were made and  $k_p$  and  $k_t^{i,i}$  taken from literature.<sup>[119,130]</sup>

Figure 4.12 compares the experimental and simulated time traces of the BA polymerization in the presence of BMPT. The influence of the cross-termination reaction between an intermediate species and a propagating radical is examined by varying

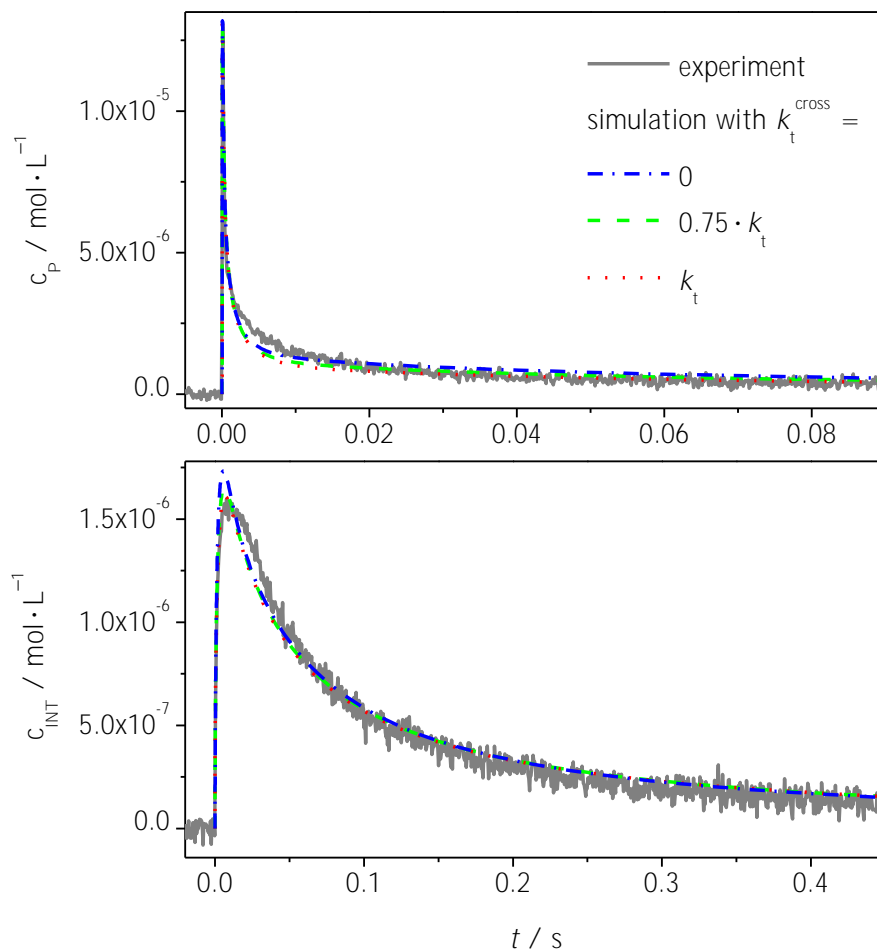


**Figure 4.11.** Comparison of simulated and experimental concentration-versus-time profiles for the propagating and the intermediate radical in BA polymerization ( $1.5 \text{ mol} \cdot \text{L}^{-1}$  in toluene) at  $-40 \text{ }^\circ\text{C}$  with EPPT being the RAFT agent ( $5.0 \times 10^{-5} \text{ mol} \cdot \text{L}^{-1}$ ) and MMMP the photoinitiator ( $1.0 \times 10^{-2} \text{ mol} \cdot \text{L}^{-1}$ ). The simulations were carried out assuming different values for the cross-termination coefficient,  $k_t^{\text{cross}}$ , which was assumed to be chain-length dependent.

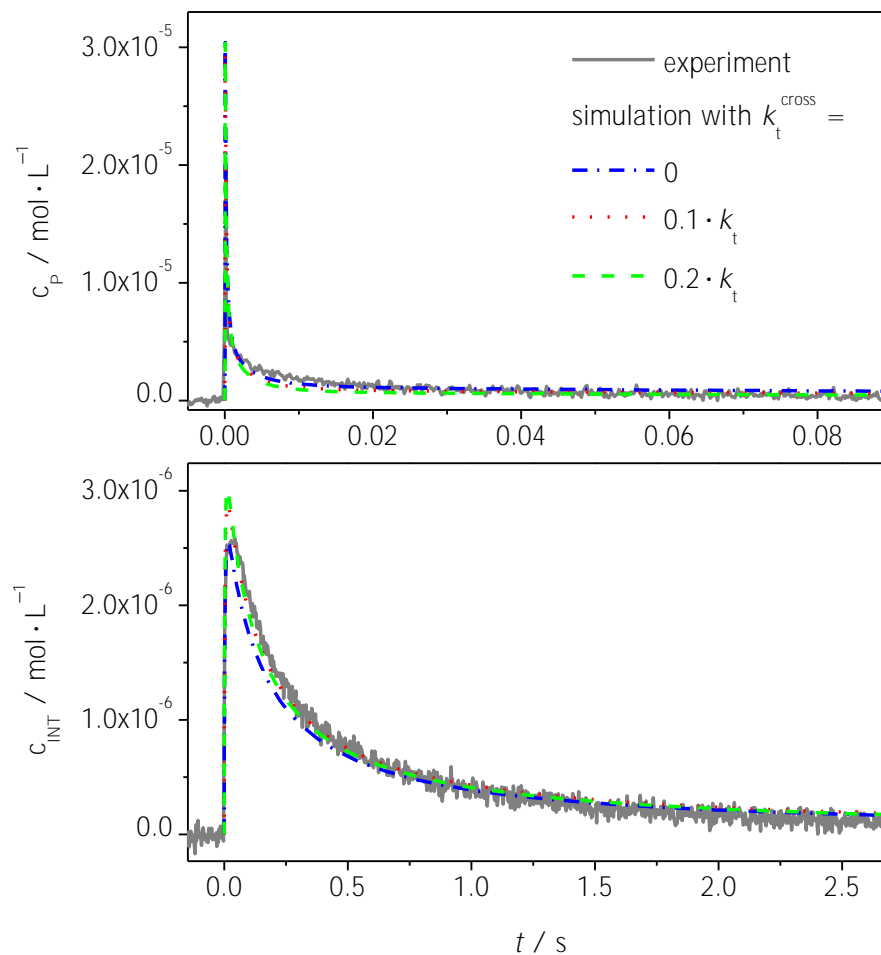


**Figure 4.12.** Comparison of simulated and experimental concentration-versus-time profiles for the propagating and the intermediate radical in BA polymerization ( $1.5 \text{ mol} \cdot \text{L}^{-1}$  in toluene) at  $-40 \text{ }^\circ\text{C}$  with BMPT being the RAFT agent ( $3.5 \times 10^{-5} \text{ mol} \cdot \text{L}^{-1}$ ) and MMMP the photoinitiator ( $1.0 \times 10^{-2} \text{ mol} \cdot \text{L}^{-1}$ ). The simulations were carried out assuming different values for the cross-termination coefficient,  $k_t^{\text{cross}}$ , which was assumed to be chain-length dependent.

**Table 4.4.** Rate coefficients and equilibrium constants for EPPT-mediated BA polymerization at  $-40\text{ }^{\circ}\text{C}$ . The following input parameters have been used in the fitting procedure:  $k_p = 2.27 \times 10^3\text{ L} \cdot \text{mol}^{-1} \cdot \text{s}^{-1}$ ,  $k_i = 2.27 \times 10^4\text{ L} \cdot \text{mol}^{-1} \cdot \text{s}^{-1}$ ,  $k_t^{1,1} = 1.65 \times 10^8\text{ L} \cdot \text{mol}^{-1} \cdot \text{s}^{-1}$ ,  $\alpha_s = 0.85$ ,  $\alpha_l = 0.22$ ,  $i_c = 30$ . The best fit was achieved using primary radical concentrations of  $c_R^0 = 2.0 \times 10^{-5}\text{ mol} \cdot \text{L}^{-1}$ .

$k_t^{\text{cross}} / k_t^{i,i}$	$k_{\text{ad}}^{\text{I}} / \text{L} \cdot \text{mol}^{-1} \cdot \text{s}^{-1}$	$k_{\text{ad}} / \text{L} \cdot \text{mol}^{-1} \cdot \text{s}^{-1}$	$k_{\beta} / \text{s}^{-1}$	$K_{\text{eq}} / \text{L} \cdot \text{mol}^{-1}$
0	$1.70 \times 10^6$	$3.16 \times 10^6$	$1.74 \times 10^2$	$1.82 \times 10^4$
0.75	$5.99 \times 10^6$	$3.60 \times 10^6$	$1.28 \times 10^2$	$2.82 \times 10^4$
1	$9.38 \times 10^6$	$3.58 \times 10^6$	$1.13 \times 10^2$	$3.17 \times 10^4$

the  $k_t^{\text{cross}}$  value between  $k_t^{\text{cross}} = 0$  and  $k_t^{\text{cross}} = 0.5 \times k_t^{i,i}$ . Good fits are obtained for  $k_t^{\text{cross}}$  values between 0 and  $0.2 \times k_t^{i,i}$ . For  $k_t^{\text{cross}} > 0.2 \times k_t^{i,i}$  the INT trace can be fitted well but the decay of the propagating radical becomes faster than observed in the experiment. There is probably less cross-termination with three-armed INTs than with two-armed INTs due to sterical hindrance.

The resulting parameters are listed in Table 4.5. The average numbers obtained are  $(4.1 \pm 0.9) \times 10^6\text{ L} \cdot \text{mol}^{-1} \cdot \text{s}^{-1}$  for the addition rate coefficient,  $(45 \pm 5)\text{ s}^{-1}$  for the fragmentation rate coefficient, and  $(9 \pm 3) \times 10^4\text{ L} \cdot \text{mol}^{-1}$  for the equilibrium constant. Whereas the addition of a growing chain to BMPT is similarly fast as the addition to EPPT, fragmentation is slower. This is reasonable as the radical is delocalized over three sulfur atoms instead of two. The resulting equilibrium constant is therefore higher for the BMPT polymerization.

### 4.2.3 Comparison of both approaches

For EPPT-mediated BA polymerization at  $-40\text{ }^{\circ}\text{C}$  the equilibrium constant obtained via the stationary approach,  $K_{\text{eq}} = (2.6 \pm 0.1) \times 10^4\text{ L} \cdot \text{mol}^{-1}$ , is in excellent agreement with the one obtained with the SP-PLP-EPR-RAFT method,  $K_{\text{eq}} = (2.6 \pm 0.8) \times 10^4\text{ L} \cdot \text{mol}^{-1}$ . For BMPT the corresponding values are  $K_{\text{eq}} = (7.0 \pm 0.2) \times 10^4\text{ L} \cdot \text{mol}^{-1}$  and  $K_{\text{eq}} = (9 \pm 3) \times 10^4\text{ L} \cdot \text{mol}^{-1}$ , respectively. The kinetic scheme used for PREDICI<sup>®</sup> simulations is therefore appropriate to describe the BA polymerization mediated by these trithiocarbonates.

The rate coefficients deduced from the single-pulse approach can be used to check whether the reaction conditions of the stationary experiments were adequate for estimating  $K_{\text{eq}}$  via Equation 3.3. An assumption made is that the rate of cross-

**Table 4.5.** Rate coefficients and equilibrium constants for BMPT-mediated BA polymerization at  $-40$  °C. The following input parameters have been used in the fitting procedure:  $k_p = 2.27 \times 10^3 \text{ L} \cdot \text{mol}^{-1} \cdot \text{s}^{-1}$ ,  $k_i = 2.27 \times 10^4 \text{ L} \cdot \text{mol}^{-1} \cdot \text{s}^{-1}$ ,  $k_t^{1,1} = 1.65 \times 10^8 \text{ L} \cdot \text{mol}^{-1} \cdot \text{s}^{-1}$ ,  $\alpha_s = 0.85$ ,  $\alpha_1 = 0.22$ ,  $i_c = 30$ . The best fit was achieved using primary radical concentrations of  $c_R^0 = 7.1 \times 10^{-5} \text{ mol} \cdot \text{L}^{-1}$  and  $k_{ad}^1$  values of  $3.0 \times 10^6 \text{ L} \cdot \text{mol}^{-1} \cdot \text{s}^{-1}$ .

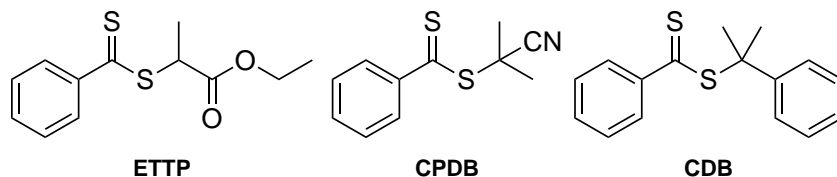
$k_t^{\text{cross}} / k_t^{i,i}$	$k_{ad} / \text{L} \cdot \text{mol}^{-1} \cdot \text{s}^{-1}$	$k_\beta / \text{s}^{-1}$	$K_{eq} / \text{L} \cdot \text{mol}^{-1}$
0	$3.15 \times 10^6$	50	$6.3 \times 10^4$
0.1	$4.23 \times 10^6$	45	$9.4 \times 10^4$
0.2	$4.98 \times 10^6$	41	$1.2 \times 10^5$
0.5	$5.50 \times 10^6$	25	$2.2 \times 10^5$

termination,  $r_t^{\text{cross}}$ , is negligibly small as compared to the addition and fragmentation rates,  $r_{ad}$  and  $r_\beta$ . These rates are therefore calculated. The absolute concentrations of INT and P are known from the EPR spectra. The maximum value of  $r_t^{\text{cross}}$  was estimated by implementing  $k_t^{\text{cross}} = k_t^{1,1}$ , which refers to the upper limit of termination taking place between a propagating and an intermediate radical, both of chain length unity. In order to consider the worst case scenario also for addition and fragmentation, both rates were estimated for the lowest EPPT and BMPT concentrations used ( $5 \times 10^{-6} \text{ mol} \cdot \text{L}^{-1}$ ). Even under these conditions,  $r_t^{\text{cross}}$  values are below  $r_{ad}$  and  $r_\beta$ , thus verifying the validity of using Equation 3.3 in the chosen EPPT and BMPT concentration range.

### 4.3 Dithiobenzoate-mediated *n*-butyl acrylate polymerization

The EPR methods developed and tested on xanthate- and trithiocarbonate-mediated polymerizations are now extended to dithiobenzoates.<sup>[132]</sup> The investigation of the mechanism of dithiobenzoate-mediated polymerizations is of particular interest as rate retardation is observed with some monomers, like styrene and acrylates, but not with methacrylates.

For evaluation of rate retardation, polymerization rate-versus-time behavior of BA bulk polymerizations was studied with cumyl dithiobenzoate (CDB), 2-(2'-cyanopropyl)-dithiobenzoate (CPDB), and ethyl *S*-thiobenzoyl-2-thiopropionate (ETTP) as RAFT agents (see Scheme 4.4). Under main-equilibrium conditions, the resonance-stabilized INT species of these RAFT agents are of identical structure (see Scheme



**Scheme 4.4.** RAFT agents under investigation: ethyl *S*-thiobenzoyl-2-thiopropionate (ETTP), 2-(2'-cyanopropyl)-dithiobenzoate (CPDB) and cumyl dithiobenzoate (CDB).

8.2 in Section 8.1). Figure 4.13 shows that pronounced rate retardation is observed with all of the three RAFT agents.

CDB-mediated polymerization at higher RAFT agent concentration exhibits an extended induction period, which is assigned to resonance stabilization of the cumyl radical. This effect is considerably larger than in case of ethyl acrylate and cyano-*iso*-propyl radicals, which are released from the primary intermediate radical species with ETTP and CPDB, respectively. The cumyl radical is less active in reinitiating polymerization. With CDB, the addition of a cumyl radical to BA, under otherwise identical conditions, is by about a factor of 700 slower than the addition of a BA radical to BA (i. e., in homo-propagation).<sup>[133,134]</sup> This factor reduces to about 10 for addition of the cyano-*iso*-propyl radical to BA and is smaller than unity in the case of addition of the ethyl acrylate radical to BA.<sup>[130,131,135]</sup> The rate coefficient for addition of the first monomer unit is expected to be well above  $k_p$  for subsequent propagation steps of larger growing radicals.<sup>[136]</sup>

No pre-equilibrium situation is observed in systems where the leaving radical moiety is of similar structure as the propagating radicals, as is the case with ETTP/BA. For CPDB where the leaving group is identical to the initiator fragments from AIBN, inhibition may be interpreted as a decrease in initiator efficiency, since reinitiation by the leaving group does not occur quantitatively until the initial RAFT agent is converted to propagating chain adducts. This effect is more pronounced at higher RAFT agent concentration due to the higher amount of leaving/inhibiting groups. In case of ETTP, reinitiation efficiency of the ethyl acrylate radicals is supposed to be much higher than for AIBN. As a consequence, no inhibition occurs. For CDB and CPDB, this interpretation is in full agreement with the current understanding of the initialization period as put forward by the Klumperman group: The rate-determining step in the initial stage of RAFT polymerization is the addition of the leaving radical moiety to a monomer molecule, unless the leaving group exhibits higher reactivity than the radical fragments from initiator decomposition (see Section 2.3).<sup>[80–84]</sup>

As soon as the initial RAFT agent has been completely transformed into macromolecular RAFT species, main-equilibrium conditions apply and the same polymerization rates are observed for the three RAFT agents (Figure 4.13). This comes as no surprise,

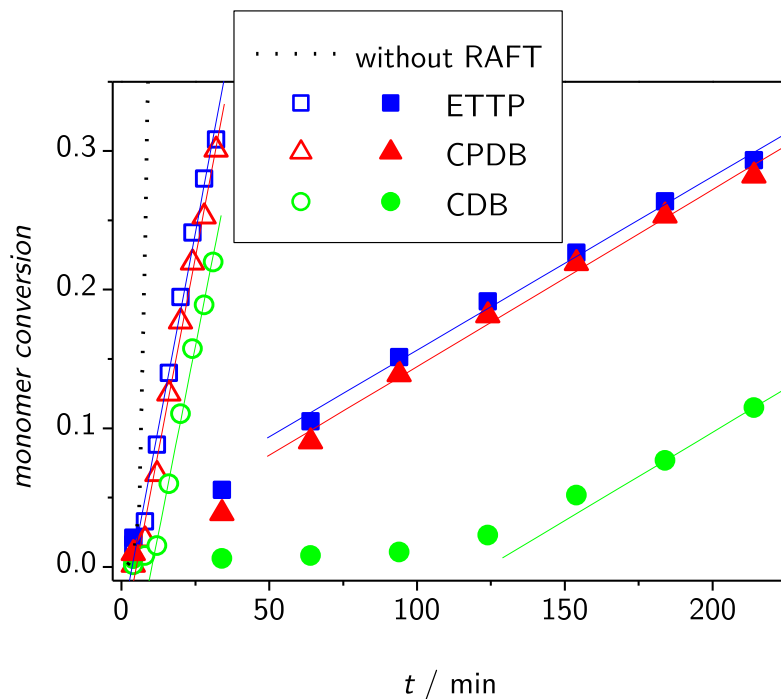


**Figure 4.13.** Induction period and rate retardation observed for BA bulk polymerizations at 70 °C mediated by ETTP, CPDB, CDB and without RAFT agent using AIBN ( $1.5 \times 10^{-3} \text{ mol} \cdot \text{L}^{-1}$ ) as the initiator. Open symbols:  $c_{\text{RAFT}} = 1.5 \times 10^{-3} \text{ mol} \cdot \text{L}^{-1}$ ; closed symbols:  $c_{\text{RAFT}} = 2.0 \times 10^{-2} \text{ mol} \cdot \text{L}^{-1}$ .

as the identical type of intermediate radical occurs under main-equilibrium conditions with CDB, CPDB, and ETTP (see Scheme 8.2). Polymerization rates are given by the slope of the straight-line fits under stationary reaction conditions. They are below the polymerization rate in the absence of RAFT agent ( $R_p = 1.4 \times 10^{-2} \text{ mol} \cdot \text{L}^{-1} \cdot \text{s}^{-1}$ ) by a factor of 10 at  $c_{\text{RAFT}} = 1.5 \times 10^{-3} \text{ mol} \cdot \text{L}^{-1}$  ( $R_p = 1.3 \times 10^{-3} \text{ mol} \cdot \text{L}^{-1} \cdot \text{s}^{-1}$ ) and by a factor of 100 at  $c_{\text{RAFT}} = 2.0 \times 10^{-2} \text{ mol} \cdot \text{L}^{-1}$  ( $R_p = 1.5 \times 10^{-4} \text{ mol} \cdot \text{L}^{-1} \cdot \text{s}^{-1}$ ).

As detailed in Section 2.3.1, the equilibrium constant may be deduced from Equations 2.2 and 2.3 proposed by Kwak *et al.*<sup>[50,90]</sup> Assuming that cross-termination between the intermediate species and propagating radicals is the main cause for the observed rate retardation, the experimental data may be plotted as  $R_p^{-2}$  versus  $c_{\text{RAFT}}^0$  (see Figure 4.14a). The slope of the straight line,  $2k_t^{\text{cross}}/k_t(R_p^0)^{-2}K_{\text{eq}}$ , is a measure for retardation. Adopting  $k_t^{\text{cross}}/k_t = 0.5$  yields an equilibrium constant of  $(4.8 \pm 0.2) \times 10^5 \text{ L} \cdot \text{mol}^{-1}$  for the dithiobenzoate-mediated BA bulk poly-



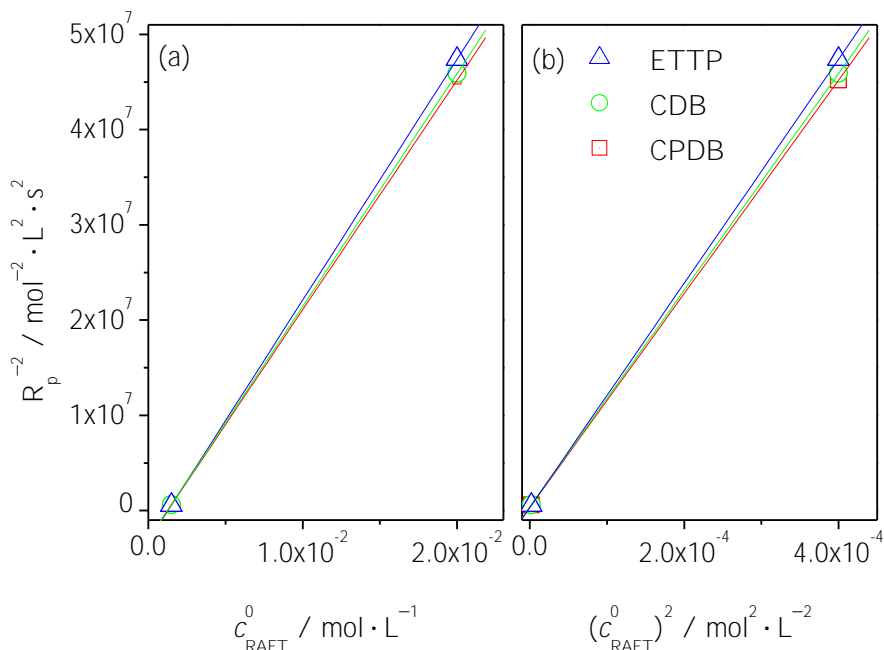


**Figure 4.14.** (a) Plot of  $R_p^{-2}$  versus  $c_{\text{RAFT}}^0$  and (b) plot of  $R_p^{-2}$  versus  $(c_{\text{RAFT}}^0)^2$  for ETTP-, CPDB- and CDB-mediated BA bulk polymerizations at 70 °C using AIBN ( $1.5 \times 10^{-3} \text{ mol} \cdot \text{L}^{-1}$ ) as the initiator.

merization at 70 °C. When the rate retardation is exclusively assigned to self-termination between two intermediate radicals, plotting  $R_p^{-2}$  versus  $(c_{\text{RAFT}}^0)^2$  results in a slope of  $k_t^{\text{self}}/k_t(R_p^0)^{-2}K_{\text{eq}}$  (see Figure 4.14b). An equilibrium constant of  $(9.5 \pm 0.2) \times 10^3 \text{ L} \cdot \text{mol}^{-1}$  is obtained, assuming  $k_t^{\text{self}}/k_t = 0.5$ . The difference in  $K_{\text{eq}}$  values of more than one order of magnitude shows that this method strongly depends on the assumptions made. Since only two different RAFT agent concentrations were studied, it cannot be decided whether cross- or self-termination is the main cause for rate retardation in these polymerizations. The  $K_{\text{eq}}$  values determined via the method described by Kwak *et al.*<sup>[50]</sup> will be compared to the EPR-derived values in the following section.

Because of the close similarity of polymerization rates under main-equilibrium conditions as indicated by Figure 4.13, EPR experiments were carried out for ETTP. This RAFT agent exhibits no induction period and is far more stable toward UV and laser irradiation than are CDB and CPDB. The decay of ETTP concentration due to broad-band UV irradiation occurs by less than 1 % within 1.3 s, which is the typical irradiation time chosen for the quasi-stationary EPR experiments with this dithiobenzoate. No decomposition of the RAFT agent however occurs even by

applying 10 laser pulses at 351 nm. To carry out the experiment, only one laser pulse is required. Since ETTP bears an acrylate leaving group, the number of rate coefficients to be fitted by PREDICI<sup>®</sup> simulations of an acrylate polymerization is lower than, e. g., in CDB-mediated BA polymerization.<sup>[122]</sup>

A reaction temperature of  $-40\text{ }^{\circ}\text{C}$  was chosen not only to avoid midchain radical formation but also to test slow-fragmentation behavior. Since a significant activation energy is expected for  $k_{\beta}$ , the intermediate radical should be extremely long-lived at  $-40\text{ }^{\circ}\text{C}$  in the case of slow fragmentation.<sup>[38]</sup>

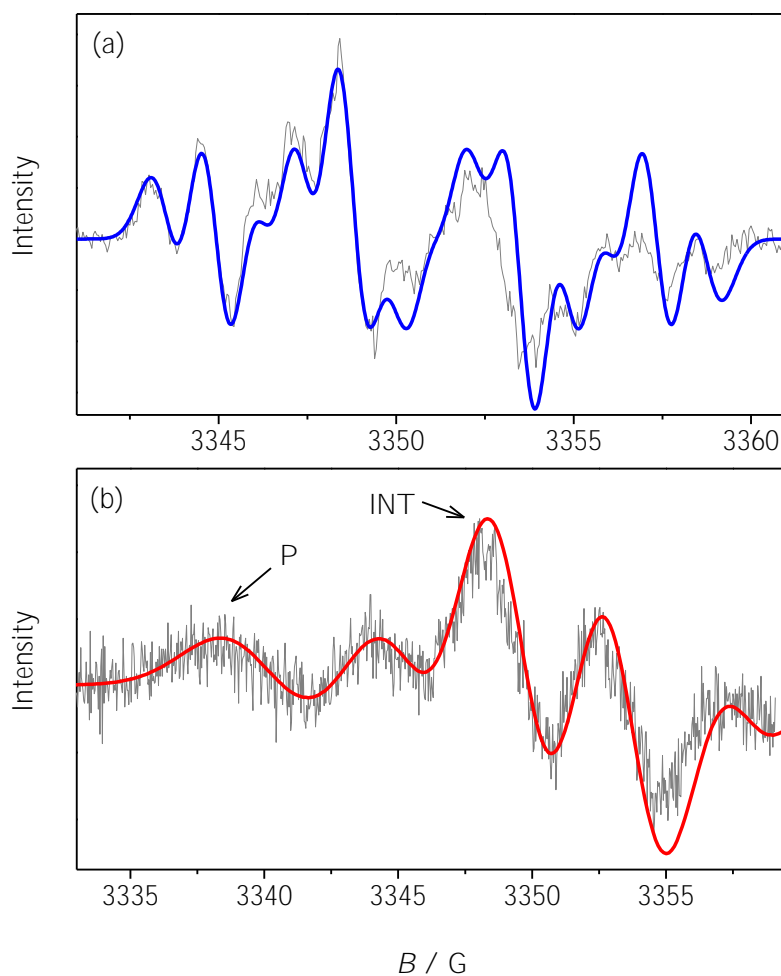
### 4.3.1 Quasi-stationary EPR experiments

Presented in Figure 4.15a is the EPR spectrum of the intermediate radical recorded during an ETTP-mediated BA polymerization at  $-40\text{ }^{\circ}\text{C}$  under laser pulsing at a repetition rate of 20 Hz. The essential features of the experimental spectrum are adequately represented by the simulated EPR curve (dashed line). Delocalization of the radical functionality over the phenyl ring is indicated by the hyperfine splitting pattern already reported for styrene and for acrylate polymerizations mediated by dithiobenzoates.<sup>[50,54,56,57,137]</sup> The EPR spectrum in Figure 4.15b has been recorded under continuous UV initiation under otherwise identical conditions.

From the EPR signals of intermediate and propagating radicals recorded during a single fast scan (Figure 4.15b), the equilibrium constant,  $K_{\text{eq}}$ , may be estimated via Equation 3.3. Because of the shorter sweep time, the spectrum is noisier than the one in Figure 4.15a. EPR spectra as in Figure 4.15b were taken at different ETTP concentrations. The measured  $c_{\text{INT}}/c_{\text{P}}$  ratios obtained by deconvolution of the EPR spectra are plotted versus ETTP concentration in Figure 4.16. The deconvolution procedure is detailed in Section 7.3.3. The coupling constants of the intermediate and propagating radical are listed in Table 4.6 of this section and in Table 4.1 of Section 4.1, respectively.

According to Equation 3.3 the slope of the straight line passing through the origin yields  $K_{\text{eq}} = (2.3 \pm 0.6) \times 10^5\text{ L} \cdot \text{mol}^{-1}$ . The accuracy of  $K_{\text{eq}}$  is essentially determined by the error associated with measuring  $c_{\text{INT}}/c_{\text{P}}$  and depends on the validity of Equation 3.3 under the specific experimental conditions. That Equation 3.3 is indeed applicable will be demonstrated further below. The observed  $K_{\text{eq}}$  value is by about 1 order of magnitude above the one found for BA polymerization mediated by trithiocarbonates (see Section 4.2) and is by 4 orders of magnitude above  $K_{\text{eq}}$  for BA polymerized under xanthate control (see Section 4.1).

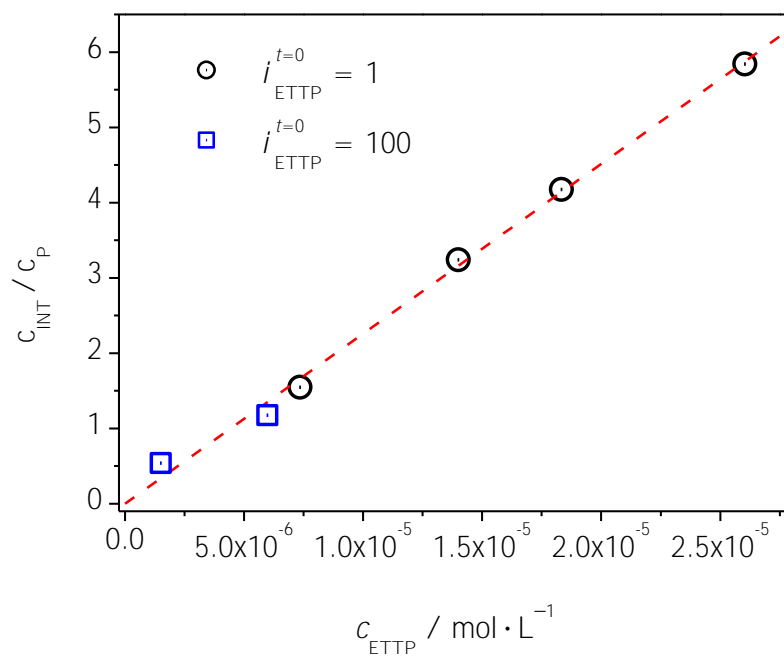
Product samples were analyzed via size-exclusion chromatography. The number averages of molar mass,  $\overline{M}_n > 700\text{ g} \cdot \text{mol}^{-1}$ , are indicative of main-equilibrium conditions. The  $\overline{M}_n$  values decrease toward higher ETTP concentration. If  $K_{\text{eq}}$  would be clearly different for pre-equilibrium and main-equilibrium conditions, the  $c_{\text{INT}}/c_{\text{P}}$  versus  $c_{\text{RAFT}}$  correlation should be nonlinear. This is, however, not what



**Figure 4.15.** EPR spectrum of the intermediate radical recorded during an ETTP-mediated polymerization of BA with MMMP as the photoinitiator at  $-40\text{ }^{\circ}\text{C}$ . (a) Pseudo-stationary conditions apply with laser pulsing at a repetition rate of 20 Hz; modulation amplitude: 3 G, microwave power: 10 mW,  $c_{\text{ETTP}} = 5 \times 10^{-4}\text{ mol} \cdot \text{L}^{-1}$ . Simulated spectrum:  $a/G = 1.3$  (2H, *meta*); 3.9 (2H, *ortho*); 4.7 (1H, *para*). (b) EPR spectrum recorded in a 1.3 s field sweep during a stationary BA polymerization ( $c_{\text{ETTP}} = 2 \times 10^{-5}\text{ mol} \cdot \text{L}^{-1}$ ) with continuous UV initiation under otherwise identical experimental conditions. The dashed line indicates the best fit of overall EPR contour by summation of the individually simulated EPR spectra for INT and P. Because of lower ETTP concentration, the P component is more pronounced in (b). The field positions for monitoring INT and P individually as a function of time after laser initiation are indicated by the arrows.

**Table 4.6.** Coupling constants deduced from the experimental spectra of INT at  $-40\text{ }^\circ\text{C}$ .

coupling constants / G		
$a_{\text{H},meta}$	$a_{\text{H},ortho}$	$a_{\text{H},para}$
1.3	3.9	4.7

**Figure 4.16.** Ratio of intermediate radical and propagating radical concentrations,  $c_{\text{INT}}/c_{\text{P}}$ , plotted versus ETTP concentration for BA polymerizations ( $1.5\text{ mol} \cdot \text{L}^{-1}$  in toluene) at  $-40\text{ }^\circ\text{C}$ ; photoinitiator: MMMP ( $1.0 \times 10^{-2}\text{ mol} \cdot \text{L}^{-1}$ ). The slope of the straight-line fit yields the equilibrium constant,  $K_{\text{eq}}$ . Stationary experiments were carried out with monomeric ( $i_{\text{ETTP}}^{t=0} = 1$ ) and macromolecular ( $i_{\text{ETTP}}^{t=0} = 100$ ) RAFT agent.

the experimental data indicate. No clear chain-length dependence is observed, which may be due to the fact that the radical which fragments from the addition product of a radical to ETTP is very similar to the growing (secondary) radical of BA polymerization at low temperature. This is not to say that the very first steps of addition and fragmentation are independent of chain length. The experiment is however not sufficiently sensitive to investigate such a dependence under pre-equilibrium conditions.

As in the case of the trithiocarbonate EPPT, the stationary EPR experiments were additionally carried out with a pre-polymerized dithiobenzoate. An initial chain-length of  $i = 100$  was chosen to cover a broad chain-length range. The measured  $c_{\text{INT}}/c_{\text{P}}$  ratios for the macromolecular RAFT agent are plotted together with the monomeric RAFT in Figure 4.16. The resulting equilibrium constant, does not vary with initial chain length, which is a further indication for the chain-length independence of  $K_{\text{eq}}$ .

As mentioned above, the determination of  $K_{\text{eq}}$  for BA polymerizations at elevated temperatures is complicated due to the occurrence of midchain radicals. However, an apparent equilibrium constant may be obtained at elevated temperatures, e. g., at 70 °C, by determination of  $c_{\text{INT}}$  and  $c_{\text{P}}$  from two independent experiments: The concentration of secondary propagating radicals,  $c_{\text{P}}$ , has been determined from the measured rate of polymerization and the known  $k_{\text{p}}$  value of these radical species,<sup>[130,138]</sup> as detailed by Kwak *et al.*<sup>[50]</sup> The resulting value is  $(5.2 \pm 0.5) \times 10^{-10} \text{ mol} \cdot \text{L}^{-1}$  for BA polymerization carried out at a RAFT agent concentration of  $c_{\text{RAFT}} = 2.0 \times 10^{-2} \text{ mol} \cdot \text{L}^{-1}$ . In addition, EPR spectra were taken during ETTP-mediated BA polymerization at 70 °C. The INT concentration is determined by double integration of the associated EPR component to be  $(3.9 \pm 0.4) \times 10^{-8} \text{ mol} \cdot \text{L}^{-1}$ . The resulting equilibrium constant is  $(75 \pm 15) \text{ L} \cdot \text{mol}^{-1}$ . It has to be mentioned that this value is an apparent one as MCRs and SPRs are present at 70 °C, whereas only SPRs occur at -40 °C. Due to the low concentration of growing radicals the exact SPR to MCR ratio has not been determined. This ratio may be lower than in the case of free-radical polymerization because Ahmad *et al.*<sup>[139]</sup> showed that controlled radical polymerizations give rise to lower levels of branching. In contrast, no difference in MCR/SPR ratio was observed between the trithiocarbonate-mediated and conventional BA polymerization (see Figure 4.9).

Nevertheless, the apparent value is close to  $K_{\text{eq}} = 55 \text{ L} \cdot \text{mol}^{-1}$  as reported by Kwak *et al.* for polystyryl dithiobenzoate-mediated styrene polymerization at 60 °C.<sup>[50]</sup> From the  $K_{\text{eq}}$  values for BA polymerization at -40 °C and at 70 °C, the difference in activation energies,  $E_{\text{a}}(K_{\text{eq}}) = E_{\text{a}}(k_{\text{ad}}) - E_{\text{a}}(k_{\beta}) = -49.5 \text{ kJ} \cdot \text{mol}^{-1}$ , is found.

The EPR-derived equilibrium constant ( $75 \text{ L} \cdot \text{mol}^{-1}$ ) is about two to four orders of magnitude below the  $K_{\text{eq}}$  values determined via Equations 2.2 and 2.3 ( $4.8 \times 10^5 \text{ L} \cdot \text{mol}^{-1}$  and  $9.5 \times 10^3 \text{ L} \cdot \text{mol}^{-1}$ , respectively). The discrepancy is probably due

to the fact that rate retardation is overestimated by the equations of Kwak *et al.*,<sup>[50]</sup> since a decrease in polymerization rate at higher RAFT agent concentrations is, at least partly, due to the chain-length dependence of the termination rate coefficient,  $k_t$ .<sup>[88]</sup> In addition, the equations were derived for only one type of propagating radical taking part in the equilibrium. However, at 70 °C SPRs and MCRs are present during polymerization and secondary and tertiary radicals probably differ significantly in their cross-termination reactivities. Equations 2.2 and 2.3 are therefore not suitable for a reliable determination of the equilibrium constant.

### 4.3.2 Time-resolved EPR experiments

Without further assumptions, the rate coefficients for addition,  $k_{ad}$ , and fragmentation,  $k_{\beta}$ , are not accessible from  $K_{eq}$ . These individual rate coefficients may, however, be deduced by measuring the concentrations of both intermediate and propagating radicals,  $c_{INT}$  and  $c_P$ , via microsecond time-resolved EPR spectroscopy after laser single pulse initiation and subsequent fitting of the experimental time traces to a kinetic scheme via PREDICI<sup>®</sup>. In Figure 4.17, the measured time evolutions of INT and P concentrations after applying the laser pulse at  $t = 0$  are shown.

In spite of resonance stabilization of radical functionality over the phenyl ring and the low temperature of  $-40$  °C, the RAFT intermediate radical decays on the time scale of a few seconds, signifying that INT is a relatively short-lived species. This observation makes slow fragmentation a very unlikely explanation for retardation in dithiobenzoate-mediated polymerization because this model predicts a half-life of more than 10 s at 60 °C, which would result in a half-life of hours at  $-40$  °C.<sup>[42]</sup> Quantitative evidence is provided by subjecting the experimental radical concentration-versus-time profiles to parameter estimation via the program package PREDICI<sup>®</sup>. The kinetic scheme, which encompasses initiation, propagation, chain-length-dependent termination, the individual RAFT pre-equilibrium and main-equilibrium reaction steps, and chain-length-dependent cross-termination of the intermediate radical, is detailed in Section 8.1. It is assumed that, due to chemical similarity of the leaving group of the reaction product from addition of the RAFT agent to the propagating BA radical, the addition and the fragmentation rate coefficients of the ETTP-derived radical should be very similar to the associated rate coefficients of growing BA radicals. Moreover, the leaving group is assumed to add to a monomer molecule, and thus reinitiate, at the same rate as the propagating radical, i. e.,  $k_p^{rein} = k_p$ . The propagation rate coefficient,  $k_p$ , and the chain-length-dependent termination rate coefficient,  $k_t^{i,i}$ , are known from the literature.<sup>[130,140,141]</sup> The initiation rate coefficient,  $k_i$ , was assumed to be by 1 order of magnitude above the propagation rate coefficient:  $k_i = 10 \times k_p$ .

The primary free-radical concentration,  $c_R^0$ , which is almost instantaneously produced by absorption of the laser pulse, is identified with the concentration of initiator

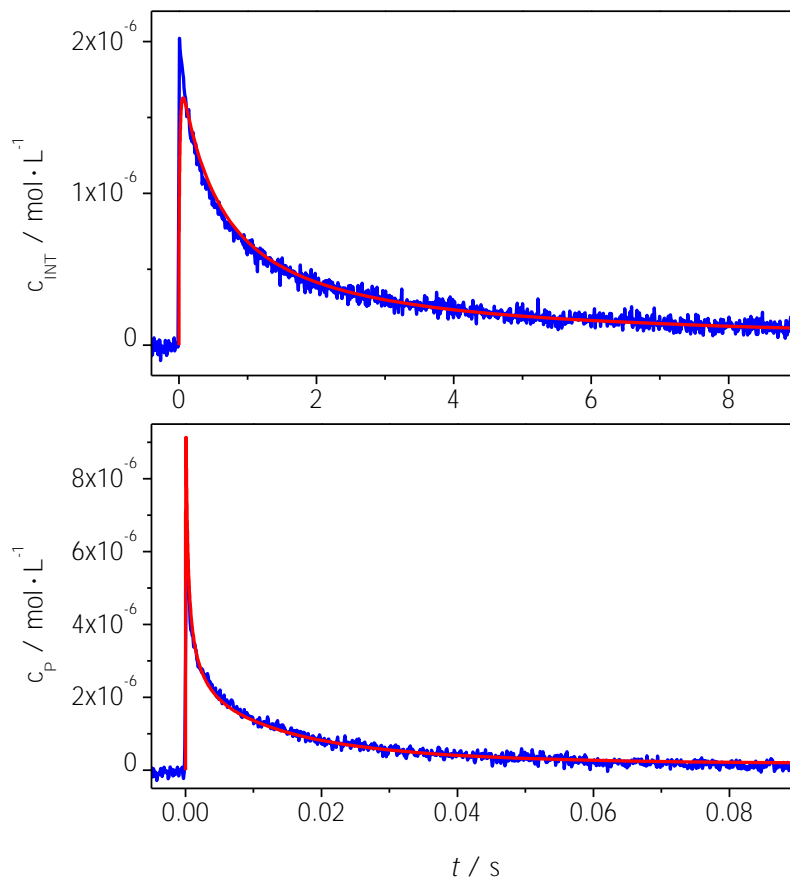


**Figure 4.17.** Simulated and experimental concentration-versus-time traces for propagating and intermediate radicals during BA polymerization ( $1.5 \text{ mol} \cdot \text{L}^{-1}$  in toluene) at  $-40 \text{ }^\circ\text{C}$ . The initial ETTP and MMMP concentrations were  $2.0 \times 10^{-5}$  and  $1.0 \times 10^{-2} \text{ mol} \cdot \text{L}^{-1}$ , respectively. The input parameters for PREDICI<sup>®</sup> simulation were  $k_p = 2.27 \times 10^3 \text{ L} \cdot \text{mol}^{-1} \cdot \text{s}^{-1}$ ,  $k_i = 2.27 \times 10^4 \text{ L} \cdot \text{mol}^{-1} \cdot \text{s}^{-1}$ ,  $c_R^0 = 1.30 \times 10^{-5} \text{ mol} \cdot \text{L}^{-1}$ ,  $k_t^{1,1} = 1.65 \times 10^8 \text{ L} \cdot \text{mol}^{-1} \cdot \text{s}^{-1}$ ,  $\alpha_s = 0.85$ ,  $\alpha_1 = 0.22$ ,  $i_c = 30$ , and  $k_t^{\text{cross}} = 0.25 \times k_t^{i,i}$ .

fragments at  $t = 0$ . The  $c_{\text{R}}^0$  value has to be varied within the simulation procedure to fit the maxima of experimental  $c_{\text{INT}}$  and  $c_{\text{P}}$  traces. The final choice of the parameters  $c_{\text{R}}^0$ ,  $k_{\text{ad}}^{\text{I}}$  and  $k_{\text{i}}$ , however, does not affect the results for the fitted parameters  $k_{\text{ad}}$  and  $k_{\beta}$ , as the impact of the reactions associated with  $c_{\text{R}}^0$ ,  $k_{\text{i}}$  and  $k_{\text{ad}}^{\text{I}}$  is essentially restricted to the increasing part of the experimental concentration-versus-time traces.

So far, no reliable number is available for the cross-termination rate coefficient. Kwak *et al.* estimated  $k_{\text{t}}^{\text{cross}}$  to be around  $0.5 \times k_{\text{t}}$ , thus allowing for rapid cross-termination between radicals of arbitrary size.<sup>[90]</sup> The chain-length dependence of  $k_{\text{t}}^{\text{cross}}$  is adopted to be identical to the one measured for  $k_{\text{t}}$ . To check for the impact of cross-termination, parameter estimates have been carried out for various sizes of relative cross-termination rate,  $C_{\text{cross}} = k_{\text{t}}^{\text{cross}}/k_{\text{t}}$ , with  $C_{\text{cross}}$  being varied from 0 to 1. Best fits of both the  $c_{\text{INT}}$  and  $c_{\text{P}}$  versus time traces from EPR spectroscopy were obtained for  $C_{\text{cross}}$  being in the range of 0.2 to 0.3. The lower value is determined by the fitting quality of  $c_{\text{P}}$  versus time and the upper value by the  $c_{\text{INT}}$  versus time fit; i. e., the decay of P suggests  $C_{\text{cross}} \geq 0.2$ , whereas the decay of INT is best fitted by  $C_{\text{cross}} \leq 0.3$ . Simultaneous fitting of both concentration-versus-time profiles thus results in a narrow range for the size of cross-termination:  $C_{\text{cross}} = 0.25 \pm 0.05$ .

Because of the need for calibration of the EPR setup and because of reduced signal-to noise quality of the spectra, the accuracy of radical concentration measurement is estimated to be about 20 %. Simulations of the experimental concentration-versus-time traces have thus been carried out for various combinations of potential uncertainty, i. e., assuming  $c_{\text{INT}}$  and  $c_{\text{P}}$  to be either as calibrated or by 10 % below or above this value.

Plotted in Figure 4.18 are the so-obtained values of addition rate coefficient,  $k_{\text{ad}}$ , and fragmentation rate coefficient,  $k_{\beta}$ , (upper part), and the resulting values of equilibrium constant,  $K_{\text{eq}} = k_{\text{ad}}/k_{\beta}$  (lower part). The smaller symbols indicate the results for a particular combination of the concentrations being taken as calibrated or as 10 % above or below this value. The larger symbols indicate the mean value obtained for the 9 combinations selected at identical  $C_{\text{cross}}$ . The error bars indicate the range of  $k_{\text{ad}}$ ,  $k_{\beta}$ , and  $K_{\text{eq}}$  values resulting from simulation of  $c_{\text{INT}}$  and  $c_{\text{P}}$  varying by  $\pm 10$  %. Toward increasing  $C_{\text{cross}}$ ,  $k_{\beta}$  slightly decreases and  $K_{\text{eq}}$  increases, whereas  $k_{\text{ad}}$  is almost insensitive toward the variation of  $C_{\text{cross}}$  within the range 0.2–0.3. The rate coefficients obtained for  $C_{\text{cross}} = 0.25$ , which allows the best fit of both radical concentration profiles (see Figure 4.17), are  $k_{\text{ad}} = (1.4 \pm 0.4) \times 10^6 \text{ L} \cdot \text{mol}^{-1} \cdot \text{s}^{-1}$  and  $k_{\beta} = (4.7 \pm 1.5) \text{ s}^{-1}$ .



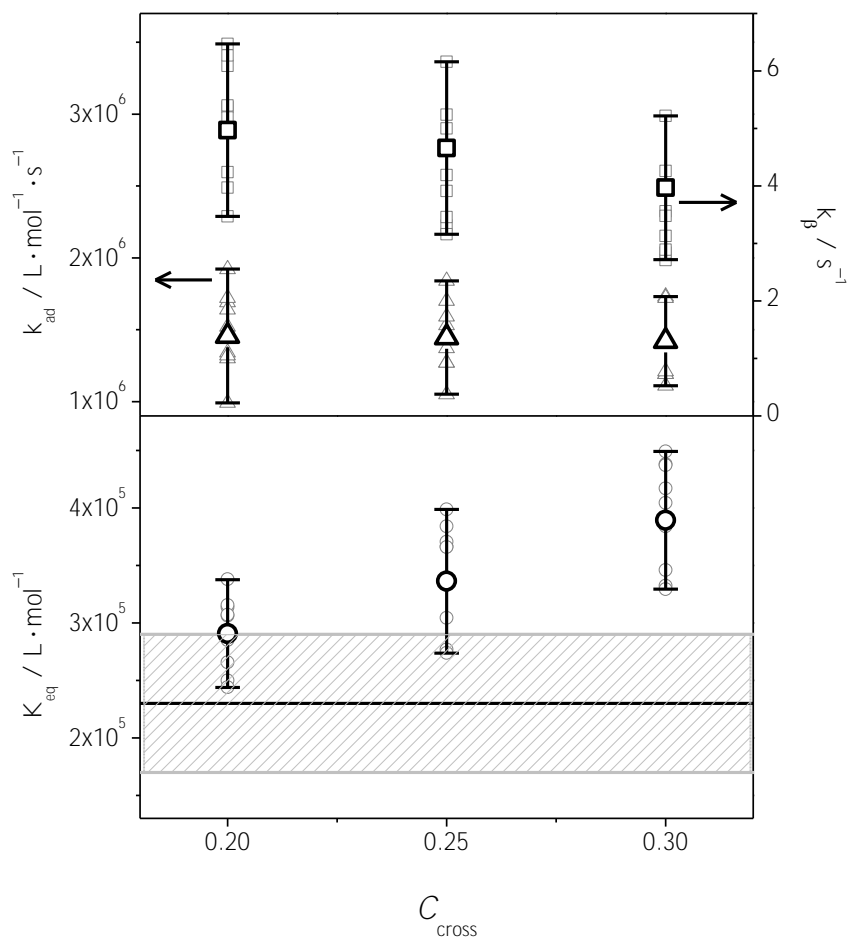


**Figure 4.18.** Results from fitting the experimental trace for ETTP-mediated BA polymerization at  $-40\text{ }^{\circ}\text{C}$  for various adopted  $C_{\text{cross}} = (k_{\text{t}}^{\text{cross}}/k_{\text{t}})$  values. Upper part:  $k_{\text{ad}}$  (triangles) and  $k_{\beta}$  (squares); lower part:  $K_{\text{eq}}$  (circles). The shaded area indicates  $K_{\text{eq}} = (2.3 \pm 0.6)\text{ L} \cdot \text{mol}^{-1} \cdot \text{s}^{-1}$  which value has been deduced from measuring  $c_{\text{INT}}/c_{\text{P}}$  during stationary RAFT polymerization.

### 4.3.3 Comparison of both approaches

From these  $k_{\text{ad}}$  and  $k_{\beta}$  values, the equilibrium constant at  $-40\text{ }^{\circ}\text{C}$  is obtained to be  $K_{\text{eq}} = (3.4 \pm 0.6) \times 10^5\text{ L} \cdot \text{mol}^{-1}$ . This number is in satisfactory agreement with  $K_{\text{eq}} = (2.3 \pm 0.6) \times 10^5\text{ L} \cdot \text{mol}^{-1}$ , as obtained from the measured ratio of INT to P concentrations under stationary polymerization conditions (see Section 4.3.1). In Figure 4.18, the range of uncertainty quoted for  $K_{\text{eq}}$  is indicated by the shaded area. The data show that  $K_{\text{eq}}$  estimated from  $k_{\text{ad}}$  and  $k_{\beta}$  for  $C_{\text{cross}} = 0.25$  is not significantly different from the corresponding value deduced from experimentally determined  $c_{\text{INT}}/c_{\text{P}}$ . The RAFT model thus appears to adequately describe the polymerization kinetics and thus should be well suited for determination of  $k_{\text{ad}}$  and  $k_{\beta}$ .

The obtained  $k_{\text{ad}}$  and  $k_{\beta}$  values may be used to check whether the reaction conditions of the stationary experiments were adequate for estimating  $K_{\text{eq}}$  via Equation 3.3, i. e., whether the rate of cross-termination,  $r_{\text{t}}^{\text{cross}}$ , is indeed negligible as compared to the addition and fragmentation rates,  $r_{\text{ad}}$  and  $r_{\beta}$ . The absolute concentrations of INT and P are known from the EPR spectra. The maximum value of  $r_{\text{t}}^{\text{cross}}$  was estimated by implementing  $k_{\text{t}}^{\text{cross}} = k_{\text{t}}^{1,1}$ , which refers to the upper limit of termination taking place between a propagating and an intermediate radical, both of chain length unity. In order to consider the worst case scenario also for addition and fragmentation, both rates were estimated for the lowest  $c_{\text{ETTP}}$ . Even under these conditions,  $r_{\text{t}}^{\text{cross}}$  is by about 1 order of magnitude below  $r_{\text{ad}}$  and  $r_{\beta}$ , thus verifying the validity of using Equation 3.3 for the ETTP concentration range selected for our experiments.

Via the activation energy  $E_{\text{a}}(K_{\text{eq}}) = -49.5\text{ kJ} \cdot \text{mol}^{-1}$  (see Section 4.3.1) and assuming that  $k_{\text{ad}}$  is associated with a low activation energy, e. g., of  $8.4\text{ kJ} \cdot \text{mol}^{-1}$ , as suggested by *ab initio* quantum-chemical calculations for the addition of small radicals to dithioester compounds,<sup>[38]</sup> the activation energy of  $k_{\beta}$  is estimated to be  $E_{\text{a}}(k_{\beta}) = 57.9\text{ kJ} \cdot \text{mol}^{-1}$ . This number together with  $k_{\beta}$  measured for  $-40\text{ }^{\circ}\text{C}$  results in a fragmentation rate coefficient of  $3.1 \times 10^4\text{ s}^{-1}$  at  $60\text{ }^{\circ}\text{C}$ , which is by orders of magnitude above  $k_{\beta}$  values predicted by the slow fragmentation model; e. g.,  $k_{\beta} = 10^{-2}\text{ s}^{-1}$  has been reported for CDB-mediated styrene polymerization at  $60\text{ }^{\circ}\text{C}$ .<sup>[43]</sup> It is very unlikely that polymerizing styrene rather than BA may be responsible for this difference by about 5 orders of magnitude. Moreover, if the monomers matters, one would expect that, with identical RAFT agent,  $k_{\beta}$  is higher for styrene than for BA, as the styryl radical is stabilized by delocalization of radical functionality over the aromatic ring.

## 4.4 Discussion

The experimentally obtained equilibrium constants and addition and fragmentation rate coefficients for the RAFT-mediated BA polymerizations at  $-40\text{ }^{\circ}\text{C}$  are listed in Table 4.7. The values for three different types of RAFT agents are compared, i. e. the xanthate EDTCP, the trithiocarbonates BMPT and EPPT, as well as the dithiobenzoate ETTP. The rate coefficients  $k_{\text{ad}}$  and  $k_{\beta}$  are the ones obtained from SP-PLP-EPR-RAFT experiments and the equilibrium constants represent the average values of the stationary and the single pulse measurements.

**Table 4.7.** Comparison of experimentally obtained equilibrium constants and addition and fragmentation rate coefficients for RAFT-mediated BA polymerizations ( $1.5\text{ mol}\cdot\text{L}^{-1}$  in toluene) at  $-40\text{ }^{\circ}\text{C}$ .

	$k_{\text{ad}} / \text{L}\cdot\text{mol}^{-1}\cdot\text{s}^{-1}$	$k_{\beta} / \text{s}^{-1}$	$K_{\text{eq}} / \text{L}\cdot\text{mol}^{-1}$
EDTCP	$(2.5 \pm 0.1) \times 10^4$	$(2.3 \pm 0.3) \times 10^3$	$12 \pm 2$
EPPT	$(3.4 \pm 0.3) \times 10^6$	$(1.4 \pm 0.4) \times 10^2$	$(2.6 \pm 0.8) \times 10^4$
BMPT	$(4.1 \pm 0.9) \times 10^6$	$45 \pm 5$	$(8 \pm 4) \times 10^4$
ETTP	$(1.4 \pm 0.4) \times 10^6$	$5 \pm 2$	$(3 \pm 1) \times 10^5$

### Comparison of addition rate coefficients

The addition of propagating radicals to the trithiocarbonate and to the dithiobenzoate is almost equally fast. This is in agreement with *ab initio* calculations predicting that for most RAFT agents, the addition rate coefficients fall into a relatively narrow range ( $10^5 - 10^7\text{ L}\cdot\text{mol}^{-1}\cdot\text{s}^{-1}$ ).<sup>[40]</sup> An exception are xanthates where the reactivity of the thiocarbonyl bond is reduced due to the free electron pair on the oxygen atom. The addition rate coefficient for the xanthate is by two orders of magnitude smaller than for the trithiocarbonate and the dithiobenzoate. Therefore, xanthates are typically used to control polymerizations of highly reactive propagating radicals, like vinyl acetate, whereas trithiocarbonates and dithiobenzoates are employed with stable propagating radicals, such as styrene. *Ab initio* calculations predict  $k_{\text{ad}}$  values around  $10^4\text{ L}\cdot\text{mol}^{-1}\cdot\text{s}^{-1}$  for xanthates at  $60\text{ }^{\circ}\text{C}$ ,<sup>[40]</sup> since the addition reaction is associated with a very low energy barrier. The calculated value is in close agreement with the experimentally obtained one.

### Comparison of fragmentation rate coefficients

Considering the low polymerization temperature, fragmentation of the intermediate species is fast for all RAFT agents. With reference to the trithiocarbonates, fragmentation is around one order of magnitude faster for the xanthate and one order of magnitude slower for the dithiobenzoate. For xanthates a fragmentation rate coefficient in the range of  $10^2 - 10^3 \text{ s}^{-1}$  is predicted by *ab initio* calculations,<sup>[40]</sup> which is close to the coefficient obtained from SP-PLP-EPR-RAFT measurements.

For the trithiocarbonate-mediated BA polymerizations  $k_{\beta}$  has not been calculated separately. However, the equilibrium constants for the trithiocarbonates are in close agreement with the calculated  $K_{\text{eq}}$  value of  $1.4 \times 10^4 \text{ L} \cdot \text{mol}^{-1}$  for the BMPT-mediated polymerization of MA in toluene at  $-30 \text{ }^{\circ}\text{C}$ <sup>[41]</sup> and calculated and experimental  $k_{\text{ad}}$  values are similar. The experimentally obtained fragmentation rate coefficient for the trithiocarbonate is therefore in agreement with the calculated one.

The dithiobenzoate-mediated BA polymerization has not been investigated with *ab initio* methods so far. The experimentally obtained  $k_{\beta}$  value can therefore only be compared with  $k_{\beta}$  in a dithiobenzoate-mediated styrene polymerization. The fragmentation rate coefficient should not significantly differ for both systems. At  $70 \text{ }^{\circ}\text{C}$ ,  $k_{\beta} = 2.5 \times 10^{-4} \text{ s}^{-1}$  deduced from *ab initio* calculations is significantly below  $k_{\beta} = 4.7 \text{ s}^{-1}$  determined from the SP-PLP-EPR-RAFT experiment. As fragmentation becomes faster with increasing temperature, there is a difference of at least 5 orders of magnitude between the calculated and experimental fragmentation rate coefficient if one adopts the styrene value for the extrapolation.

### Comparison of equilibrium constants

The equilibrium constants for the trithiocarbonates and the dithiobenzoate are three to four orders of magnitude above the  $K_{\text{eq}}$  value for the xanthate. The low equilibrium constant results from a combination of slow addition of BA to the thiocarbonyl bond of the xanthate and the fast fragmentation of the intermediate radical species. A key aspect to controlling radical polymerization by RAFT is the rapid exchange between the propagating species and dormant macroRAFT agent, which entails that both the addition and the fragmentation reactions are sufficiently fast. The significantly lower  $k_{\text{ad}}$  value for the xanthate system therefore explains why acrylate polymerizations are less well controlled by xanthates compared with trithiocarbonates or dithiobenzoates.

The equilibrium constants for the trithiocarbonates are only one order of magnitude smaller than for the dithiobenzoate. This is caused by the slightly faster fragmentation of the intermediate radical in trithiocarbonate-mediated polymerizations. The theoretically predicted  $K_{\text{eq}}$  value for xanthate-mediated polymerizations is around 10 to  $100 \text{ L} \cdot \text{mol}^{-1}$ ,<sup>[40]</sup> which is in good agreement with the experimental value of  $12 \text{ L} \cdot \text{mol}^{-1}$ . A good correlation between experiment and *ab initio* prediction is

also found for the trithiocarbonates, with the calculated value of  $1.4 \times 10^4 \text{ L} \cdot \text{mol}^{-1}$  being close to the experimental ones,  $2.6 \times 10^4$  and  $8 \times 10^4 \text{ L} \cdot \text{mol}^{-1}$  for EPPT and BMPT, respectively.<sup>[41]</sup> The equilibrium constant for the dithiobenzoate expected from *ab initio* studies is  $4 \times 10^9 \text{ L} \cdot \text{mol}^{-1}$  at  $70 \text{ }^\circ\text{C}$ .<sup>[39]</sup> Since  $K_{\text{eq}}$  increases with decreasing temperature, the difference between the experimental ( $3 \times 10^5 \text{ L} \cdot \text{mol}^{-1}$ ) and theoretical value is even more pronounced at  $-40 \text{ }^\circ\text{C}$ .

In summary, the rate coefficients determined by EPR spectroscopy are in good agreement with the calculated ones reported by the Coote group,<sup>[40,41]</sup> with the exception of dithiobenzoate being the RAFT agent.<sup>[39]</sup> For dithiobenzoate-mediated polymerizations slow fragmentation of the intermediate radical is predicted, which is in sharp contrast to the fast decay of INT concentration monitored by EPR spectroscopy after laser single pulse initiation. A chain-length dependence of  $K_{\text{eq}}$  was checked by monitoring stationary BA polymerizations mediated by a pre-polymerized trithiocarbonate and a pre-polymerized dithiobenzoate, respectively. No pronounced chain-length dependence, as predicted by *ab initio* studies, was found.<sup>[39]</sup>

The accuracy of the determination of the RAFT equilibrium constant via the novel EPR methods represents an enormous advantage over the approach suggested by Kwak *et al.*,<sup>[50]</sup> where  $K_{\text{eq}}$  is deduced by comparing polymerization rates at different RAFT agent contents (see Section 4.3). In addition, the EPR strategies are not restricted to polymerizations which exhibit rate retardation and they provide access to the individual addition and fragmentation rate coefficients. No control of polymerization is required, so that all RAFT agent/monomer combinations may be investigated. The EPR experiments can be carried out over a wide range of temperatures but are restricted to ambient pressure, since no pressure-resistant EPR tubes have been developed so far.

The EPR methods may be applied to other RAFT agents, like dithiocarbamates, and other monomers, like methacrylates or vinyl acetate. However, the EPR investigation of styrene polymerization still poses a problem since the radical delocalization into the aromatic ring of the propagating radical gives rise to a multi-line spectrum. During normal polymerization conditions this spectrum can hardly be distinguished from noise. Further development of EPR instrumentation will increase the signal-to-noise ratio and the detection limit, so that this monomer should be measurable in the near future. Meanwhile, the investigation of an appropriate model system provides insight into the dithiobenzoate-mediated styrene polymerization (see Section 5.3).

Studies of BA polymerizations at higher temperatures are complicated by the occurrence of MCRs. Thus, three radicals are detected in the EPR spectrum. Deconvolution of such a spectrum poses no general problem, but single-pulse experiments with subsequent PREDICI<sup>®</sup> fitting of the radical concentration-versus-time profiles becomes more difficult due to the increased number of unknown rate coefficients.

It would therefore be recommendable to separately investigate the RAFT equilibrium with a system which only contains MCRs. This may be possible by applying acrylate-type macromonomers. By initiation of such macromonomers radical species are produced which are similar to MCRs formed during acrylate polymerization.

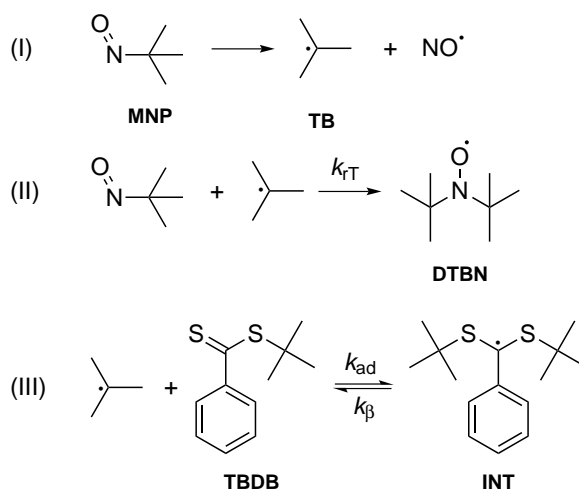
# 5

## EPR with monomer-free model systems

The results from the EPR experiments with macromolecular systems are in good agreement with the theoretically predicted ones for xanthate- and trithiocarbonate-mediated RAFT polymerizations, but there remains a huge difference for dithiobenzoates. To exclude that the discrepancy is due to possible chain-length dependencies of  $k_{\text{ad}}$ ,  $k_{\beta}$  or  $k_{\text{t}}^{\text{cross}}$ , this chapter deals with model systems which contain no monomer but the compounds which are used for *ab initio* calculations. In this way, the direct comparison of experimental and theoretical values becomes possible. For the investigated model systems the attacking radicals (*tert*-butyl, cyano-*iso*-propyl and phenylethyl, respectively) are identical to the leaving group of the dithiobenzoate.

### 5.1 *tert*-Butyl/*tert*-butyl dithiobenzoate

The first attempt to use a model reaction for comparing experimental and theoretical  $K_{\text{eq}}$  values was made by Chernikova *et al.*,<sup>[100]</sup> who applied a spin trap method in conjunction with EPR spectroscopy. As spin trap agent, 2-methyl-2-nitrosopropane (MNP) was used which simultaneously functioned as a visible-light photoinitiator. This initiator decomposes into *tert*-butyl and NO radicals (see reaction I in Scheme 5.1). The *tert*-butyl radical adds to another MNP molecule resulting in the stable nitroxide radical di-*tert*-butyl nitroxide (DTBN in reaction II). The *tert*-butyl radical may also add to *tert*-butyl dithiobenzoate (TBDB in reaction III), which was used as RAFT agent. The resulting intermediate radical INT and the nitroxide radical DTBN can be monitored by EPR spectroscopy.



**Scheme 5.1.** Reactions that were considered by Chernikova *et al.* for  $K_{\text{eq}}$  determination of the TB/TBDB system.<sup>[100]</sup>

Tracing INT and DTBN concentrations after irradiation of the reaction mixture with visible light and subsequent fitting of the concentration profiles resulted in an equilibrium constant of  $K_{\text{eq}} = (6 \pm 4) \times 10^8 \text{ L} \cdot \text{mol}^{-1}$  for the TB/TBDB system in benzene solution at 20 °C. Simultaneously performed quantum-chemical calculations resulted in  $K_{\text{eq}} = 4.5 \times 10^8 \text{ L} \cdot \text{mol}^{-1}$ .<sup>[100]</sup>

From Scheme 5.1 one would expect that the consumption of INT after switching off the irradiation source equals the accumulation of the nitroxide spin trap DTBN. This is however only the case for  $c_{\text{TBDB}}^0/c_{\text{MNP}}^0 = 1$ . For the other concentration ratios, e. g. for  $c_{\text{TBDB}}^0/c_{\text{MNP}}^0 = 9$ , less DTBN than expected is formed. Chernikova *et al.* assigned the effect to self-termination of INT.<sup>[100]</sup> This conclusion is however in conflict with the  $\ln(c_{\text{INT}})$ -versus-time curves being linear which indicates a first-order decay of INT as one would expect with unimolecular decomposition. Yet, a clearly non-linear INT decay is predicted by PREDICI<sup>®</sup> simulations when self-termination is included to the extent indicated by Chernikova *et al.*<sup>[100,108]</sup> Scheme 5.1 is thus not sufficient to describe the kinetics of this particular model system.

The problem of the spin trap method is that the reaction mechanism is far more complex than brief inspection may indicate and that the system involves at least four types of radicals. In addition to TB and INT, the radicals DTBN and NO are present, which may add to the RAFT agent forming additional INT species or undergo further reactions. For example, evidence for the combination of TB and NO radicals can be found in literature.<sup>[142]</sup> Thus, only part of the resulting complexity has been considered by Chernikova *et al.*<sup>[100]</sup>



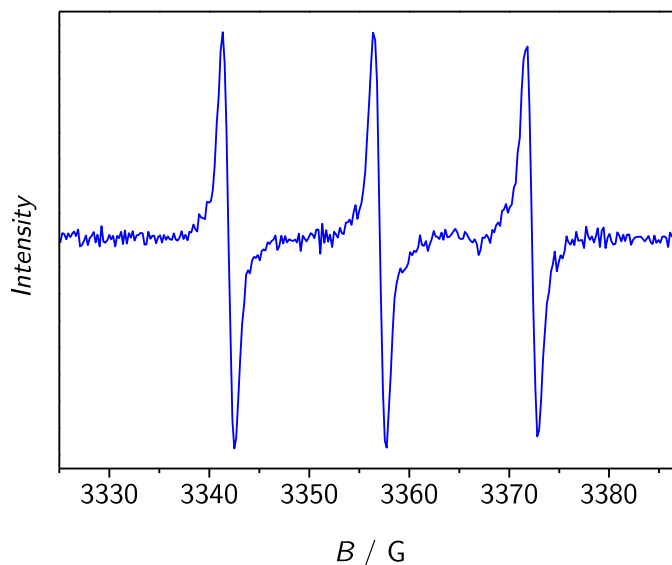
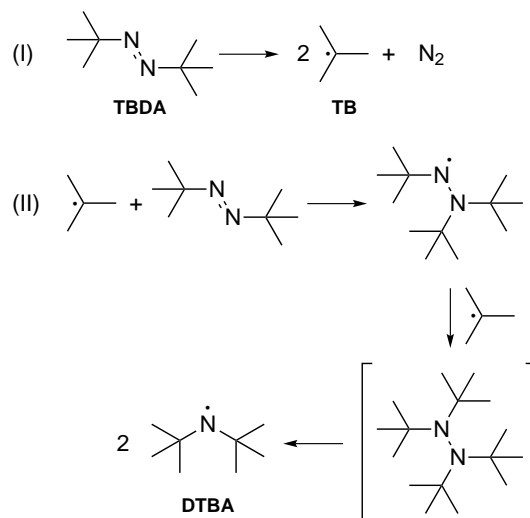


**Figure 5.1.** Radical formed when TBDA decomposes thermally at 80 °C. The hyperfine coupling constant,  $a = 15.3$  G, and the intensity ratio of the EPR lines, 1:1:1, point to a nitrogen-centered radical.

### 5.1.1 Choice of the initiator

Since the model reaction is apparently disturbed by the occurrence of too many radical species, it is preferable to develop a system of lower complexity. This can be achieved by producing TB from an initiator which only decomposes into the desired radicals and an inert molecule which does not react with any species taking part in the RAFT equilibrium such as symmetrical azo-initiators. Therefore, EPR spectroscopy was used to check whether 1,2-di-*tert*-butyldiazene (TBDA) is suitable for this purpose.

Thermal decomposition of TBDA at 80 °C, however, does not only lead to the expected TB radical. Instead, the EPR spectrum shown in Figure 5.1 points to the formation of a nitrogen-centered radical, probably di-*tert*-butylamine (DTBA), which could be formed via the mechanism shown in Scheme 5.2. This reaction probably only plays an important role below the temperature at which the initiator decomposes at a reasonable rate. Normally, TBDA is used in high-pressure ethene polymerization and the thermal decomposition rate coefficient,  $k_d$ , is around  $0.5 \text{ s}^{-1}$  at 280 °C.<sup>[143]</sup> At such high temperatures the addition rate of the TB radical to TBDA should become negligibly small as compared to the rate of termination between two TB radicals. Hence, TBDA is not suitable for confirming the  $K_{\text{eq}}$  value derived by Chernikova *et al.* for the TB/TBDB system at lower temperatures (up to 100 °C).<sup>[100]</sup>



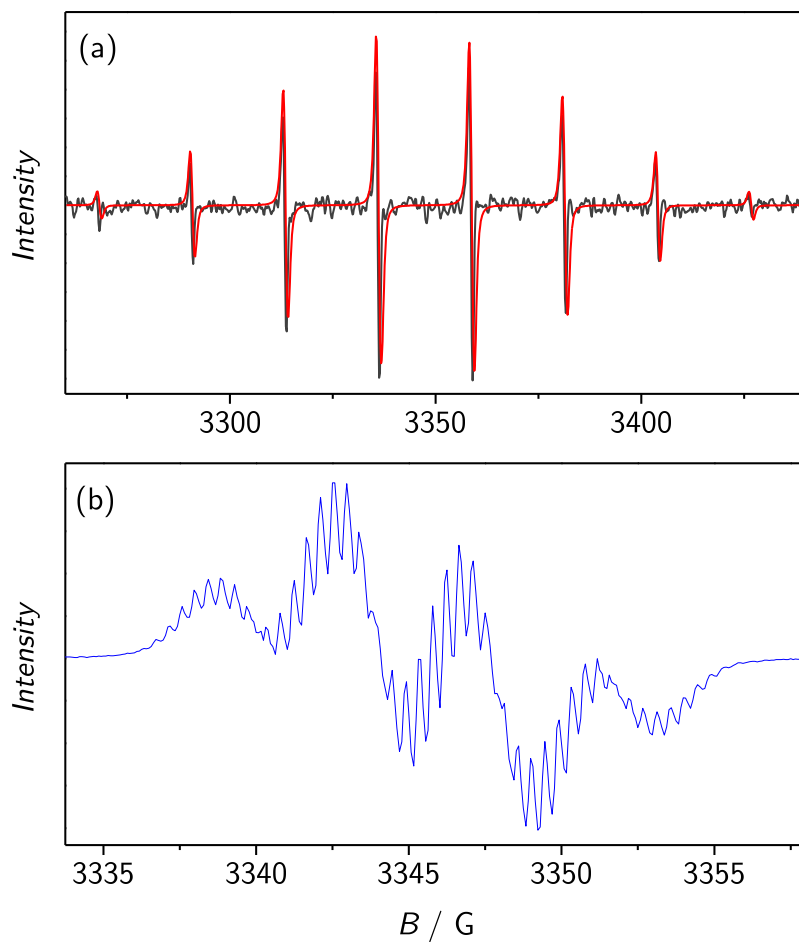
**Scheme 5.2.** Assumed reaction mechanism for the decomposition of TBDA at 80 °C and formation of DTBA. The shown cross-termination reaction (IV) represents one of the possible reaction pathways. Cross-termination reactions may occur with all resonance structures depicted in Scheme 2.4.

In an attempt to find another initiator which does not form any additional radicals at temperatures below 100 °C Tetramethylpropyl peroxyvalate (TMPPP) was investigated. Its  $k_d$  value in high-pressure ethene polymerizations is  $0.5 \text{ s}^{-1}$  at 147 °C and it should therefore decompose sufficiently fast at temperatures around 70 °C in toluene.<sup>[144]</sup> As shown in Scheme 5.3, TMPPP decomposes thermally into TB, acetone and  $\text{CO}_2$ .<sup>[145,146]</sup> The EPR spectrum of the TB radical is presented in Figure 5.2a. The corresponding coupling constants and line width, deduced from the experimental spectrum by fitting with the EasySpin toolbox (see Section 7.3.3), are presented in Table 5.1.

### 5.1.2 Determination of the equilibrium constant

A degassed solution of TMPPP ( $0.3 \text{ mol} \cdot \text{L}^{-1}$ ) and TBDB ( $4.5 \times 10^{-3} \text{ mol} \cdot \text{L}^{-1}$ ) in toluene has been prepared and the reaction mixture was monitored at 70 °C via EPR spectroscopy. The EPR spectrum of the INT radical resulting from the addition of TB to the RAFT agent TBDB is shown in Figure 5.2b, which can be simulated using the coupling constants listed in Table 5.1.

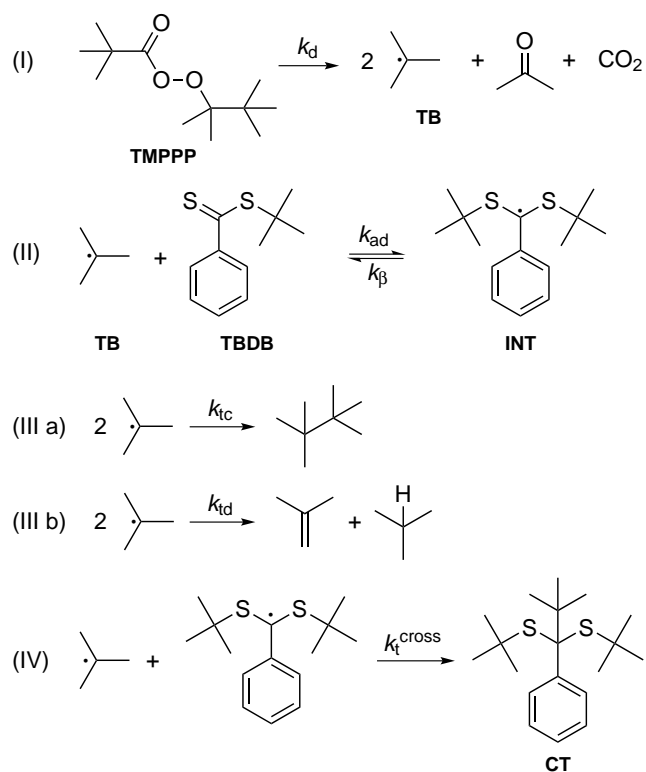
The concentration profiles of the INT and TB radical are illustrated in Figure 5.3. At the beginning of the reaction the INT concentration is very high and the TB radical is not detectable. A fast decay of the INT species is observed and after 300 s INT disappears completely. Only then TB concentration becomes measurable, which



**Figure 5.2.** (a) Simulated and experimental TB spectrum; (b) experimental INT spectrum; obtained of EPR scans at 70 °C, an initial initiator concentration of  $c_{\text{TMPPP}} = 0.30 \text{ mol} \cdot \text{L}^{-1}$ , and a RAFT agent concentration of  $c_{\text{CPDB}} = 4.5 \times 10^{-3} \text{ mol} \cdot \text{L}^{-1}$ . The EPR parameters are listed in Table 5.1. Note the different abscissa scales.

**Table 5.1.** Coupling constants and line widths deduced from experimental spectra of INT and TB in toluene at 70 °C.

radical	coupling constants / G				line width / G
TB	$a_{\text{H}}$ 22.6				0.1
INT	$a_{\text{H},\text{meta}}$ 1.3	$a_{\text{H},\text{ortho}}$ 3.7	$a_{\text{H},\text{para}}$ 4.2	$a_{\text{H},\delta}$ 0.4	0.1

**Scheme 5.3.** Assumed reaction scheme for the model system TB/TBDB.

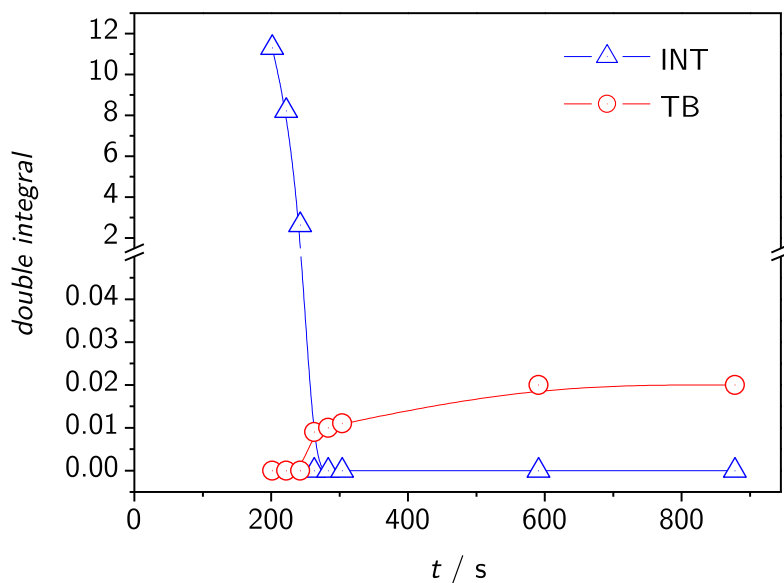


**Figure 5.3.** Concentration profiles of TB and INT during the decomposition of TMPPP ( $c_{\text{TMPPP}} = 0.3 \text{ mol} \cdot \text{L}^{-1}$ ) in the presence of  $4.5 \times 10^{-3} \text{ mol} \cdot \text{L}^{-1}$  TBDB in toluene at  $70 \text{ }^\circ\text{C}$ . Note that the concentration of the radical species is proportional to the double integral of the signal.

indicates that INT and TB are consumed by cross-termination until the RAFT agent concentration is completely depleted (see Scheme 5.3). The sudden and pronounced decay of RAFT would also explain the decolorization of the solution which was observed during the reaction. Due to the apparently high cross-termination rate, determination of  $K_{\text{eq}}$  via Equation 3.3 is not possible. The extrapolation of the  $c_{\text{INT}}/c_{\text{TB}}$  ratio to  $t = 0$  can however provide a rough estimate. With the concentration ratio being above 1000 and an initial RAFT agent concentration of  $4.5 \times 10^{-3} \text{ mol} \cdot \text{L}^{-1}$ ,  $K_{\text{eq}}$  exceeds  $10^5 \text{ L} \cdot \text{mol}^{-1}$ . Although no exact  $K_{\text{eq}}$  may be obtained from this experiment, the result confirms that  $K_{\text{eq}}$  is high, which is consistent with the  $K_{\text{eq}}$  value proposed by Chernikova *et al.*<sup>[100]</sup>

It appears from the experiments described above that  $K_{\text{eq}}$  for the TB/TBDB system is probably in the range of  $10^5$  to  $10^9 \text{ L} \cdot \text{mol}^{-1}$  (between  $20$  and  $70 \text{ }^\circ\text{C}$ ). Adopting an addition rate coefficient of  $k_{\text{ad}} = 5 \times 10^6 \text{ L} \cdot \text{mol}^{-1} \cdot \text{s}^{-1}$ , as proposed by the spin trap method, yields fragmentation rate coefficients of  $k_{\beta} = 8 \times 10^{-3}$  to  $50 \text{ s}^{-1}$ . In another study, Chernikova *et al.* observed high intermediate radical concentrations during the

early stage of a TBDB-mediated BA polymerization.<sup>[56]</sup> These experimental results suggest slow fragmentation of the intermediate radical in dithiobenzoate-mediated polymerizations. This conclusion is however misleading as the *tert*-butyl radical does not resemble any monomer in its chemical properties. The *tert*-butyl radical is less stabilized than styrene, acrylate or methacrylate radicals and common RAFT leaving groups, such as cumyl or cyano-*iso*-propyl. The results from this model system can therefore not be transferred directly to other dithiobenzoate systems.

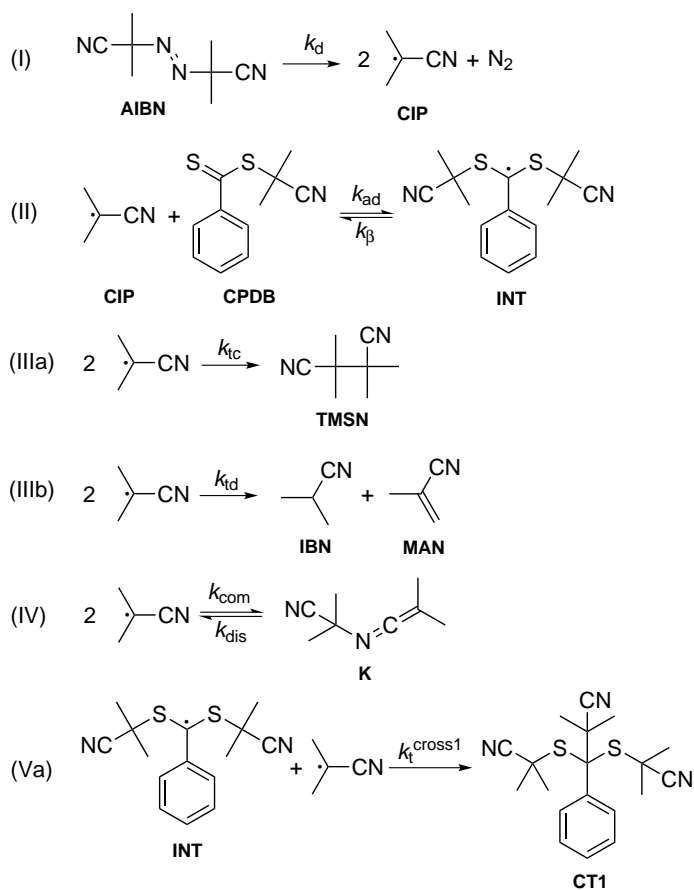
Since neither the spin trap method reported by Chernikova *et al.*<sup>[100]</sup> nor the EPR experiment described above provide an exact value for the equilibrium constant, none of the both approaches can be used for checking the accuracy of the calculated  $K_{\text{eq}}$  value ( $4.5 \times 10^8 \text{ L} \cdot \text{mol}^{-1}$ ). The theoretical equilibrium constant lies within the range of  $10^5$  to  $10^9 \text{ L} \cdot \text{mol}^{-1}$ , which constitutes a rough estimate of  $K_{\text{eq}}$  obtained from the experiments. This does not necessarily mean that the quantum-chemical studies by Coote and co-workers yield exact  $K_{\text{eq}}$  values for other dithiobenzoate-containing systems. For this particular model system the approximations made and the method used for modeling solvation energies differ from previous studies (see Table 5.8 and the Supporting Information of the corresponding publications).<sup>[39,98,100]</sup>

## 5.2 Cyano-*iso*-propyl/2-(2'-cyanopropyl)-dithiobenzoate

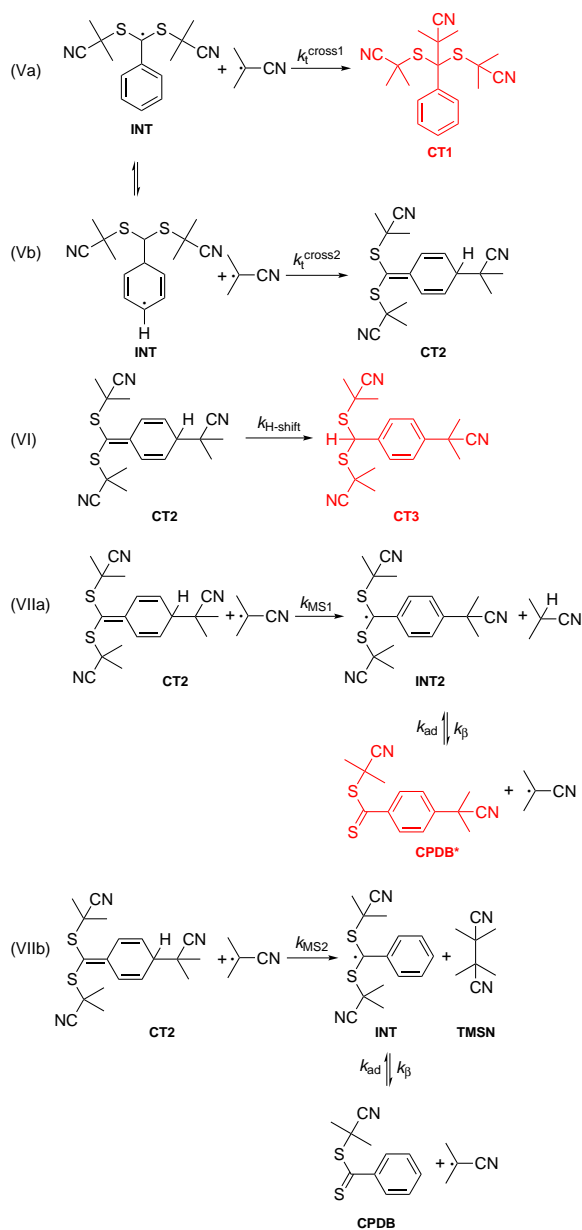
In order to meet the requirement of using a model system of low complexity, which resembles monomer addition and fragmentation and allows at the same time for testing of quantum-chemical calculations, 2,2'-azobis(2-methylpropionitrile) (AIBN) was selected as thermal initiator and 2-(2'-cyanopropyl)-dithiobenzoate (CPDB) as the RAFT agent. The enormous advantage of this model system relates to the fact that only two radical species are present, the intermediate radical, INT, and the CIP radical, which are both easily monitored by EPR spectroscopy. Moreover, quantum-chemical estimates of  $K_{\text{eq}}$  have been made for a system composed of these two radical species.<sup>[39,98]</sup> The results of the following section have already been published.<sup>[147,148]</sup>

The kinetic scheme associated with the CIP/CPDB system is given in Scheme 5.4. It includes AIBN decomposition into two cyano-*iso*-propyl (CIP) radicals (I), addition of CIP to CPDB and fragmentation of the resulting INT species (II), self-termination of two CIP species via reaction IIIa, IIIb or IV,<sup>[149]</sup> and cross-termination between CIP and INT (Va). By means of PREDICI<sup>®</sup> simulation it was verified that reactions III to IV do not affect  $K_{\text{eq}}$  measurement under the reaction conditions selected.

To check whether side reactions occur which may interfere with the determination of  $K_{\text{eq}}$  via Equation 3.3, NMR analyses of the product mixture of the CIP + CPDB reaction after 18 h at 80 °C were performed. The experimental procedure as well as the NMR and mass spectrometry data of the entire set of products are given in Section 7.3.4.



**Scheme 5.4.** Kinetic scheme for the model system CIP/CPDB. AIBN: 2,2'-azobis(2-methylpropionitrile); CIP: cyano-*iso*-propyl radical; CPDB: 2-(2'-cyanopropyl)-dithiobenzoate; INT: intermediate radical; TMSN: tetramethylsuccinonitrile; IBN: *iso*-butyronitrile; MAN: methacrylonitrile; K: ketenimine; CT1: cross-termination product 1.



**Scheme 5.5.** Products (highlighted in red) found after complete decomposition of  $0.3 \text{ mol} \cdot \text{L}^{-1}$  AIBN in the presence of  $0.75 \text{ mol} \cdot \text{L}^{-1}$  CPDB in toluene at  $80 \text{ }^\circ\text{C}$ . CT1, CT2, CT3: cross-termination products 1, 2, 3, respectively; INT2: ring-substituted intermediate radical; CPDP\*: ring-substituted CPDB. The red structures indicate the side products.



The observed side products and the mechanism of their formation are shown in Scheme 5.5. As expected, cross-termination product CT1 has been found (Va), whereas cross-termination product CT2 is missing (Vb). The absence of CT2 may be explained by the lower stability of this compound, which exhibits no extended delocalization of radical functionality over the cyclic moiety. Aromaticity may be gained back by an H-shift reaction of CT2 to yield CT3 (VI). Alternatively, the hydrogen atom in *para* position may be abstracted by another radical (VIIa), which process is one out of a multitude of so-called “missing step” reactions<sup>[105]</sup> resulting in the formation of the intermediate radical, INT2. This species may fragment and produce the ring-substituted RAFT agent CPDB\*, which should be less prone to cross-termination than CPDB. The “missing step” process may also occur according to step VIIb, which goes with the formation of the resonance-stabilized INT radical plus a stable molecule from a highly reactive radical and relatively labile molecule. Fragmentation subsequent to step VIIb restores CPDB. Further side products were not detected at our reaction conditions, which indicates that cross-termination via an intermediate radical with the radical functionality in *ortho* position plays no significant role. Products resulting from self-termination between two INT radicals were also missing. These reaction steps are therefore not included in Scheme 5.5.

The occurrence of products from cross-termination and “missing step” reactions is no surprise because of the enormous driving force behind both processes.<sup>[105]</sup> DFT calculations of reaction enthalpies for the ethyl radical/ethyl dithiobenzoate system suggest that step Va is faster than Vb, since step Vb is accompanied by a loss of ring aromaticity. However, due to the bulkiness of the CIP radical, step Va should be more demanding with the system under investigation and thus may be of comparable rate or even slower than step Vb. The absence of product CT2 in the final reaction mixture is most likely due to the fast follow-up reactions (VI through VIIb). The intramolecular H-shift step VI has not been investigated in the earlier DFT study,<sup>[105]</sup> but is assumed to be comparably fast as reaction steps VIIa and VIIb. Within the latter three processes, products with resonance stabilization over the entire aromatic ring are obtained.

It should be noted that the enthalpies from *ab initio* calculations for the ethyl radical/ethyl dithiobenzoate system differ only by about 5 % for reactions VIIa and VIIb.<sup>[105]</sup> This finding is of relevance, as high rates for radical abstraction from a cross-termination product by another radical, e.g., via step VIIb, account for the absence of three-arm star polymeric material in RAFT polymerizations and thus invalidate objections against the intermediate radical termination model which are based on significant amounts of star-shaped species being absent. “Missing step” reactions of CT1 have not been included into Scheme 5.5, as DFT calculations indicate a significantly lower enthalpy for this reaction.<sup>[105]</sup> Moreover, hydrogen abstraction is unlikely to occur with CT1.

**Table 5.2.** Coupling constants and line widths deduced from the experimental spectra of INT and CIP.

radical	coupling constants / G				line widths / G
CIP	$a_{\text{H}}$		$a_{\text{N}}$		0.6
	20.5		3.3		
INT	$a_{\text{H},meta}$	$a_{\text{H},ortho}$	$a_{\text{H},para}$	$a_{\text{H},\delta}$	0.5
	1.3	3.7	4.2	0.4	

The occurrence of the cross-termination product CT1 and of the “missing step” product CPDB\* has already been reported by Moad *et al.* for AIBN decomposition in the presence of benzyl dithiobenzoate.<sup>[106]</sup> They did not observe the product CT1 during RAFT polymerization, probably because monomer addition to CIP is faster than cross-termination. In addition, they found a by-product under polymerization conditions, which originates from the ketenimine K (see reaction IV in Scheme 5.4). The molecular structure of this by-product has not been identified so far and could not be detected in the experiment carried out as described in Section 7.3.4. However, the product was also detected by real-time NMR when AIBN was used as initiator for a trithiocarbonate-mediated polymerization.<sup>[150]</sup>

Formation of CT1 and CT3 may interfere with the determination of  $K_{\text{eq}}$  via Equation 3.3. To determine whether this is the case, one has to check

- (I) whether the radical concentration ratio  $c_{\text{INT}}/c_{\text{CIP}}$  decreases with ongoing reaction and
- (II) whether significant amounts of CT1 and CT3 are formed.

(I) The radical concentration ratio  $c_{\text{INT}}/c_{\text{CIP}}$  was monitored via EPR spectroscopy. For this purpose, the EPR spectra of the individual species need to be known. In contrast to the situation met in the studies of the RAFT-mediated BA polymerization (see Section 4) the EPR signals of the CIP radical and of INT are not fully separated. Thus, the following deconvolution procedure has been applied. The EPR spectrum of CIP, as recorded after heating a degassed AIBN solution in toluene to 80 °C, was simulated. The coupling constants,  $a$ , obtained from least-squares fitting via the Nelder-Mead simplex algorithm of the EasySpin toolbox (see Section 7.3.3), are listed in Table 5.2. The simulated CIP spectrum is illustrated in Figure 5.4a.

[hb]

From the EPR spectra measured of AIBN- and CPDB-containing solutions the simulated CIP radical spectrum was subtracted, which procedure yields an EPR

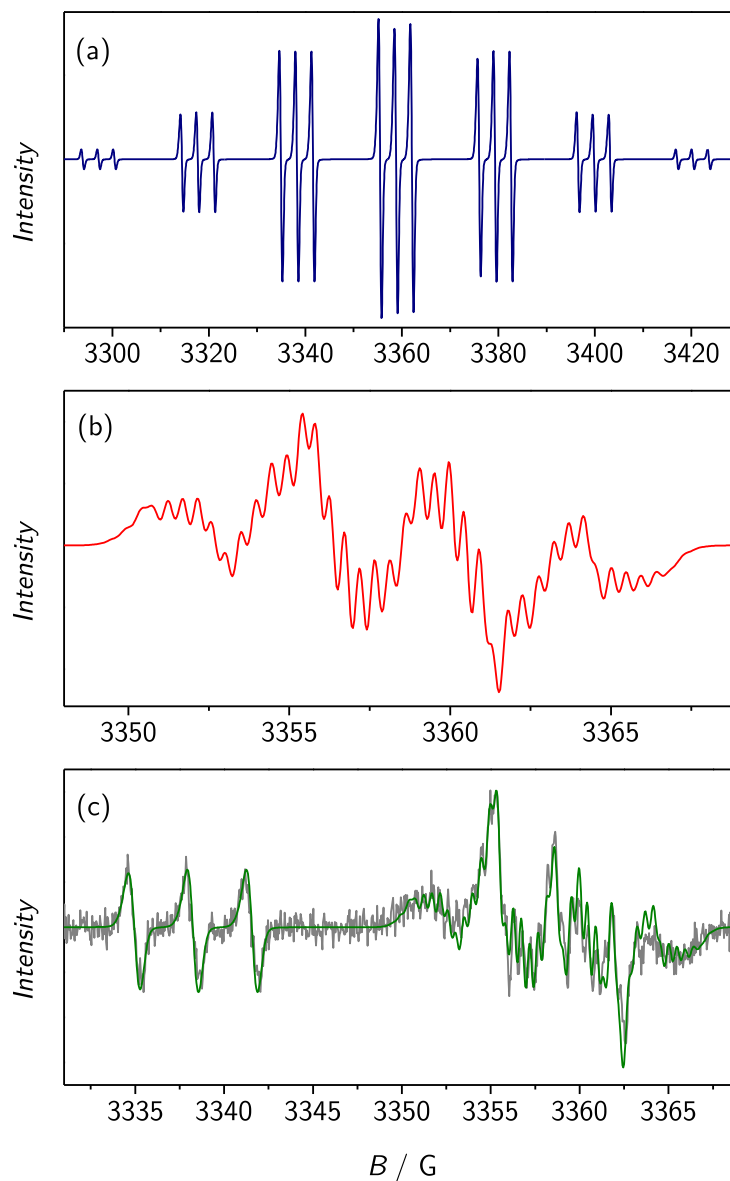


**Figure 5.4.** (a) Simulated CIP spectrum; (b) simulated INT spectrum; (c) experimental spectrum (gray line) obtained by co-addition of 10 EPR scans at 80 °C, an initial initiator concentration of  $c_{\text{AIBN}} = 0.30 \text{ mol} \cdot \text{L}^{-1}$ , and a RAFT agent concentration of  $c_{\text{CPDB}} = 0.60 \text{ mol} \cdot \text{L}^{-1}$ . The green line in (c) represents the summation over the simulated CIP and INT spectra. The EPR parameters are listed in Table 5.2. Note the different abscissa scales.

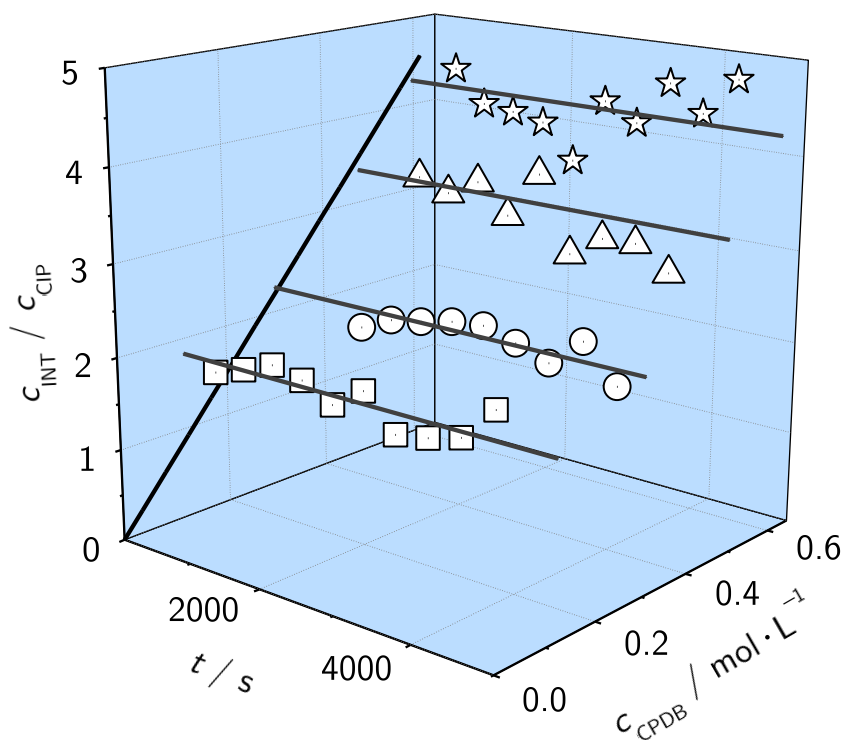
spectrum that should entirely originate from the INT species. Fitting of the so-obtained INT spectrum (Figure 5.4b) via EasySpin yields as best fit parameters the values listed in Table 5.2. To enhance signal-to-noise quality several EPR scans were coadded and only part of the magnetic field range in Figure 5.4a has been recorded for evaluation of  $c_{\text{INT}}/c_{\text{CIP}}$ . Coaddition of 10 EPR scans results in the spectrum illustrated by the gray line in Figure 5.4c. The green line in Figure 5.4c represents the sum of simulated CIP and INT spectra.

The concentration ratio  $c_{\text{INT}}/c_{\text{CIP}}$  was obtained from the ratio of the double integrals of the simulated INT and CIP contributions of each EPR spectrum. This ratio was determined at several points in time during the reaction of CPDB and AIBN at temperatures between 60 and 100 °C. Spectral analysis was carried out using the MATLAB code given in Appendix B.

The resulting numbers for 80 °C are plotted in Figure 5.5. The ratio  $c_{\text{INT}}/c_{\text{CIP}}$  does not, at least not significantly, vary with reaction time. No decay of  $c_{\text{INT}}/c_{\text{CIP}}$  is seen at 80 °C up to 4000 s, where about 50 % of initial AIBN has undergone thermal decomposition. The scattering of the  $c_{\text{INT}}/c_{\text{CIP}}$  data increases toward higher CPDB concentration, as the concentrations of INT and CIP become more dissimilar. At identical temperature, the scattering is lower for  $c_{\text{INT}}/c_{\text{CIP}}$  being close to unity, as the deconvolution procedure is associated with smaller uncertainty in case of similar INT and CIP concentrations. At lower temperatures, longer reaction periods have been selected and more EPR scans were taken.

At temperatures between 60 and 100 °C no  $c_{\text{INT}}/c_{\text{CIP}}$  decrease has been observed, which indicates that the RAFT agent is not measurably consumed by cross-termination or self-termination reactions of INT. Thus  $K_{\text{eq}}$  may be deduced from Equation 3.3, i. e., from the slope to the straight-line plot of  $c_{\text{INT}}/c_{\text{CIP}}$  versus  $c_{\text{CPDB}}$ . RAFT equilibrium constants determined for the temperature range 60 to 100 °C are listed in Table 5.3. Plotted in Figure 5.6 is an Arrhenius-type representation of  $K_{\text{eq}}$  with the associated difference in activation energies for  $k_{\text{ad}}$  and  $k_{\beta}$  being  $E_{\text{a}}(K_{\text{eq}}) = E_{\text{a}}(k_{\text{ad}}) - E_{\text{a}}(k_{\beta}) = (-28 \pm 4) \text{ kJ} \cdot \text{mol}^{-1}$ .

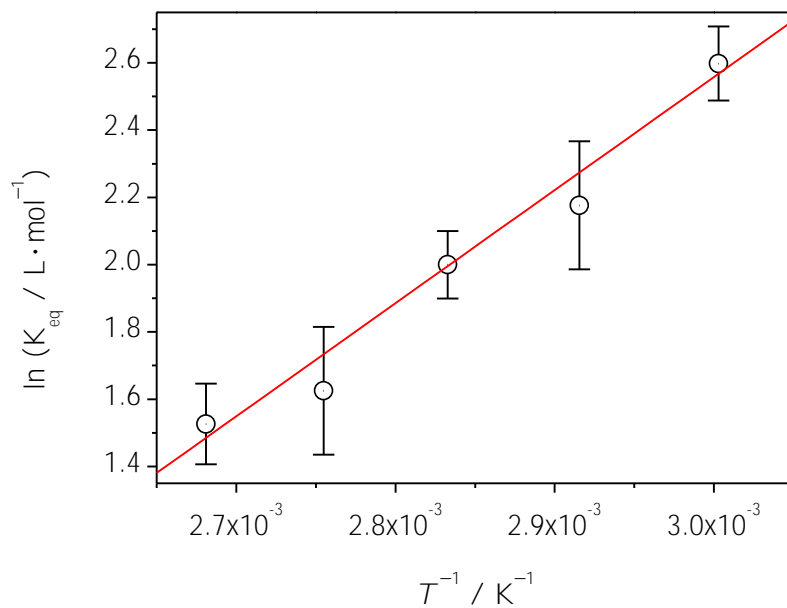
(II) The  $c_{\text{INT}}/c_{\text{CIP}}$  does not decrease during the reaction and the EPR approach using Equation 3.3 to determine  $K_{\text{eq}}$  should therefore be valid. Nevertheless, Junkers *et al.*<sup>[107]</sup> claimed that this EPR approach would be model dependent and that the data could be equally well fitted by assuming slow addition of radicals to the RAFT agent in conjunction with slow fragmentation of the so-obtained intermediate radical as well as a high cross-termination rate. The method for disproving this assumption is straight-forward: The amount of cross-termination products in the composition of the product mixture of AIBN and CPDB in toluene has to be analyzed. Subsequently, this amount is compared to the amount of cross-termination products expected when the SF and the IRT model are assumed at the same time.



**Figure 5.5.** Ratios of radical concentration,  $c_{\text{INT}}/c_{\text{CIP}}$ , plotted versus reaction time for different initial CPDB concentrations:  $c_{\text{CPDB}}/\text{mol} \cdot \text{L}^{-1} = 0.12$  (squares), 0.30 (circles), 0.48 (triangles), 0.60 (stars) at 80 °C. The black line for  $t = 0$  indicates the linear regression of  $c_{\text{INT}}/c_{\text{CIP}}$  versus  $c_{\text{CPDB}}$  according to Equation 3.3 with  $c_{\text{INT}}/c_{\text{CIP}}$  being obtained as the arithmetic mean value over the full reaction time period of each experiment, as represented by the gray lines. The time period up to 4000 s roughly corresponds to the decomposition half-life of AIBN at 80 °C.

**Table 5.3.** Equilibrium constants obtained at temperatures from 60 to 100 °C.

$T / ^\circ\text{C}$	$K_{\text{eq}} / \text{L} \cdot \text{mol}^{-1}$
60	$13 \pm 1$
70	$9 \pm 1$
80	$7.4 \pm 0.7$
90	$5.1 \pm 0.9$
100	$4.6 \pm 0.5$

**Figure 5.6.** Arrhenius-type plot of  $K_{\text{eq}}$  in the temperature range 60 to 100 °C. The difference in activation energies of  $k_{\text{ad}}$  and  $k_{\beta}$ ,  $E_{\text{a}}(K_{\text{eq}}) = -28.4 \text{ kJ} \cdot \text{mol}^{-1}$ , has been determined from the slope to the linear regression (gray line).

**Table 5.4.** Product composition of a solution of CPDB ( $0.75 \text{ mol} \cdot \text{L}^{-1}$ ) and AIBN ( $0.30 \text{ mol} \cdot \text{L}^{-1}$ ) in toluene after stirring for 18 h at  $80 \text{ }^\circ\text{C}$ .

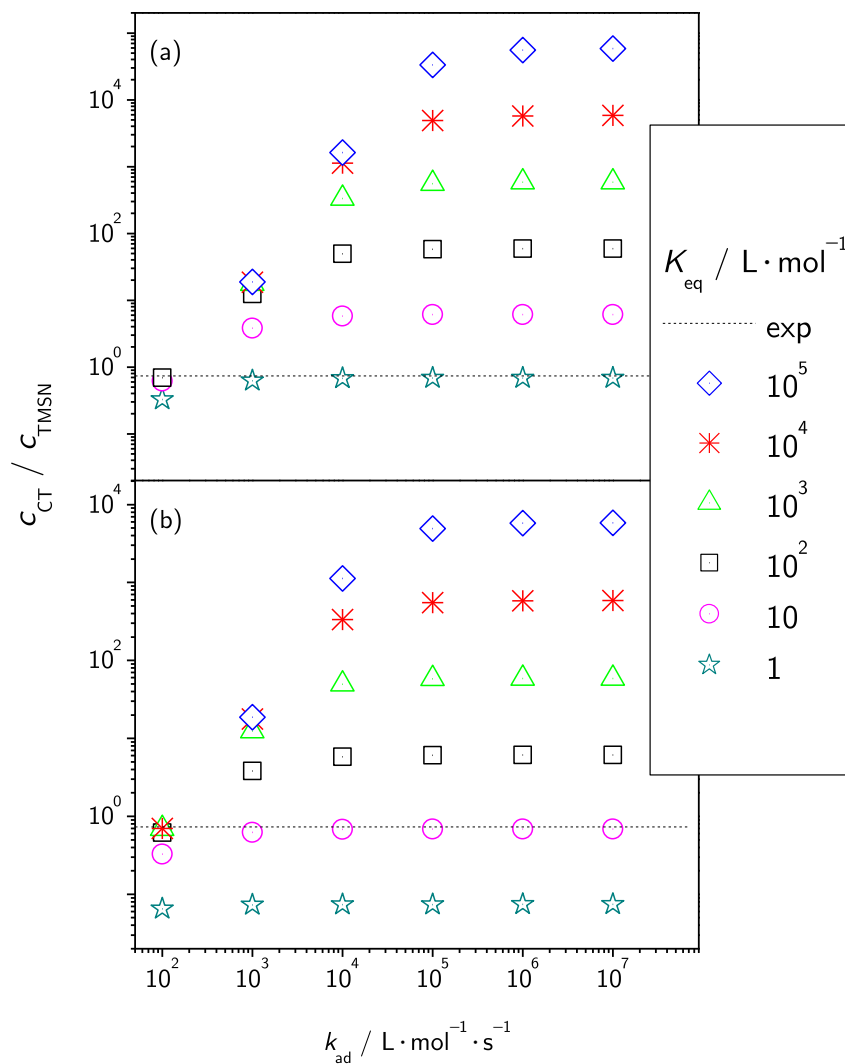
product	AIBN	CPDB	TMSN	CT1	CT3	CPDB*
percentage in product mixture	0	71	15	3	8	3

Table 5.4 shows the product composition, analyzed by  $^1\text{H}$  NMR, after stirring a solution of  $0.75 \text{ mol} \cdot \text{L}^{-1}$  CPDB and  $0.30 \text{ mol} \cdot \text{L}^{-1}$  AIBN in toluene for 18 h at  $80 \text{ }^\circ\text{C}$ . In what follows, it will be shown that these numbers prove cross-termination to be no important reaction channel as compared to addition and fragmentation.

The ratio of cross-termination products to products resulting from CIP combination,  $c_{\text{CT}}/c_{\text{TMSN}}$ , is 0.73 with  $c_{\text{CT}}$  being the sum of  $c_{\text{CT1}}$  and  $c_{\text{CT3}}$ . This measured ratio may be compared to the ratio, which is estimated by PREDICI<sup>®</sup> simulation of experimental  $c_{\text{INT}}/c_{\text{CIP}}$  data adopting a range of  $K_{\text{eq}}$  and  $k_{\text{ad}}$  values and using a) the cross-termination rate coefficient suggested by Junkers *et al.*,<sup>[107]</sup>  $k_{\text{t}}^{\text{cross}} = 1.0 \times 10^9 \text{ L} \cdot \text{mol}^{-1} \cdot \text{s}^{-1}$  as well as b)  $k_{\text{t}}^{\text{cross}} = 1.0 \times 10^8 \text{ L} \cdot \text{mol}^{-1} \cdot \text{s}^{-1}$ . The  $k_{\text{t}}^{\text{cross}}$  value has been varied for illustrating the impact on the concentration of cross-termination products. The comparison is shown in Figure 5.7. The experimental  $c_{\text{CT}}/c_{\text{TMSN}}$  ratio at  $80 \text{ }^\circ\text{C}$  is represented by the dotted line.

Figure 5.7 demonstrates that – if SF and IRT are operative at the same time as stated by Junkers *et al.*<sup>[107]</sup> – experimental data can only be fitted assuming an unrealistically low  $k_{\text{ad}}$  values of  $1.0 \times 10^2 \text{ L} \cdot \text{mol}^{-1} \cdot \text{s}^{-1}$ . Even for  $k_{\text{ad}} = 1.0 \times 10^3 \text{ L} \cdot \text{mol}^{-1} \cdot \text{s}^{-1}$ ,  $c_{\text{CT}}$  should be at least 10 times larger than  $c_{\text{TMSN}}$ , i. e.,  $c_{\text{CT}}/c_{\text{TMSN}}$  should be above 10, which disagrees with the experimental  $c_{\text{CT}}/c_{\text{TMSN}}$  being below unity. For more realistic  $k_{\text{ad}}$  values, i. e., of  $k_{\text{ad}}$  above  $1.0 \times 10^5 \text{ L} \cdot \text{mol}^{-1} \cdot \text{s}^{-1}$ , TMSN should be virtually absent for  $K_{\text{eq}}$  above  $10^4$ . The closest match between experimental and simulated  $c_{\text{CT}}/c_{\text{TMSN}}$  is found for  $K_{\text{eq}} = 1.0 \text{ L} \cdot \text{mol}^{-1}$  and  $K_{\text{eq}} = 10 \text{ L} \cdot \text{mol}^{-1}$  with  $k_{\text{t}}^{\text{cross}} = 1.0 \times 10^9 \text{ L} \cdot \text{mol}^{-1} \cdot \text{s}^{-1}$  (Figure 5.7a) and  $k_{\text{t}}^{\text{cross}} = 1.0 \times 10^8 \text{ L} \cdot \text{mol}^{-1} \cdot \text{s}^{-1}$  (Figure 5.7b), respectively. If one assumes  $K_{\text{eq}}$  to be above  $10 \text{ L} \cdot \text{mol}^{-1}$ , experimental  $c_{\text{CT}}/c_{\text{TMSN}}$  may only be fitted by lowering  $k_{\text{t}}^{\text{cross}}$  by orders of magnitude. Thus high  $K_{\text{eq}}$  in conjunction with high  $k_{\text{t}}^{\text{cross}}$ , as claimed by Junkers *et al.*,<sup>[107]</sup> is not in agreement with experimental data.

In an attempt to check for consistency of the strategy of deducing  $K_{\text{eq}}$  from Equation 3.3, the size of the individual terms on the r. h. s. of Equation 3.1 have been estimated. These terms refer to the rates of addition, fragmentation and cross-



**Figure 5.7.** Dependence of the ratio  $c_{CT}/c_{TMSN}$  on  $k_{ad}$  and  $K_{eq}$  for  $c_{CPDB} = 0.75 \text{ mol} \cdot \text{L}^{-1}$ ,  $c_{AIBN} = 0.30 \text{ mol} \cdot \text{L}^{-1}$ , assuming a)  $k_t^{\text{cross}} = k_t = 1.0 \times 10^9 \text{ L} \cdot \text{mol}^{-1} \cdot \text{s}^{-1}$  and b)  $k_t^{\text{cross}} = 0.10 \times k_t = 1.0 \times 10^8 \text{ L} \cdot \text{mol}^{-1} \cdot \text{s}^{-1}$ . Note that at constant  $k_{ad}$  increasing  $K_{eq}$  goes with a lowering of  $k_{\beta}$ . Scheme 5.4 and the literature  $k_d$  value<sup>[151]</sup> were used for PREDICI<sup>®</sup> simulation.



termination, respectively. The radical concentrations  $c_{\text{INT}}$  and  $c_{\text{CIP}}$  do not exceed  $1.0 \times 10^{-6} \text{ mol} \cdot \text{L}^{-1}$  whereas  $c_{\text{CPDB}}$  will be above  $0.1 \text{ mol} \cdot \text{L}^{-1}$ . The maximum value of  $k_{\text{t}}^{\text{cross}}$  should be  $1.0 \times 10^9 \text{ L} \cdot \text{mol}^{-1} \cdot \text{s}^{-1}$ . Adopting  $k_{\text{ad}}$  to be  $1.0 \times 10^6 \text{ L} \cdot \text{mol}^{-1} \cdot \text{s}^{-1}$  or higher, as is indicated by the quantum-chemical calculations,<sup>[38]</sup> in conjunction with the experimental  $K_{\text{eq}} = (7.4 \pm 0.7) \text{ L} \cdot \text{mol}^{-1}$ , yields a fragmentation rate coefficient of  $k_{\beta} \approx 10^5 \text{ s}^{-1}$ . The resulting rates of addition, fragmentation and cross-termination (in  $\text{mol} \cdot \text{L}^{-1} \cdot \text{s}^{-1}$ ) are:  $r_{\text{ad}} = r_{\beta} \approx 10^{-1} \gg r_{\text{t}}^{\text{cross}} \approx 10^{-3}$ . On the basis of the  $K_{\text{eq}}$  value at  $80 \text{ }^{\circ}\text{C}$  (see Table 5.3), these numbers demonstrate that cross-termination rate is negligible as compared to both the rate of addition and of fragmentation.

It should be noted that the rate of the “missing step” reaction (VIIIb in Scheme 5.5), which contributes another term to the r. h. s. of Equation 3.1, is even smaller than the one of cross-termination. This “missing step” rate can be estimated from  $r_{\text{MS2}} = k_{\text{MS2}} \times c_{\text{CIP}} \times c_{\text{CT2}}$ . For an upper limiting value of  $k_{\text{MS2}} = 1.0 \times 10^9 \text{ L} \cdot \text{mol}^{-1} \cdot \text{s}^{-1}$ , PREDICI<sup>®</sup> simulation predicts  $c_{\text{CT2}}$  to be below  $1.0 \times 10^{-7} \text{ mol} \cdot \text{L}^{-1}$ . Thus  $r_{\text{MS2}}$  should not exceed  $1.0 \times 10^{-4} \text{ mol} \cdot \text{L}^{-1} \cdot \text{s}^{-1}$ .

From Figure 5.7 it becomes clear that assuming SF *and* IRT can only match experimental data if  $k_{\text{ad}} \leq 10^2 \text{ L} \cdot \text{mol}^{-1} \cdot \text{s}^{-1}$ . However, no experimental evidence for slow addition of CIP to dithiobenzoates has been put forward so far. If  $k_{\text{ad}}$  were of such small size, the addition of the CIP radical to the C=S double bond would be slower than to a C=C double bond.<sup>[131]</sup> One would however expect the opposite to be true, since the barrier for addition of a radical to a C=S double bond is below the one for addition to a C=C bond:<sup>[152]</sup> For methyl radical addition to  $\text{CH}_2 = \text{CH}_2$  and  $\text{CH}_2 = \text{S}$  at 0 K, reaction barriers of  $\Delta H_0^{\ddagger} = 38.4 \text{ kJ} \cdot \text{mol}^{-1}$  and  $\Delta H_0^{\ddagger} = 9.0 \text{ kJ} \cdot \text{mol}^{-1}$ , respectively, have been calculated using high-level *ab initio* calculations. As a consequence, the addition of a radical to the C=S bond is by about three orders of magnitude faster than addition to the C=C bond of alkenes.<sup>[152]</sup>

Junkers *et al.*<sup>[107]</sup> try to assign the suggested low  $k_{\text{ad}}$  to the homoanomeric effect, i. e., to the electron-withdrawing cyano group of the CIP radical which reduces the ability of sulfur to stabilize the resulting intermediate radical via lone pair donation. They suggest that pseudo- $\pi$  acceptance by the antibonding orbital of the C=S bond weakens the forming bond and increases the barrier for addition. *Ab initio* calculations however do not predict this homoanomeric effect, e. g., for the addition of CIP to a dithiobenzoate RAFT agent bearing methyl as the Z-group,  $k_{\text{ad}} = 8.29 \times 10^5 \text{ L} \cdot \text{mol}^{-1} \cdot \text{s}^{-1}$  has been calculated for  $60 \text{ }^{\circ}\text{C}$ .<sup>[38]</sup> With phenyl being the Z-group of the dithiobenzoates, as in the CIP/CPDB system, the intermediate radical should exhibit even better stabilization and  $k_{\text{ad}}$  values in the order of  $1.0 \times 10^6 \text{ L} \cdot \text{mol}^{-1} \cdot \text{s}^{-1}$  must be expected.

From the transfer coefficient for CIP to poly(methyl methacrylate) dithiobenzoate at  $60 \text{ }^{\circ}\text{C}$ , determined by Chong *et al.*, a  $k_{\text{ad}}$  value of  $7.2 \times 10^5 \text{ L} \cdot \text{mol}^{-1} \cdot \text{s}^{-1}$  can be

estimated.<sup>[74]</sup> In addition, Houshyar *et al.* investigated the single unit monomer insertion into a cyano-*iso*-propyl trithiocarbonate.<sup>[150]</sup> Their kinetic simulations resulted in a value of  $1.0 \times 10^4 \text{ L} \cdot \text{mol}^{-1} \cdot \text{s}^{-1}$  for the addition of CIP to the trithiocarbonate. EPR-derived  $k_{\text{ad}}$  values for trithiocarbonate- and dithiobenzoate-mediated *n*-butyl acrylate polymerizations suggest that the addition of a radical to a trithiocarbonate is about one order of magnitude slower than the addition to a dithiobenzoate (see Chapter 4). Hence, these experimental results are also indicating a minimum  $k_{\text{ad}}$  value of at least  $10^5 \text{ L} \cdot \text{mol}^{-1} \cdot \text{s}^{-1}$ .

If the barrier for addition of CIP would be enhanced by a homoanomeric effect, similar behavior would be expected for methacrylates and acrylates, as the carbonyl moiety is also electron withdrawing. Slow addition would be associated with poor control of dithiobenzoate-mediated (meth)acrylate polymerization, which is not what is experimentally found. Moreover, this argument would not be in line with the high addition rate coefficients from experiment and calculation: The reported experimental values are  $1.5 \times 10^6 \text{ L} \cdot \text{mol}^{-1} \cdot \text{s}^{-1}$  for addition of a methyl acrylate radical to a dithioacetate at 80 °C,<sup>[153]</sup> and  $2.0 \times 10^6 \text{ L} \cdot \text{mol}^{-1} \cdot \text{s}^{-1}$ ,<sup>[153]</sup>  $1.7 \times 10^6 \text{ L} \cdot \text{mol}^{-1} \cdot \text{s}^{-1}$ <sup>[154]</sup> and  $2.4 \times 10^6 \text{ L} \cdot \text{mol}^{-1} \cdot \text{s}^{-1}$ ,<sup>[155]</sup> respectively, for methyl acrylate, butyl acrylate, and dodecyl acrylate radicals adding to a trithiocarbonate. The values were determined from the analysis of molar mass versus monomer conversion plots of RAFT-mediated polymerizations displaying hybrid behavior.

These high  $k_{\text{ad}}$  values are confirmed by direct time-resolved observation of intermediate radical concentration in RAFT-mediated *n*-butyl acrylate polymerizations via EPR detection after almost instantaneous production of primary photoinitiator-derived radicals. These experiments also demonstrate that the peak concentration of radicals is reached a few milliseconds after applying the laser pulse and the intermediate radical concentration starts to decline immediately (see Section 4.3). A  $k_{\text{ad}}$  value as low as suggested by Junkers *et al.*<sup>[107]</sup> would result in a significantly slower increase of INT concentration. It would take several seconds to reach the maximum radical concentration, if  $k_{\text{ad}}$  were around  $10^5 \text{ L} \cdot \text{mol}^{-1} \cdot \text{s}^{-1}$ , and minutes if  $k_{\text{ad}}$  were of the order of  $10^3 \text{ L} \cdot \text{mol}^{-1} \cdot \text{s}^{-1}$ .

The EPR-derived values for addition rate coefficients are close to the *ab initio* values for addition of several small radicals to RAFT agents.<sup>[38]</sup> The entire body of existing experimental evidence supports  $k_{\text{ad}}$  to be of the order of  $10^5$  to  $10^6 \text{ L} \cdot \text{mol}^{-1} \cdot \text{s}^{-1}$  at the reaction conditions of our experiment and thus disagrees with the assumption made by Junkers *et al.* of  $k_{\text{ad}}$  being around  $10^3 \text{ L} \cdot \text{mol}^{-1} \cdot \text{s}^{-1}$ .

## 5.3 Phenylethyl/1-phenylethyl dithiobenzoate

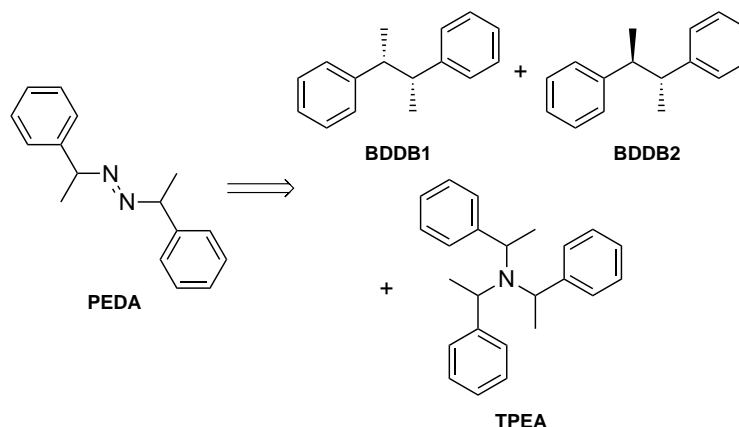
The above-described model reactions are essential for testing *ab initio* methods. However, TB and CIP are non-monomeric radicals, which makes direct comparison with RAFT polymerizations difficult. Therefore, an additional model system, phenylethyl radical/phenylethyl dithiobenzoate, has been investigated. The phenylethyl radical (PE) – which is equivalent to the styrene radical – is of particular interest, as the controversy concerning rate retardation is mainly based on different evaluation procedures of experimental data from dithiobenzoate-mediated styrene polymerizations.<sup>[42–44,46,48,50,57,58,64,84,90,94,109,110,156–159]</sup>

Under polymerization conditions, styrene radicals are barely detectable via EPR spectroscopy.<sup>[160,161]</sup> The equilibrium constant is therefore not accessible via the strategies outlined in Chapter 4. The problems met with the styrene radical relate to the fact that hyperfine coupling with the aromatic and vicinal hydrogen atoms leads to a multi-line spectrum. This dramatically reduces the intensity of each line, which makes some kinetic investigations, like  $k_t$  measurements, nearly impossible. Using deuterated compounds is one approach to reduce the number of EPR lines.<sup>[162,163]</sup> Hyperfine coupling of the radical with a deuterium atom is only  $1/6.5$  of that with a proton,<sup>[164]</sup> so that more lines are condensed into a single line. The drawbacks of this strategy are the high cost of deuterated chemicals and, more importantly, that an impact of C–D bonds on the rate coefficients cannot be ruled out. For example, Clouet *et al.*<sup>[165]</sup> observed a 1.2 times higher  $k_p$  value for styrene- $d_8$  than for normal styrene.

### 5.3.1 Investigation of initiator kinetics

Using a model reaction allows for producing significantly higher radical concentrations than in the presence of monomer, where polymerization would proceed far too rapidly for recording EPR spectra. An appropriate initiator for producing high PE radical concentrations is *meso*-1,2-bis(1-phenylethyl)diazene (PEDA). Its decomposition mechanism has not been thoroughly investigated before. For that purpose, degassed solutions of the initiator in toluene were stirred under an argon atmosphere at 80, 100 and 110 °C, respectively. Subsequently, the solvent and volatile products were removed under reduced pressure and the product mixture was analyzed by NMR spectroscopy and mass spectrometry (see Section 7.3.5). The resulting products are depicted in Scheme 5.6 and their fractions at each reaction temperature are listed in Table 5.5.

At 110 °C only the expected products 2,3-butane-2,3-diylidibenzene 1 and 2 (BDDDB1, BDDDB2) are found. They are formed via termination by combination of two PE radicals. The lower the temperature, however, the higher is the amount of a by-product, which according to NMR data could be tris(1-phenylethyl)amine (TPEA). 2D



**Scheme 5.6.** PEDA decomposition products found after stirring the initiator solution in toluene at 80, 100 and 110 °C for 20 h. BDDDB1 and BDDDB2: 2,3-butane-2,3-diyl dibenzene; TPEA: tris(1-phenylethyl)amine.

**Table 5.5.** PEDA decomposition products found after stirring the initiator solution in toluene at different temperatures.

$T / ^\circ\text{C}$	product fraction in %		
	BDDDB1	BDDDB2	TPEA
80	10.5	10.5	79.0
100	39.2	40.8	20.0
110	48.0	52.0	0

NMR spectra show that the methyl and methine protons correlate with the aromatic carbons and the nitrogen. Based on the connectivity of the atoms three structures are possible, but because of the chemical shifts in the  $^1\text{H}$  and  $^{13}\text{C}$  NMR spectra and the lack of correlations of nitrogen with other protons, 1-phenylethylamine and *N,N*-bis(1-phenylethyl)amine can be ruled out (see Section 7.3.5). Further confirmation of the structure by mass spectrometry was not possible. A molecular ion peak was not observed, due to the instability of the compound.

The formation of TPEA probably follows the mechanism outlined in Scheme 5.2 for decomposition of 1,2-di-*tert*-butyldiazene: A nitrogen-centered radical bearing two PE units may be formed, which acts as a spin trap. Reaction of this spin trap with a PE radical affords TPEA.

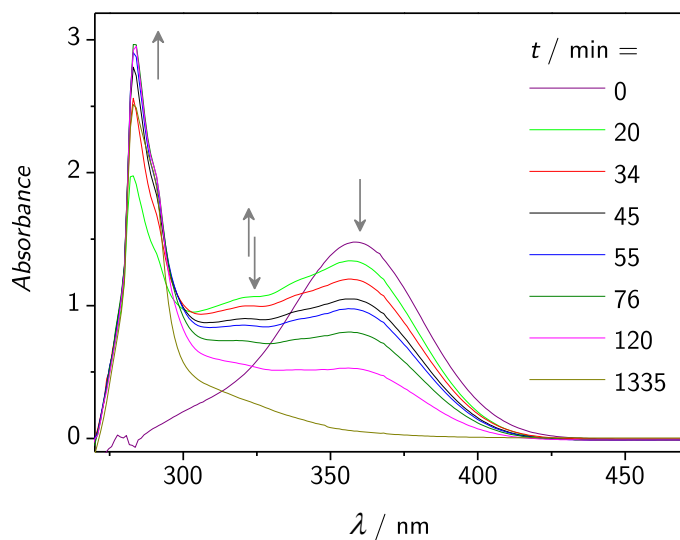


**Figure 5.8.** UV/VIS spectra recorded during the decomposition of  $3.2 \times 10^{-2} \text{ mol} \cdot \text{L}^{-1}$  PEDA in toluene under an argon atmosphere at 110 °C. The time period depicted is 22 h. The arrows indicate the formation of products BDDB1 and BDDB2 at 283 nm, the formation and subsequent decay of an intermediate product at 315 nm, and the decay of the initiator at 358 nm.

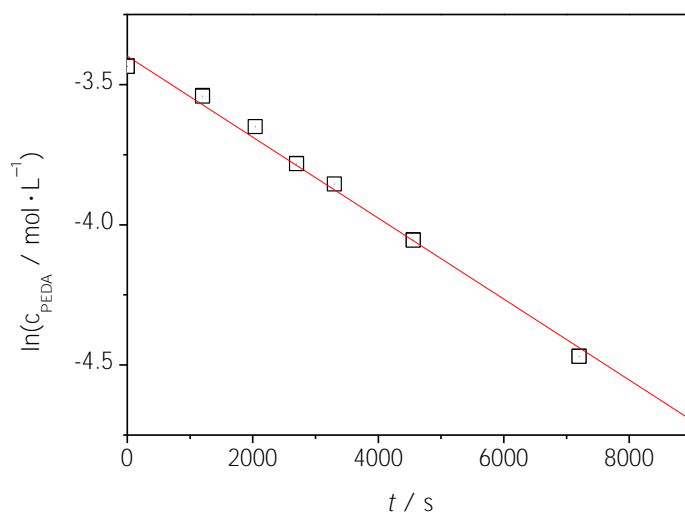


**Figure 5.9.** First order  $\ln(c_{\text{PEDA}})$ -versus-time plot for the decomposition of  $3.2 \times 10^{-2} \text{ mol} \cdot \text{L}^{-1}$  PEDA in toluene at 110 °C.

The occurrence of radicals others than the PE radical could lead to unexpected reactions with the RAFT agent or the intermediate radical. This potentially interferes with  $K_{\text{eq}}$  evaluation via Equation 3.3. All experiments were therefore carried out at 110 °C. Decomposition of PEDA at 110 °C has, however, not been investigated so far. Cohen and Wang<sup>[166]</sup> determined the rates of PEDA decomposition in toluene at 43 and 53 °C by measuring the volume of evolved nitrogen as a function of time. Extrapolation of their values to 110 °C gives  $k_{\text{d}} = 9.75 \times 10^{-2} \text{ s}^{-1}$ . However, below 110 °C the concentration of produced  $\text{N}_2$  is most likely not proportional to the concentration of decomposed initiator, as significant amounts of the side product TPEA are formed (see Scheme 5.6 and Table 5.5). Consequently, the data might be erroneous and should not be used for extrapolation to higher temperatures. In this work, the initiator decomposition rate coefficient was determined by UV/VIS spectroscopy monitoring the decay in absorption of the N=N double bond at  $\lambda = 358 \text{ nm}$ .

The spectral series for the decomposition of  $3.2 \times 10^{-2} \text{ mol} \cdot \text{L}^{-1}$  PEDA in toluene under argon atmosphere at 110 °C shown in Figure 5.8 covers a time period of 22 h. The solution was degassed by three freeze–pump–thaw cycles prior to the experiment. As indicated by the arrows, formation of products BDDB1 and BDDB2 is responsible for the growing peak at 283 nm. The barely discernible absorbance at 315 nm is presumably due to an intermediate product, which disappears completely after 2 h.

According to the Beer-Lambert law,<sup>[167]</sup> the characteristic absorbance of a species is proportional to its concentration. The absorbances obtained from the spectra of PEDA decomposition allow for the determination of  $k_{\text{d}}$  by plotting  $\ln(c_{\text{PEDA}})$  versus time. From the slope of the straight line in Figure 5.9 the coefficient  $k_{\text{d}} = (1.3 \pm 0.2) \times 10^{-4} \text{ s}^{-1}$  is obtained at 110 °C. This value differs by more than two orders of magnitude from  $k_{\text{d}} = 9.75 \times 10^{-2}$ , which was extrapolated from the decomposition rates determined by Cohen and Wang<sup>[166]</sup> at 43 and 53 °C. This discrepancy is probably due to the fact, that the extrapolation over a wide temperature range is associated with a high degree of uncertainty. In addition, the data at 43 and 53 °C is probably erroneous because of the side reactions of the initiator, which were not taken into account by Cohen and Wang. In the following,  $k_{\text{d}} = 1.3 \times 10^{-4} \text{ s}^{-1}$  will therefore be used for evaluating further kinetic data.

As the next step, termination kinetics of the PE radical are investigated. Figure 5.11a illustrates the PE spectrum at 110 °C in toluene, which may be simulated using the coupling constants listed in Table 5.6 that are close to the numbers reported in the literature.<sup>[162]</sup> Recording consecutive spectra during PEDA decomposition yields the PE concentration-versus-time plot shown in Figure 5.10. The experimental concentration profile was simulated with PREDICI<sup>®</sup> to give the first EPR-derived rate coefficient for the termination of two styrene radicals of chain length unity,  $k_{\text{t}}^{1,1}$ . The value of  $3.25 \times 10^{10} \text{ L} \cdot \text{mol}^{-1} \cdot \text{s}^{-1}$  is close to the diffusion-controlled rate coefficient,

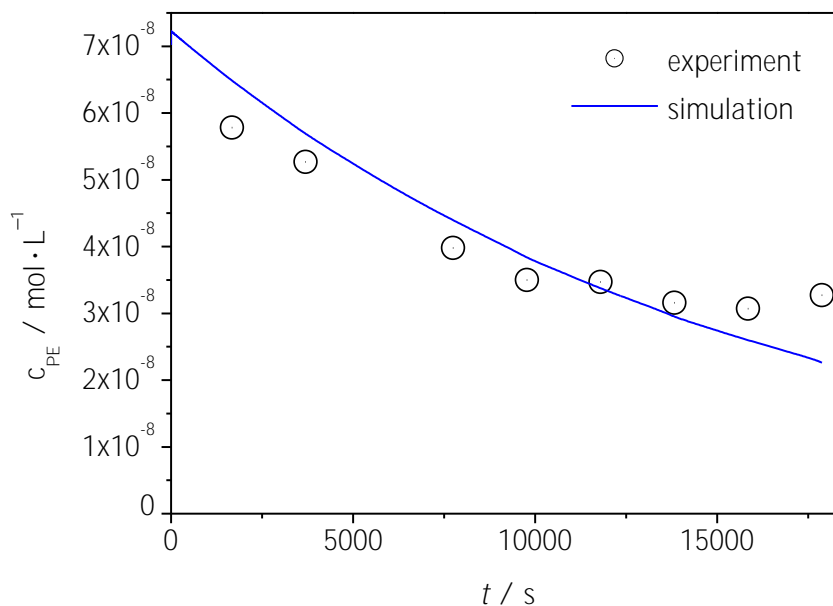


**Figure 5.10.** Experimental and simulated decay of PE radical concentration for a solution containing  $1.3 \text{ mol} \cdot \text{L}^{-1}$  PEDA in toluene at  $110 \text{ }^\circ\text{C}$  for determining  $k_t$ .

$k_{\text{diff}} = 3.38 \times 10^{10} \text{ L} \cdot \text{mol}^{-1} \cdot \text{s}^{-1}$ , which was estimated from the Smoluchowski and Stokes-Einstein equation via<sup>[168]</sup>

$$k_{\text{diff}} = \frac{8RT}{3\eta} \quad (5.1)$$

where  $R$  is the gas constant and  $\eta$  the viscosity of toluene at  $110 \text{ }^\circ\text{C}$ , which was taken from the literature.<sup>[169]</sup> The close match between the experimental  $k_t^{1,1}$  and the calculated  $k_{\text{diff}}$  indicates that the termination between two PE radicals is a diffusion-controlled process. This is due to the stability of the radical by delocalization into the aromatic ring so that almost all collisions of two PE radicals lead to reaction.

**Table 5.6.** Coupling constants deduced from the experimental spectra of PE and INT at 110 °C.

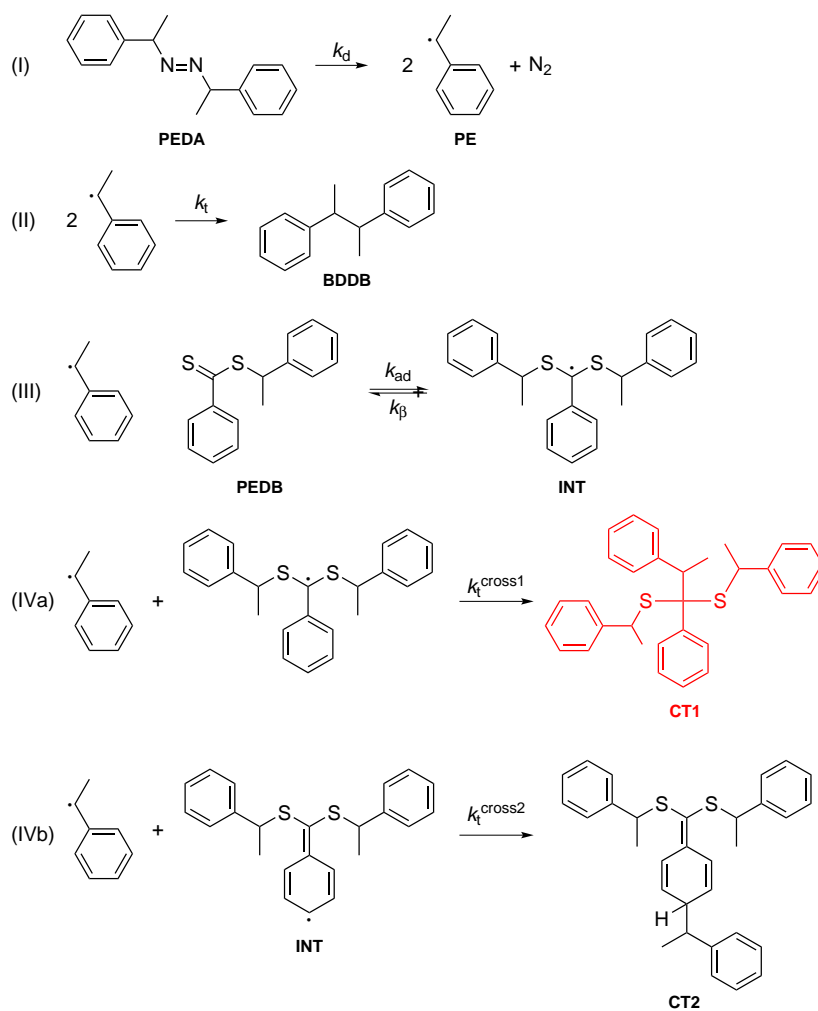
radical	coupling constants / G				
PE	$a_{\text{H},\alpha}$	$a_{\text{H},\beta}$	$a_{\text{H},meta}$	$a_{\text{H},ortho}$	$a_{\text{H},para}$
	16.7	17.8	1.7	4.9	6.1
INT	$a_{\text{H},\gamma}$	$a_{\text{H},meta}$	$a_{\text{H},ortho}$	$a_{\text{H},para}$	
	0.4	1.3	3.7	4.2	

### 5.3.2 Determination of the equilibrium constant

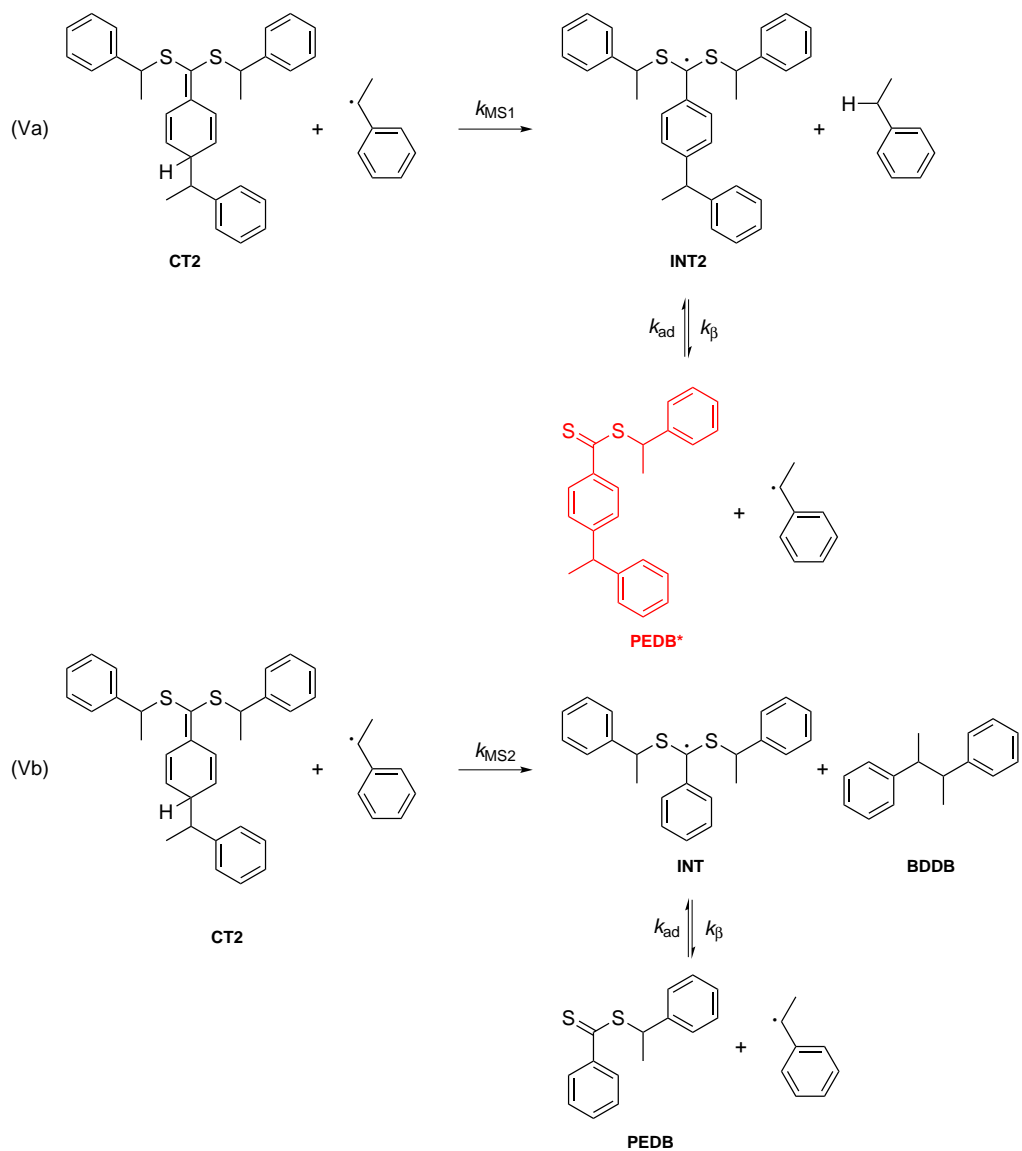
In order to establish a mechanistic model for the reaction of PEDA and PEDB in toluene at 110 °C, the product mixture was analyzed. The experimental procedure as well as the NMR and mass spectrometry data of the entire set of products are given in Section 7.3.6. The kinetic scheme 5.7 involves decomposition of the initiator (I), termination of two PE radicals (II), addition of PE to the RAFT agent PEDB and fragmentation of the resulting INT species (III), cross-termination between PE and INT (IVa and IVb), as well as “missing step” reactions (Va and Vb). Products resulting from other cross-termination reactions have not been detected at 110 °C. The product resulting from a hydrogen shift in CT2 which was detected in the CIP/CPDB reaction is missing (see Scheme 5.5). Below 110 °C additional side products were found. These side products have not been characterized so far. Furthermore, the main product of initiator decomposition at 80 °C, TPEA, is not formed in the presence of RAFT agent.

When 0.43 mol · L<sup>-1</sup> PEDA and 0.43 mol · L<sup>-1</sup> PEDB were stirred in toluene at 110 °C up to complete decomposition of the initiator, 23 % of the product mixture was made up of CT1 compared to 44 % PEDB, 3 % PEDB\*, and 30 % BDDDB1 and BDDDB2. Thus, a higher amount of cross-termination product CT1 is formed than in the CIP/CPDB model experiment, which means that reaction step IVa plays an important role in the PE/PEDB system. Formation of a cross-termination product is in accordance with the study of de Brouwer *et al.*,<sup>[170]</sup> who reported the occurrence of a three-arm star after irradiating polystyryl dithiobenzoate with UV light in a monomer-free model experiment. Another model experiment conducted by Kwak *et al.*<sup>[90]</sup> also gave rise to a three-arm species. When polystyryl dithiobenzoate reacted with polystyryl radicals (produced from an ATRP initiator) a stable compound of threefold molecular weight was detected by size-exclusion chromatography. It was shown that the cross-termination reaction is irreversible at 60 °C. Only after 25 h of





**Scheme 5.7.** Kinetic scheme for the model system PE/PEDB. PEDA: *meso*-1,2-bis(1-phenylethyl)diazene; PE: phenylethyl radical; BDDB: 2,3-butane-2,3-diyl-dibenzene; PEDB: 1-phenylethyl dithiobenzoate; INT: intermediate radical; CT1: cross-termination product 1. The side products are highlighted in red.



**Scheme 5.7.** Kinetic scheme for the model system PE/PEDB (continued). CT2: cross-termination product 2; INT2: ring-substituted intermediate radical; PEDB\*: ring-substituted PEDB. The side products are highlighted in red.

heating to 120 °C a slight decrease of the species was observed. One may conclude that the formation of CT1 at the chosen reaction conditions proceeds irreversibly.

The low amount of the “missing step” product PEDB\* as compared to the cross-termination product CT1 indicates that the reaction barrier for cross-termination of PE with the radical site at the carbon between the two sulfur atoms of the INT species is reduced as compared to the cross-termination with CIP. This may be due to the radical delocalization being possible in the case of the PE radical, which is captured rapidly by INT. Subsequent rearrangement of the resulting product affords CT1. In addition, PE is a secondary radical and the cross-termination at the carbon between the two sulfur atoms of the INT is less impeded by steric hindrance.

By analogy to the  $K_{\text{eq}}$  determination of the CIP/CPDB system (see Section 5.2) the radical concentration ratio  $c_{\text{INT}}/c_{\text{PE}}$  was obtained from consecutively recorded EPR spectra during the reaction of PEDA and PEDB in toluene at 110 °C. The EPR signals were not fully separated. Consequently, the strategy applied in Section 5.2 was adopted. First, EPR spectra of the individual compounds were recorded by using conditions where only one radical species was present. The PE spectrum was obtained by monitoring PEDA decomposition in toluene as described above. Employing a high PEDB concentration gave the INT spectrum shown in Figure 5.11b.

To obtain the molar fractions of the individual species, the two-component spectrum is modeled as a linear combination of the individual INT and PE spectra. The least-square fitting was performed using EXCEL. Due to the high signal-to-noise ratio of the experimental PE spectrum, the spectrum was smoothed by applying a Fourier filter prior to the fitting procedure. The simulated spectrum was not used, because it did not entirely match the experimental one. Figure 5.11c proves that this strategy leads to a close agreement between the experimental two-component spectrum and the simulated one.

Figure 5.12 shows the  $c_{\text{INT}}/c_{\text{PE}}$  ratios observed during the reaction for various initial RAFT agent concentrations,  $c_{\text{PEDA}}^0$ . Contrary to the CIP/CPDB system a clear decay of the radical concentration ratio is seen. It is therefore necessary to check whether  $K_{\text{eq}}$  may be calculated from Equation 3.3 since the decay indicates that cross-termination is considerable compared to addition and fragmentation. A first estimate of  $K_{\text{eq}}$  is obtained by extrapolating  $c_{\text{INT}}/c_{\text{PE}}$  to  $t = 0$ . Plotting  $c_{\text{INT}}/c_{\text{PE}}$  versus  $\sqrt{t}$  and  $\ln(c_{\text{INT}}/c_{\text{PE}})$  versus  $t$  (see Figure 5.12a and b, respectively) yields straight line fits. Both methods however have no theoretical basis. Interestingly, plots with almost the same slope (around  $-1.3 \times 10^{-4} \text{ s}^{-1}$ ) are observed in the latter case. The only exception is the data with an initial PEDB concentration of  $4.4 \times 10^{-2} \text{ mol} \cdot \text{L}^{-1}$ . The different slope is due to scattering in  $c_{\text{INT}}/c_{\text{PE}}$  ratios at longer reaction times. A deviation for this concentration is therefore also observed in the  $\ln(c_{\text{INT}}/c_{\text{PE}})$ -versus- $t$  diagram.

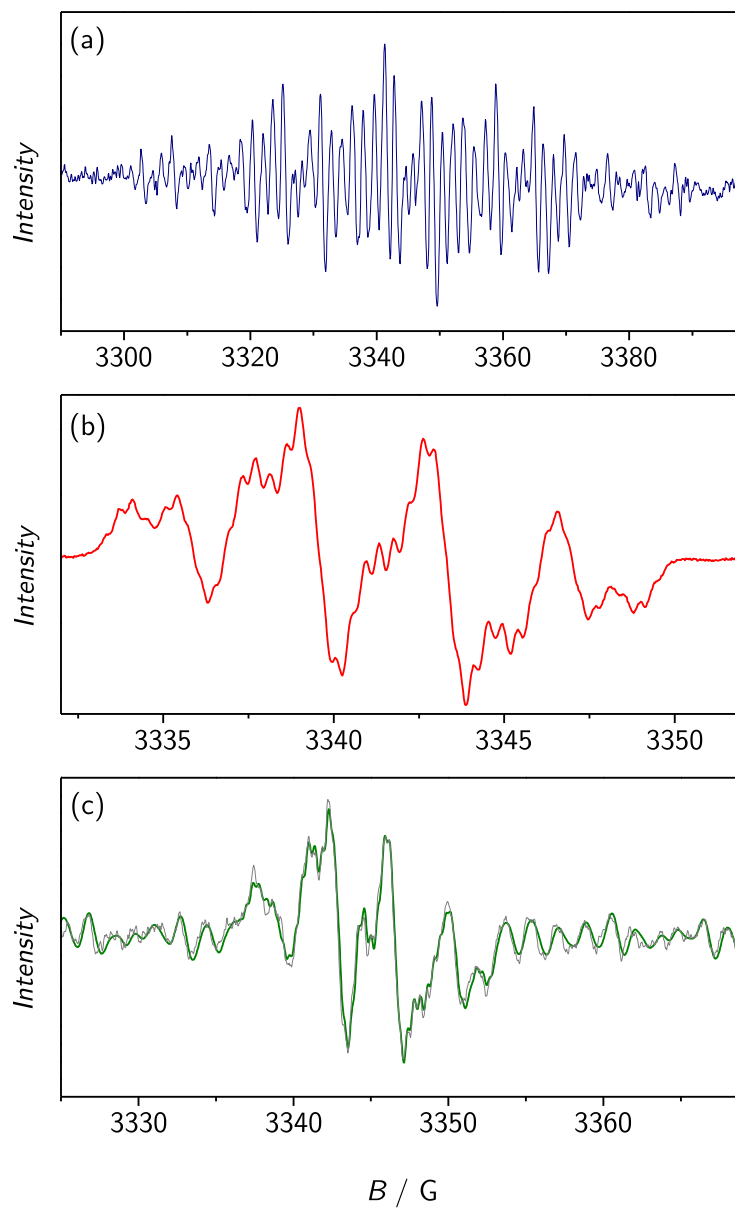


**Figure 5.11.** (a) Spectrum of the PE radical; (b) spectrum of INT; (c) best fit and experimental spectrum of INT and PE obtained by co-addition of 8 EPR scans at 110 °C, a RAFT agent concentration of  $c_{\text{PEDB}} = 5.6 \times 10^{-2} \text{ mol} \cdot \text{L}^{-1}$ , and an initiator concentration of  $c_{\text{PEDA}} = 0.8 \text{ mol} \cdot \text{L}^{-1}$ . Note the different abscissa scales.

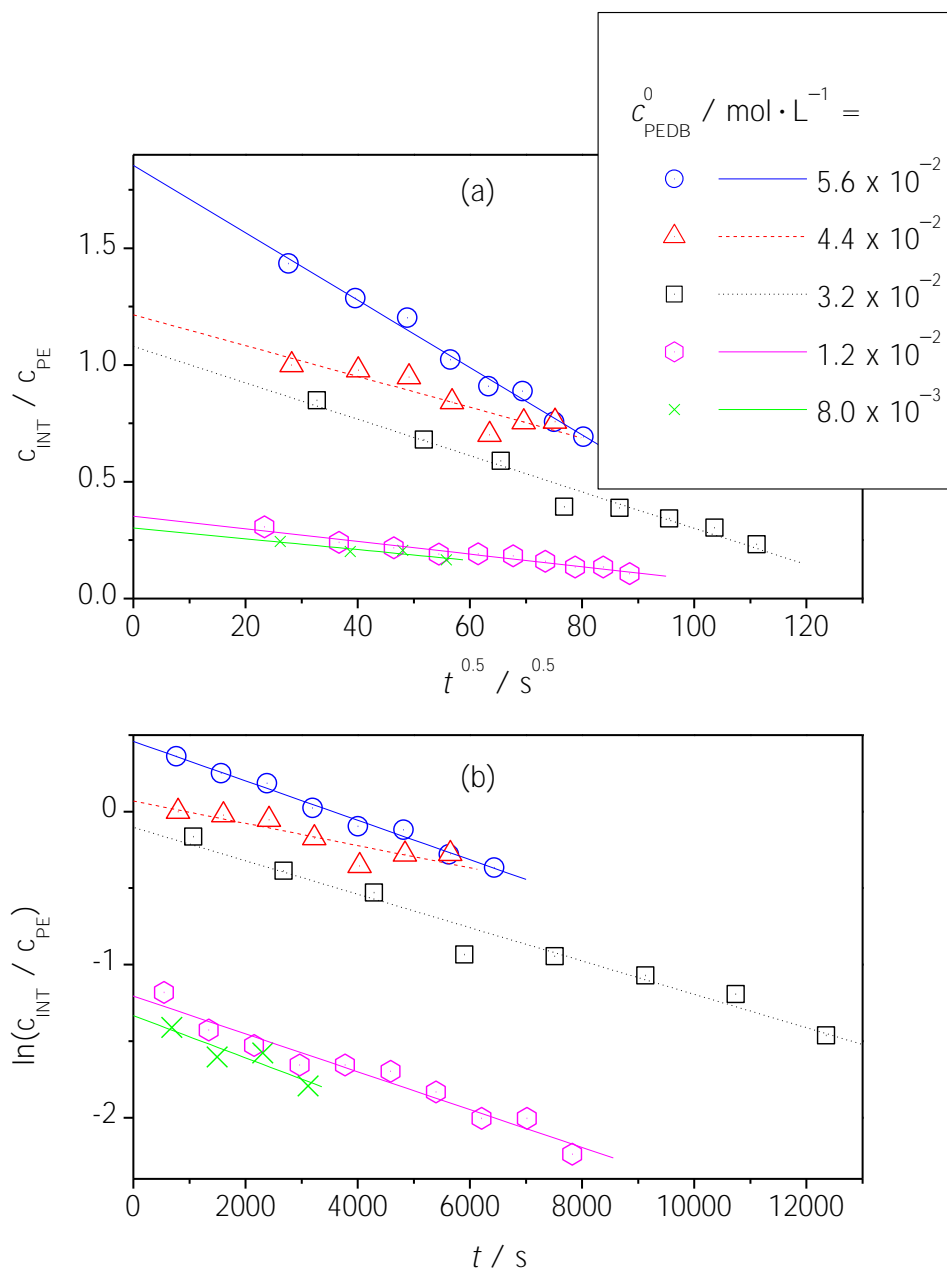


**Figure 5.12.** Decay of  $c_{\text{INT}}/c_{\text{PE}}$  ratio at 110 °C for extrapolation to  $c_{\text{INT}}/c_{\text{PE}}(t = 0)$ . (a)  $c_{\text{INT}}/c_{\text{PE}}$  versus  $\sqrt{t}$ ; (b)  $\ln(c_{\text{INT}}/c_{\text{PE}})$  versus  $t$  for various initial RAFT agent concentrations,  $c_{\text{PEDB}}^0$ .

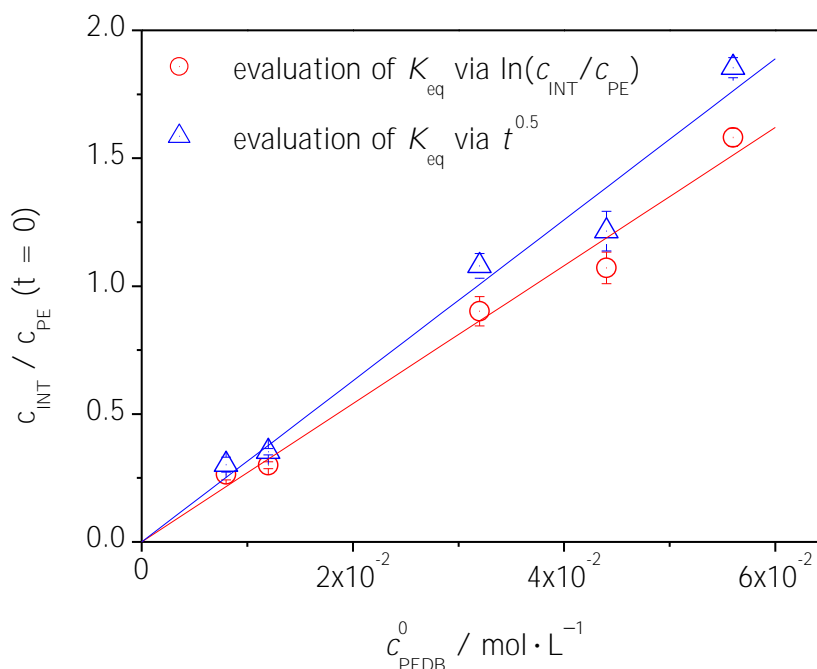


**Figure 5.13.**  $c_{\text{INT}}/c_{\text{PE}}(t = 0)$  versus initial PEDB concentration for determination of  $K_{\text{eq}}$  at 110 °C.  $c_{\text{INT}}/c_{\text{PE}}(t = 0)$  ratios were obtained from Figure 5.12 by extrapolation of  $c_{\text{INT}}/c_{\text{PE}}$  versus  $\sqrt{t}$  and  $\ln(c_{\text{INT}}/c_{\text{PE}})$  versus  $t$ , respectively.

In Figure 5.13 the  $c_{\text{INT}}/c_{\text{PE}}(t = 0)$  values are plotted versus initial RAFT agent concentration. Evaluating the EPR data using the  $\sqrt{t}$ -based method gives  $K_{\text{eq}} = (31 \pm 1) \text{ L} \cdot \text{mol}^{-1}$ . Interpretation via  $\ln(c_{\text{INT}}/c_{\text{PE}})$  yields  $K_{\text{eq}} = (27 \pm 1) \text{ L} \cdot \text{mol}^{-1}$ . Thus, the first estimate affords an average  $K_{\text{eq}}$  of  $(29 \pm 3) \text{ L} \cdot \text{mol}^{-1}$ .

To check for the consistency of the estimate via Equation 3.3, the EPR setup was calibrated by using solutions of TEMPO in toluene. This procedure is applied because neither PEDA nor PEDB increases the polarity of the sample significantly. The quality factor  $Q$  and the difference in field strength between sample and reference remain unchanged (see Section 7.3.2). The concentration profiles are illustrated in Figure 5.14. All profiles were fitted simultaneously using the reactions depicted in Scheme 5.7. In addition, the concentration of the cross-termination product CT1, found in the experiment designed to identify all side products (see Section 7.3.6), should be reproduced by the PREDICI<sup>®</sup> simulation.

Figure 5.14 shows the best fits for the various initial RAFT agent concentrations using  $k_{\text{ad}} = 10^7 \text{ L} \cdot \text{mol}^{-1} \cdot \text{s}^{-1}$  and the  $k_{\text{d}}$  and  $k_{\text{t}}^{1,1}$  values from the above described

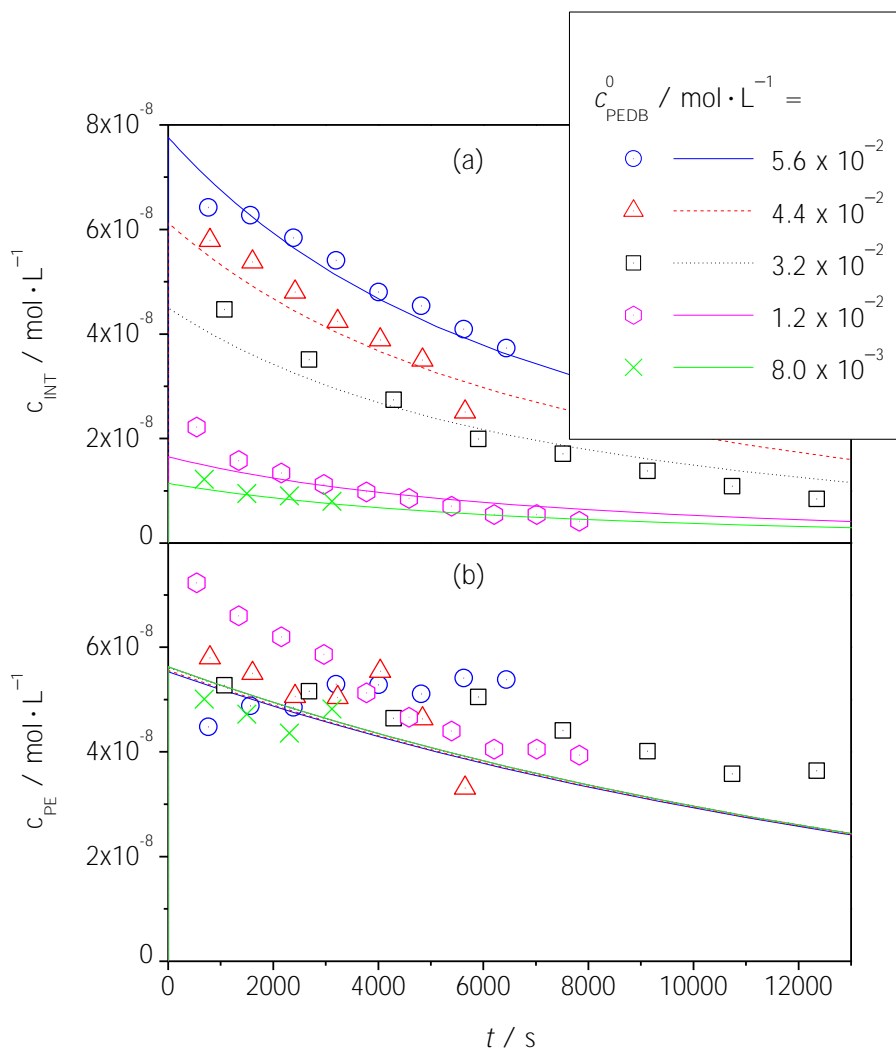


**Figure 5.14.** Experimental and simulated decay of PE and INT radical concentrations for various initial RAFT agent concentrations,  $c_{\text{PEDB}}^0$ , at 110 °C for determining  $K_{\text{eq}}$  and  $k_t^{\text{cross}}$  using  $k_{\text{ad}} = 10^7 \text{ L} \cdot \text{mol}^{-1} \cdot \text{s}^{-1}$ .

experiments. Since the INT concentration can be measured with higher accuracy than the PE concentration, less scattering is seen in the INT traces and these profiles are therefore more suitable for fitting. It should be noted however that it makes no difference whether all profiles are used for parameter estimation or only the INT traces. The same rate coefficients are obtained.

The addition rate coefficient was varied in the range of  $10^4$  to  $10^{10}$   $\text{L} \cdot \text{mol}^{-1} \cdot \text{s}^{-1}$ . The experimental data could be fitted equally well for all  $k_{\text{ad}}$  values and the corresponding numbers for  $K_{\text{eq}}$  and  $k_{\text{t}}^{\text{cross}}$  are listed in Table 5.7. For  $k_{\text{ad}} < 10^4$   $\text{L} \cdot \text{mol}^{-1} \cdot \text{s}^{-1}$  fitting was not successful anymore. It becomes clear that neither  $K_{\text{eq}}$  nor  $k_{\text{t}}^{\text{cross}}$  do depend significantly on  $k_{\text{ad}}$ . The experimental  $c_{\text{CT1}}/c_{\text{PEDB}}$  ratio is 0.52, compared to 0.59 predicted by simulation. The experimental  $c_{\text{CT1}}/c_{\text{BDDDB1+2}}$  ratio is 0.76, compared to the calculated number of 0.59. For  $k_{\text{ad}}$  being between  $10^5$  to  $10^{10}$   $\text{L} \cdot \text{mol}^{-1} \cdot \text{s}^{-1}$  the  $K_{\text{eq}}$  values are within the error margin of the equilibrium constant estimated via Equation 3.3.

Mean values of  $K_{\text{eq}} = (31.5 \pm 0.3)$   $\text{L} \cdot \text{mol}^{-1}$  and  $k_{\text{t}}^{\text{cross}} = 1.8 \times 10^9$   $\text{L} \cdot \text{mol}^{-1} \cdot \text{s}^{-1}$  are obtained at 110 °C. In comparison, the equilibrium constant estimated via Equation 3.3 is  $(29 \pm 3)$   $\text{L} \cdot \text{mol}^{-1}$ . The close agreement between the constants obtained from the two different approaches shows that extrapolation of  $c_{\text{INT}}/c_{\text{PE}}$  to  $t = 0$  minimizes the error induced by the high cross-termination rate. The average  $K_{\text{eq}}$  from Equation 3.3 and PREDICI<sup>®</sup> fitting is  $(30 \pm 4)$   $\text{L} \cdot \text{mol}^{-1}$ .

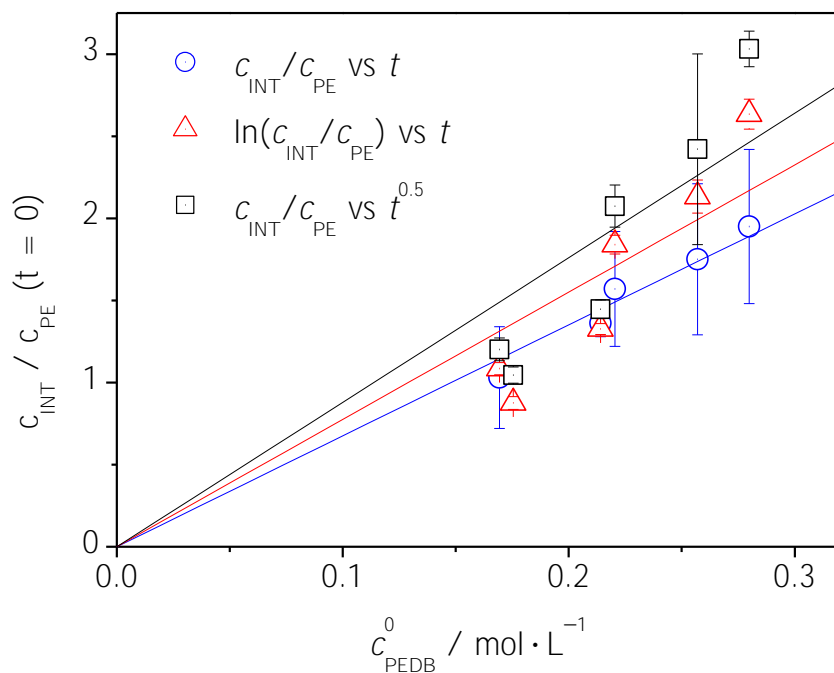
With  $k_{\text{ad}}$  being in the range of  $10^5$ – $10^{10}$   $\text{L} \cdot \text{mol}^{-1} \cdot \text{s}^{-1}$  and an equilibrium constant of 30  $\text{L} \cdot \text{mol}^{-1}$  the fragmentation step proceeds at a rate constant of  $3 \times 10^3$  to  $3 \times 10^8$   $\text{s}^{-1}$ . Assuming  $k_{\text{ad}}$  to be  $2 \times 10^6$   $\text{L} \cdot \text{mol}^{-1} \cdot \text{s}^{-1}$ , as derived for the polystyryl dithiobenzoate-mediated styrene polymerization at 40 °C studied by Goto *et al.*,<sup>[66]</sup> yields  $k_{\beta} \approx 6.7 \times 10^4$   $\text{s}^{-1}$ . This value is in agreement with  $k_{\beta} = 1.8 \times 10^4$   $\text{s}^{-1}$  obtained by Kwak *et al.* during a polystyryl dithiobenzoate-mediated styrene polymerization at 60 °C.<sup>[90]</sup> The authors used EPR spectroscopy to determine the intermediate radical concentration and dilatometry to calculate the propagating radical concentration. Barner-Kowollik *et al.* deduced a value of  $k_{\beta} = 3 \times 10^{-2}$   $\text{s}^{-1}$  for the cumyl dithiobenzoate-mediated styrene polymerization at 60 °C by modeling of the time-dependent evolution of experimental molecular mass distributions. The latter approach however fails to predict intermediate radical concentrations correctly.<sup>[45,46]</sup> It is thus reasonable to conclude that fragmentation is fast for the PE/PEDB system.

The PE/PEDB reaction was also investigated at 150 °C to estimate  $E_{\text{a}}(K_{\text{eq}})$ , as it is likely that less side reactions occur at elevated temperatures. At 80 and 100 °C, not yet identified side products were found, which are probably related to the side product TPEA observed during initiator decomposition at these temperatures. Toluene has a boiling point of 110.6 °C<sup>[171]</sup> and could therefore not be used as the solvent. Instead, naphthalene with a boiling point of 218 °C<sup>[171]</sup> was employed. A decrease of  $c_{\text{INT}}/c_{\text{PE}}$  is seen comparable with the one observed at 110 °C. Using naphthalene as a solvent,



**Table 5.7.** Equilibrium constants and cross-termination rate coefficients derived from the best fits of the experimental data shown in Figure 5.14.

$k_{\text{ad}} / \text{L} \cdot \text{mol}^{-1} \cdot \text{s}^{-1}$	$K_{\text{eq}} / \text{L} \cdot \text{mol}^{-1}$	$k_{\text{t}}^{\text{cross}} / \text{L} \cdot \text{mol}^{-1} \cdot \text{s}^{-1}$
$10^4$	38.1	$1.7 \times 10^9$
$10^5$	31.8	$1.8 \times 10^9$
$10^6$ – $10^{10}$	31.2	$1.8 \times 10^9$

**Figure 5.15.**  $c_{\text{INT}}/c_{\text{PE}}(t=0)$  versus initial PEDB concentration,  $c_{\text{PEDB}}^0$ , for determination of  $K_{\text{eq}}$  at 150 °C.  $c_{\text{INT}}/c_{\text{PE}}(t=0)$  ratios were obtained by extrapolation of  $c_{\text{INT}}/c_{\text{PE}}$  versus  $t$ ,  $c_{\text{INT}}/c_{\text{PE}}$  versus  $\sqrt{t}$  and  $\ln(c_{\text{INT}}/c_{\text{PE}})$  versus  $t$ , respectively.

however, complicates EPR calibration and thus determination of  $k_d$  and  $k_t$ , since it is a solid at room temperature (melting point  $80.3\text{ }^\circ\text{C}$ <sup>[171]</sup>). The equilibrium constant may therefore only be estimated from Equation 3.3. The above detailed strategy of  $c_{\text{INT}}/c_{\text{PE}}$  extrapolation to  $t = 0$  was used. The  $c_{\text{INT}}/c_{\text{PE}}(t = 0)$  versus  $c_{\text{PEDB}}^0$  plots are shown in Figure 5.15. Evaluation of the data via  $c_{\text{INT}}/c_{\text{PE}}$  versus time,  $\ln(c_{\text{INT}}/c_{\text{PE}})$  versus time and  $c_{\text{INT}}/c_{\text{PE}}$  versus  $\sqrt{t}$  yield  $K_{\text{eq}} = (6.8 \pm 0.2)$ ,  $(7.8 \pm 0.7)$  and  $(8.8 \pm 0.8)\text{ L} \cdot \text{mol}^{-1}$ , respectively. The average  $K_{\text{eq}}$  is  $(8 \pm 2)\text{ L} \cdot \text{mol}^{-1}$ . Note that the product analysis by NMR does not exclude the possibility of side reactions because the solvent naphthalene cannot be easily removed from the mixture. The signal-to-noise ratio was too high for reliable identification of reaction products due to the huge naphthalene fraction. From the equilibrium constants at 110 and 150  $^\circ\text{C}$  the apparent activation energy was determined to be:  $E_a(K_{\text{eq}}) = E_a(k_{\text{ad}}) - E_a(k_{\beta}) \approx -44.5\text{ kJ} \cdot \text{mol}^{-1}$ . This value is in close agreement with  $-40.5\text{ kJ} \cdot \text{mol}^{-1}$  obtained by Arita *et al.*<sup>[157]</sup> for cumyl dithiobenzoate-mediated styrene polymerizations between 120 and 180  $^\circ\text{C}$ .

## 5.4 Discussion

In Table 5.8 the experimentally obtained and theoretically predicted equilibrium constants for dithiobenzoate model systems and dithiobenzoate-mediated polymerizations are listed. The temperatures and solvents used in the study are given below each value. Experimental activation energies are also provided.

Note that the theoretical equilibrium constants calculated by Coote and co-workers are mainly listed for the sake of completeness and since there is no *a priori* reasons to assume that the general trends are not a true reflection of what can be expected in a RAFT polymerization. One has to be careful however in taking the calculated equilibrium constants as face values since they are significantly influenced by solvation effects. Coote and co-workers compared calculated gas- and solution-phase free energies and found that the gas-phase values are up to  $-30\text{ kJ} \cdot \text{mol}^{-1}$  more exothermic, i. e., the gas-phase equilibrium constants are up to six orders of magnitude higher.<sup>[41]</sup> A particularly strong influence of solvation effects was found for acrylates due to their greater polarity and their greater potential for hydrogen bonding as compared to other monomers.

In the following, radical stabilization energies (RSEs) are used to explain the experimental results. The radical stabilization energy is a thermodynamic measure of relative radical stability.<sup>[172]</sup> It compares the energy of the radical  $\text{R}^\bullet$  to a reference species  $\text{CH}_3^\bullet$ . The standard RSE is the difference of the corresponding  $\text{R-H}$  and  $\text{CH}_3\text{-H}$  bond dissociation enthalpies (BDEs):  $\text{RSE} = \text{BDE}[\text{CH}_3\text{-H}] - \text{BDE}[\text{R-H}]$ . When the RSE for radical  $\text{R}^\bullet$  is positive,  $\text{R}^\bullet$  is more stabilized than  $\text{CH}_3^\bullet$  and if the RSE is negative,  $\text{R}^\bullet$  is less stabilized.<sup>[173]</sup>

**Table 5.8.** Comparison of equilibrium constants and activation energies for dithiobenzoate model systems and dithiobenzoate-mediated polymerizations. The theoretical values were obtained using (A) B3LYP/6-13G(d) for geometry optimization, W1-ONIOM for energy calculations and COSMO-RS for modeling of solvation energies, (B) B3LYP/6-13G(d), W1-ONIOM with PCM-UAHF for modeling of solvation energies, (C) B3LYP/6-31G(d), W1-ONIOM. The *ab initio* methods are explained in the references provided in the table. (D) The values refer to apparent activation energies. See text for further details.

	$K_{\text{eq}}^{\text{exp}} / \text{L} \cdot \text{mol}^{-1}$	$K_{\text{eq}}^{\text{theo}} / \text{L} \cdot \text{mol}^{-1}$	$E_{\text{a}}(K_{\text{eq}}) / \text{kJ} \cdot \text{mol}^{-1}$
model systems			
TB/TBDB	$> 10^5$ 70 °C in toluene	$2.55 \times 10^{10}$ 25 °C in MMA <sup>[98], A</sup>	–
	$(6 \pm 4) \times 10^8$ 20 °C in benzene <sup>[100]</sup>	$4.5 \times 10^8$ 20 °C in benzene <sup>[100], B</sup>	
CIP/CPDB	$9 \pm 1$ 70 °C in toluene	$2.35 \times 10^5$ 70 °C in gas phase <sup>[39], C</sup>	–28.4 60 to 100 °C
		$3.51 \times 10^3$ 25 °C in MMA <sup>[98], A</sup>	
PE/PEDB	$30 \pm 4$ 110 °C in toluene	$3.45 \times 10^8$ 70 °C in gas phase <sup>[39], C</sup>	–44.5 <sup>D</sup> 110 and 150 °C
macromolecular systems			
PS/PSDB	55 60 °C in styrene <sup>[90]</sup>	$2.06 \times 10^{11}$ 70 °C in gas phase <sup>[39], C</sup>	–40.5 <sup>[157]</sup> 120 to 180 °C
BA/ETTP	75 70 °C in toluene	–	–49.5 <sup>D</sup> –40 and 70 °C

### Comparison of equilibrium constants of model systems

The values for CIP/CPDB and PE/PEDB are extrapolated to 20 °C, using the activation energies given in Table 5.8, to allow for direct comparison of the equilibrium constants. The resulting values are  $K_{\text{eq}} = 53 \text{ L} \cdot \text{mol}^{-1}$  for the CIP/CPDB system and  $K_{\text{eq}} = 2.2 \times 10^3 \text{ L} \cdot \text{mol}^{-1}$  for the PE/PEDB system. The value reported by Chernikova *et al.* for the TB/TBDB system is  $K_{\text{eq}} = 6 \times 10^8 \text{ L} \cdot \text{mol}^{-1}$ .<sup>[100]</sup> Thus, there is a 5 to 7 orders of magnitude difference in  $K_{\text{eq}}$  for the equilibrium involving *tert*-butyl to the ones involving phenylethyl and cyano-*iso*-propyl, respectively. This is due to the lower radical stabilization energy of TB ( $28.5 \text{ kJ} \cdot \text{mol}^{-1}$ )<sup>[173]</sup> versus CIP ( $58.3 \text{ kJ} \cdot \text{mol}^{-1}$ )<sup>[173]</sup> or PE ( $68.3 \text{ kJ} \cdot \text{mol}^{-1}$ )<sup>[174]</sup> which shifts the addition-fragmentation equilibrium from the side of the *tert*-butyl radical towards the one of the intermediate radical (see reaction II in Scheme 5.3). Since *tert*-butyl does not resemble a monomeric species, the model equilibrium constant does not provide evidence for slow fragmentation being the cause of rate retardation in other dithiobenzoate-mediated polymerizations.

Considering the radical stabilization energies of CIP and PE one would expect a larger equilibrium constant for CIP than for PE. However, the PE/PEDB value is around 40 times higher than the one for CIP/CPDB. This is caused by the electron-withdrawing cyano-*iso*-propyl which exerts a significant homoanomeric effect by weakening the bond formed between the sulfur and the attacking radical. The CIP radical therefore adds at a slower rate to the C=S double bond and fragments faster from the RAFT intermediate.<sup>[74]</sup> As a result, the equilibrium constant is smaller than expected from radical stabilization energy.<sup>[40]</sup> For a methyl methacrylate/dithiobenzoate system a similar equilibrium constant is expected, as the radical stabilization energy of MMA ( $54.6 \text{ kJ} \cdot \text{mol}^{-1}$ )<sup>[173]</sup> is close to the one of CIP and as MMA also bears an electron-withdrawing group. This assumption is supported by *ab initio* calculations.<sup>[98]</sup>

The homoanomeric effect also plays a role in acrylate-dithiobenzoate systems. However, the radical stabilization energy of ethyl acrylate ( $42.0 \text{ kJ} \cdot \text{mol}^{-1}$ )<sup>[173]</sup> is much lower than for CIP or MMA and the equilibrium constant should therefore be higher. This could explain why rate retardation has been observed with acrylates but not in methyl methacrylate polymerization.<sup>[88]</sup>

### Comparison of experimental and theoretical equilibrium constants

For the TB/TBDB model system experimental  $K_{\text{eq}}$  values are not in conflict with the theoretical ones. The difference of two orders of magnitude between the theoretical values in benzene and MMA is most likely due to the different solvent methods used for calculation, i. e. COSMO-RS and PCM-UAHF, respectively.<sup>[98]</sup>

The higher  $K_{\text{eq}}^{\text{theo}}$  value for the CIP/CPDB system listed in Table 5.8 was calculated in the gas phase. The lower  $K_{\text{eq}}^{\text{theo}}$  was calculated in MMA as the solvent and refers to the addition of CIP to TBDB. Calculations were carried out using COSMO-RS as a solvent model. The authors recommend, however, PCM-UAHF for the prediction of RAFT-based solvation energies. With this model, equilibrium constants are reduced up to two orders of magnitude.<sup>[98]</sup> Additional calculations of the CIP/CPDB equilibrium using PCM-UAHF for calculating solvation energies may therefore yield the same results as the experiment.

For PE/PEDB only gas-phase calculations have been carried out so far. The calculated value is around six orders of magnitude above the experimental one. Comparison with CIP/CPDB shows that – if the solvent environment is considered –  $K_{\text{eq}}^{\text{theo}}$  may be reduced up to four orders of magnitude. Still, a difference of two orders of magnitude remains. A particular difficulty of quantum-chemical calculations for this system may be associated with adequately taking the delocalization of radical functionality for both species, PE and INT, into account. It therefore appears recommendable to revise the *ab initio* calculations for this system.

### Comparison of model systems and macromolecular systems

A direct comparison between model and macromolecular system is possible in the case of PE/PEDB and polystyryl/polystyryl dithiobenzoate (PS/PSDB). Extrapolation of  $K_{\text{eq}}$  to 60 °C yields  $K_{\text{eq}} = 244 \text{ L} \cdot \text{mol}^{-1}$  using the apparent activation energy  $E_a(K_{\text{eq}}) = -44.5 \text{ kJ} \cdot \text{mol}^{-1}$ . Thus,  $K_{\text{eq}}$  for the model system is about four times above  $K_{\text{eq}}$  for dithiobenzoate-mediated styrene polymerization. This may be due to a chain-length dependence of  $K_{\text{eq}}$ . *Ab initio* calculations predict an even more pronounced chain-length effect of three orders of magnitude. However, the chain-length effect is contrary to the observed one, i. e. fragmentation of a growing chain should be much slower than the fragmentation of a phenylethyl radical.<sup>[39]</sup>

It should be noted that Suzuki *et al.*<sup>[95,96]</sup> measured rates of dithiobenzoate-mediated styrene polymerization in bulk and in miniemulsion and found significantly higher rates for miniemulsion polymerization. The experimental observation cannot be understood by the slow fragmentation model, but is adequately described by the intermediate termination model assuming a relatively high fragmentation rate coefficient and a high rate coefficient for termination between the intermediate radical, INT, and a

propagating radical. These conclusions are in full agreement with the EPR data and clearly contradict the high equilibrium constant from *ab initio* calculations.

The investigation into the *n*-butyl acrylate polymerization mediated by ethyl *S*-thiobenzoyl-2-thiopropionate, which is a dithiobenzoate RAFT agent with an acrylate leaving group (see Section 4.3), yielded  $K_{\text{eq}} = 75 \text{ L} \cdot \text{mol}^{-1}$  at 70 °C. This latter value for BA polymerization is affected by the simultaneous occurrence of secondary propagating chain-end radicals (SPRs) and midchain radicals (MCRs) produced by backbiting reactions of SPRs. Both radicals with their relative concentration being temperature dependent may add to the RAFT agent.  $K_{\text{eq}}$  for BA/ETTP should therefore be considered as an apparent value. As expected by comparison of radical stabilization energies (see above),  $K_{\text{eq}}$  is higher for acrylate polymerization than for the CIP/CPDB system. The homoanomeric effect causes the styrene and acrylate polymerizations to have similar equilibrium constants despite the difference in radical stabilization energy of more than 25 kJ · mol<sup>-1</sup>.

### Comparison of activation energies

Whereas the experimental equilibrium constants listed in Table 5.8 were measured with high accuracy and are therefore exact values, the accuracy of the experimental activation energies is limited. This is due to the narrow temperature range investigated and do to the fact that different solvents had to be used in order to cover a larger temperature range.

The difference in activation energies for  $k_{\text{ad}}$  and  $k_{\beta}$  for the CIP/CPDB system is  $E_{\text{a}}(K_{\text{eq}}) = (-28 \pm 4) \text{ kJ} \cdot \text{mol}^{-1}$ . This number is slightly below the styrene model system and styrene polymerization. Arita *et al.* obtained  $E_{\text{a}}(K_{\text{eq}}) = -40.5 \text{ kJ} \cdot \text{mol}^{-1}$  for the cumyl dithiobenzoate-mediated styrene polymerization.<sup>[157,175]</sup> This value is in close agreement with the PE/PEDB model system, although the activation energy is slightly uncertain as solvents were changed from toluene at 110 °C to naphthalene at 150 °C. The value for dithiobenzoate-mediated BA polymerization is also an apparent value and is based on the measurement of  $K_{\text{eq}}$  at two different temperatures. At higher temperatures, midchain radicals occur, which have a higher radical stabilization energy (54.7 compared to 42.0 kJ · mol<sup>-1</sup>). The higher radical stabilization energy of the MCRs should lower  $K_{\text{eq}}$ , so that the activation energy for SPRs could be even higher than the one listed in Table 5.8.

Activation energies from *ab initio* calculations for various model systems, e. g., for reaction of CH<sub>3</sub>, CH<sub>2</sub>COOCH<sub>3</sub>, CH<sub>2</sub>Ph, or C(CH<sub>3</sub>)<sub>2</sub>CN radicals with RAFT agents bearing a CH<sub>3</sub> leaving group and a CH<sub>3</sub>, phenyl, or benzyl Z-group, are in the range of -95 to -34 kJ · mol<sup>-1</sup>.<sup>[38]</sup>

# 6

## Closing Remarks

The novel EPR strategies presented in this thesis are highly advantageous compared to previously used methods for deducing the RAFT equilibrium constant,  $K_{\text{eq}}$ , and the rate coefficients for addition,  $k_{\text{ad}}$ , and fragmentation,  $k_{\beta}$ . Due to direct monitoring of the radical species involved in the RAFT equilibrium, determination of  $K_{\text{eq}}$  without assuming a kinetic model becomes possible. Tracing of intermediate radical concentration after laser single pulse initiation provides information about the lifetime of this species. The two methods allow for independent access to  $K_{\text{eq}}$ . In addition, the EPR experiments are not restricted to RAFT agents which induce rate retardation, but can be applied to all types of RAFT agents.

Lower  $K_{\text{eq}}$  values were observed in BA polymerizations mediated by xanthate and trithiocarbonate than the ones mediated by dithiobenzoate. This is consistent with the experimental finding, that dithiobenzoates control acrylate polymerizations better than xanthates or trithiocarbonates. The equilibrium constants for the latter two types of RAFT agents are in agreement with *ab initio* values calculated by Coote *et al.*<sup>[40,41]</sup> The equilibrium constant for the dithiobenzoate is, however, by six orders of magnitude smaller than the theoretically predicted one. Therefore, monomer-free model systems with dithiobenzoates were investigated to check the accuracy of the quantum-chemical methods. Since the  $K_{\text{eq}}$  values of the model systems also deviate significantly from the calculated ones, it appears highly advisable to revisit the *ab initio* method employed for dithiobenzoates.

Quantum-chemical calculations for the model systems cyano-*iso*-propyl/2-(2'-cyano-propyl)-dithiobenzoate and phenylethyl/1-phenylethyl dithiobenzoate are currently underway in the "Computational Chemistry and Biochemistry" research group of

Jun.-Prof. Dr. Ricardo Mata at the University of Göttingen. Preliminary equilibrium constants are much closer to the values obtained from the EPR measurements<sup>[176]</sup> than the theoretical values calculated by the Coote group.<sup>[39]</sup> Both groups carried out their *ab initio* calculations for the gas phase, showing that the discrepancy between theoretically and experimentally obtained equilibrium constants cannot be attributed to solvent effects. It is more likely that the new *ab initio* method developed in the Mata group is capable of describing the delocalization of the radical function into the aromatic ring.

The model systems investigated in this thesis can explain the rate retardation phenomena observed in dithiobenzoate-mediated polymerizations. In CIP/CPDB-related polymerizations, such as the dithiobenzoate-mediated MMA polymerization, no rate retardation is observed due to the relatively low equilibrium constant and cross-termination being slow as compared to addition and fragmentation. Part of the cross-terminated species undergo “missing step” reactions to either yield back the RAFT agent or a RAFT agent being substituted at the *para* position of the aromatic ring. To check whether the results from the CIP/CPDB model system can be transferred to dithiobenzoate-mediated polymerizations of tertiary monomers, studies into the MMA polymerization mediated by a dithiobenzoate with MMA leaving group are currently underway in our laboratory.<sup>[177]</sup>

For dithiobenzoate-mediated styrene polymerizations cross-termination seems to be the main cause for rate retardation. “Missing step” reactions play a minor role with this monomer. In *tert*-butyl dithiobenzoate-mediated polymerizations strong inhibition is seen in the early stages of the polymerization due to a combination of slow fragmentation of *tert*-butyl from the RAFT adduct radical and fast cross-termination of *tert*-butyl radicals with intermediate radicals.

The presented results thus indicate that rate retardation in some RAFT polymerizations is due to a reduced fragmentation rate, which however is by orders of magnitude faster than proposed by the supporters of the slow fragmentation model. The reduced fragmentation rate of the RAFT adduct only serves to increase its concentration, and thus makes cross-termination more likely than in the corresponding non-retarded systems.

Cross-termination occurs at the *para* position of the phenyl group and at the carbon between the two sulfur atoms of the INT species. The other possible sites, like the *ortho* position, are not affected. This may be explained by the fact that the aromatic system remains intact when cross-termination occurs at the carbon between the two sulfur atoms. Despite the steric hindrance, cross-termination at this position therefore takes place. In the case of xanthates or trithiocarbonates this reaction site does not cause rate retardation since  $K_{\text{eq}}$  is lower than for dithiobenzoates and the lifetime of



---

the intermediate radical is reduced. Cross-termination may therefore only occur to a very limited extent.

For dithiobenzoates, cross-termination preferably takes place at the *para* position instead of the *ortho* position of the phenyl ring, due to less steric hindrance. For the same reason, tertiary radicals preferably add to the *para* position and secondary radicals to the carbon between the two sulfur atoms. The cross-termination product resulting from the addition at the *para* position is not overly stable. Consecutive reaction steps which restore the aromaticity of the phenyl ring are fast. Therefore, significant amounts of “missing step” products are found when tertiary radicals are involved in the RAFT process.

The main factors that contribute to the reduction of cross-termination during the course of dithiobenzoate-mediated polymerizations are the chain-length dependence of  $k_t^{\text{cross}}$  and the transformation of part of the original RAFT agent into a “missing step” product, which is less prone to cross-termination. Adopting a reasonable chain-length dependence of  $k_t^{\text{cross}}$  together with fast fragmentation, yields excellent fits of the presented EPR data. In addition, experimental evidence for chain-length-dependent cross-termination has been deduced by Ting *et al.* from dithiobenzoate-mediated styrene polymerization, where only radicals of chain length  $i > 50$  were present.<sup>[111]</sup> The absence of significant rate retardation with long-chain radicals is most likely due to the fact that in macroRAFT-mediated and conventional polymerization (without RAFT agent) almost exclusively large radicals are present. From the composite model it is well known, that large radicals exhibit only minor differences in termination rate that are not easily detected.<sup>[178]</sup> On the other hand, RAFT polymerization at low degrees of conversion exhibits quite different termination behavior, as almost all radicals are of small size and thus terminate much faster. The behavior under such conditions is quite different from the one of a conventional polymerization, where large radicals are present from the very beginning on. As a consequence, compared to conventional polymerization, a clear retardation is seen with RAFT-mediated polymerization at small chain lengths, i. e., at low degrees of monomer conversion.

To confirm the results of this thesis, the EPR strategies developed herein should be applied to a broad range of monomer/RAFT agent combinations. Pre-polymerized RAFT agents in conjunction with macromonomers may be used in SP-PLP-EPR-RAFT experiments to investigate a possible chain-length dependence of the individual rate coefficients,  $k_{\text{ad}}$  and  $k_{\beta}$ . For the determination of the activation energies of these coefficients monomers which do not undergo backbiting reactions are well suited.

The novel EPR techniques are also useful for investigating other reversible-deactivation radical polymerizations, where two species taking part in the equilibrium can be monitored by EPR spectroscopy. Recently, first SP-PLP-EPR experiments were

## 6 Closing Remarks

---

carried out in our laboratory to determine the deactivation rate coefficient in ATRP polymerization.<sup>[179]</sup> EPR spectroscopy may also provide further insight into NMP and RTCP polymerization.

# 7

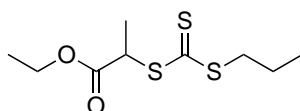
## Experimental

This chapter focuses on the synthesis of transfer agents and initiators and lists the solvents, monomers and calibration standards used in this thesis. Experimental procedures and data treatment are detailed and the instrumentation employed is presented.

### 7.1 Chemicals

#### 7.1.1 Transfer agents

##### **S-Ethyl propan-2-ylonate-*S'*-propyl trithiocarbonate**



*S*-Ethyl propan-2-ylonate-*S'*-propyl trithiocarbonate (EPPT,  $M = 252.42 \text{ g} \cdot \text{mol}^{-1}$ ) was prepared according to the procedure described by Rotzoll<sup>[180]</sup> for a similar trithiocarbonate. To a solution of sodium methoxide (10.8 g, 11.4 mL, 0.05 mol, 25 wt % in methanol) in methanol (15 mL), propanethiol (3.8 g, 4.5 mL, 0.05 mol) was added dropwise at 0 °C. The reaction mixture was stirred for 2 h and carbon disulfide (3.8 g, 3.0 mL, 0.05 mol) was added. After stirring for another 3 h at 0 °C, ethyl-2-bromopropionate (9.1 g, 6.5 mL, 0.05 mol) was added and the mixture was stirred for 20 h at ambient temperature. Methanol was removed *in vacuo* and the crude

## 7 Experimental

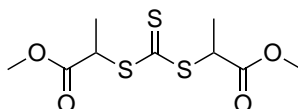
---

product was purified by column chromatography ( $\text{SiO}_2$ , *n*-pentane,  $R_f$ : 0.17). The product was isolated as a yellowish oil. According to NMR the purity was at least 98 %.

$^1\text{H}$  NMR (300 MHz,  $\text{CDCl}_3$ ):  $\delta(\text{ppm}) = 1.00$  (t, 3 H,  $J = 7.4$  Hz,  $\text{CH}_2\text{-CH}_2\text{-CH}_3$ ), 1.26 (t, 3 H,  $J = 7.1$  Hz,  $\text{O-CH}_2\text{-CH}_3$ ), 1.58 (d, 3 H,  $J = 7.4$  Hz,  $\text{CH-CH}_3$ ), 1.72 (tq, 2 H,  $J = 7.4$  Hz, 7.4 Hz,  $\text{CH}_2\text{-CH}_2\text{-CH}_3$ ), 3.33 (t, 2 H,  $J = 7.4$  Hz,  $\text{CH}_2\text{-CH}_2\text{-CH}_3$ ), 4.17 (q, 2 H,  $J = 7.1$  Hz,  $\text{O-CH}_2\text{-CH}_3$ ), 4.79 (q, 1 H,  $J = 7.4$  Hz,  $\text{CH-CH}_3$ ).

$^{13}\text{C}$  NMR (75 MHz,  $\text{CDCl}_3$ ):  $\delta(\text{ppm}) = 13.6$  ( $\text{CH}_2\text{-CH}_2\text{-CH}_3$ ), 14.2 ( $\text{O-CH}_2\text{-CH}_3$ ), 17.1 ( $\text{CH-CH}_3$ ), 21.6 ( $\text{CH}_2\text{-CH}_2\text{-CH}_3$ ), 39.1 ( $\text{CH}_2\text{-CH}_2\text{-CH}_3$ ), 48.1 ( $\text{CH-CH}_3$ ), 61.9 ( $\text{O-CH}_2\text{-CH}_3$ ), 171.2 ( $\text{C=O}$ ), 222.2 ( $\text{C=S}$ ).

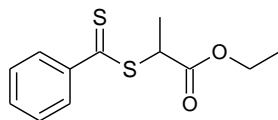
### ***S,S'*-Bis(methyl-propion-2-ylate) trithiocarbonate**



*S,S'*-Bis(methyl-propion-2-ylate) trithiocarbonate (BMPT,  $M = 282.40 \text{ g} \cdot \text{mol}^{-1}$ ) was synthesized according to the procedure described by Tamami and Kiasat.<sup>[181]</sup> Dried Ambersep 900 (30 g) was dispersed in carbon disulfide (150 mL) and stirred for approximately 10 min at ambient temperature. The anion-exchange resin changed from light yellow to dark red immediately. Subsequently, methyl-2-bromopropionate (10 g) as the alkylating agent was added dropwise. The reaction mixture was then stirred at room temperature for 30 h. After filtration and extraction, the organic layer was dried over sodium sulfate, concentrated and purified by column chromatography ( $\text{SiO}_2$ , toluene). The trithiocarbonate was obtained as a yellow liquid. Its structure and purity were determined by NMR.

$^1\text{H}$  NMR (300 MHz,  $\text{CDCl}_3$ ):  $\delta(\text{ppm}) = 1.58$  (d, 6 H,  $J = 7.2$  Hz,  $\text{CH-CH}_3$ ), 3.71 (s, 6 H,  $\text{O-CH}_3$ ), 4.78 (q, 2 H,  $J = 7.2$  Hz,  $\text{CH-CH}_3$ ).

$^{13}\text{C}$  NMR (75 MHz,  $\text{CDCl}_3$ ):  $\delta(\text{ppm}) = 17.2$  ( $\text{CH-CH}_3$ ), 48.3 ( $\text{CH-CH}_3$ ), 53.2 ( $\text{O-CH}_3$ ), 171.5 ( $\text{C=O}$ ), 219.7 ( $\text{C=S}$ ).

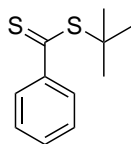
**Ethyl *S*-thiobenzoyl-2-thiopropionate**

Ethyl *S*-thiobenzoyl-2-thiopropionate (ETTP,  $M = 254.39 \text{ g} \cdot \text{mol}^{-1}$ ) was synthesized similar to the procedure described by Chong *et al.*<sup>[74]</sup> for the synthesis of a similar dithiobenzoate. Phenylmagnesium bromide was prepared from bromobenzene (6.28 g, 4.21 mL, 0.04 mol) and magnesium turnings (1.00 g, 0.04 mol) in dry THF (30 mL). The solution was warmed to 40 °C and carbon disulfide (3.05 g, 2.41 mL, 0.04 mol) was added over 15 min while maintaining the reaction temperature at 40 °C. Ethyl-2-bromopropionate (7.24 g, 5.20 mL, 0.04 mol) was added to the resultant dark brown solution and the reaction temperature was raised to 80 °C and maintained for 60 h. Ice-water (50 mL) was added, and the organic products were extracted with diethyl ether (3 x 50 mL). The combined organic extracts were washed with water and brine and dried over anhydrous magnesium sulfate. After removal of solvent and purification by column chromatography ( $\text{SiO}_2$ , *n*-hexane/diethyl ether 9:1,  $R_f = 0.21$ ). Ethyl *S*-thiobenzoyl-2-thiopropionate was obtained as a red oil. According to NMR the purity was at least 98 %.

**$^1\text{H}$  NMR** (300 MHz,  $\text{CDCl}_3$ ):  $\delta(\text{ppm}) = 1.25$  (t, 3 H,  $J = 6.3$  Hz,  $\text{CH}_2\text{-CH}_3$ ), 1.64 (d, 3 H,  $J = 6.6$  Hz,  $\text{CH-CH}_3$ ), 4.21 (q, 2 H,  $J = 6.3$  Hz,  $\text{CH}_2\text{-CH}_3$ ), 4.72 (q, 1 H,  $J = 6.6$  Hz,  $\text{CH-CH}_3$ ), 7.33–7.40 (m, 2 H,  $\text{C}_6\text{H}_5$ ), 7.49–7.58 (m, 1 H,  $\text{C}_6\text{H}_5$ ), 7.94–8.00 (d, 2 H,  $\text{C}_6\text{H}_5$ ).

**$^{13}\text{C}$  NMR** (75 MHz,  $\text{CDCl}_3$ ):  $\delta(\text{ppm}) = 14.1$  ( $\text{CH}_2\text{-CH}_3$ ), 16.5 ( $\text{CH-CH}_3$ ), 48.6 ( $\text{CH-CH}_3$ ), 61.8 ( $\text{CH}_2\text{-CH}_3$ ), 126.9, 128.4, 132.6, 144.4 ( $\text{C}_6\text{H}_5$ ), 171.1 ( $\text{C=O}$ ), 225.9 ( $\text{C=S}$ ).

**ESI-HRMS**  $m/z$ :  $[\text{M} + \text{H}]^+$  calcd for  $\text{C}_{12}\text{H}_{14}\text{O}_2\text{S}_2$  255.0508, found 255.0509.

***tert*-Butyl dithiobenzoate**

*tert*-Butyl dithiobenzoate (TBDB,  $M = 210.36 \text{ g} \cdot \text{mol}^{-1}$ ) was synthesized according to the procedure described by Ladav.<sup>[65]</sup> *S*-(thiobenzoyl)thioglycolic acid (10 g, 47 mmol)

## 7 Experimental

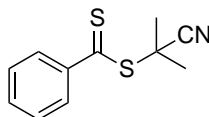
---

was dissolved in dilute alkaline solution containing 2 eq of NaOH (3.8 g, 94 mmol in 400 mL of H<sub>2</sub>O). Then, 2-methyl-2-propanethiol (4.67 g, 52 mmol) was added and the mixture was stirred at room temperature for a period of 20.5 h. *tert*-Butyl dithiobenzoate, which separated out as a dark, pink oil, was extracted with diethyl ether (1 × 600 mL, 1 × 300 mL). The organic extracts were washed with 0.1 N aqueous NaOH (3 × 330 mL) and water (3 × 300 mL), dried over sodium sulfate, filtered, and evaporated. The product was left overnight under vacuum (4 × 10<sup>-2</sup> mbar, 25 °C) to eliminate the residual 2-methyl-2-propanethiol. The yield of *tert*-butyl dithiobenzoate, which remained as a dark pink oil, was 59 %.

**<sup>1</sup>H NMR** (300 MHz, CDCl<sub>3</sub>): δ(ppm) = 1.71 (s, 9 H, C(CH<sub>3</sub>)<sub>3</sub>), 7.31–7.41 (m, 2 H, C<sub>6</sub>H<sub>5</sub>), 7.45–7.55 (m, 1 H, C<sub>6</sub>H<sub>5</sub>), 7.86–7.92 (m, 2 H, C<sub>6</sub>H<sub>5</sub>).

**<sup>13</sup>C NMR** (75 MHz, CDCl<sub>3</sub>): δ(ppm) = 28.3 (C(CH<sub>3</sub>)<sub>3</sub>), 52.2 (C(CH<sub>3</sub>)<sub>3</sub>), 126.7, 128.1, 131.7, 147.2 (C<sub>6</sub>H<sub>4</sub>), 230.3 (C=S).

### 2-(2'-Cyanopropyl)-dithiobenzoate

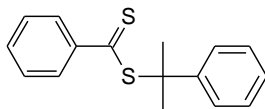


2-(2'-Cyanopropyl)-dithiobenzoate (CPDB,  $M = 221.34 \text{ g} \cdot \text{mol}^{-1}$ ) was synthesized as described in literature.<sup>[85,182,183]</sup> The purity was better than 98 % as verified by <sup>1</sup>H NMR analysis.

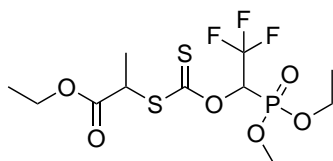
**<sup>1</sup>H NMR** (300 MHz, CDCl<sub>3</sub>): δ(ppm) = 1.92 (s, 6 H, CH<sub>3</sub>), 7.37 (t, 2 H,  $J = 7.2 \text{ Hz}$ , C<sub>6</sub>H<sub>5</sub>), 7.54 (t, 1 H,  $J = 7.2 \text{ Hz}$ , C<sub>6</sub>H<sub>5</sub>), 7.89 (d, 2 H,  $J = 7.2 \text{ Hz}$ , C<sub>6</sub>H<sub>5</sub>).

**<sup>13</sup>C NMR** (75 MHz, CDCl<sub>3</sub>): δ(ppm) = 26.7 (CH<sub>3</sub>), 42.0 (C(CH<sub>3</sub>)<sub>2</sub>C≡N), 120.2 (C≡N), 126.9, 128.8, 133.1, 144.8 (C<sub>6</sub>H<sub>5</sub>), 223.4 (C(=S)S).

**EI-HRMS**  $m/z$ : [M + Na]<sup>+</sup> clcd for C<sub>11</sub>H<sub>11</sub>NS<sub>2</sub> 244.0232, found 244.0232.

**Cumyl dithiobenzoate**

Cumyl dithiobenzoate (CDB) was synthesized according to a literature procedure.<sup>[85]</sup> The purity was  $\geq 98\%$  according to NMR spectroscopy.

**Ethyl 2-[1-diethoxyphosphoryl-2,2,2-trifluoroethoxythio carbonylsulfanyl] propionate**

Ethyl 2-[1-diethoxyphosphoryl-2,2,2-trifluoroethoxythio carbonylsulfanyl] propionate (EDTCP,  $M = 412.38 \text{ g} \cdot \text{mol}^{-1}$ ) was synthesized according to a two-step procedure described by Destarac:<sup>[128]</sup> A solution of fluoral hydrate (10.0 g of a 75 % aqueous solution, 64.6 mmol) and diethylphosphite  $\text{HP}(\text{O})(\text{OEt})_2$  (64.6 mmol) in triethylamine (9.0 ml, 64.6 mmol) was stirred at room temperature for 15 h. The mixture was rapidly concentrated under partial vacuum while keeping the temperature below 40 °C. The residue was purified by flash chromatography ( $\text{SiO}_2$ , *n*-heptane/acetone 10:1, then diethyl ether, then diethyl ether/methanol: 10:1) to give diethyl 2,2,2-trifluoro-1-hydroxyethylphosphonate.

A solution of this alcohol (5.0 g, 21.18 mmol) in DMF (6 ml) was added dropwise to a suspension of sodium hydride (1.03 g of a 60 % dispersion in mineral oil, 25.75 mmol) in DMF (30 ml) and cooled to 0 °C. After 30 min at 0 °C, carbon disulfide (2.65 ml, 44 mmol) was added and stirring was continued for another 15 min. Ethyl 2-bromopropionate (3.51 ml, 26.7 mmol) was added and the mixture kept at 0 °C for 23 h. It was neutralized with saturated aqueous ammonium chloride solution, extracted three times with ethyl acetate, and the combined organic layers were dried over magnesium sulfate. The solvent was removed under vacuum and the residue was purified by flash column chromatography ( $\text{SiO}_2$ , *n*-hexane/ethyl acetate 7:3) to give the pure product.

<sup>1</sup>H NMR (300 MHz,  $\text{CDCl}_3$ ):  $\delta(\text{ppm}) = 1.23\text{--}1.40$  (m, 9 H,  $\text{O-CH}_2\text{-CH}_3$ ), 1.62 (d, 3 H,  $J = 6.8 \text{ Hz}$ ,  $\text{CH-CH}_3$ ), 4.10–4.46 (m, 7 H,  $\text{O-CH}_2\text{-CH}_3$ ,  $\text{CH-CH}_3$ ), 6.67 (m, 1 H,  $\text{CH-CF}_3$ ).

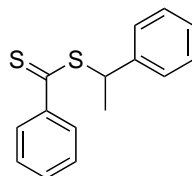
## 7 Experimental

---

**$^{13}\text{C}$  NMR** (75 MHz,  $\text{CDCl}_3$ ):  $\delta(\text{ppm}) = 14.2$  ( $\text{C}(=\text{O})\text{O}-\text{CH}_2-\text{CH}_3$ ), 16.5 ( $\text{P}-\text{O}-\text{CH}_2-\text{CH}_3$ ), 17.2 ( $\text{CH}-\text{CH}_3$ ), 48.8 ( $\text{CH}-\text{CH}_3$ ), 62.2 ( $\text{C}(=\text{O})\text{O}-\text{CH}_2-\text{CH}_3$ ), 64.6 ( $\text{P}-\text{O}-\text{CH}_2-\text{CH}_3$ ), 71.8 ( $\text{CH}-\text{CF}_3$ ), 121.6 ( $\text{CH}-\text{CF}_3$ ), 170.5 ( $\text{C}=\text{O}$ ), 211.2 ( $\text{C}=\text{S}$ ).

**EI-MS**  $m/z$ :  $[\text{M} + \text{Na}]^+$  calcd for  $\text{C}_{12}\text{H}_{20}\text{F}_3\text{O}_6\text{PS}_2$  435.0283, found 435.0294.

### 1-Phenylethyl dithiobenzoate



1-Phenylethyl dithiobenzoate (PEDB,  $M = 258.40 \text{ g} \cdot \text{mol}^{-1}$ ) was synthesized similar to the procedure described by Perrier.<sup>[85]</sup> Benzyl bromide (171.0 g, 1.0 mol) was added dropwise over two hours to a round bottomed flask containing elemental sulfur (64.1 g, 2.0 mol), 25 % sodium methoxide solution in methanol (432 g) and methanol (300 mL). The solution was refluxed for 6 h at 80 °C and stirred at room temperature over night. The mixture was filtered to remove the white solid (sodium bromide) and the methanol was removed under reduced pressure. The resulting brown solid was dissolved in water (1200 mL) and washed three times with diethyl ether (2400 mL total). A final layer of diethyl ether was added to the solution and the two-phase mixture was then acidified with 37 % aqueous HCl until the aqueous layer lost its characteristic brown color and the top layer was deep purple. The etherous layer was dried over magnesium sulfate and the solvent was removed under reduced pressure to yield dithiobenzoic acid as a deep purple oil.

Part of the acid (10.0 g, 64.8 mmol) was dissolved in *n*-pentane (300 mL) and styrene (8.1 g, 77.8 mmol). *Para*-toluenesulfonic acid (0.1 g, 0.7 mmol) was added as catalyst and the reaction mixture was stirred for 13 h at room temperature. The product was purified by column chromatography ( $\text{SiO}_2$ , *n*-heptane) to give 1-phenylethyl dithiobenzoate in 11 % yield.

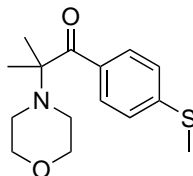
**$^1\text{H}$  NMR** (300 MHz,  $\text{CDCl}_3$ ):  $\delta(\text{ppm}) = 1.82$  (d, 3 H,  $J = 7.1 \text{ Hz}$ ,  $\text{CH}_3$ ), 5.26 (q, 1 H,  $J = 7.1 \text{ Hz}$ ,  $\text{CH}$ ), 7.28–7.38 (m, 5 H,  $\text{C}_6\text{H}_5$ ), 7.43–7.51 (m, 3 H,  $\text{C}_6\text{H}_5$ ), 7.94–7.98 (m, 2 H,  $\text{C}_6\text{H}_5$ ).

**$^{13}\text{C}$  NMR** (75 MHz,  $\text{CDCl}_3$ ):  $\delta(\text{ppm}) = 20.9$  ( $\text{CH}_3$ ), 50.4 ( $\text{CH}$ ), 127.0, 127.8, 128.0, 128.4, 128.8, 132.4, 141.4, 145.1 ( $\text{C}_6\text{H}_5$ ), 226.9 ( $\text{C}=\text{S}$ ).



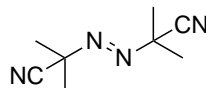
### 7.1.2 Initiators

#### 2-Methyl-1-[4-(methylthio)phenyl]-2-morpholin-4-ylpropan-1-one



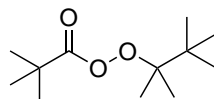
The photoinitiator 2-methyl-1-[4-(methylthio)phenyl]-2-morpholin-4-ylpropan-1-one (MMMP,  $M = 279.40 \text{ g} \cdot \text{mol}^{-1}$ , Aldrich, > 98 %) was used as received.

#### 2,2'-Azobis(2-methylpropionitrile)



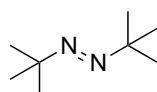
2,2'-Azobis(2-methylpropionitrile) (AIBN,  $M = 164.21 \text{ g} \cdot \text{mol}^{-1}$ , Akzo Nobel, 98 %) was recrystallized twice from diisopropyl ether prior to use.

#### Tetramethylpropyl peroxyvalate

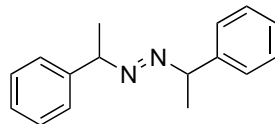


Tetramethylpropyl peroxyvalate (TMPPP,  $M = 216.32 \text{ g} \cdot \text{mol}^{-1}$ ) has been provided by Akzo Nobel (Polymer Chemicals Research Center Deventer) in 90.9 % purity.

#### 1,2-Di-*tert*-butyldiazene



1,2-Di-*tert*-butyldiazene (TBDA,  $M = 142.24 \text{ g} \cdot \text{mol}^{-1}$ , Aldrich, 97 %) was used as received.

**meso-1,2-bis(1-Phenylethyl)diazene**

Two syntheses for the azo-initiator *meso*-1,2-bis(1-phenylethyl)diazene (PEDA,  $M = 238.15 \text{ g} \cdot \text{mol}^{-1}$ ) are described in literature. Smolyar<sup>[184]</sup> reported that the reaction of acetophenone oxime with hydrazine hydrate gives the azo-initiator in 99.9 % yield. However, this one-step procedure results in the exclusive formation of acetophenone azine as can be proven by NMR.

Thus, the initiator was synthesized according to the three-step procedure described by Daub:<sup>[185]</sup> Acetophenone (50 mL, 428 mmol), hydrazine hydrate (50–60 %, 12 mL, 214 mmol) and glacial acetic acid (0.9 mL) were refluxed in ethanol (200 mL) for 4 h. After cooling to room temperature acetophenone azine (> 98 % yield,  $R_f$ : 0.80 in 3 : 1 toluene/ethyl acetate) precipitated as yellow crystals, which were filtered and air-dried.

Acetophenone azine (15.1 g, 63.8 mmol) was dissolved in dry ethyl acetate (500 mL) under argon atmosphere and Pd/C (10 %, 6.8 g, 6.4 mmol) was added. Subsequently, the argon atmosphere was replaced by hydrogen and the reaction mixture stirred at room temperature for 48 h. After completion of the reaction (TLC control,  $R_f$  of 1,2-bis(1-phenylethyl)diazene: 0.28 in 3 : 1 toluene/ethyl acetate) the mixture was filtered over celite to remove the catalyst.

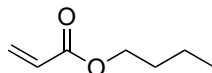
The filtrate was transferred into a round-bottomed flask and stirred under oxygen atmosphere until the reaction was completed (TLC). The solvent was evaporated at 30 °C under reduced pressure, methanol was added and the solution stored at –10 °C overnight. The colorless crystals were filtered off and washed with ice-cold methanol. The product was recrystallized twice from methanol to give 3.2 g (13.4 mmol, 21 % yield from acetophenone azine,  $R_f$ : 0.72 in 3 : 1 toluene/ethyl acetate) of *meso*-1,2-bis(1-phenylethyl)diazene. The purity was checked by NMR.

**<sup>1</sup>H NMR** (300 MHz, CDCl<sub>3</sub>):  $\delta$ (ppm) = 1.56 (d, 6 H,  $J = 6.8 \text{ Hz}$ , CH–CH<sub>3</sub>), 4.66 (q, 2 H,  $J = 6.8 \text{ Hz}$ , CH–CH<sub>3</sub>), 7.28–7.47 (m, 10 H, C<sub>6</sub>H<sub>5</sub>).

**<sup>13</sup>C NMR** (75 MHz, CDCl<sub>3</sub>):  $\delta$ (ppm) = 20.4 (CH–CH<sub>3</sub>), 76.8 (CH–CH<sub>3</sub>), 127.5, 128.7, 141.4 (C<sub>6</sub>H<sub>5</sub>).

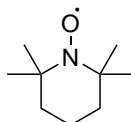
### 7.1.3 Miscellaneous

#### *n*-Butyl acrylate



The monomer *n*-butyl acrylate (BA,  $M = 128.17 \text{ g} \cdot \text{mol}^{-1}$ , Fluka, purum, 99.5 %, stabilized by hydroquinone monomethylether) was purified by passing over a column filled with inhibitor remover (Aldrich) prior to use.

#### (2,2,6,6-Tetramethylpiperidine-1-yl)oxyl



The EPR calibration standard (2,2,6,6-tetramethylpiperidine-1-yl)oxyl (TEMPO,  $M = 156.25 \text{ g} \cdot \text{mol}^{-1}$ , Aldrich, 99 %) was used as received.

#### Solvents

The principal solvents used for the EPR studies were obtained in high quality form and were used without further purification: Toluene (99.8 %, Sigma-Aldrich), naphthalene ( $\geq 99.7$  %, Fluka) and benzene (99.8 %, Sigma-Aldrich).

## 7.2 Instrumentation

### 7.2.1 Electron paramagnetic resonance spectroscopy

EPR experiments were performed on a Bruker Elexsys E 500 series CW (continuous wave) spectrometer operating at X-band frequency.<sup>[186]</sup> A schematic view of the spectrometer arrangement is illustrated in Figure 7.1. The microwave bridge houses the electromagnetic radiation source and the detector. The optical transmission cavity is a metal box into which the sample tube is placed. It is equipped with a grid which can be opened for experiments where irradiation of the sample is required. The cavity amplifies weak signals from the sample and is characterized by its quality factor  $Q$ , which indicates how efficiently the cavity stores microwave energy. As  $Q$  is inversely proportional to the amount of energy lost during one microwave period, an increasing  $Q$  enhances the sensitivity of the spectrometer. The magnet tunes the electronic energy levels and the console contains signal processing and control

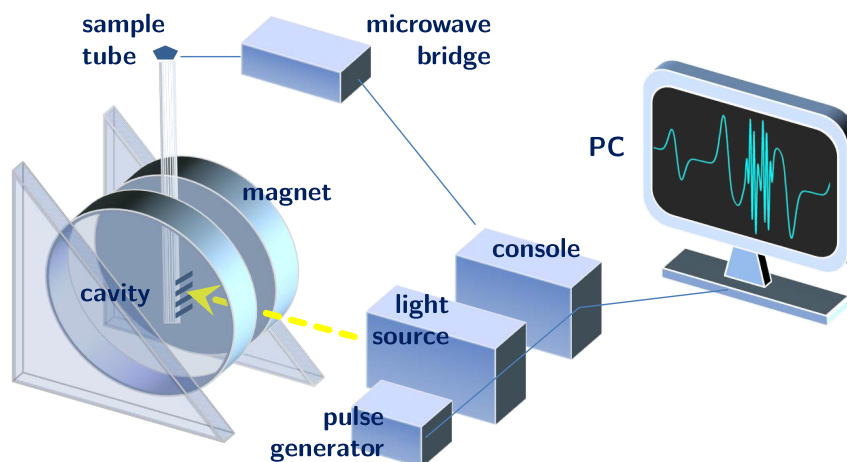


**Figure 7.1.** Schematic view of the EPR setup.

electronics. Temperature control was achieved via an ER 4131VT unit (Bruker) by purging the sample cavity with nitrogen.

For investigations which need a light source, additional components complete the setup: A 500 W mercury UV lamp (LAX, Mueller Elektronik) was used for continuous irradiation of the sample and a XeF excimer laser (COMPex 102, Lambda Physik) for generating short laser pulses at 351 nm. The laser source is triggered by the pulse generator Quantum Composers 9314 (Scientific Instruments). The spectrometer is connected to a computer, which is used for analyzing data as well as coordinating all the units for acquiring a spectrum.

The spectrometer settings were carefully chosen for each set of experiments to reduce potential errors (see Section 7.3.2). For best signal-to-noise ratio a field modulation frequency of 100 kHz was used, modulation amplitudes were varied between 0.5 and 3 G, and microwave powers ranged between 2 and 20 mW. With laser energies between 20 and 80 mJ per pulse and pulse repetition rates up to 20 Hz, spectra of the desired quality were obtained. The sweep time for recording one single spectrum depends largely on the radical concentration and ranges from 2 s to 10 min. At very low radical concentrations, instead of the sweep time, the number of added scans was increased to avoid a shift in the baseline of the spectrum. The signal channel digitizer was chosen to record full EPR spectra and the fast digitizer for acquiring time scans at a constant magnetic field value.

### 7.2.2 Size-exclusion chromatography

Product solutions were collected and subjected to size-exclusion chromatography (SEC) after evaporation of residual monomer and solvent. As the eluent, tetrahydrofuran for SEC (THF, Carl Roth, Rotipuran, stabilized with 2,6-di-*tert*-butyl-4-methylphenol) was used without further purification. Molar mass distributions were determined by means of SEC using a Waters 515 HPLC pump, three PSS-SDV columns with nominal 5 mm particle size and pore sizes of 105, 103, and 102 Å, and a Waters 2410 refractive index detector. The SEC setup was operated at 35 °C with a flow rate of 1 mL · min<sup>-1</sup> and was calibrated against polystyrene standards of narrow polydispersity ( $M_P = 800\text{--}2,000,000 \text{ g} \cdot \text{mol}^{-1}$ , Polymer Standards Service). As Mark-Houwink parameters for polyBA,  $K = 12.2 \times 10^{-5} \text{ dL} \cdot \text{g}^{-1}$  and  $a = 0.70$ ,<sup>[187]</sup> were used.

### 7.2.3 UV Spectroscopy

Measurements of the stability of RAFT agents under UV irradiation, of the RAFT agent concentrations in pre-polymerized samples, and of the decay of azo-initiators were performed on a Cary 100 UV-Vis spectrometer. The spectra were processed via the spectrometer software (Bruker).

### 7.2.4 NMR Spectroscopy

NMR spectra were recorded on a Varian Unity 300 spectrometer using CDCl<sub>3</sub> or CDCN as the solvent. The analyte concentrations were in the range of 20–60 g · L<sup>-1</sup>. The residual proton signal of the deuterated solvent served as internal standard for the <sup>1</sup>H and <sup>13</sup>C NMR spectra. The NMR data were processed with the program MestReNova 7.0.3-8830 (MESTRELAB RESEARCH).

## 7.3 Experimental Procedures

### 7.3.1 Sample preparation for EPR experiments

In case of liquid solvents the RAFT agent and the monomer were deoxygenated by three freeze-pump-thaw cycles. The solution was mixed with the initiator in a glove box under an argon atmosphere. The mixture was transferred into an EPR quartz tube of 5 mm outer and 4 mm inner diameter. The tube was sealed with a screw cap with teflon liner and protected from light prior to the experiment. In case of solid solvents the RAFT agent, the initiator and the solvent were directly weighed into the EPR tube and transferred to the glove box for deoxygenating and sealing. The volume of the samples was calculated from the filling level of the tube at the temperature used in the experiment.

### 7.3.2 Calibration of the EPR setup

EPR spectroscopy is the only technique that can directly detect and quantify the concentration of free radicals. Therefore, it plays an important role in investigating the RAFT equilibrium in which two radical species are present. The concentration of intermediate radicals cannot be determined by any other experimental technique and the concentration of propagating radicals is only indirectly accessible through the polymerization rate.

The absolute radical concentration of a sample is normally obtained by comparison with a standard sample of known concentration. Potential errors might be reduced to 3–5 % if the calibration conditions are chosen carefully.<sup>[188]</sup> The largest source of uncertainty has been assigned to the difference in field strength between sample and reference.<sup>[189]</sup> Therefore, several precautions were taken: The reference and sample were positioned identically in the cavity, they were measured in sample tubes of same material, diameter and wall thickness, the same sample volumes were used and the reference was dissolved in the same solvent/monomer mixture as the sample. Since the sensitivity of the EPR spectrometer depends on several experimental parameters which may change with temperature,<sup>[160]</sup> EPR calibration has been carried out at the actual reaction temperatures. In addition, the same spectroscopical parameters, i. e. microwave power, modulation amplitude, sweep time, number of recorded points and time constant, were used for sample and reference. For the correct determination of absolute radical concentrations it is further required to avoid signal saturation. To check for the absence of saturation, the microwave power was decreased and it was verified that the signal intensity also decreased by the square root of the microwave power.<sup>[186]</sup>

The double integral of the EPR first derivative spectrum is correlated with the concentration of the radical. Thus, the intensities of the reference and the sample were determined by double integration of the full spectra. In this work TEMPO was used as calibration standard since it is a stable radical which could be dissolved in all solvent/monomer mixtures used. In addition, its  $g$  value is close to the ones of the investigated radical species so that the absolute radical concentration of the sample,  $c_S$ , can be calculated from Equation 7.1<sup>[189,190]</sup>

$$c_S = c_R \cdot \frac{\iint I_{Ssc}}{\iint I_{Rsc}} = h_1 \cdot \iint I_{Ssc} \quad (7.1)$$

with  $c_R$  being the concentration of the reference and  $\iint I_{Ssc}$  and  $\iint I_{Rsc}$  being the double integrals of the sample spectrum and the reference spectrum, respectively. The index sc refers to the recording of the spectrum via the signal channel. Equation 7.1 is also valid for spectra acquired with the fast digitizer.

For determining the radical concentration of the sample from a recorded spectrum TEMPO standards were prepared. The standards contained radical concentrations

close to the experimentally observed ones. The double integral of the EPR signal intensities were plotted versus TEMPO concentration to yield a straight line with the slope  $h_1$  which is the proportionality constant between  $c_S$  and  $\iint I_{\text{Ssc}}$ .

Time scans were recorded at a constant magnetic field,  $B_x$ . Thus, the intensity of the recorded line has to be correlated to the double integral of the full spectrum. For different concentrations of one type of radical the double integral is plotted versus the intensity of the signal. Both quantities should be correlated linearly according to Equation 7.2

$$\iint I_{\text{Ssc}} = h_2 \cdot I_{\text{Ssc}}(B_x) \quad (7.2)$$

The constant  $h_2$  is the slope of the regression line and characteristic for each type of radical. Since it does not depend on the digitizer, the relation is also valid for the fast digitizer

$$\iint I_{\text{Sfd}} = h_2 \cdot I_{\text{Sfd}}(B_x) \quad (7.3)$$

Since the decay of radical species was traced with the fast digitizer the sensitivity has to be correlated with the signal channel detection. Hence, the double integrals of the TEMPO spectra recorded with the fast digitizer,  $\iint I_{\text{Sfd}}$ , are compared to the ones recorded with the signal channel,  $\iint I_{\text{Ssc}}$  using Equation 7.4

$$\iint I_{\text{Ssc}} = h_3 \cdot \iint I_{\text{Sfd}} \quad (7.4)$$

For the EPR spectrometer used the proportional constant  $h_3$  is around 2 and independent of radical concentration and temperature.

At a given time point, the radical concentration of a sample which contains one radical species is obtained by combining Equation 7.1 to 7.4

$$c_S(t) = h_1 \cdot h_2 \cdot h_3 \cdot I_{\text{Sfd}}(B_x)(t) \quad (7.5)$$

A detailed illustration of the calibration procedure may be found in the PhD thesis of P. Hesse.<sup>[191]</sup>

### 7.3.3 Deconvolution of EPR spectra

For samples containing more than one radical species the calibration procedure described in Section 7.3.2 has to be extended by a deconvolution procedure. This additional step yields the molar fractions of all contributing radical species. It is assumed that the EPR spectrum consists of a superposition of the individual EPR components.<sup>[129,192]</sup> Therefore, the spectra of the individual species needed to be known. This was achieved by recording them under conditions where only one of the radical species was present. Subsequently, the EPR spectra were simulated either with SIMFONIA (Bruker, version 1.25) or with EasySpin, version 3.1.6 (a MATLAB

based computational package). The simulated EPR spectra of the species were fitted to the experimental spectra using a least-squares method. Fitting was performed either by EXCEL (Microsoft Office 2007) or by a MATLAB code (see Appendix B). Note that a newer version of the EasySpin toolbox is now available, which includes the fitting of a two-component spectrum. Prior to the fitting, very noisy spectra were smoothed by applying a Fourier filter. In case where simulation of the spectrum of an individual species was not possible, i. e. the phenylethyl radical, several EPR spectra were coadded, further noise reduction was achieved by Fourier transformation and the resulting spectrum was then used for least-square fitting of the mixed spectra. The deconvolution procedure is illustrated in detail in Chapter 4 and 5.

If the radical ratio stays constant during the field scan the so-obtained molar fraction of the radical,  $x_i$ , can be used to calculate the time-dependent concentration of that radical

$$c_{S,i}(t) = h_1 \cdot h_{2,i} \cdot h_3 \cdot x_i \cdot I_{\text{Sfd}}(B_x)(t) \quad (7.6)$$

During UV-initiated RAFT polymerization a high percentage of the radicals is already destroyed during the field scan. The first laser pulse is therefore used for the time scan and no full spectrum is available for the deconvolution procedure. In this case molar fractions were calculated using the concentration ratio  $c_i/c_j$  obtained from separate UV experiments:

$$x_i = 1 - x_j \quad \text{and} \quad x_j = \frac{1}{1 + c_i/c_j} \quad (7.7)$$

### 7.3.4 Identification of side products in the model systems cyano-*iso*-propyl/2-(2'-cyanopropyl)-dithiobenzoate

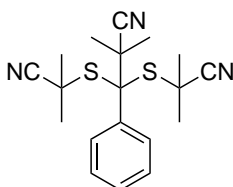
A solution of CPDB in toluene ( $0.75 \text{ mol} \cdot \text{L}^{-1}$ ) was deoxygenated by three freeze-pump-thaw cycles. AIBN was added to the degassed solution in a glove box under an argon atmosphere to yield concentrations of  $0.30 \text{ mol} \cdot \text{L}^{-1}$ . The solution was filled into a glass vial and sealed with a screw cap. The reaction mixture was stirred for 18 h at  $80 \text{ }^\circ\text{C}$ . After removal of the solvent and the volatile products under vacuum, the remaining product mixture was analyzed by  $^1\text{H}$  and  $^{13}\text{C}$  NMR for determination of the fraction of each product. Subsequently, CPDB and TMSN were separated from the other products by column chromatography ( $\text{SiO}_2$ , *n*-pentane/ethyl acetate 98:2). The residual side product mixture was again subjected to column chromatography ( $\text{SiO}_2$ , dichloromethane/*n*-pentane 2:1) to yield the “missing step” product CPDB\* as a red solid and a mixture of the cross-termination products CT1 and CT3 as a yellow oil. The isolated side products were identified via ESI-MS, 1D ( $^1\text{H}$ ,  $^{13}\text{C}$ ) and 2D (COSY, HSQC, HMBC) NMR spectroscopy.



**2,2,3,3-Tetramethylsuccinonitrile (TMSN)**

$^1\text{H NMR}$  (300 MHz,  $\text{CDCl}_3$ ):  $\delta(\text{ppm}) = 1.53$  (s,  $\text{C-CH}_3$ ).

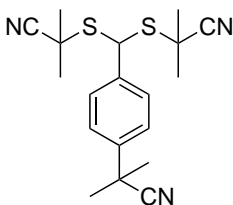
$^{13}\text{C NMR}$  (75 MHz,  $\text{CDCl}_3$ ):  $\delta(\text{ppm}) = 23.5$  ( $\text{C-CH}_3$ ), 39.5 ( $\text{C-CH}_3$ ), 121.5 ( $\text{C}\equiv\text{N}$ ).

**2,2'-((2-Cyano-2-methyl-1-phenylpropane-1,1-diyl)bis(sulfanediy))bis(2-methylpropanenitrile) (CT1)**

$^1\text{H NMR}$  (300 MHz,  $\text{CDCl}_3$ ):  $\delta(\text{ppm}) = 1.62$  (s, 6 H,  $\text{C-C-CH}_3$ ), 1.66 (s, 6 H,  $\text{S-C-CH}_3$ ), 1.71 (s, 6 H,  $\text{S-C-CH}_3$ ), 7.44 (m, 2 H,  $\text{C}_6\text{H}_5$ ), 7.46 (m, 1 H,  $\text{C}_6\text{H}_5$ ), 8.15 (m, 2 H,  $\text{C}_6\text{H}_5$ ).

$^{13}\text{C NMR}$  (75 MHz,  $\text{CDCl}_3$ ):  $\delta(\text{ppm}) = 26.8$  ( $\text{C-C-CH}_3$ ), 29.1 ( $\text{S-C-CH}_3$ ), 30.1 ( $\text{S-C-CH}_3$ ), 41.9 ( $\text{C-C-CH}_3$ ), 44.8 ( $\text{C-C-CH}_3$ ), 128.9 ( $\text{C}_6\text{H}_5$ ), 130.5 ( $\text{C}_6\text{H}_5$ ), 131.8 ( $\text{C}_6\text{H}_5$ ).

**ESI-HRMS**  $m/z$ :  $[\text{M} + \text{Na}]^+$  calcd for  $\text{C}_{19}\text{H}_{23}\text{N}_3\text{S}_2$  380.1226, found 380.1226.

**2,2'-(((4-(2-Cyanopropan-2-yl)phenyl)methylene)bis(sulfanediy))bis(2-methylpropanenitrile) (CT3)**

## 7 Experimental

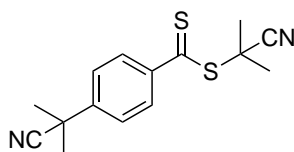
---

**$^1\text{H}$  NMR** (300 MHz,  $\text{CDCl}_3$ ):  $\delta(\text{ppm}) = 1.50$  (s, 6 H, S-C- $\text{CH}_3$ ), 1.69 (s, 6 H, C-C- $\text{CH}_3$ ), 1.71 (s, 6 H, S-C- $\text{CH}_3$ ), 5.48 (s, 1 H, S-CH-S), 7.53 (m, 2 H,  $\text{C}_6\text{H}_4$ ), 7.59 (m, 2 H,  $\text{C}_6\text{H}_4$ ).

**$^{13}\text{C}$  NMR** (75 MHz,  $\text{CDCl}_3$ ):  $\delta(\text{ppm}) = 28.2$  (S-C- $\text{CH}_3$ ), 28.4 (S-C- $\text{CH}_3$ ), 29.1 (C-C- $\text{CH}_3$ ), 37.9 (C-C- $\text{CH}_3$ ), 40.0 (S-C- $\text{CH}_3$ ), 52.5 (S-CH-S), 122.8 (S-C- $\text{C}\equiv\text{N}$ ), 125.4 (C-C- $\text{C}\equiv\text{N}$ ), 126.9 ( $\text{C}_6\text{H}_4$ ), 129.4 ( $\text{C}_6\text{H}_4$ ), 140.0 ( $\text{C}_6\text{H}_4$ ), 143.6 ( $\text{C}_6\text{H}_4$ ).

**ESI-HRMS**  $m/z$ :  $[\text{M} + \text{Na}]^+$  clcd for  $\text{C}_{19}\text{H}_{23}\text{N}_3\text{S}_2$  380.1226, found 380.1226.

### 2-Cyanopropan-2-yl 4-(2-cyanopropan-2-yl)benzodithioate (CPDB\*)



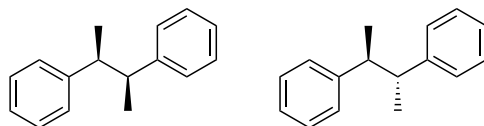
**$^1\text{H}$  NMR** (300 MHz,  $\text{CDCl}_3$ ):  $\delta(\text{ppm}) = 1.75$  (s, 6 H, C-C- $\text{CH}_3$ ), 1.95 (s, 6 H, S-C- $\text{CH}_3$ ), 7.53 (m, 2 H,  $\text{C}_6\text{H}_4$ ), 7.95 (m, 2 H,  $\text{C}_6\text{H}_4$ ).

**$^{13}\text{C}$  NMR** (75 MHz,  $\text{CDCl}_3$ ):  $\delta(\text{ppm}) = 26.6$  (S-C- $\text{CH}_3$ ), 29.1 (C-C- $\text{CH}_3$ ), 37.4 (C-C- $\text{CH}_3$ ), 42.0 (S-C- $\text{CH}_3$ ), 119.9 (S-C- $\text{C}\equiv\text{N}$ ), 123.9 (C-C- $\text{C}\equiv\text{N}$ ), 125.5 ( $\text{C}_6\text{H}_4$ ), 127.4 ( $\text{C}_6\text{H}_4$ ), 144.1 ( $\text{C}_6\text{H}_4$ ), 146.3 ( $\text{C}_6\text{H}_4$ ), 221.9 (C=S).

**ESI-HRMS**  $m/z$ :  $[\text{M} + \text{Na}]^+$  clcd for  $\text{C}_{15}\text{H}_{16}\text{N}_2\text{S}_2$  289.0828, found 289.0827.

### 7.3.5 Identification of PEDA decomposition products

To identify all initiator decomposition products a solution of *meso*-1,2-bis(1-phenylethyl)diazene (0.59 g, 2.5 mmol) in toluene (5 mL) was thoroughly degassed by three freeze-pump-thaw cycles. In an argon-filled glove box the solution was transferred into a glass vial which was sealed with a screw cap. The reaction mixture was stirred at 100 °C for 19 h. Subsequently, the solvent and volatile products were removed under reduced pressure. The  $^1\text{H}$  and  $^{13}\text{C}$  NMR spectra revealed the existence of three products which were separated by column chromatography ( $\text{SiO}_2$ , *n*-pentane/dichloromethane 1:0  $\rightarrow$  0:1). The isolated products were identified via EI-MS, 1D ( $^1\text{H}$ ,  $^{13}\text{C}$ ) and 2D (COSY, HSQC, HMBC) NMR spectroscopy. The same procedure was applied to identify the decomposition products at 80 and 110 °C.

**(2S,3S)-Butane-2,3-diylidibenzene and (2R,3S)-butane-2,3-diylidibenzene (BDDDB1 and BDDDB2)**

**<sup>1</sup>H NMR** (300 MHz, CDCl<sub>3</sub>):  $\delta$ (ppm) = 1.02 (d, 6 H,  $J$  = 6.8 Hz, CH<sub>3</sub>), 2.80 (ddq, 2 H,  $J$  = 6.8, 4.8, 2.4 Hz, CH), 7.19–7.25 (m, 6 H, C<sub>6</sub>H<sub>5</sub>), 7.28–7.35 (m, 4 H, C<sub>6</sub>H<sub>5</sub>).

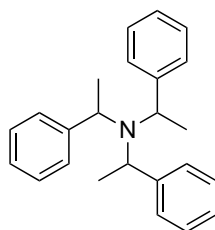
**<sup>13</sup>C NMR** (75 MHz, CDCl<sub>3</sub>):  $\delta$ (ppm) = 21.2 (CH<sub>3</sub>), 47.4 (CH), 126.2, 127.8, 128.4, 145.4 (C<sub>6</sub>H<sub>5</sub>).

**EI-MS**  $m/z$ : calcd for C<sub>16</sub>H<sub>18</sub> 210.1, found 210.2.

**<sup>1</sup>H NMR** (300 MHz, CDCl<sub>3</sub>):  $\delta$ (ppm) = 1.29 (d, 6 H,  $J$  = 7.0 Hz, CH<sub>3</sub>), 2.95 (ddq, 2 H,  $J$  = 7.0, 4.8, 2.1 Hz, CH), 6.99–7.05 (m, 4 H, C<sub>6</sub>H<sub>5</sub>), 7.06–7.13 (m, 2 H, C<sub>6</sub>H<sub>5</sub>), 7.14–7.21 (m, 4 H, C<sub>6</sub>H<sub>5</sub>).

**<sup>13</sup>C NMR** (75 MHz, CDCl<sub>3</sub>):  $\delta$ (ppm) = 18.1 (CH<sub>3</sub>), 46.6 (CH), 125.8, 127.9, 128.0, 146.0 (C<sub>6</sub>H<sub>5</sub>).

**EI-MS**  $m/z$ : calcd for C<sub>16</sub>H<sub>18</sub> 210.1, found 210.2.

**Tris(1-phenylethyl)amine (TPEA)**

**<sup>1</sup>H NMR** (300 MHz, CDCl<sub>3</sub>):  $\delta$ (ppm) = 1.54 (d, 3 H,  $J$  = 6.9 Hz, CH<sub>3</sub>), 4.64 (q, 1 H,  $J$  = 6.9 Hz, CH), 7.27–7.45 (m, 5 H, C<sub>6</sub>H<sub>5</sub>).

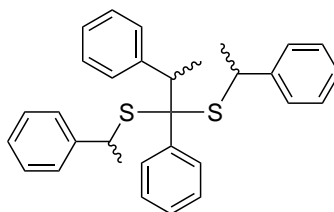
$^{13}\text{C}$  NMR (75 MHz,  $\text{CDCl}_3$ ):  $\delta(\text{ppm}) = 20.4$  ( $\text{CH}_3$ ), 76.8 ( $\text{CH}$ ), 127.5, 127.5, 141.4 ( $\text{C}_6\text{H}_5$ ).

$^{15}\text{N}$  HMBC NMR (30 MHz,  $\text{CDCl}_3$ ):  $\delta(\text{ppm}) = -253.4$ .

### 7.3.6 Identification of side products in the model system phenylethyl/1-phenylethyl dithiobenzoate

PEDA (0.22 g, 0.91 mmol) was added to a solution of PEDB (0.24 g, 0.91 mmol) in toluene (2.1 mL). The solution was degassed by three freeze–pump–thaw cycles. In an argon glove box the solution was transferred into a glass vial and sealed with a screw cap. The reaction mixture was stirred at 110 °C for 19 h. Subsequently, the solvent and volatile products were removed under reduced pressure. NMR spectra showed a mixture of various products, which were separated by column chromatography ( $\text{SiO}_2$ , *n*-heptane/ethyl acetate 99:1) yielding the RAFT agent, initiator decomposition products and a fraction which contained the side products. This side product mixture was again subjected to column chromatography ( $\text{SiO}_2$ , *n*-heptane) The isolated products were identified via ESI-MS, 1D ( $^1\text{H}$ ,  $^{13}\text{C}$ ) and 2D (COSY, HSQC, HMBC) NMR spectroscopy. The same procedure was applied to identify the side products in the PE/PEDB model system at 80 and 100 °C.

#### (1,2-Diphenylpropane-1,1-diyl)bis((1-phenylethyl)sulfane) (CT1)



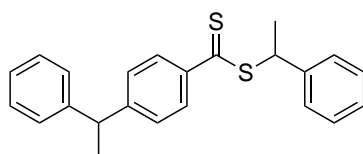
$^1\text{H}$  NMR (300 MHz,  $\text{CDCl}_3$ ):  $\delta(\text{ppm}) = 0.77$  (d, 3 H,  $J = 7.2$  Hz,  $\text{CH}_3$ ), 0.79 (d, 3 H,  $J = 7.2$  Hz,  $\text{CH}_3$ ), 1.07 (d, 3 H,  $J = 7.3$  Hz,  $\text{CH}_3$ ), 1.21 (d, 3 H,  $J = 7.2$  Hz,  $\text{CH}_3$ ), 1.22 (d, 3 H,  $J = 7.2$  Hz,  $\text{CH}_3$ ), 1.24 (d, 3 H,  $J = 7.2$  Hz,  $\text{CH}_3$ ), 1.37 (d, 3 H,  $J = 7.2$  Hz,  $\text{CH}_3$ ), 1.39 (d, 3 H,  $J = 7.2$  Hz,  $\text{CH}_3$ ), 1.65 (d, 3 H,  $J = 7.2$  Hz,  $\text{CH}_3$ ), 1.66 (d, 3 H,  $J = 7.2$  Hz,  $\text{CH}_3$ ), 1.74 (d, 3 H,  $J = 7.4$  Hz,  $\text{CH}_3$ ), 1.78 (d, 3 H,  $J = 7.2$  Hz,  $\text{CH}_3$ ), 2.81 (q, 1 H,  $J = 7.0$  Hz,  $\text{CH}$ ), 2.97 (q, 1 H,  $J = 7.1$  Hz,  $\text{CH}$ ), 3.40 (q, 1 H,  $J = 7.0$  Hz,  $\text{CH}$ ), 3.55 (q, 1 H,  $J = 7.1$  Hz,  $\text{CH}$ ), 3.83 (q, 2 H,  $J = 7.3$  Hz,  $\text{CH}$ ), 4.10 (q, 2 H,  $J = 7.4$  Hz,  $\text{CH}$ ), 4.21 (q, 1 H,  $J = 7.1$  Hz,  $\text{CH}$ ), 4.30 (q, 1 H,  $J = 7.2$  Hz,  $\text{CH}$ ), 4.35 (q, 1 H,  $J = 7.2$  Hz,  $\text{CH}$ ), 4.72 (q, 1 H,  $J = 7.4$  Hz,  $\text{CH}$ ), 6.30–7.68 (m, 80 H,  $\text{C}_6\text{H}_5$ ).

$^{13}\text{C}$  NMR (75 MHz,  $\text{CDCl}_3$ ):  $\delta(\text{ppm}) = 17.7$  (2C), 18.4 (2C), 23.5, 23.9, 24.8, 25.2, 25.3, 25.4, 25.9, 26.1 ( $\text{CH}_3$ ), 44.3, 44.4, 44.7, 45.0, 45.1 (2C), 45.5, 45.8, 48.1, 48.6, 49.7, 50.1 ( $\text{CH}$ ), 126.0, 126.1, 126.3, 126.4, 126.6, 126.7, 126.8 (2C), 126.9, 127.0, 127.1 (2C), 127.3, 127.4, 127.7, 127.8 (2C), 127.9, 128.0, 128.4, 128.5 (3C), 128.7, 130.3 (2C), 130.4 (2C), 130.5, 130.7, 130.8 (2C), 136.7, 136.9, 138.6, 138.8, 140.9, 141.0 (2C), 141.1, 144.4, 145.2, 145.5, 145.6, 146.0, 146.1, 146.3, 146.5 ( $\text{C}_6\text{H}_5$ ).

Note: The quaternary carbons between the sulfur atoms are not resolved due to the poor signal-to-noise ratio.

**ESI-HRMS**  $m/z$ :  $[\text{M} + \text{Na}]^+$  clcd for  $\text{C}_{31}\text{H}_{32}\text{S}_2$  491.1838, found 491.1831.

### 1-Phenylethyl 4-(1-phenylethyl)benzodithioate (PEDB\*)



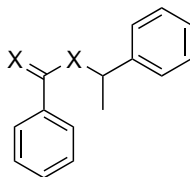
$^1\text{H}$  NMR (300 MHz,  $\text{CDCl}_3$ ):  $\delta(\text{ppm}) = 1.63$  (d, 3H,  $J = 7.1$  Hz,  $\text{S}-\text{CH}-\text{CH}_3$ ), 1.79 (d, 3H,  $J = 7.0$  Hz,  $\text{C}-\text{CH}-\text{CH}_3$ ), 4.16 (q, 1H,  $J = 7.1$  Hz,  $\text{S}-\text{CH}-\text{CH}_3$ ), 5.25 (q, 1H,  $J = 7.0$  Hz,  $\text{C}-\text{CH}-\text{CH}_3$ ), 7.15–7.23 (m, 5H,  $\text{C}_6\text{H}_5$  or  $\text{C}_6\text{H}_4$ ), 7.25–7.38 (m, 5H,  $\text{C}_6\text{H}_5$  or  $\text{C}_6\text{H}_4$ ), 7.40–7.45 (m, 2H,  $\text{C}_6\text{H}_5$  or  $\text{C}_6\text{H}_4$ ), 7.86–7.93 (m, 2H,  $\text{C}_6\text{H}_5$  or  $\text{C}_6\text{H}_4$ ).

$^{13}\text{C}$  NMR (75 MHz,  $\text{CDCl}_3$ ):  $\delta(\text{ppm}) = 21.0$  ( $\text{C}-\text{CH}-\text{CH}_3$ ), 21.6 ( $\text{S}-\text{CH}-\text{CH}_3$ ), 127.2, 127.7, 127.7, 128.0, 128.6, 128.8 ( $\text{C}_6\text{H}_5$  and  $\text{C}_6\text{H}_4$ ).

Note: Tertiary and quaternary carbons are not resolved due to the poor signal-to-noise ratio. The red color of the compound is however suggestive of the  $\text{C}=\text{S}$  double bond.

**ESI-HRMS**  $m/z$ :  $[\text{M} + \text{H}]^+$  clcd for  $\text{C}_{23}\text{H}_{22}\text{S}_2$  363.1236, found 363.1237.

**not yet identified product**



**<sup>1</sup>H NMR** (300 MHz, CDCl<sub>3</sub>):  $\delta$ (ppm) = 1.78 (d, 3 H,  $J$  = 7.1 Hz, CH<sub>3</sub>), 4.97 (q, 1 H,  $J$  = 7.1 Hz, CH), 7.15–7.38 (m, 9 H, C<sub>6</sub>H<sub>5</sub>), 7.43–7.50 (m, 1 H, C<sub>6</sub>H<sub>5</sub>), 7.92–7.97 (m, 2 H, C<sub>6</sub>H<sub>5</sub>).

**<sup>13</sup>C NMR** (75 MHz, CDCl<sub>3</sub>):  $\delta$ (ppm) = 22.5 (CH<sub>3</sub>), 43.2 (CH), 127.4 (2C), 127.5 (3C), 128.7 (2C), 128.8 (2C), 133.5, 137.1, 142.8 (C<sub>6</sub>H<sub>5</sub>), 191.3 (C=X).

Note: The signals are very similar to PEDB, but the product is yellow and the <sup>13</sup>C signal is shifted from 226.9 to 191.3 ppm.

**ESI-MS**  $m/z$ : [M + Na]<sup>+</sup> 265.1.

# 8

## Development of PREDICI models

For the accurate determination of the rate coefficients relevant to the RAFT equilibria, simulations of the complete kinetic scheme had to be performed. RAFT polymerization was previously studied with different modeling strategies including Monte Carlo simulations,<sup>[193]</sup> the discrete Galerkin approach,<sup>[64]</sup> and the method of moments.<sup>[45,194]</sup>

In this thesis the commercial software package PREDICI<sup>®</sup> (Version 6.4.8) provided by CiT (Computing in Technology, GmbH) was used. It is based on the h-p Galerkin method,<sup>[195]</sup> which is a numerical method for solving differential equations employing elements of defined size,  $h$ , and polynomial degree,  $p$ . By using a commercially available software, simulation results can be compared. PREDICI<sup>®</sup> works by creating a reaction mechanism from a database of pre-defined reaction step patterns. It is able to compute concentrations and full molecular mass distributions of polymeric species and includes a parameter estimation tool for fitting experimental data – a feature which is valuable for the determination of rate coefficients.<sup>[196]</sup>

PREDICI<sup>®</sup> does not include a direct reversible reaction between macromolecules in its reaction step database. In order to implement reactions such as the addition and fragmentation reactions of RAFT, where the intermediate radical is composed of two or three “arms” which differ in chain length, temporary chain size memory species have to be used. It has been shown that mathematically this approach is the same as having the direct reversible steps.<sup>[197–199]</sup>

The xanthate EDTCP, the trithiocarbonate EPPT and the dithiobenzoate ETTP form intermediate radicals bearing two growing chains. These intermediates are described by a two-dimensional (2D) chain-length distribution. The trithiocarbonate BMPT forms an intermediate radical bearing three growing chains, which is described

by a three-dimensional (3D) chain-length distribution. Since PREDICI<sup>®</sup> provides no reaction steps for equilibria containing two- or three-dimensional species, the 2D and 3D problem have to be translated to a 1D problem. The deviation of these translations is detailed in the following sections. To ensure that the output is correct, species concentrations from the full molecular mass distribution simulation and the moments simulation were checked for agreement.

## 8.1 Implementation of the 2D RAFT mechanism into PREDICI

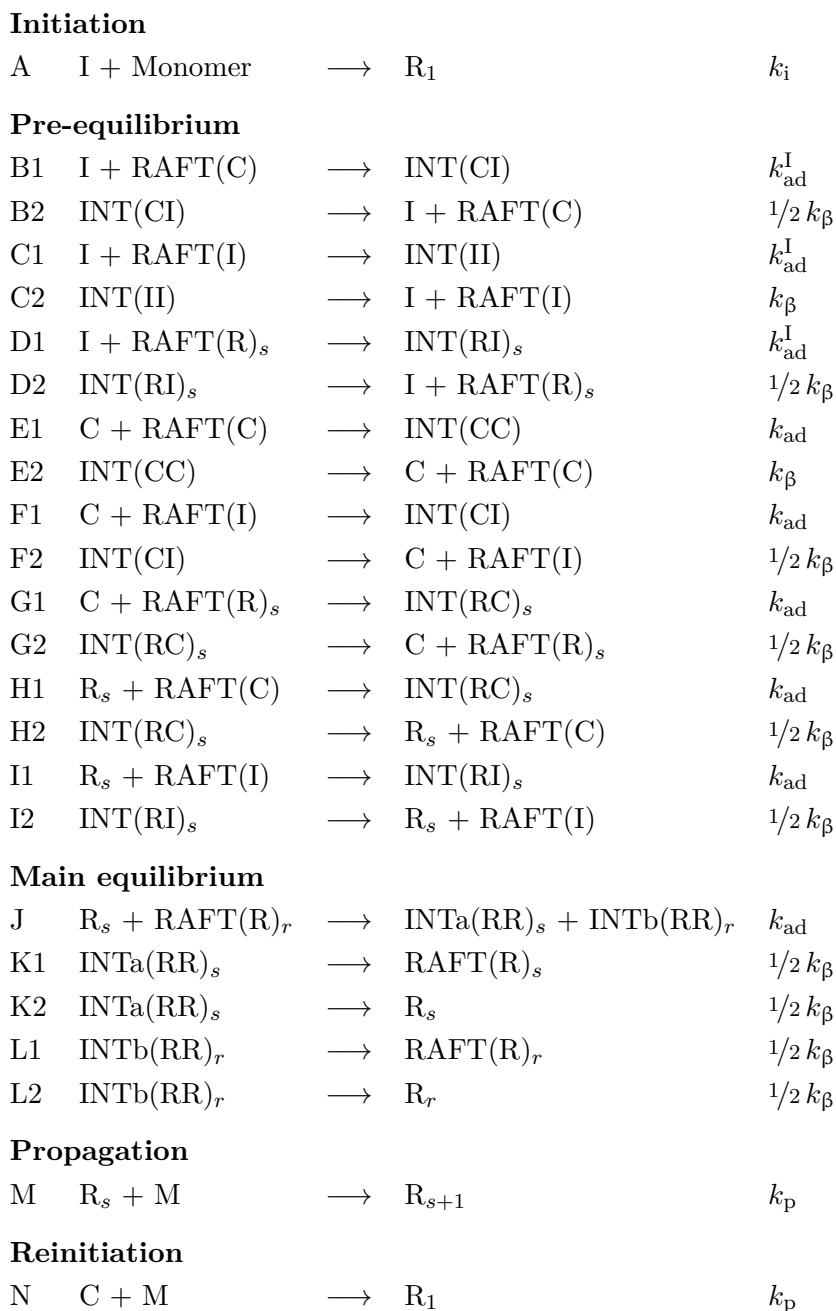
Scheme 8.1 shows the reactions and associated rate coefficients that have been translated into differential equations in the program package PREDICI<sup>®</sup>. The detailed kinetic scheme consists of initiation (reaction step A), propagation (M), termination (O-R3), the individual RAFT pre-equilibrium (B1-I2) and main equilibrium reaction steps (J-L2), reinitiation of the leaving group (N), and cross-termination of the intermediate radical species (S1-Y12).

The model considers 3 RAFT species and 6 INT species, which differ in their chemical structure. A RAFT species may either bear an initiator-derived radical, I, or the leaving group, C, or a growing chain, R, whereas an intermediate radical may bear a combination of two arms, i. e. I, C and R (see Scheme 8.2). The arguments  $s$  and  $r$  refer to the chain length of the species.

An intermediate radical bearing two chemically different arms, for example INT(CI), may either fragment into an initiator-derived radical plus the original RAFT agent (reaction B2) or the leaving group and a RAFT agent bearing an initiator-derived species (reaction F2). As the reaction proceeds to either one side or the other,  $k_{\beta}$  has to be divided by two. The same is valid for the pre-equilibrium reaction steps D2, and G2 to I2.

In the main equilibrium, a propagating chain adds to the macromolecular RAFT agent to form an intermediate radical, which carries two polymeric chains that may differ in chain length (reaction J). The arms of the intermediate radical bearing two growing chains are described by a two-dimensional (2D) chain-length distribution. Since the calculation of a 2D problem requires extensive numerical efforts, the reactions involving an intermediate radical, which carries two polymeric chains (J to L2 and Y1 to Y12), have been translated to a 1D problem via the approach of boundary density integrals. The mathematical basis of this procedure is detailed by Wulkow *et al.* and its validity was independently verified by Gao and Zhu.<sup>[197,200,201]</sup> According to this method, two temporary chain size memory species, INTa(RR) and INTb(RR), have been introduced, each acting as a chain length memory for the macroRAFT species, RAFT(R). Similar to the pre-equilibrium, the RAFT end group may either remain on the original growing radical chain or exchange its place to the other growing chain.





Scheme 8.1. Kinetic scheme for the 2D models.

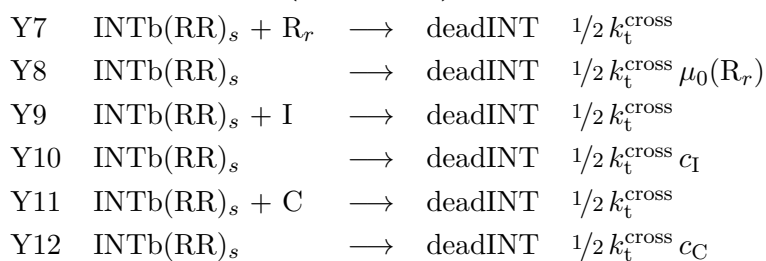
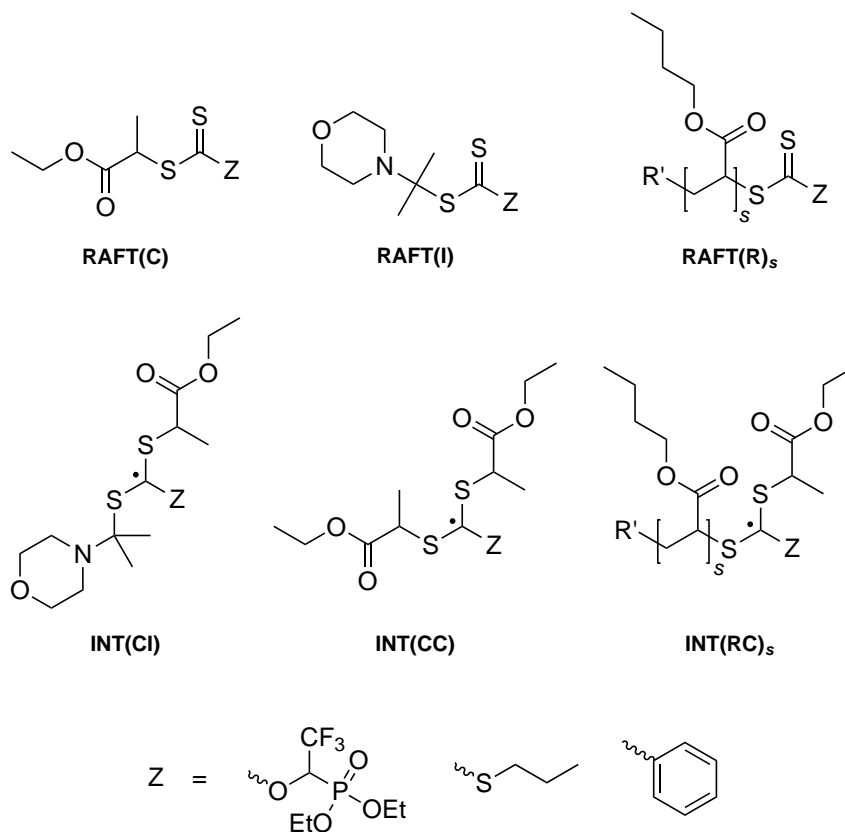
**Termination**

O	$R_s + R_r$	$\longrightarrow$	$P_{r+s}$	$k_t^{i,i}$
P	$R_s + I$	$\longrightarrow$	$P_s$	$k_t^{i,i}$
Q	$R_s + C$	$\longrightarrow$	$P_s$	$k_t^{i,i}$
R1	$C + C$	$\longrightarrow$	CC	$k_t^{1,1}$
R2	$I + I$	$\longrightarrow$	II	$k_t^{1,1}$
R3	$C + I$	$\longrightarrow$	CI	$k_t^{1,1}$

**Cross-termination**

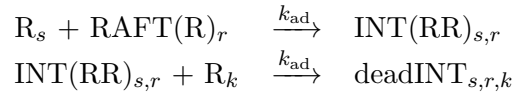
S1	$\text{INT}(\text{CI}) + R_s$	$\longrightarrow$	deadINT	$k_t^{\text{cross}}$
S2	$\text{INT}(\text{CI}) + I$	$\longrightarrow$	deadINT	$k_t^{\text{cross}}$
S3	$\text{INT}(\text{CI}) + C$	$\longrightarrow$	deadINT	$k_t^{\text{cross}}$
T1	$\text{INT}(\text{CC}) + R_s$	$\longrightarrow$	deadINT	$k_t^{\text{cross}}$
T2	$\text{INT}(\text{CC}) + I$	$\longrightarrow$	deadINT	$k_t^{\text{cross}}$
T3	$\text{INT}(\text{CC}) + C$	$\longrightarrow$	deadINT	$k_t^{\text{cross}}$
U1	$\text{INT}(\text{RC})_s + R_r$	$\longrightarrow$	deadINT	$k_t^{\text{cross}}$
U2	$\text{INT}(\text{RC})_s + I$	$\longrightarrow$	deadINT	$k_t^{\text{cross}}$
U3	$\text{INT}(\text{RC})_s + C$	$\longrightarrow$	deadINT	$k_t^{\text{cross}}$
V1	$\text{INT}(\text{II}) + R_s$	$\longrightarrow$	deadINT	$k_t^{\text{cross}}$
V2	$\text{INT}(\text{II}) + I$	$\longrightarrow$	deadINT	$k_t^{\text{cross}}$
V3	$\text{INT}(\text{II}) + C$	$\longrightarrow$	deadINT	$k_t^{\text{cross}}$
X1	$\text{INT}(\text{RI})_s + R_r$	$\longrightarrow$	deadINT	$k_t^{\text{cross}}$
X2	$\text{INT}(\text{RI})_s + I$	$\longrightarrow$	deadINT	$k_t^{\text{cross}}$
X3	$\text{INT}(\text{RI})_s + C$	$\longrightarrow$	deadINT	$k_t^{\text{cross}}$
Y1	$\text{INTa}(\text{RR})_s + R_r$	$\longrightarrow$	deadINT	$1/2 k_t^{\text{cross}}$
Y2	$\text{INTa}(\text{RR})_s$	$\longrightarrow$	deadINT	$1/2 k_t^{\text{cross}} \mu_0(R_r)$
Y3	$\text{INTa}(\text{RR})_s + I$	$\longrightarrow$	deadINT	$1/2 k_t^{\text{cross}}$
Y4	$\text{INTa}(\text{RR})_s$	$\longrightarrow$	deadINT	$1/2 k_t^{\text{cross}} c_I$
Y5	$\text{INTa}(\text{RR})_s + C$	$\longrightarrow$	deadINT	$1/2 k_t^{\text{cross}}$
Y6	$\text{INTa}(\text{RR})_s$	$\longrightarrow$	deadINT	$1/2 k_t^{\text{cross}} c_C$

Scheme 8.1. (continued)

**Cross-termination (continued)****Scheme 8.1.** (continued)**Scheme 8.2.** All possible RAFT species and 3 of 6 possible intermediate radical species that have been considered in the kinetic scheme for BA polymerizations mediated by the xanthate EDTCP, the trithiocarbonate EPPT and the dithiobenzoate ETTP, respectively.

For an overall balanced process, the decomposition is implemented twice (reactions K1 to L2) and  $k_\beta$  was divided by two. The change in the temporary chain size memory species, INTa(RR) and INTb(RR), can be formulated as decoupled (either K1 and K2 or L1 and L2) because it is a unimolecular reaction.

The approach of boundary density integrals was also applied to implement the cross-termination reactions. The method is illustrated by example of the addition of a propagating radical to a macroRAFT species and the subsequent termination of the resulting intermediate radical:



Here  $\mathbf{R}_s$  and  $\text{RAFT}(\mathbf{R})_r$  describe 1D polymer distributions,  $\text{INT}(\text{RR})_{s,r}$  denotes a 2D distribution consisting of sub-chains of lengths  $s$  and  $r$  and  $\text{deadINT}_{s,r,k}$  refers to the corresponding 3D distribution.

This leads to the following differential equation system where the chain lengths  $s$ ,  $r$ ,  $k$  are written as subscript and  $\mu_0$  denotes the zero moment of a distribution:

$$\frac{\delta \mathbf{R}_s}{\delta t} = -k_{\text{ad}} \cdot \mathbf{R}_s \cdot \mu_0(\text{RAFT}(\mathbf{R})_r) - k_{\text{t}}^{\text{cross}} \cdot \mathbf{R}_s \cdot \mu_{0,0}(\text{INT}(\text{RR})_{s,r}) \quad (8.1)$$

$$\frac{\delta \text{RAFT}(\mathbf{R})_s}{\delta t} = -k_{\text{ad}} \cdot \mu_0(\mathbf{R}_s) \cdot \text{RAFT}(\mathbf{R})_r \quad (8.2)$$

$$\frac{\delta \text{INT}(\text{RR})_{s,r}}{\delta t} = k_{\text{ad}} \cdot \mathbf{R}_s \cdot \text{RAFT}(\mathbf{R})_r - k_{\text{t}}^{\text{cross}} \cdot \mu_0(\mathbf{R}_s) \cdot \text{INT}(\text{RR})_{s,r} \quad (8.3)$$

$$\frac{\delta \text{deadINT}_{s,r,k}}{\delta t} = -k_{\text{t}}^{\text{cross}} \cdot \mathbf{R}_s \cdot \text{INT}(\text{RR})_{s,r} \quad (8.4)$$

Since a full computation of the 2D and 3D distribution is not necessary for computing the molecular mass distributions of  $\mathbf{R}_s$  and  $\text{RAFT}_r$ , the following boundary density integrals are introduced:

$$\text{INTa}(\text{RR})_s = \sum_r \text{INT}(\text{RR})_{s,r} \quad (8.5)$$

$$\text{INTb}(\text{RR})_r = \sum_s \text{INT}(\text{RR})_{s,r} \quad (8.6)$$

$$\text{deadINTa}(\text{RRR})_s = \sum_{r,k} \text{deadINT}(\text{RRR})_{s,r,k} \quad (8.7)$$

$$\text{deadINTb}(\text{RRR})_r = \sum_{s,k} \text{deadINT}(\text{RRR})_{s,r,k} \quad (8.8)$$

$$\text{deadINTc}(\text{RRR})_k = \sum_{s,r} \text{deadINT}(\text{RRR})_{s,r,k} \quad (8.9)$$

The overall concentration of the  $\text{INT}(\text{RR})_{s,r}$  species is given by:

$$\mu_{0,0}(\text{INT}(\text{RR})_{s,r}) = \sum_s \sum_r \text{INT}(\text{RR})_{s,r} \quad (8.10)$$

Using the definitions of Equation 8.5 and 8.6 we derive the following:

$$\begin{aligned} \mu_{0,0}(\text{INT}(\text{RR})_{s,r}) &= \sum_s \sum_r \text{INT}(\text{RR})_{s,r} \\ &= \sum_r \text{INTa}(\text{RR})_s = \sum_s \text{INTb}(\text{RR})_r \\ &= \mu_0(\text{INTa}(\text{RR})_s) = \mu_0(\text{INTb}(\text{RR})_r) \end{aligned} \quad (8.11)$$

In the same way, the overall concentration of the  $\text{deadINT}_{s,r,k}$  species is given by:

$$\begin{aligned} \mu_{0,0,0}(\text{deadINT}(\text{RRR})_{s,r,k}) &= \sum_s \sum_r \sum_k \text{deadINT}(\text{RRR})_{s,r,k} \\ &= \sum_s \text{deadINTa}(\text{RRR})_s \\ &= \sum_r \text{deadINTb}(\text{RRR})_r \\ &= \sum_k \text{deadINTc}(\text{RRR})_k \\ &= \mu_0(\text{deadINTa}(\text{RRR})_s) \\ &= \mu_0(\text{deadINTb}(\text{RRR})_r) \\ &= \mu_0(\text{deadINTc}(\text{RRR})_k) \end{aligned} \quad (8.12)$$

Substituting the expressions 8.5 to 8.12 into the differential equations 8.1 to 8.4 yields:

$$\begin{aligned} \frac{\delta R_s}{\delta t} &= -k_{\text{ad}} \cdot R_s \cdot \mu_0(\text{RAFT}(\text{R})_r) \\ &\quad - \frac{1}{2} \cdot k_t^{\text{cross}} \cdot R_s \cdot \left( \mu_0(\text{INTa}(\text{RR})_s) + \mu_0(\text{INTb}(\text{RR})_r) \right) \end{aligned} \quad (8.13)$$

$$\frac{\delta \text{RAFT}(\text{R})_r}{\delta t} = -k_{\text{ad}} \cdot \mu_0(R_s) \cdot \text{RAFT}(\text{R})_r \quad (8.14)$$

$$\frac{\delta \text{INTa}(\text{RR})_s}{\delta t} = k_{\text{ad}} \cdot R_s \cdot \text{RAFT}(\text{R})_r - k_t^{\text{cross}} \cdot \mu_0(R_s) \cdot \text{INTa}(\text{RR})_s \quad (8.15)$$

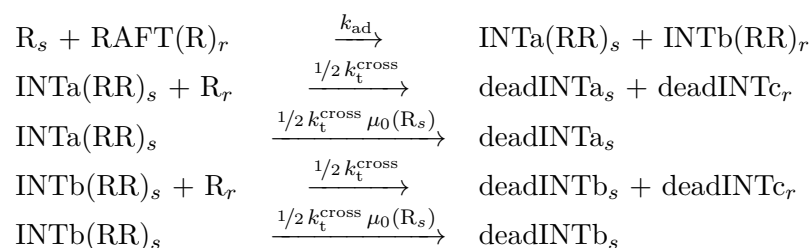
$$\frac{\delta \text{INTb}(\text{RR})_s}{\delta t} = k_{\text{ad}} \cdot R_s \cdot \text{RAFT}(\text{R})_r - k_t^{\text{cross}} \cdot \mu_0(R_s) \cdot \text{INTb}(\text{RR})_s \quad (8.16)$$

$$\frac{\delta \text{deadINTa(RRR)}_s}{\delta t} = k_t^{\text{cross}} \cdot R_s \cdot \text{INTa(RR)}_s \quad (8.17)$$

$$\frac{\delta \text{deadINTb(RRR)}_r}{\delta t} = k_t^{\text{cross}} \cdot R_s \cdot \text{INTb(RR)}_r \quad (8.18)$$

$$\frac{\delta \text{deadINTc(RRR)}_k}{\delta t} = \frac{1}{2} \cdot k_t^{\text{cross}} \cdot R_s \cdot \left( \mu_0(\text{INTa(RR)}_s) + \mu_0(\text{INTb(RR)}_r) \right) \quad (8.19)$$

This new set of equations 8.13 to 8.19 can then be translated back to a reaction system:



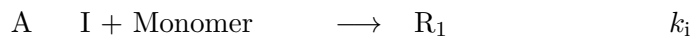
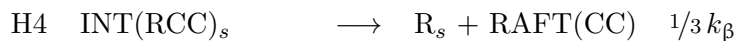
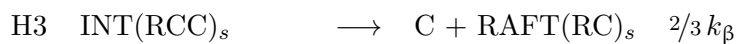
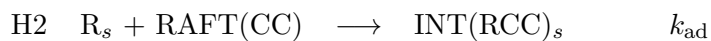
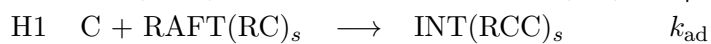
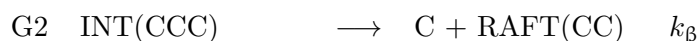
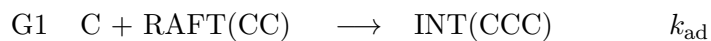
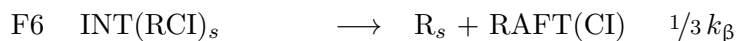
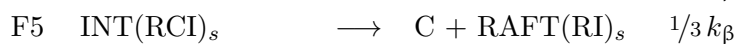
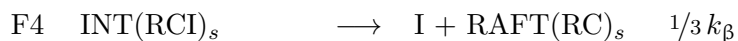
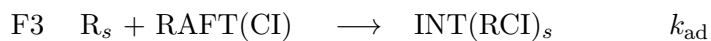
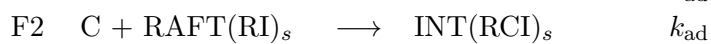
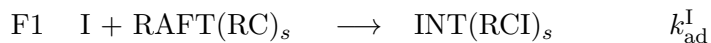
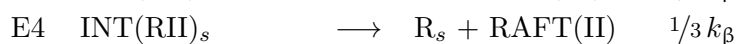
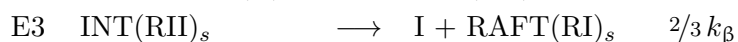
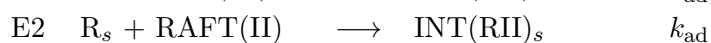
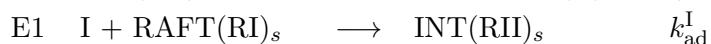
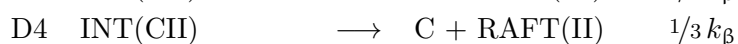
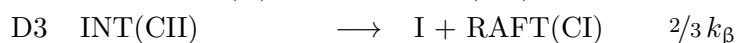
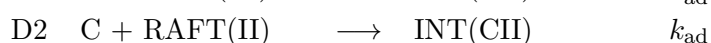
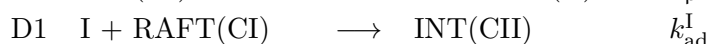
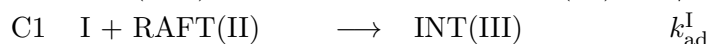
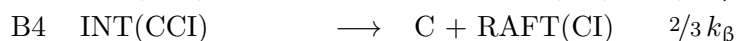
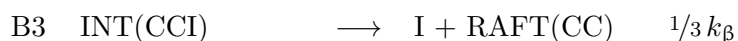
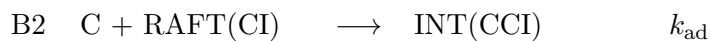
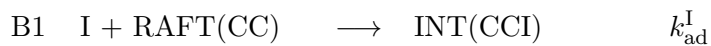
Since the concentration of the terminated intermediate radical is too low to be detected in the reaction mixture, it was not necessary to obtain any exact values for the termination product and the temporary chain size memory species, deadINTa, deadINTb and deadINTc, were not distinguished. Instead a general species, deadINT, was used and the reaction system obtained is described by reactions J, Y1, Y2, Y7 and Y8.

The same method was applied to implement the addition of an initiator-derived radical to the intermediate radical (reactions Y3, Y4, Y9 and Y10) and the addition of the leaving group to intermediate radical (reactions Y5, Y6, Y11 and Y12).

## 8.2 Implementation of the 3D RAFT mechanism into PREDICI

As in the case of the 2D model the full kinetic scheme consists of initiation (reaction step A), propagation (M), termination (O-R3), the individual RAFT pre- and main equilibrium reaction steps (B1-L9), reinitiation of the leaving group radical (N), and cross-termination of the intermediate radical species (S1-ZC18). The reaction steps are listed in Scheme 8.3.

The model considers 6 RAFT species and 10 INT species, which differ in their chemical structure. Scheme 8.4 shows 3 possible RAFT and INT structures, respectively. Each RAFT species bears a combination of 2 arms and each INT species a combination of 3 arms, with the arms being the initiator-derived radical, I, the leaving group, C, or a growing chain, R.

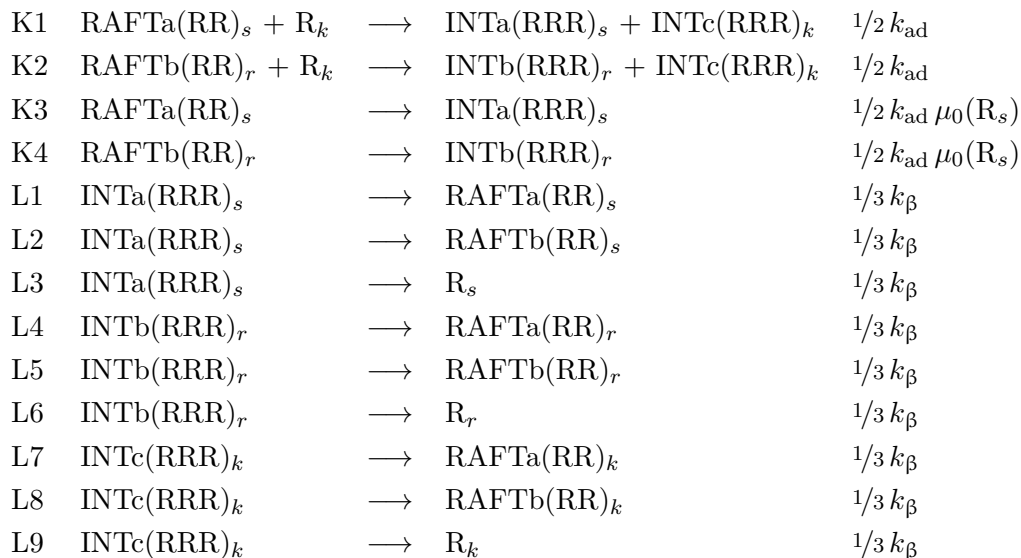
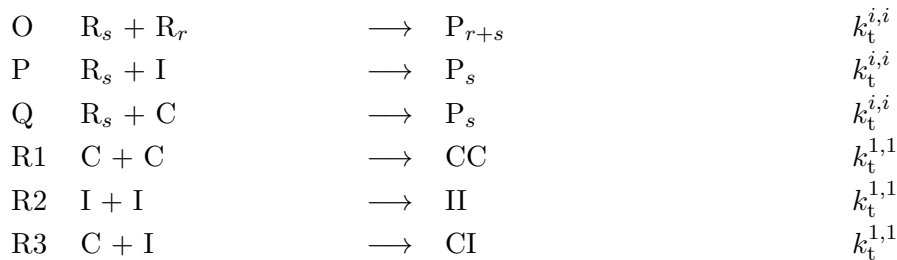
**Initiation****Pre-equilibrium****Scheme 8.3.** Kinetic scheme for the 3D model.

**Pre-equilibrium (continued)**

I1	$R_s + \text{RAFT}(\text{RI})_r$	$\longrightarrow$	$\text{INTa}(\text{RRI})_s + \text{INTb}(\text{RRI})_r$	$k_{\text{ad}}$
I2	$I + \text{RAFTa}(\text{RR})_s$	$\longrightarrow$	$\text{INTa}(\text{RRI})_s$	$1/2 k_{\text{ad}}^{\text{I}}$
I3	$I + \text{RAFTb}(\text{RR})_r$	$\longrightarrow$	$\text{INTb}(\text{RRI})_r$	$1/2 k_{\text{ad}}^{\text{I}}$
I4	$\text{RAFTa}(\text{RR})_s$	$\longrightarrow$	$\text{INTa}(\text{RRI})_s$	$1/2 k_{\text{ad}}^{\text{I}} c_{\text{I}}$
I5	$\text{RAFTb}(\text{RR})_r$	$\longrightarrow$	$\text{INTb}(\text{RRI})_r$	$1/2 k_{\text{ad}}^{\text{I}} c_{\text{I}}$
I6	$\text{INTa}(\text{RRI})_s$	$\longrightarrow$	$I + \text{RAFTa}(\text{RR})_s$	$1/6 k_{\beta}$
I7	$\text{INTa}(\text{RRI})_s$	$\longrightarrow$	$\text{RAFTb}(\text{RR})_s$	$1/6 k_{\beta}$
I8	$\text{INTb}(\text{RRI})_r$	$\longrightarrow$	$I + \text{RAFTb}(\text{RR})_r$	$1/6 k_{\beta}$
I9	$\text{INTb}(\text{RRI})_r$	$\longrightarrow$	$\text{RAFTa}(\text{RR})_r$	$1/6 k_{\beta}$
I10	$\text{INTa}(\text{RRI})_s$	$\longrightarrow$	$\text{RAFT}(\text{RI})_s$	$1/3 k_{\beta}$
I11	$\text{INTa}(\text{RRI})_s$	$\longrightarrow$	$R_s$	$1/3 k_{\beta}$
I12	$\text{INTb}(\text{RRI})_r$	$\longrightarrow$	$\text{RAFT}(\text{RI})_r$	$1/3 k_{\beta}$
I13	$\text{INTb}(\text{RRI})_r$	$\longrightarrow$	$R_r$	$1/3 k_{\beta}$
J1	$R_s + \text{RAFT}(\text{RC})_r$	$\longrightarrow$	$\text{INTa}(\text{RRC})_s + \text{INTb}(\text{RRC})_s$	$k_{\text{ad}}$
J2	$C + \text{RAFTa}(\text{RR})_s$	$\longrightarrow$	$\text{INTa}(\text{RRC})_s$	$1/2 k_{\text{ad}}$
J3	$C + \text{RAFTb}(\text{RR})_r$	$\longrightarrow$	$\text{INTb}(\text{RRC})_r$	$1/2 k_{\text{ad}}$
J4	$\text{RAFTa}(\text{RR})_s$	$\longrightarrow$	$\text{INTa}(\text{RRC})_s$	$1/2 k_{\text{ad}} c_{\text{C}}$
J5	$\text{RAFTb}(\text{RR})_r$	$\longrightarrow$	$\text{INTb}(\text{RRC})_r$	$1/2 k_{\text{ad}} c_{\text{C}}$
J6	$\text{INTa}(\text{RRC})_s$	$\longrightarrow$	$C + \text{RAFTa}(\text{RR})_s$	$1/6 k_{\beta}$
J7	$\text{INTa}(\text{RRC})_s$	$\longrightarrow$	$\text{RAFTb}(\text{RR})_s$	$1/6 k_{\beta}$
J8	$\text{INTb}(\text{RRC})_r$	$\longrightarrow$	$C + \text{RAFTb}(\text{RR})_r$	$1/6 k_{\beta}$
J9	$\text{INTb}(\text{RRC})_r$	$\longrightarrow$	$\text{RAFTa}(\text{RR})_r$	$1/6 k_{\beta}$
J10	$\text{INTa}(\text{RRC})_s$	$\longrightarrow$	$\text{RAFT}(\text{RC})_s$	$1/3 k_{\beta}$
J11	$\text{INTa}(\text{RRC})_s$	$\longrightarrow$	$R_s$	$1/3 k_{\beta}$
J12	$\text{INTb}(\text{RRC})_r$	$\longrightarrow$	$\text{RAFT}(\text{RC})_r$	$1/3 k_{\beta}$
J13	$\text{INTb}(\text{RRC})_r$	$\longrightarrow$	$R_r$	$1/3 k_{\beta}$

**Scheme 8.3.** (continued)



**Main equilibrium****Propagation****Reinitiation****Termination**

Scheme 8.3. (continued)

**Cross-termination**

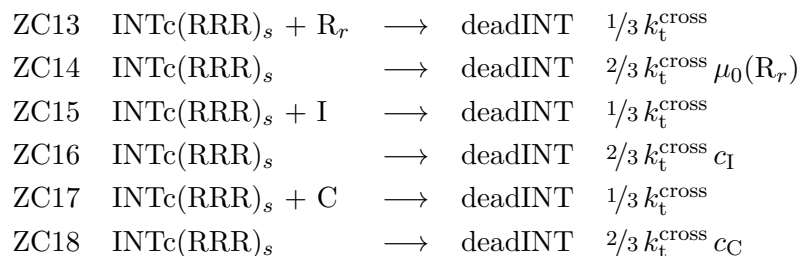
S1	$\text{INT}(\text{CCI}) + \text{R}_s$	$\longrightarrow$	deadINT	$k_t^{\text{cross}}$
S2	$\text{INT}(\text{CCI}) + \text{I}$	$\longrightarrow$	deadINT	$k_t^{\text{cross}}$
S3	$\text{INT}(\text{CCI}) + \text{C}$	$\longrightarrow$	deadINT	$k_t^{\text{cross}}$
T1	$\text{INT}(\text{III}) + \text{R}_s$	$\longrightarrow$	deadINT	$k_t^{\text{cross}}$
T2	$\text{INT}(\text{III}) + \text{I}$	$\longrightarrow$	deadINT	$k_t^{\text{cross}}$
T3	$\text{INT}(\text{III}) + \text{C}$	$\longrightarrow$	deadINT	$k_t^{\text{cross}}$
U1	$\text{INT}(\text{CII}) + \text{R}_s$	$\longrightarrow$	deadINT	$k_t^{\text{cross}}$
U2	$\text{INT}(\text{CII}) + \text{I}$	$\longrightarrow$	deadINT	$k_t^{\text{cross}}$
U3	$\text{INT}(\text{CII}) + \text{C}$	$\longrightarrow$	deadINT	$k_t^{\text{cross}}$
V1	$\text{INT}(\text{RII})_s + \text{R}_r$	$\longrightarrow$	deadINT	$k_t^{\text{cross}}$
V2	$\text{INT}(\text{RII})_s + \text{I}$	$\longrightarrow$	deadINT	$k_t^{\text{cross}}$
V3	$\text{INT}(\text{RII})_s + \text{C}$	$\longrightarrow$	deadINT	$k_t^{\text{cross}}$
W1	$\text{INT}(\text{RCI})_s + \text{R}_r$	$\longrightarrow$	deadINT	$k_t^{\text{cross}}$
W2	$\text{INT}(\text{RCI})_s + \text{I}$	$\longrightarrow$	deadINT	$k_t^{\text{cross}}$
W3	$\text{INT}(\text{RCI})_s + \text{C}$	$\longrightarrow$	deadINT	$k_t^{\text{cross}}$
X1	$\text{INT}(\text{CCC}) + \text{R}_s$	$\longrightarrow$	deadINT	$k_t^{\text{cross}}$
X2	$\text{INT}(\text{CCC}) + \text{I}$	$\longrightarrow$	deadINT	$k_t^{\text{cross}}$
X3	$\text{INT}(\text{CCC}) + \text{C}$	$\longrightarrow$	deadINT	$k_t^{\text{cross}}$
Y1	$\text{INT}(\text{RCC})_s + \text{R}_r$	$\longrightarrow$	deadINT	$k_t^{\text{cross}}$
Y2	$\text{INT}(\text{RCC})_s + \text{I}$	$\longrightarrow$	deadINT	$k_t^{\text{cross}}$
Y3	$\text{INT}(\text{RCC})_s + \text{C}$	$\longrightarrow$	deadINT	$k_t^{\text{cross}}$
ZA1	$\text{INTa}(\text{RRI})_s + \text{R}_r$	$\longrightarrow$	deadINT	$1/2 k_t^{\text{cross}}$
ZA2	$\text{INTa}(\text{RRI})_s$	$\longrightarrow$	deadINT	$1/2 k_t^{\text{cross}} \mu_0(\text{R}_r)$
ZA3	$\text{INTa}(\text{RRI})_s + \text{I}$	$\longrightarrow$	deadINT	$1/2 k_t^{\text{cross}}$
ZA4	$\text{INTa}(\text{RRI})_s$	$\longrightarrow$	deadINT	$1/2 k_t^{\text{cross}} c_I$
ZA5	$\text{INTa}(\text{RRI})_s + \text{C}$	$\longrightarrow$	deadINT	$1/2 k_t^{\text{cross}}$
ZA6	$\text{INTa}(\text{RRI})_s$	$\longrightarrow$	deadINT	$1/2 k_t^{\text{cross}} c_C$
ZA7	$\text{INTb}(\text{RRI})_s + \text{R}_r$	$\longrightarrow$	deadINT	$1/2 k_t^{\text{cross}}$
ZA8	$\text{INTb}(\text{RRI})_s$	$\longrightarrow$	deadINT	$1/2 k_t^{\text{cross}} \mu_0(\text{R}_r)$

**Scheme 8.3.** (continued)

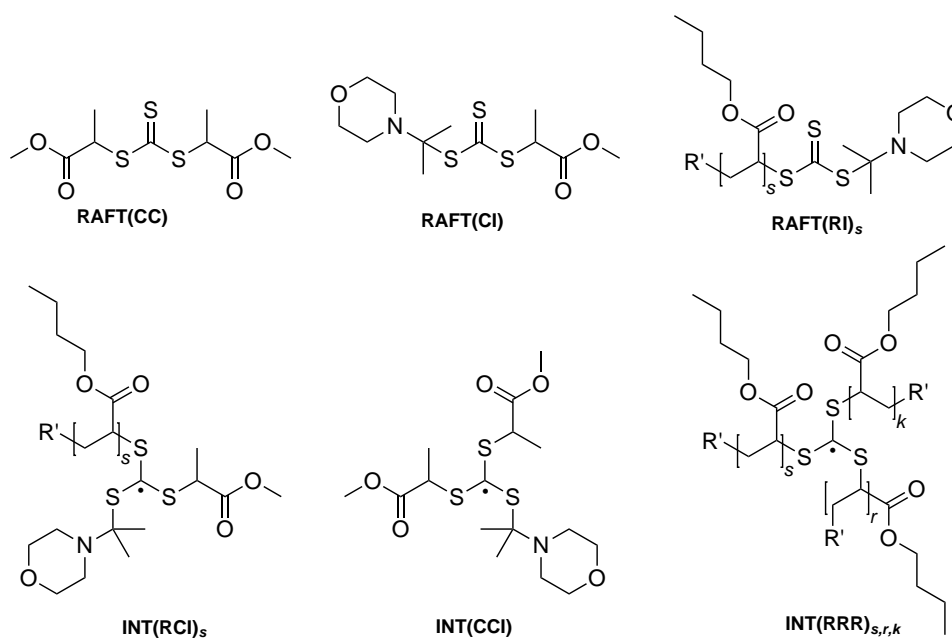
**Cross-termination (continued)**

ZA9	$\text{INTb(RRI)}_s + \text{I}$	$\longrightarrow$	deadINT	$1/2 k_t^{\text{cross}}$
ZA10	$\text{INTb(RRI)}_s$	$\longrightarrow$	deadINT	$1/2 k_t^{\text{cross}} c_I$
ZA11	$\text{INTb(RRI)}_s + \text{C}$	$\longrightarrow$	deadINT	$1/2 k_t^{\text{cross}}$
ZA12	$\text{INTb(RRI)}_s$	$\longrightarrow$	deadINT	$1/2 k_t^{\text{cross}} c_C$
ZB1	$\text{INTa(RRC)}_s + \text{R}_r$	$\longrightarrow$	deadINT	$1/2 k_t^{\text{cross}}$
ZB2	$\text{INTa(RRC)}_s$	$\longrightarrow$	deadINT	$1/2 k_t^{\text{cross}} \mu_0(\text{R}_r)$
ZB3	$\text{INTa(RRC)}_s + \text{I}$	$\longrightarrow$	deadINT	$1/2 k_t^{\text{cross}}$
ZB4	$\text{INTa(RRC)}_s$	$\longrightarrow$	deadINT	$1/2 k_t^{\text{cross}} c_I$
ZB5	$\text{INTa(RRC)}_s + \text{C}$	$\longrightarrow$	deadINT	$1/2 k_t^{\text{cross}}$
ZB6	$\text{INTa(RRC)}_s$	$\longrightarrow$	deadINT	$1/2 k_t^{\text{cross}} c_C$
ZB7	$\text{INTb(RRC)}_s + \text{R}_r$	$\longrightarrow$	deadINT	$1/2 k_t^{\text{cross}}$
ZB8	$\text{INTb(RRC)}_s$	$\longrightarrow$	deadINT	$1/2 k_t^{\text{cross}} \mu_0(\text{R}_r)$
ZB9	$\text{INTb(RRC)}_s + \text{I}$	$\longrightarrow$	deadINT	$1/2 k_t^{\text{cross}}$
ZB10	$\text{INTb(RRC)}_s$	$\longrightarrow$	deadINT	$1/2 k_t^{\text{cross}} c_I$
ZB11	$\text{INTb(RRC)}_s + \text{C}$	$\longrightarrow$	deadINT	$1/2 k_t^{\text{cross}}$
ZB12	$\text{INTb(RRC)}_s$	$\longrightarrow$	deadINT	$1/2 k_t^{\text{cross}} c_C$
ZC1	$\text{INTa(RRR)}_s + \text{R}_r$	$\longrightarrow$	deadINT	$1/3 k_t^{\text{cross}}$
ZC2	$\text{INTa(RRR)}_s$	$\longrightarrow$	deadINT	$2/3 k_t^{\text{cross}} \mu_0(\text{R}_r)$
ZC3	$\text{INTa(RRR)}_s + \text{I}$	$\longrightarrow$	deadINT	$1/3 k_t^{\text{cross}}$
ZC4	$\text{INTa(RRR)}_s$	$\longrightarrow$	deadINT	$2/3 k_t^{\text{cross}} c_I$
ZC5	$\text{INTa(RRR)}_s + \text{C}$	$\longrightarrow$	deadINT	$1/3 k_t^{\text{cross}}$
ZC6	$\text{INTa(RRR)}_s$	$\longrightarrow$	deadINT	$2/3 k_t^{\text{cross}} c_C$
ZC7	$\text{INTb(RRR)}_s + \text{R}_r$	$\longrightarrow$	deadINT	$1/3 k_t^{\text{cross}}$
ZC8	$\text{INTb(RRR)}_s$	$\longrightarrow$	deadINT	$2/3 k_t^{\text{cross}} \mu_0(\text{R}_r)$
ZC9	$\text{INTb(RRR)}_s + \text{I}$	$\longrightarrow$	deadINT	$1/3 k_t^{\text{cross}}$
ZC10	$\text{INTb(RRR)}_s$	$\longrightarrow$	deadINT	$2/3 k_t^{\text{cross}} c_I$
ZC11	$\text{INTb(RRR)}_s + \text{C}$	$\longrightarrow$	deadINT	$1/3 k_t^{\text{cross}}$
ZC12	$\text{INTb(RRR)}_s$	$\longrightarrow$	deadINT	$2/3 k_t^{\text{cross}} c_C$

**Scheme 8.3.** (continued)



Scheme 8.3. (continued)

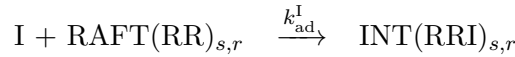


**Scheme 8.4.** 3 out of 6 possible RAFT species and 3 out of 10 possible intermediate radical species that have been considered in the kinetic scheme for BA polymerizations mediated by BMPT.

An intermediate radical bearing two chemically different arms, e. g. INT(CCI), may either fragment into an initiator-derived radical, I, plus the original RAFT agent, RAFT(CC) (reaction B3), or the leaving group, C, and a RAFT agent bearing C and I, RAFT(CI). As the reaction proceeds with a possibility of  $1/3$  in the direction of I fragmentation and a possibility of  $2/3$  in the direction of C fragmentation, reaction step B3 proceeds with a fragmentation rate coefficient of  $1/3 k_{\beta}$  and B4 with a fragmentation rate coefficient of  $2/3 k_{\beta}$ . The same principle applies to the reaction steps D3, D4, E3, E4, F4–F6, H3, and H4.

Steps I1 to J13 describe the pre-equilibria involving intermediate radicals and RAFT species bearing two growing chains that may differ in chain length. Since these compounds are described by a 2D chain-length distribution, the equilibria involved have been translated to a 1D problem by introducing the temporary chain size memory species INTa(RRI)<sub>s</sub>, INTb(RRI)<sub>r</sub>, INTa(RRC)<sub>s</sub>, INTb(RRC)<sub>r</sub>, RAFTa(RR)<sub>s</sub> and RAFTb(RR)<sub>r</sub>.

The addition of an initiator-derived radical to a RAFT agent bearing two growing chains reads:



The corresponding differential equation system is:

$$\frac{\delta \text{I}}{\delta t} = -k_{\text{ad}}^{\text{I}} \cdot \text{I} \cdot \mu_{0,0}(\text{RAFT}(\text{RR})_{s,r}) \quad (8.20)$$

$$\frac{\delta \text{RAFT}(\text{RR})_{s,r}}{\delta t} = -k_{\text{ad}}^{\text{I}} \cdot \text{I} \cdot \text{RAFT}(\text{RR})_{s,r} \quad (8.21)$$

$$\frac{\delta \text{INT}(\text{RRI})_{s,r}}{\delta t} = k_{\text{ad}}^{\text{I}} \cdot \text{I} \cdot \text{RAFT}(\text{RR})_{s,r} \quad (8.22)$$

The following boundary density integrals are introduced:

$$\text{INTa}(\text{RRI})_s = \sum_r \text{INT}(\text{RRI})_{s,r} \quad (8.23)$$

$$\text{INTb}(\text{RRI})_r = \sum_s \text{INT}(\text{RRI})_{s,r} \quad (8.24)$$

$$\text{RAFTa}(\text{RR})_s = \sum_r \text{RAFT}(\text{RR})_{s,r} \quad (8.25)$$

$$\text{RAFTb}(\text{RR})_r = \sum_s \text{RAFT}(\text{RR})_{s,r} \quad (8.26)$$

The overall concentration of the INT(RRI)<sub>s,r</sub> species is given by:

$$\begin{aligned} \mu_{0,0}(\text{INT}(\text{RRI})_{s,r}) &= \sum_s \sum_r \text{INT}(\text{RRI})_{s,r} \\ &= \sum_r \text{INTa}(\text{RRI})_s = \sum_s \text{INTb}(\text{RRI})_r \\ &= \mu_0(\text{INTa}(\text{RRI})_s) = \mu_0(\text{INTb}(\text{RRI})_r) \end{aligned} \quad (8.27)$$

The overall concentration of the RAFT(RR)<sub>s,r</sub> species is given by:

$$\begin{aligned}
 \mu_{0,0}(\text{RAFT}(\text{RR})_{s,r}) &= \sum_s \sum_r \text{RAFT}(\text{RR})_{s,r} \\
 &= \sum_r \text{RAFTa}(\text{RR})_s = \sum_s \text{RAFTb}(\text{RR})_r \\
 &= \mu_0(\text{RAFTa}(\text{RR})_s) = \mu_0(\text{RAFTb}(\text{RR})_r)
 \end{aligned} \tag{8.28}$$

Substituting the expressions 8.23 to 8.28 into the differential equations 8.20 to 8.22 yields:

$$\frac{\delta I}{\delta t} = -\frac{1}{2} \cdot k_{\text{ad}}^{\text{I}} \cdot I \cdot \left( \mu_0(\text{RAFTa}(\text{RR})_s) + \mu_0(\text{RAFTb}(\text{RR})_r) \right) \tag{8.29}$$

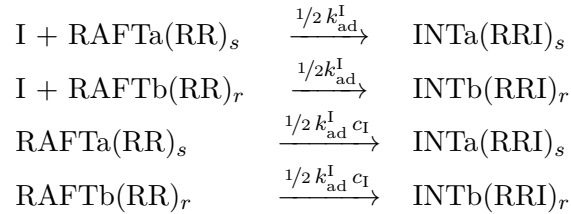
$$\frac{\delta \text{RAFTa}(\text{RR})_s}{\delta t} = -k_{\text{ad}}^{\text{I}} \cdot I \cdot \text{RAFTa}(\text{RR})_s \tag{8.30}$$

$$\frac{\delta \text{RAFTb}(\text{RR})_r}{\delta t} = -k_{\text{ad}}^{\text{I}} \cdot I \cdot \text{RAFTb}(\text{RR})_r \tag{8.31}$$

$$\frac{\delta \text{INTa}(\text{RRI})_s}{\delta t} = k_{\text{ad}}^{\text{I}} \cdot I \cdot \text{RAFTa}(\text{RR})_s \tag{8.32}$$

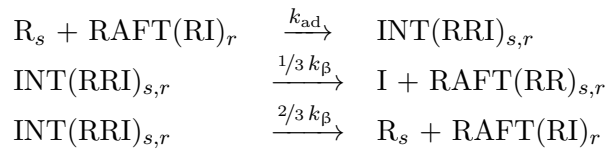
$$\frac{\delta \text{INTb}(\text{RRI})_r}{\delta t} = k_{\text{ad}}^{\text{I}} \cdot I \cdot \text{RAFTb}(\text{RR})_r \tag{8.33}$$

The equation set 8.29 to 8.33 is translated back to the following reaction system:



The same translation is applied for the addition of C to RAFT(RR)<sub>s,r</sub> and the reactions are described in Scheme 8.3 by steps I1 to I5 and J1 to J5, respectively.

The reaction system for the addition of a polymeric radical, R<sub>s</sub>, to RAFT(RI)<sub>r</sub> and the subsequent fragmentation reactions reads:



These reactions are described by the following differential equation system:

$$\frac{\delta I}{\delta t} = \frac{1}{3} \cdot k_{\beta} \cdot \mu_{0,0}(\text{INT}(\text{RRI})_{s,r}) \quad (8.34)$$

$$\frac{\delta R_s}{\delta t} = -k_{\text{ad}} \cdot R_s \cdot \mu_0(\text{RAFT}(\text{RI})_r) + \frac{2}{3} \cdot k_{\beta} \cdot \mu_{0,0}(\text{INT}(\text{RRI})_{s,r}) \quad (8.35)$$

$$\frac{\delta \text{RAFT}(\text{RI})_r}{\delta t} = -k_{\text{ad}} \cdot \mu_0(R_s) \cdot \text{RAFT}(\text{RI})_r + \frac{2}{3} \cdot k_{\beta} \cdot \mu_{0,0}(\text{INT}(\text{RRI})_{s,r}) \quad (8.36)$$

$$\frac{\delta \text{RAFT}(\text{RR})_{s,r}}{\delta t} = \frac{1}{3} \cdot k_{\beta} \cdot \mu_{0,0}(\text{INT}(\text{RRI})_{s,r}) \quad (8.37)$$

$$\frac{\delta \text{INT}(\text{RRI})_{s,r}}{\delta t} = k_{\text{ad}} \cdot R_s \cdot \text{RAFT}(\text{RI})_r - k_{\beta} \cdot \text{INT}(\text{RRI})_{s,r} \quad (8.38)$$

Substituting the expressions 8.23 to 8.28 into the differential equations 8.34 to 8.38 yields:

$$\frac{\delta I}{\delta t} = \frac{1}{6} \cdot k_{\beta} \cdot \left( \mu_0(\text{INTa}(\text{RRI})_s) + \mu_0(\text{INTb}(\text{RRI})_r) \right) \quad (8.39)$$

$$\begin{aligned} \frac{\delta R_s}{\delta t} &= -k_{\text{ad}} \cdot R_s \cdot \mu_0(\text{RAFT}(\text{RI})_r) \\ &\quad + \frac{1}{3} \cdot k_{\beta} \cdot \left( \mu_0(\text{INTa}(\text{RRI})_s) + \mu_0(\text{INTb}(\text{RRI})_r) \right) \end{aligned} \quad (8.40)$$

$$\begin{aligned} \frac{\delta \text{RAFT}(\text{RI})_r}{\delta t} &= -k_{\text{ad}} \cdot \mu_0(R_s) \cdot \text{RAFT}(\text{RI})_r \\ &\quad + \frac{1}{3} \cdot k_{\beta} \cdot \left( \mu_0(\text{INTa}(\text{RRI})_s) + \mu_0(\text{INTb}(\text{RRI})_r) \right) \end{aligned} \quad (8.41)$$

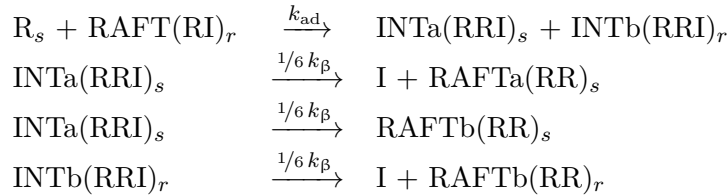
$$\frac{\delta \text{RAFTa}(\text{RR})_s}{\delta t} = \frac{1}{6} \cdot k_{\beta} \cdot \left( \mu_0(\text{INTa}(\text{RRI})_s) + \mu_0(\text{INTb}(\text{RRI})_r) \right) \quad (8.42)$$

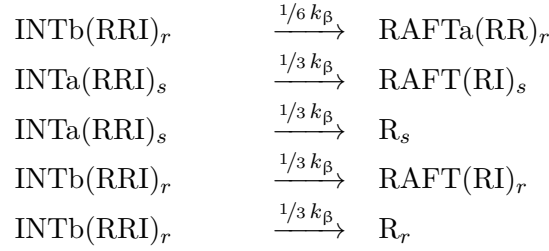
$$\frac{\delta \text{RAFTb}(\text{RR})_r}{\delta t} = \frac{1}{6} \cdot k_{\beta} \cdot \left( \mu_0(\text{INTa}(\text{RRI})_s) + \mu_0(\text{INTb}(\text{RRI})_r) \right) \quad (8.43)$$

$$\frac{\delta \text{INTa}(\text{RRI})_s}{\delta t} = k_{\text{ad}} \cdot R_s \cdot \text{RAFT}(\text{RI})_r - k_{\beta} \cdot \text{INTa}(\text{RRI})_s \quad (8.44)$$

$$\frac{\delta \text{INTb}(\text{RRI})_r}{\delta t} = k_{\text{ad}} \cdot R_s \cdot \text{RAFT}(\text{RI})_r - k_{\beta} \cdot \text{INTb}(\text{RRI})_r \quad (8.45)$$

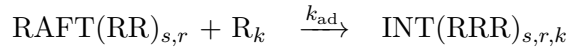
The differential equations 8.39 to 8.45 represent the following reactions:





This reaction scheme is illustrated by steps I1 and I6 to I13. The same translation can be applied to the addition of  $\text{R}_s$  to  $\text{RAFT(RC)}_r$  and subsequent fragmentation of the intermediate radicals. The corresponding reactions are given by steps J1 and J6 to J13 in Scheme 8.3.

The main equilibrium consists of the one-dimensional species  $\text{R}_k$ , the two-dimensional macromolecular RAFT agent,  $\text{RAFT(RR)}_{s,r}$ , and the three-dimensional macromolecular intermediate radical,  $\text{INT(RRR)}_{s,r,k}$ :



The corresponding differential equations read:

$$\begin{aligned}
 \frac{\delta \text{RAFT(RR)}_{s,r}}{\delta t} &= -k_{\text{ad}} \cdot \mu_0(\text{R}_k) \cdot \text{RAFT(RR)}_{s,r} \\
 &\quad + k_\beta \cdot \mu_{0,0,0}(\text{INT(RRR)}_{s,r,k})
 \end{aligned} \tag{8.46}$$

$$\begin{aligned}
 \frac{\delta \text{R}_k}{\delta t} &= -k_{\text{ad}} \cdot \text{R}_k \cdot \mu_{0,0}(\text{RAFT(RR)}_{s,r}) \\
 &\quad + k_\beta \cdot \mu_{0,0,0}(\text{INT(RRR)}_{s,r,k})
 \end{aligned} \tag{8.47}$$

$$\frac{\delta \text{INT(RRR)}_{s,r,k}}{\delta t} = k_{\text{ad}} \cdot \mu_0(\text{R}_k) \cdot \text{RAFT(RR)}_{s,r} - k_\beta \cdot \text{INT(RRR)}_{s,r,k} \tag{8.48}$$

The full two- and three-dimensional distributions  $\text{RAFT(RR)}_{s,r}$  and  $\text{INT(RRR)}_{s,r,k}$  are not necessary for the balance of the one-dimensional species  $\text{R}_k$ . Therefore, the following temporary chain size memory species are introduced:

$$\text{RAFTa(RR)}_s = \sum_r \text{RAFT(RR)}_{s,r} \tag{8.49}$$

$$\text{RAFTb(RR)}_r = \sum_s \text{RAFT(RR)}_{s,r} \tag{8.50}$$

$$\text{INTa(RRR)}_s = \sum_{r,k} \text{INT(RRR)}_{s,r,k} \tag{8.51}$$



$$\text{INTb(RRR)}_r = \sum_{s,k} \text{INT(RRR)}_{s,r,k} \quad (8.52)$$

$$\text{INTc(RRR)}_k = \sum_{s,r} \text{INT(RRR)}_{s,r,k} \quad (8.53)$$

The overall concentration of  $\text{RAFT(RR)}_{s,r}$  species is given by:

$$\mu_{0,0}(\text{RAFT(RR)}_{s,r}) = \sum_s \sum_r \text{RAFT(RR)}_{s,r} \quad (8.54)$$

Using the definitions 8.49 and 8.50 we derive the following:

$$\begin{aligned} \mu_{0,0}(\text{RAFT(RR)}_{s,r}) &= \sum_s \text{RAFTa(RR)}_s = \sum_r \text{RAFTb(RR)}_r \\ &= \mu_0(\text{RAFTa(RR)}_s) = \mu_0(\text{RAFTb(RR)}_r) \end{aligned} \quad (8.55)$$

The overall concentration of  $\text{INT(RRR)}_{s,r,k}$  species is given by:

$$\mu_{0,0,0}(\text{INT(RRR)}_{s,r,k}) = \sum_s \sum_r \sum_k \text{INT(RRR)}_{s,r,k} \quad (8.56)$$

Using the definitions 8.51 to 8.53 we derive the following:

$$\begin{aligned} \mu_{0,0,0}(\text{INT(RRR)}_{s,r,k}) &= \mu_0(\text{INTa(RRR)}_s) \\ &= \mu_0(\text{INTb(RRR)}_r) \\ &= \mu_0(\text{INTc(RRR)}_k) \end{aligned} \quad (8.57)$$

Applying equations 8.49 to 8.57 to the differential equation system 8.46 to 8.48 yields:

$$\begin{aligned} \frac{\delta \text{RAFTa(RR)}_s}{\delta t} &= -k_{\text{ad}} \cdot \mu_0(\text{R}_k) \cdot \text{RAFTa(RR)}_s \\ &\quad + \frac{1}{3} \cdot k_{\beta} \cdot \left( \mu_0(\text{INTa(RRR)}_s) + \mu_0(\text{INTb(RRR)}_r) \right. \\ &\quad \left. + \mu_0(\text{INTc(RRR)}_k) \right) \end{aligned} \quad (8.58)$$

$$\begin{aligned} \frac{\delta \text{RAFTb(RR)}_r}{\delta t} &= -k_{\text{ad}} \cdot \mu_0(\text{R}_k) \cdot \text{RAFTb(RR)}_r \\ &\quad + \frac{1}{3} \cdot k_{\beta} \cdot \left( \mu_0(\text{INTa(RRR)}_s) + \mu_0(\text{INTb(RRR)}_r) \right. \\ &\quad \left. + \mu_0(\text{INTc(RRR)}_k) \right) \end{aligned} \quad (8.59)$$

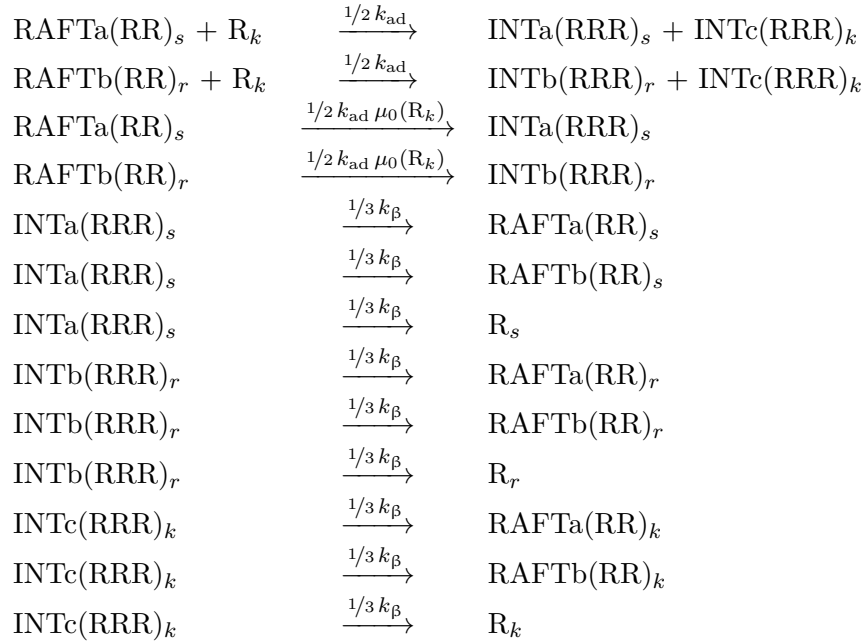
$$\begin{aligned} \frac{\delta R_k}{\delta t} = & -k_{\text{ad}} \cdot R_k \cdot \left( \mu_0(\text{RAFTa}(\text{RR})_s) + \mu_0(\text{RAFTb}(\text{RR})_r) \right) \\ & + \frac{1}{3} \cdot k_{\beta} \cdot \left( \mu_0(\text{INTa}(\text{RRR})_s) + \mu_0(\text{INTb}(\text{RRR})_r) \right) \\ & + \mu_0(\text{INTc}(\text{RRR})_k) \end{aligned} \quad (8.60)$$

$$\frac{\delta \text{INTa}(\text{RRR})_s}{\delta t} = k_{\text{ad}} \cdot \mu_0(R_k) \cdot \text{RAFTa}(\text{RR})_s - k_{\beta} \cdot \text{INTa}(\text{RRR})_s \quad (8.61)$$

$$\frac{\delta \text{INTb}(\text{RRR})_r}{\delta t} = k_{\text{ad}} \cdot \mu_0(R_k) \cdot \text{RAFTb}(\text{RR})_r - k_{\beta} \cdot \text{INTb}(\text{RRR})_r \quad (8.62)$$

$$\begin{aligned} \frac{\delta \text{INTc}(\text{RRR})_k}{\delta t} = & \frac{1}{2} \cdot k_{\text{ad}} \cdot R_k \cdot \left( \mu_0(\text{RAFTa}(\text{RR})_s) + \mu_0(\text{RAFTb}(\text{RR})_r) \right) \\ & - k_{\beta} \cdot \text{INTc}(\text{RRR})_k \end{aligned} \quad (8.63)$$

The differential equations 8.58 to 8.63 can be translated back to a reaction system:



The reaction system is given in Scheme 8.3 by steps K1 to L9.

For the cross-termination reactions S1 to ZC18 the translation into the 1D model was done in analogy to the translation in Section 8.1.

# Appendix

## A Abbreviations

$a$	EPR hyperfine coupling constant
$A$	absorbance
AIBN	azobis- <i>iso</i> -butyronitrile
$\alpha_l$	power-law exponent describing the chain-length dependence of $k_t$ for long-chain radicals
$\alpha_s$	power-law exponent describing the chain-length dependence of $k_t$ for short-chain radicals
ATRP	atom transfer radical polymerization
BA	<i>n</i> -butyl acrylate
BDDDB	2,3-butane-2,3-diylidibenzene
BMPT	<i>S,S'</i> -bis(methyl-propion-2-ylate) trithiocarbonate
BPT	benzyl propyl trithiocarbonate
$B_x$	magnetic field
C	RAFT leaving group in the PREDICI <sup>®</sup> models
$C_{\text{cross}}$	relative cross-termination rate
CDB	cumyl dithiobenzoate
$\text{CDCl}_3$	deuterated chloroform
CDCN	deuterated acetonitrile
CIP	cyano- <i>iso</i> -propyl radical
clcd	calculated
CLRP	controlled/living radical polymerization
COSY	correlation spectroscopy
CPDB	cyano- <i>iso</i> -propyl dithiobenzoate
CPDB*	ring-substituted CPDB
CT	cross-termination product

CW	continuous wave
$c_X$	concentration of substance X
$c_X^0$	initial concentration of substance X
$\delta$	chemical shift in NMR spectroscopy
d	doublet
deadINT	cross-termination product in PREDICI <sup>®</sup> models
DNA	deoxyribonucleic acid
DFT	density functional theory
DTBA	di- <i>tert</i> -butylamine
DTBN	di- <i>tert</i> -butylnitroxide
$E_a$	activation energy
e. g.	for example
EI-(HR)MS	electron ionization (high resolution) mass spectrometry
EPPT	<i>S</i> -ethyl propan-2-ylonate- <i>S'</i> -propyl trithiocarbonate
EPR	electron paramagnetic resonance
ESI-(HR)MS	electrospray ionization (high resolution) mass spectrometry
<i>et al.</i>	and others
ETTP	ethyl <i>S</i> -thiobenzoyl-2-thiopropionate
$g$	g-factor in EPR spectroscopy
g	gram
G	Gauss
$H$	reaction enthalpy
$h_1, h_2, h_3$	proportionality constants used for EPR calibration
HMBC	heteronuclear multiple bond correlation
HPLC	high-performance liquid chromatography
HSQC	heteronuclear single quantum coherence
Hz	hertz [ $s^{-1}$ ]
I	initiator-derived radical
IBN	<i>iso</i> -butyronitrile
$i_c$	crossover chain length
i. e.	that is
INT	RAFT intermediate radical
$I_{Rsc}$	intensity of the EPR reference spectrum recorded with the signal channel digitizer
IRT	intermediate radical termination
$I_{Ssc}$	intensity of the EPR sample spectrum recorded with the

---

	signal channel digitizer
$I_{\text{Sfd}}$	intensity of the EPR sample spectrum recorded with the fast digitizer
IUPAC	International Union of Pure and Applied Chemistry
$J$	NMR coupling constant
K	ketenimine
$K$	Mark-Houwink parameter
$k_{\text{ad}}$	addition rate coefficient
$k_{\text{ad}}^{\text{I}}$	addition rate coefficient for the initiator fragment
$k_{\beta}$	fragmentation rate coefficient
$k_{\text{d}}$	initiator decomposition rate coefficient
$k_{\text{diff}}$	diffusion-controlled rate coefficient
$K_{\text{eq}}$	RAFT equilibrium constant
$k_{\text{i}}$	initiation rate coefficient
$k_{\text{MS}}$	“missing step” rate coefficient
$k_{\text{p}}$	propagation rate coefficient
$k_{\text{p}}^{\text{rein}}$	reinitiation rate coefficient
$k_{\text{t}}$	termination rate coefficient
$k_{\text{t}}^{\text{cross}}$	cross-termination rate coefficient
$k_{\text{t}}^{i,i}$	chain-length dependent termination rate coefficient
$k_{\text{t}}^{1,1}$	termination rate coefficient of two radicals with chain length one
$k_{\text{t}}^{\text{self}}$	self-termination rate coefficient
$\lambda$	wavelength
L	liter
ln	natural logarithm
m	meter, milli, multiplet
$M$	molar mass
$\mu_0$	zero moment of a distribution
MADIX	macromolecular design via the interchange of xanthates
MALDI-TOF-MS	matrix-assisted laser desorption ionization time-of-flight mass spectrometry
MAN	methacrylonitrile
MCR	midchain radical
mJ	millijoule
$\overline{M}_n$	number average molecular weight

---

MNP	2-methyl-2-nitrosopropane
MMMP	2-methyl-1-[4-(methylthio)phenyl]-2-morpholin-4-ylpropan-1-one
$m/z$	mass-to-charge ratio
$\eta$	viscosity
nm	nanometer
NMP	nitroxide-mediated polymerization
NMR	nuclear magnetic resonance
NO	nitric oxide radical
P	propagating radical
<i>PDI</i>	polydispersity index
PE	phenylethyl radical
PEDA	<i>meso</i> -1,2-bis(1-phenylethyl)diazene
PEDB	1-phenylethyl dithiobenzoate
PEDB*	ring-substituted PEDB
ppm	parts per million
PREDICI <sup>®</sup>	Polyreaction Distributions by Countable System Integration
PSS	Polymer Standards Service
$Q$	quality factor
q	quartet
R	leaving group radical
$R$	ideal gas constant
$r_{ad}$	addition rate
RAFT	reversible addition-fragmentation chain transfer
$r_{\beta}$	fragmentation rate
RP	radical polymerization
$R_p$	polymerization rate
RSE	radical stabilization energy
RTCP	reversible chain transfer catalyzed polymerization
$r_t^{cross}$	cross-termination rate
s	second, singlet
SEC	size-exclusion chromatography
SF	slow fragmentation
SiO <sub>2</sub>	silica
SP-PLP-EPR	single pulse-pulsed laser polymerization-electron paramagnetic resonance

SPR	secondary propagating radical
<i>t</i>	time
t	triplet
<i>T</i>	temperature
TB	<i>tert</i> -butyl radical
TBDA	1,2-di- <i>tert</i> -butyldiazene
TBDB	<i>tert</i> -butyl dithiobenzoate
TEMPO	(2,2,6,6-tetramethylpiperidine-1-yl)oxyl
TMPPP	tetramethylpropyl peroxyvalate
TMSN	tetramethylsuccinonitrile
TPEA	tris(1-phenylethyl)amine
UV	ultraviolet
W	Watt
$x_X$	molar fraction of compound X
Z	stabilizing group of the RAFT agent

## B Matlab Code

```
1 % Load EasySpin
2 easyspin;
3
4 % Load and display spectrum
5
6 % Load spectrum from folder
7 [specdat,pathdat] = uigetfile('d:\Doktorarbeit\ESR-Experimente\*.txt',
8
9 addpath(pathdat);
10 data1 = importdata(specdat);
11
12 % Identify spectral data
13 a=getfield(data1, 'data');
14 dimension=size(a);
15 for i=1:dimension(1,1)
16     B(i,1)=a(i,2);
17     CorrSpec(i,1)=a(i,dimension(1,2));
18 end;
19
20 % Ask for measuring conditions
21 rg=input('receiver gain: ');
22 scans=input('number of added scans: ');
23 Anfangsfeld=min(B)/10;
24 Endfeld=max(B)/10;
25 MwFrequenz=input('Mikrowellenfrequenz / GHz: ');
26 np=i;
27
28 % Convert field values from G to mT
29 B=B/10; ...
30
31 % Convert to receiver gain 50
32 dimension=size(CorrSpec);
33 for i=1: dimension(1,1)
34     if CorrSpec(i,1) < 0
35         spc1(i,1)=CorrSpec(i,1)*(-1);
36         spc1(i,1)=(10^(0.0502*(50-rg)+log10(spc1(i,1))))/scans;
37         spc1(i,1)=spc1(i,1)*(-1);
38     end;
39     if CorrSpec(i,1) > 0
40         spc1(i,1)=(10^(0.0502*(50-rg)+log10(CorrSpec(i,1))))/scans;
41     end;
42     end; ...
43
44 % Correction of the baseline
45 CorrSpec = basecorr(spc,1,0);
46 [CorrSpec,BLine] = basecorr(spc,1,0);
47 clear spc;
48
```



```
49 % Fitting of the first species
50
51 % Define range where only one species is present
52 Spec=[B,CorrSpec];
53 plot(Spec(1:np,1),Spec(1:np,2), 'c') ;
54 v2=axis;
55 disp('Please define the range of the spectrum you like to use (by expanding)');
56 nix=input('press any key (and RETURN) to continue');
57 clear nix;
58 v=axis;
59
60 startspektrum=v(1,1);
61 endspektrum=v(1,2);
62
63 if v2==v
64     startspektrum=v(1,1)+1;
65     endspektrum=v(1,2)-1;
66 end;
67
68 r=size(B);
69 zaehler=0;
70
71 for i=1:r(1,1)
72     if B(i)<startspektrum
73         zaehler=zaehler+1;
74     end;
75
76     if B(i)>startspektrum
77         if B(i)<endspektrum
78             nB(i-zaehler)=B(i);
79             nCorrSpec(i-zaehler)=CorrSpec(i);
80         end;
81     end;
82 end;
83
84 nB=nB';
85 nCorrSpec=nCorrSpec';
86 np1=size(nB);
87 np1=np1(1,1);
88 close all;
89
90 % g value of first radical
91 gFaktor=2.0053;
92
93 % Coupling constants of first radical
94 A1=2.053;
95 A2=0.331;
96 A1= mt2mhz(A1,gFaktor);
97 A2= mt2mhz(A2,gFaktor);
98
```

## Appendix

---

```
99 % Line width of first radical
100 linewidthgaussian=0.054;
101 linewidthlorenzian=0.006;
102
103 % Fitting (g value)
104 Sys1.g = gFaktor;
105 Sys1.Nucs = '1H, 14N';
106 Sys1.n = [6 1];
107 Exp.mwFreq = MwFrequenz;
108 Exp.Range = [startspektrum endspektrum];
109 Exp.nPoints = np1;
110 Sys1.A = [A1 A2];
111 Sys1.lwpp = [linewidthgaussian linewidthlorenzian];
112 Vary1.g=[0.001];
113 [BestSys1,BestSpc1]=esfit('garlic',nCorrSpec,Sys1,Vary1,Exp);
114
115 % Fitting (Coupling constants)
116 clear Vary1;
117 clear A1;
118 clear A2;
119 clear gFaktor;
120 clear linewidthgaussian;
121 clear linewidthlorenzian;
122 clear Anfangsfeld;
123 clear Endfeld;
124 clear MwFrequenz;
125 clear dimension;
126 clear i;
127 clear m;
128 clear np;
129 Sys1.g = BestSys1.g;
130 Sys1.Nucs = BestSys1.Nucs;
131 Sys1.A = BestSys1.A;
132 Sys1.lwpp = BestSys1.lwpp;
133 Vary1.A=[0 0.01];
134 [BestSys1,BestSpc1]=esfit('garlic',nCorrSpec,Sys1,Vary1,Exp);
135 clear Vary1;
136
137 % Fitting (line width)
138 Sys1.A = BestSys1.A;
139 Vary1.lwpp=[0.1 0.1];
140 [BestSys1,BestSpc1]=esfit('garlic',nCorrSpec,Sys1,Vary1,Exp);
141
142 % Maximum of simulated spectrum
143 IsnB=max(BestSpc1);
144
145 % Maximum of experimental spectrum in selected range
146 IeB=max(nCorrSpec);
147 BestSpc1=BestSpc1*IeB*IsnB; ...
148
```

```
149 % Simulate spectrum over full measuring range
150 Anfangsfeld=min(B);
151 Endfeld=max(B);
152 np=size(B);
153 np=np(1,1);
154 Exp.Range=[Anfangsfeld Endfeld];
155 Exp.nPoints=np;
156 [x,BestSpc1b]=garlic(Sys1,Exp);
157 BestSpc1b=BestSpc1b';
158
159 % Bring simulated spectrum to same intensity as BestSpc1
160 zaehler=0;
161 for i=1:r(1,1)
162     if x(i)<startspektrum
163         zaehler=zaehler+1;
164     end;
165
166     if x(i)>startspektrum
167         if x(i)<endspektrum
168             nx(i-zaehler)=x(i);
169             nBestSpc1b(i-zaehler)=BestSpc1b(i);
170         end;
171     end;
172 end;
173
174 nx=nx';
175 nBestSpc1b=nBestSpc1b';
176
177 BestSpc1b=BestSpc1b*max(BestSpc1)/max(nBestSpc1b); ...
178
179 % Simulate complete spectrum of first species
180 Exp.Range=[325 345];
181 Exp.nPoints=5000;
182 [x2,BestSpc1c]=garlic(Sys1,Exp);
183 BestSpc1c=BestSpc1c';
184 x2=x2';
185
186 % Bring spectrum to same intensity as fitted one
187 BestSpc1c=BestSpc1c*max(BestSpc1b)/max(BestSpc1c); ...
188
189 % Fitting of the second species
190
191 % Subtract simulated spectrum of 1st species of experimental one
192 ExpSpec2=CorrSpec-BestSpc1c;
193
194 % Remove noise
195 y2=ExpSpec2;
196 m = 5; % half-width of smoothing window
197 y_sg2 = smooth(y2,m,'savgol',2); % Savitzky-Golay moving average
198
```

## Appendix

---

```
199 % Coupling constants
200 A1=0.134;
201 A2=0.366;
202 A3=0.42;
203 A4=0.042;
204 A1= mt2mhz(A1,BestSys1.g);
205 A2= mt2mhz(A2, BestSys1.g);
206 A3= mt2mhz(A3, BestSys1.g );
207 A4= mt2mhz(A4, BestSys1.g );
208
209 % Line width
210 linewidth=0.045;
211
212 % Fitting of 2nd species (g value)
213 Anfangsfeld=min(B);
214 Endfeld=max(B);
215 np=size(B);
216 np=np(1,1);
217 Exp.Range=[Anfangsfeld Endfeld];
218 Exp.nPoints=np;
219 Sys2.Nucs = '1H,1H,1H,1H';
220 Sys2.A = [A1 A2 A3 A4];
221 Sys2.n = [2 2 1 12];
222 Sys2.g = BestSys1.g;
223 Sys2.lwpp = [linewidth];
224 Vary2.g=[0.01];
225 [BestSys2,BestSpc2]=esfit('garlic',y_sg2,Sys2,Vary2,Exp);
226
227 % Fitting of 2nd species (Coupling constants)
228 clear Vary2;
229 Sys2.A = [A1 A2 A3 A4];
230 Sys2.g = BestSys2.g;
231 Vary2.A=[0.1 0.1 0 0];
232 [BestSys2,BestSpc2]=esfit('garlic',y_sg2,Sys2,Vary2,Exp);
233
234 clear Vary2;
235 Sys2.A = BestSys2.A
236 Vary2.A=[0.1 0.1 0.1 0];
237 Vary2.lwpp=[0.1];
238 [BestSys2,BestSpc2]=esfit('garlic',y_sg2,Sys2,Vary2,Exp);
239
240 clear Vary2;
241 Sys2.lwpp=BestSys2.lwpp;
242 Sys2.A = BestSys2.A;
243 Vary2.A=[0 0 0 0.1];
244 Vary2.g=[0.01];
245 [BestSys2,BestSpc2]=esfit('garlic',y_sg2,Sys2,Vary2,Exp);
246
247 clear Vary2;
248 Sys2.A = BestSys2.A
```

```
249 Vary2.A=[0.1 0.1 0.1 0.1];
250 [BestSys2,BestSpc2]=esfit('garlic',y_sg2,Sys2,Vary2,Exp);
251
252 %Spektrum der zweiten Spezies fitten (g-Wert)
253 Sys2.A = BestSys2.A;
254 Sys2.g = BestSys1.g;
255 Vary2.g=[0.01];
256 [BestSys2,BestSpc2]=esfit('garlic',ExpSpec2,Sys2,Vary2,Exp);
257
258 %Spektrum der zweiten Spezies fitten (Kopplungskonstanten)
259 clear Vary2;
260 Sys2.A = [A1 A2 A3 A4];
261 Sys2.g = BestSys2.g;
262 Vary2.A=[0.1 0.1 0 0];
263 [BestSys2,BestSpc2]=esfit('garlic',ExpSpec2,Sys2,Vary2,Exp); ...
264
265 % Bring simulated spectrum to same intensity as ExpSpec2
266 BestSpc2b=BestSpc2*max(ExpSpec2);
267 BestSpc2b= BestSpc2b';
268
269 simges=BestSpc1b+BestSpc2b;
270 res=CorrSpec-simges; ...
271
272 % Write fitting results into a table
273 Kopplungskonstanten = mhz2mt(BestSys2.A,BestSys2.g);
274 BestSys2.A=Kopplungskonstanten;
275 Kopplungskonstanten = mhz2mt(BestSys1.A,BestSys1.g);
276 BestSys1.A=Kopplungskonstanten;
277 clear Kopplungskonstanten;
278
279 % Calculate the ratio of double integrals
280
281 % Double integral of 1st species
282 x2=10*x2;
283 IntSpezies1=cumtrapz(x2,BestSpc1c);
284 DIntSpezies1=cumtrapz(x2,IntSpezies1);
285 maxDIntSpezies1=max(DIntSpezies1);
286
287 % Double integral of 2nd species
288 B=10*B;
289 IntSpezies2=cumtrapz(B,BestSpc2b);
290 DIntSpezies2=cumtrapz(B,IntSpezies2);
291 maxDIntSpezies2=max(DIntSpezies2);
292
293 % Ratio of double integrals
294 VerhaeltnisINTzuP=maxDIntSpezies2/maxDIntSpezies1; ...
295
296 % Display results
297
298 % Subtract simulated spectrum of 2nd species from experimental one
```

```

299 ExpSpec1=CorrSpec-BestSpc2b;
300
301 close all;
302 figure
303 subplot(2,2,1); plot(B,BestSpc1b,B,ExpSpec1); title('Radikal 1')
304 subplot(2,2,2); plot(B,simges,B,CorrSpec); title('beide Radikale')
305 subplot(2,2,3); plot(B,ExpSpec2,B,BestSpc2b); title('Radikal 2')
306 subplot(2,2,4); plot(B,res); title('Residuum');
307
308 figure
309 subplot(2,1,1); plot(x2,BestSpc1c,x2,IntSpezies1,x2,DIntSpezies1);
310 title('Doppelintegral Radikal 1')
311 subplot(2,1,2); plot(B,BestSpc2b,B,IntSpezies2,B,DIntSpezies2);
312 title('Doppelintegral Radikal 2')
313
314 BestFit=[B,CorrSpec,BestSpc1b,BestSpc2b,simges,res];
315 Doppelintegrale=[maxDIntSpezies1,maxDIntSpezies2,VerhaeltnisINTzuP];
316 Spezies1ges=[x2,BestSpc1c,IntSpezies1,DIntSpezies1];
317 Spezies2ges=[B,BestSpc2b,IntSpezies2,DIntSpezies2]; ...
318
319 Ergebnisse=[Doppelintegrale,BestSys1.A,BestSys1.g,BestSys2.A,BestSys2.g];

```

# Bibliography

- [1] H.-G. Elias, *An Introduction to Polymer Science*, 1st Ed., VCH Weinheim, **1997**.
- [2] L. H. Baekeland, US Patent 942 699, **1907**.
- [3] H. Staudinger, J. Fritsch, *Helvetica Chimica Acta* **1922**, *5*, 785–806.
- [4] K. Matyjaszewski, W. A. Braunecker, Y. Gnanou, L. Leibler, *Macromolecular Engineering. Precise Synthesis, Materials Properties, Applications*, (Ed.: Wiley-VCH), Matyjaszewski, K, **2007**.
- [5] Plastics – the Facts 2011: An analysis of European plastics production, demand and recovery for 2010, [www.plasticseurope.de](http://www.plasticseurope.de) (10.04.2012), **2011**.
- [6] K. Matyjaszewski, *Controlled and Living Polymerization*, WILEY-VCH, Chap. Radical Polymerization, **2009**, 103–166.
- [7] M. Semsarilar, S. Perrier, *Nature Chemistry* **2010**, *2*, 811–820.
- [8] M. Szwarc, *Nature* **1956**, *178*, 1168–1169.
- [9] M. Szwarc, *Journal of Polymer Science Part A-Polymer Chemistry* **1998**, *36*, IX–XV.
- [10] IUPAC. Compendium of Chemical Terminology, 2nd Ed. (the "Gold Book"), compiled by A. D. McNaught and A. Wilkinson, Blackwell Scientific Publications, Oxford, **1997**.
- [11] C. J. Hawker, A. W. Bosman, E. Harth, *Chemical Reviews* **2001**, *101*, 3661–3688.
- [12] J. S. Wang, K. Matyjaszewski, *Journal of the American Chemical Society* **1995**, *117*, 5614–5615.

## Bibliography

---

- [13] M. Kato, M. Kamigaito, M. Sawamoto, T. Higashimura, *Macromolecules* **1995**, *28*, 1721–1723.
- [14] J. Chiefari, Y. K. Chong, F. Ercole, J. Krstina, J. Jeffery, T. P. T. Le, R. T. A. Mayadunne, G. F. Meijs, C. L. Moad, G. Moad, E. Rizzardo, S. H. Thang, *Macromolecules* **1998**, *31*, 5559–5562.
- [15] A. Goto, H. Zushi, N. Hirai, T. Wakada, Y. Tsojii, T. Fukuda, *Journal of the American Chemical Society* **2007**, *129*, 13347–13354.
- [16] A. Goto, N. Hirai, K. Nagasawa, Y. Tsujii, T. Fukuda, H. Kaji, *Macromolecules* **2010**, *43*, 7971–7978.
- [17] A. Wolpers, L. Ackermann, P. Vana, *Macromolecular Chemistry and Physics* **2011**, *212*, 259–265.
- [18] D. Greszta, D. Mardare, K. Matyjaszewski, *Macromolecules* **1994**, *27*, 638–644.
- [19] A. D. Jenkins, R. G. Jones, G. Moad, *Pure and Applied Chemistry* **2010**, *82*, 483–491.
- [20] A. B. Lowe, C. L. McCormick, *Progress in Polymer Science* **2007**, *32*, 283–351.
- [21] K. J. Thurecht, A. M. Gregory, S. Villarroya, J. Zhou, A. Heise, S. M. Howdle, *Chemical Communications* **2006**, 4383–4385.
- [22] J. F. Quinn, E. Rizzardo, T. P. Davis, *Chemical Communications* **2001**, *11*, 1044–1045.
- [23] Y. Wang, A.-L. Li, H. Liang, J. Lu, *European Polymer Journal* **2006**, *42*, 2695–2702.
- [24] C. Boyer, V. Bulmus, T. P. Davis, V. Ladmiral, J. Liu, S. Perrier, *Chemical Reviews* **2009**, *109*, 5402–5436.
- [25] Y. K. Chong, T. P. T. Le, G. Moad, E. Rizzardo, S. H. Thang, *Macromolecules* **1999**, *32*, 2071–2074.
- [26] Y. Z. You, C. Y. Hong, W. P. Wang, W. Q. Lu, C. Y. Pan, *Macromolecules* **2004**, *37*, 9761–9767.
- [27] P. Relogio, M. T. Charreyre, J. P. S. Farinha, J. M. G. Martinho, C. Pichot, *Polymer* **2004**, *45*, 8639–8649.
- [28] M. Stenzel-Rosenbaum, T. P. Davis, V. Chen, A. G. Fane, *Journal of Polymer Science Part A-Polymer Chemistry* **2001**, *39*, 2777–2783.



- [29] V. Darcos, A. Dureault, D. Taton, Y. Gnanou, P. Marchand, A.-M. Caminade, J.-P. Majoral, M. Destarac, F. Leising, *Chemical Communications* **2004**, *18*, 2110–2111.
- [30] M. H. Stenzel-Rosenbaum, T. P. Davis, A. G. Fane, V. Chen, *Angewandte Chemie International Edition* **2001**, *40*, 3428–3432.
- [31] C. Barner-Kowollik, M. Coote, E. Krenske, E. Izgorodina, G. Moad, T. Junkers, T. Lovestead, S. Zard, E. Rizzardo, S. Thang, A. Lowe, C. McCormick, C. Urbani, M. Monteiro, M. Stenzel, D. Taton, M. Destarac, Y. Li, L. Schadler, B. Benicewicz, L. Barner, S. Perrier, A. Favier, B. de Lambert, M.-T. Charreyre, *Handbook of RAFT Polymerization*, (Ed.: Barner-Kowollik, Christopher), Wiley-VCH, **2008**.
- [32] A. W. York, S. E. Kirkland, C. L. McCormick, *Advanced Drug Delivery Reviews* **2008**, *60*, 1018–1036.
- [33] M. H. Stenzel, *Chemical Communications* **2008**, 3486–3503.
- [34] C. Barner-Kowollik, H. Dalton, T. P. Davis, M. H. Stenzel, *Angewandte Chemie International Edition* **2003**, *42*, 3664–3668.
- [35] X. Hao, M. H. Stenzel, C. Barner-Kowollik, T. P. Davis, E. Evans, *Polymer* **2004**, *45*, 7401–7415.
- [36] M. L. Coote, L. Radom, *Journal of the American Chemical Society* **2003**, *125*, 1490–1491.
- [37] M. L. Coote, *Macromolecules* **2004**, *37*, 5023–5031.
- [38] M. L. Coote, *Journal of Physical Chemistry A* **2005**, *109*, 1230–1239.
- [39] M. L. Coote, E. I. Izgorodina, E. H. Krenske, M. Busch, C. Barner-Kowollik, *Macromolecular Rapid Communications* **2006**, *27*, 1015–1022.
- [40] M. L. Coote, E. H. Krenske, E. I. Izgorodina, *Macromolecular Rapid Communications* **2006**, *27*, 473–497.
- [41] C. Y. Lin, M. L. Coote, *Australian Journal of Chemistry* **2009**, *62*, 1479–1483.
- [42] A. Feldermann, M. L. Coote, M. H. Stenzel, T. P. Davis, C. Barner-Kowollik, *Journal of the American Chemical Society* **2004**, *126*, 15915–15923.
- [43] C. Barner-Kowollik, J. F. Quinn, D. R. Morsley, T. P. Davis, *Journal of Polymer Science Part A-Polymer Chemistry* **2001**, *39*, 1353–1365.

## Bibliography

---

- [44] C. Barner-Kowollik, M. L. Coote, T. P. Davis, L. Radom, P. Vana, *Journal of Polymer Science Part A-Polymer Chemistry* **2003**, *41*, 2828–2832.
- [45] A. R. Wang, S. P. Zhu, *Journal of Polymer Science Part A-Polymer Chemistry* **2003**, *41*, 1553–1566.
- [46] A. R. Wang, S. P. Zhu, Y. W. Kwak, A. Goto, T. Fukuda, M. S. Monteiro, *Journal of Polymer Science Part A-Polymer Chemistry* **2003**, *41*, 2833–2839.
- [47] G. Moad, J. Chiefari, Y. K. Chong, J. Krstina, R. T. A. Mayadunne, A. Postma, E. Rizzardo, S. H. Thang, *Polymer International* **2000**, *49*, 993–1001.
- [48] M. J. Monteiro, H. de Brouwer, *Macromolecules* **2001**, *34*, 349–352.
- [49] M. Buback, P. Vana, *Macromolecular Rapid Communications* **2006**, *27*, 1299–1305.
- [50] Y. Kwak, A. Goto, Y. Tsujii, Y. Murata, K. Komatsu, T. Fukuda, *Macromolecules* **2002**, *35*, 3026–3029.
- [51] P. Vana, C. Barner-Kowollik, T. P. Davis, K. Matyjaszewski, *Encyclopedia Of Polymer Science and Technology*, 3rd Ed., Wiley-Interscience, Hoboken, Vol. 11, Chap. Radical Polymerization, **2003**, 359–472.
- [52] A. Alberti, M. Benaglia, M. Laus, D. Macciantelli, K. Sparnacci, *Macromolecules* **2003**, *36*, 736–740.
- [53] A. Alberti, M. Benaglia, H. Fischer, M. Guerra, M. Laus, D. Macciantelli, A. Postma, K. Sparnacci, *Helvetica Chimica Acta* **2006**, *89*, 2103–2118.
- [54] D. G. Hawthorne, G. Moad, E. Rizzardo, S. H. Thang, *Macromolecules* **1999**, *32*, 5457–5459.
- [55] M. Drache, G. Schmidt-Naake, M. Buback, P. Vana, *Polymer* **2005**, *46*, 8483–8493.
- [56] E. Chernikova, A. Morozov, E. Leonova, E. Garina, V. Golubev, C. O. Bui, B. Charleux, *Macromolecules* **2004**, *37*, 6329–6339.
- [57] F. Calitz, M. P. Tonge, R. D. Sanderson, *Macromolecules* **2003**, *36*, 5–8.
- [58] F. M. Calitz, J. B. McLeary, J. M. McKenzie, M. P. Tonge, B. Klumperman, R. D. Sanderson, *Macromolecules* **2003**, *36*, 9687–9690.
- [59] T. Junkers, PhD thesis, Georg-August-Universität Göttingen, **2006**.

- [60] R. Rotzoll, PhD thesis, Georg-August-Universität Göttingen, **2011**.
- [61] S. W. Benson, A. M. North, *Journal of the American Chemical Society* **1959**, *81*, 1339–1345.
- [62] S. W. Benson, A. M. North, *Journal of the American Chemical Society* **1962**, *84*, 935–940.
- [63] R. T. A. Mayadunne, E. Rizzardo, J. Chiefari, Y. K. Chong, G. Moad, S. H. Thang, *Macromolecules* **1999**, *32*, 6977–6980.
- [64] C. Barner-Kowollik, J. F. Quinn, T. L. U. Nguyen, J. P. A. Heuts, T. P. Davis, *Macromolecules* **2001**, *34*, 7849–7857.
- [65] C. Ladaviere, N. Dorr, J. P. Claverie, *Macromolecules* **2001**, *34*, 5370–5372.
- [66] A. Goto, K. Sato, Y. Tsujii, T. Fukuda, G. Moad, E. Rizzardo, S. H. Thang, *Macromolecules* **2001**, *34*, 402–408.
- [67] M. Destarac, D. Charmot, X. Franck, S. Z. Zard, *Macromolecular Rapid Communications* **2000**, *21*, 1035–1039.
- [68] M. S. Donovan, A. B. Lowe, B. S. Sumerlin, C. L. McCormick, *Macromolecules* **2002**, *35*, 4123–4132.
- [69] M. S. Donovan, T. A. Sanford, A. B. Lowe, B. S. Sumerlin, Y. Mitsukami, C. L. McCormick, *Macromolecules* **2002**, *35*, 4570–4572.
- [70] R. Severac, P. Lacroix-Desmazes, B. Boutevin, *Polymer International* **2002**, *51*, 1117–1122.
- [71] E. Rizzardo, J. Chiefari, R. T. A. Mayadunne, G. Moad, S. H. Thang, *ACS Symposia Series* **2000**, *768*, 278–296.
- [72] B. S. Sumerlin, M. S. Donovan, Y. Mitsukami, A. B. Lowe, C. L. McCormick, *Macromolecules* **2001**, *34*, 6561–6564.
- [73] J. Chiefari, R. T. A. Mayadunne, C. L. Moad, G. Moad, E. Rizzardo, A. Postma, M. A. Skidmore, S. H. Thang, *Macromolecules* **2003**, *36*, 2273–2283.
- [74] Y. K. Chong, J. Krstina, T. P. T. Le, G. Moad, A. Postma, E. Rizzardo, S. H. Thang, *Macromolecules* **2003**, *36*, 2256–2272.
- [75] M. Benaglia, E. Rizzardo, A. Alberti, M. Guerra, *Macromolecules* **2005**, *38*, 3129–3140.

## Bibliography

---

- [76] R. T. A. Mayadunne, E. Rizzardo, J. Chiefari, J. Krstina, G. Moad, A. Postma, S. H. Thang, *Macromolecules* **2000**, *33*, 243–245.
- [77] R. Francis, A. Ajayaghosh, *Macromolecules* **2000**, *33*, 4699–4704.
- [78] G. Moad, E. Rizzardo, S. H. Thang, *Australian Journal of Chemistry* **2009**, *62*, 1402–1472.
- [79] G. Moad, E. Rizzardo, S. H. Thang, *Australian Journal of Chemistry* **2006**, *59*, 669–692.
- [80] J. B. McLeary, J. M. McKenzie, M. P. Tonge, R. D. Sanderson, B. Klumperman, *Chemical Communications* **2004**, *17*, 1950–1951.
- [81] J. B. McLeary, F. M. Calitz, J. M. McKenzie, M. P. Tonge, R. D. Sanderson, B. Klumperman, *Macromolecules* **2004**, *37*, 2383–2394.
- [82] G. Pound, J. B. McLeary, J. M. McKenzie, R. F. M. Lange, B. Klumperman, *Macromolecules* **2006**, *39*, 7796–7797.
- [83] E. T. A. van den Dungen, H. Matahwa, J. B. McLeary, R. D. Sanderson, B. Klumperman, *Journal of Polymer Science Part A-Polymer Chemistry* **2008**, *46*, 2500–2509.
- [84] B. Klumperman, E. T. A. van den Dungen, J. P. A. Heuts, M. M. J., *Macromolecular Rapid Communications* **2010**, *31*, 1846–1862.
- [85] S. Perrier, C. Barner-Kowollik, J. F. Quinn, P. Vana, T. P. Davis, *Macromolecules* **2002**, *35*, 8300–8306.
- [86] C. Barner-Kowollik, M. Buback, B. Charleux, M. L. Coote, M. Drache, T. Fukuda, A. Goto, B. Klumperman, A. B. Lowe, J. B. Mcleary, G. Moad, M. J. Monteiro, R. D. Sanderson, M. P. Tonge, P. Vana, *Journal of Polymer Science Part A-Polymer Chemistry* **2006**, *44*, 5809–5831.
- [87] M. J. Monteiro, *Journal of Polymer Science Part A-Polymer Chemistry* **2005**, *43*, 3189–3204.
- [88] M. Buback, W. Meiser, P. Vana, *Australian Journal of Chemistry* **2009**, *62*, 1484–1487.
- [89] T. P. Davis, C. Barner-Kowollik, T. L. U. Nguyen, M. H. Stenzel, J. F. Quinn, P. Vana, *ACS Symposia Series* **2003**, *854*, 551–569.
- [90] Y. Kwak, A. Goto, T. Fukuda, *Macromolecules* **2004**, *37*, 1219–1225.

- [91] M. P. Tonge, F. M. Calitz, R. D. Sanderson, *Macromolecular Chemistry and Physics* **2006**, *207*, 1852–1860.
- [92] R. Venkatesh, B. B. P. Staal, B. Klumperman, M. J. Monteiro, *Macromolecules* **2004**, *37*, 7906–7917.
- [93] P. Geelen, B. Klumperman, *Macromolecules* **2007**, *40*, 3914–3920.
- [94] Y. W. Luo, R. Wang, L. Yang, B. Yu, B. G. Li, S. P. Zhu, *Macromolecules* **2006**, *39*, 1328–1337.
- [95] K. Suzuki, Y. Nishimura, Y. Kanematsu, Y. Masuda, S. Satoh, H. Tobita, *Macromolecular Reaction Engineering* **2012**, *6*, 17–23.
- [96] H. Tobita, *Macromolecular Theory and Simulations* **2011**, *20*, 709–720.
- [97] E. I. Izgorodina, M. L. Coote, *Macromolecular Theory and Simulations* **2006**, *15*, 394–403.
- [98] C. Y. Lin, M. L. Coote, *Australian Journal of Chemistry* **2011**, *64*, 747–756.
- [99] C. Barner-Kowollik, P. Vana, J. F. Quinn, T. P. Davis, *Journal of Polymer Science Part A-Polymer Chemistry* **2002**, *40*, 1058–1063.
- [100] E. Chernikova, V. Golubev, A. Filippov, C. Y. Lin, M. L. Coote, *Polymer Chemistry* **2010**, *1*, 1437–1440.
- [101] P. Vana, L. Albertin, L. Barner, T. P. Davis, C. Barner-Kowollik, *Journal of Polymer Science Part A-Polymer Chemistry* **2002**, *40*, 4032–4037.
- [102] A. A. Toy, P. Vana, T. P. Davis, C. Barner-Kowollik, *Macromolecules* **2004**, *37*, 744–751.
- [103] A. Feldermann, A. A. Toy, T. P. Davis, M. H. Stenzel, C. Barner-Kowollik, *Polymer* **2005**, *46*, 8448–8457.
- [104] C. Barner-Kowollik, T. Junkers, *Journal of Polymer Science Part A-Polymer Chemistry* **2011**, *49*, 1293–1297.
- [105] M. Buback, O. Janssen, R. Oswald, S. Schmatz, P. Vana, *Macromolecular Symposia* **2007**, *248*, 158–167.
- [106] G. Moad, Y. K. Chong, R. Mulder, E. Rizzardo, S. H. Thang, *ACS Symposium Series* **2009**, *k.a.*, 1–15.
- [107] T. Junkers, C. Barner-Kowollik, M. L. Coote, *Macromolecular Rapid Communications* **2011**, *32*, 1891–1898.

## Bibliography

---

- [108] T. Junkers, *Journal of Polymer Science Part A-Polymer Chemistry* **2011**, *49*, 4154–4163.
- [109] D. Konkolewicz, B. Hawkett, A. Gray-Weale, S. Perrier, *Macromolecules* **2008**, *41*, 6400–6412.
- [110] D. Konkolewicz, B. S. Hawkett, A. Gray-Weale, S. Perrier, *Journal of Polymer Science Part A-Polymer Chemistry* **2009**, *47*, 3455–3466.
- [111] S. R. S. Ting, T. P. Davis, P. B. Zetterlund, *Macromolecules* **2011**, *44*, 4187–4193.
- [112] M. G. Froehlich, P. Vana, G. Zifferer, *Journal of Chemical Physics* **2007**, *127*, 1649061–1649067.
- [113] D. Boschmann, R. Edam, P. J. Schoenmakers, P. Vana, *Polymer* **2008**, *49*, 5199–5208.
- [114] B. Friedman, B. O’Shaughnessy, *Macromolecules* **1993**, *26*, 5726–5739.
- [115] A. R. Khokhlov, *Makromolekulare Chemie - Rapid Communications* **1981**, *2*, 633–636.
- [116] F. R. Mayo, *Journal of the American Chemical Society* **1943**, *65*, 2324–2329.
- [117] A. Goto, T. Fukuda, *Progress in Polymer Science* **2004**, *29*, 329–385.
- [118] J. Barth, M. Buback, W. Meiser, P. Vana, *Macromolecules* **2010**, *43*, 51–54.
- [119] J. Barth, M. Buback, P. Hesse, T. Sergeeva, *Macromolecules* **2010**, *43*, 4023–4031.
- [120] M. Buback, P. Hesse, T. Junkers, P. Vana, *Macromolecular Rapid Communications* **2006**, *27*, 182–187.
- [121] M. Buback, A. Kuelppmann, *Macromolecular Chemistry and Physics* **2003**, *204*, 632–637.
- [122] W. Meiser, M. Buback, J. Barth, P. Vana, *Polymer* **2010**, *51*, 5977–5982.
- [123] D. Charmot, P. Corpart, H. Adam, S. Z. Zard, T. Biadatti, G. Bouhadir, *Macromolecular Symposia* **2000**, *150*, 23–32.
- [124] M. Buback, H. Frauendorf, F. Guenzler, P. Vana, *Polymer* **2007**, *48*, 5590–5598.
- [125] M. Buback, H. Frauendorf, O. Janssen, P. Vana, *Journal of Polymer Science Part A-Polymer Chemistry* **2008**, *46*, 6071–6081.

- 
- [126] M. H. Stenzel, L. Cummins, G. E. Roberts, T. P. Davis, P. Vana, C. Barner-Kowollik, *Macromolecular Chemistry and Physics* **2003**, *204*, 1160–1168.
- [127] D. Boschmann, P. Vana, *Polymer Bulletin* **2005**, *53*, 231–242.
- [128] M. Destarac, W. Bzducha, D. Taton, I. Gauthier-Gillaizeau, S. Z. Zard, *Macromolecular Rapid Communications* **2002**, *23*, 1049–1054.
- [129] R. X. E. Willemse, A. M. van Herk, E. Panchenko, T. Junkers, M. Buback, *Macromolecules* **2005**, *38*, 5098–5103.
- [130] M. Buback, C. H. Kurz, C. Schmaltz, *Macromolecular Chemistry and Physics* **1998**, *199*, 1721–1727.
- [131] H. Fischer, L. Radom, *Angewandte Chemie-International Edition* **2001**, *40*, 1340–1371.
- [132] W. Meiser, J. Barth, M. Buback, H. Kattner, P. Vana, *Macromolecules* **2011**, *44*, 2474–2480.
- [133] N. T. McManus, A. Penlidis, M. A. Dube, *Polymer* **2002**, *43*, 1607–1614.
- [134] M. L. Coote, T. P. Davis, *Macromolecules* **1999**, *32*, 4290–4298.
- [135] J. B. L. de Kock, PhD thesis, Technical University of Eindhoven, **1999**.
- [136] A. A. Gridnev, S. D. Ittel, *Macromolecules* **1996**, *29*, 5864–5874.
- [137] F. S. Du, M. Q. Zhu, H. Q. Guo, Z. C. Li, F. M. Li, M. Kamachi, A. Kajiwara, *Macromolecules* **2002**, *35*, 6739–6741.
- [138] C. Barner-Kowollik, F. Guenzler, T. Junkers, *Macromolecules* **2008**, *41*, 8971–8973.
- [139] N. Ahmad, B. Charleux, C. Farcet, C. Ferguson, S. Gaynor, B. Hawket, F. Heatley, B. Klumperman, D. Konkolewicz, P. Lovell, K. Matyjaszewski, R. Venkatesh, *Macromolecular Rapid Communications* **2009**, *30*, 2002–2021.
- [140] J. Barth, M. Buback, P. Hesse, T. Sergeeva, *Macromolecular Rapid Communications* **2009**, *30*, 1969–1974.
- [141] J. M. Asua, S. Beuermann, M. Buback, P. Castignolles, B. Charleux, R. G. Gilbert, R. A. Hutchinson, J. R. Leiza, A. N. Nikitin, J. P. Vairon, A. M. van Herk, *Macromolecular Chemistry and Physics* **2004**, *205*, 2151–2160.
- [142] J. B. Levy, B. K. W. Copeland, *Journal of the American Chemical Society* **1960**, *82*, 5314–5318.

- [143] S. Jauer, PhD thesis, Georg-August-Universität Göttingen, **2005**.
- [144] M. Buback, B. Fischer, S. Hinrichs, S. Jauer, J. Meijer, J. Sandmann, *Macromolecular Chemistry and Physics* **2007**, *208*, 772–783.
- [145] M. Buback, J. Sandmann, *Zeitschrift fuer Physikalische Chemie–International Journal of Research in Physical Chemistry & Chemical Physics* **2000**, *214*, 583–607.
- [146] M. Buback, D. Nelke, H. P. Vogele, *Zeitschrift fuer Physikalische Chemie–International Journal of Research in Physical Chemistry & Chemical Physics* **2003**, *217*, 1169–1191.
- [147] W. Meiser, M. Buback, *Macromolecular Rapid Communications* **2011**, *32*, 1490–1494.
- [148] W. Meiser, M. Buback, *Macromolecular Rapid Communications* **2012**, DOI: 10.1002/marc.201200068.
- [149] G. Moad, J. Chiefari, R. T. A. Mayadunne, C. L. Moad, A. Postma, E. Rizzardo, S. H. Thang, *Macromolecular Symposia* **2002**, *182*, 65–80.
- [150] S. Houshyar, D. J. Keddie, G. Moad, R. J. Mulder, S. Saubern, J. Tsanaktsidis, *Polymer Chemistry* **2012**, DOI: 10.1039/C2PY00529H.
- [151] AKZO Nobel Chemicals, *Initiators for High Polymers*, **2006**.
- [152] D. J. Henry, M. L. Coote, R. Gomez-Balderas, L. Radom, *Journal of the American Chemical Society* **2004**, *126*, 1732–1740.
- [153] A. Theis, A. Feldermann, N. Charton, M. H. Stenzel, T. P. Davis, C. Barner-Kowollik, *Macromolecules* **2005**, *38*, 2595–2605.
- [154] T. Junkers, A. Theis, M. Buback, T. P. Davis, M. H. Stenzel, P. Vana, C. Barner-Kowollik, *Macromolecules* **2005**, *38*, 9497–9508.
- [155] A. Theis, A. Feldermann, N. Charton, T. P. Davis, M. H. Stenzel, C. Barner-Kowollik, *Polymer* **2005**, *46*, 6797–6809.
- [156] T. Arita, M. Buback, O. Janssen, P. Vana, *Macromolecular Rapid Communications* **2004**, *25*, 1376–1381.
- [157] T. Arita, M. Buback, P. Vana, *Macromolecules* **2005**, *38*, 7935–7943.
- [158] J. F. Quinn, L. Barner, C. Barner-Kowollik, E. Rizzardo, T. P. Davis, *Macromolecules* **2002**, *35*, 7620–7627.



- 
- [159] P. Vana, T. P. Davis, C. Barner-Kowollik, *Macromolecular Theory and Simulations* **2002**, *11*, 823–835.
- [160] M. P. Tonge, A. Kajiwara, M. Kamachi, R. G. Gilbert, *Polymer* **1998**, *39*, 2305–2313.
- [161] B. Yamada, M. Kageoka, T. Otsu, *Macromolecules* **1991**, *24*, 5234–5236.
- [162] B. Yamada, S. Tagashira, K. Sakamoto, Y. Nagano, Y. Miura, *Polymer Bulletin* **1997**, *38*, 339–346.
- [163] J. Barth, M. Buback, *Macromolecular Rapid Communications* **2009**, *30*, 1805–1811.
- [164] P. D. Sullivan, N. A. Brette, *Journal of Physical Chemistry* **1975**, *79*, 474–479.
- [165] G. Clouet, P. Chaffanjon, *Journal of Macromolecular Science - Chemistry* **1990**, *A27*, 193–212.
- [166] S. G. Cohen, C. H. Wang, *Journal of the American Chemical Society* **1953**, *75*, 5504–5507.
- [167] A. Beer, *Annalen der Physik und Chemie* **1852**, *86*, 78–88.
- [168] M. von Smoluchowski, *Zeitschrift für Physikalische Chemie* **1917**, *92*, 129–168.
- [169] F. J. V. Santos, C. A. N. de Castro, J. H. Dymond, N. K. Dalaouti, M. J. Assael, A. Nagashima, *Journal of Physical and Chemical Reference Data* **2006**, *35*, 1–8.
- [170] H. de Brouwer, M. A. J. Schellekens, B. Klumperman, M. J. Monteiro, A. L. German, *Journal of Polymer Science Part A-Polymer Chemistry* **2000**, *38*, 3596–3603.
- [171] D. R. Lide, *Handbook of Chemistry and Physics*, 84 Ed., CRC Press, **2004**.
- [172] D. Griller, K. U. Ingold, *Accounts of Chemical Research* **1976**, *9*, 13–19.
- [173] M. L. Coote, C. Y. Lin, A. L. J. Beckwith, A. A. Zavitsas, *Physical Chemistry Chemical Physics* **2010**, *12*, 9597–9610.
- [174] C. Y. Lin, S. R. A. Marque, K. Matyjaszewski, M. L. Coote, *Macromolecules* **2011**, *44*, 7568–7583.
- [175] P. Vana, *Macromolecular Symposia* **2007**, *248*, 71–81.
- [176] J. Oliveira, personal communication, **2012**.

## Bibliography

---

- [177] A. Schlieper, personal communication, **2012**.
- [178] G. Smith, G. Russell, J. Heuts, *Macromolecular Theory and Simulations* **2003**, *12*, 299–314.
- [179] N. Soerensen, J. Barth, M. Buback, J. Morick, H. Schroeder, K. Matyjaszewski, *Macromolecules* **2012**, *45*, 3797–3801.
- [180] R. Rotzoll, P. Vana, *Journal of Polymer Science Part A-Polymer Chemistry* **2008**, *46*, 7656–7666.
- [181] B. Tamami, A. R. Kiasat, *Journal of Chemical Research-S* **1998**, *8*, 454–455.
- [182] G. Bouhadir, N. Legrand, B. Quiclet-Sire, S. Z. Zard, *Tetrahedron Letters* **1999**, *40*, 277–280.
- [183] W. G. Weber, J. B. McLeary, R. D. Sanderson, *Tetrahedron Letters* **2006**, *47*, 4771–4774.
- [184] N. N. Smolyar, *Russian Journal of Organic Chemistry* **2010**, *46*, 122–125.
- [185] G. H. Daub, L. F. Cannizzo, *Journal of Organic Chemistry* **1982**, *47*, 5034–5035.
- [186] J. J. Jiang, R. T. Weber, *Bruker Elecsys E 500 User's Manual*, **2001**.
- [187] R. A. Hutchinson, J. H. McMinn, D. A. Paquet, S. Beuermann, C. Jackson, *Industrial & Engineering Chemistry Research* **1997**, *36*, 1103–1113.
- [188] M. Mazur, *Analytica Chimica Acta* **2006**, *561*, 1–15.
- [189] A. Lund, M. Shiotani, S. Shimada, *Principles and Applications of ESR Spectroscopy*, 1st Ed., Springer Science + Business Media, **2011**, 430.
- [190] V. Y. Nagy, *Analytica Chimica Acta* **1997**, *339*, 1–11.
- [191] P. Hesse, PhD thesis, Georg-August-Universität Göttingen, **2008**.
- [192] E. Sato, T. Emoto, P. B. Zetterlund, B. Yamada, *Macromolecular Chemistry and Physics* **2004**, *205*, 1829–1839.
- [193] H. Chaffey-Millar, D. Stewart, M. M. T. Chakravarty, G. Keller, C. Barner-Kowollik, *Macromolecular Theory and Simulations* **2007**, *16*, 575–592.
- [194] M. Zhang, W. H. Ray, *Industrial & Engineering Chemistry Research* **2001**, *40*, 4336–4352.
- [195] M. Wulkow, *Macromolecular Theory and Simulations* **1996**, *5*, 393–416.

- [196] M. Wulkow, *PREDICI - Simulation package for polyreactions*, Computing in Technology GmbH, **2003**.
- [197] M. Wulkow, M. Busch, T. P. Davis, C. Barner-Kowollik, *Journal of Polymer Science Part A-Polymer Chemistry* **2004**, *42*, 1441–1448.
- [198] P. Deuffhard, W. Huisinga, T. Jahnke, M. Wulkow, *SIAM Journal on Scientific Computing* **2008**, *30*, 2990–3011.
- [199] J. Pallares, G. Jaramillo-Soto, C. Flores-Cataño, E. V. Lima, L. M. F. Lona, A. Penlidis, *Journal of Macromolecular Science, Part A: Pure and Applied Chemistry* **2006**, *43*, 1293–1322.
- [200] M. Wulkow, *Macromolecular Reaction Engineering* **2008**, *2*, 461–494.
- [201] X. Gao, S. Zhu, *Journal of Applied Polymer Science* **2011**, *122*, 497–508.



# Danksagung

Ich danke Herrn Prof. Dr. Michael Buback für die interessante Themenstellung sowie die vielen aufschlussreichen Diskussionen beim Erarbeiten meiner Doktorarbeit. Bei Herrn Prof. Dr. Philipp Vana möchte ich mich für die Übernahme des Korreferats für diese Arbeit danken.

Außerdem bedanke ich mich bei Jun.-Prof. Dr. Ricardo Mata und João Oliveira aus der Arbeitsgruppe *Computational Chemistry and Biochemistry* für die quantenchemischen Berechnungen ausgewählter Modellsysteme.

Allen Mitgliedern der Arbeitsgruppen *Makromolekulare Chemie* und *Technische und Makromolekulare Chemie* danke ich für die freundliche und offene Arbeitsatmosphäre sowie die stete Hilfsbereitschaft. Besonderen Dank gilt hier natürlich meinen Bürokollegen Joachim, Bastian, Vanessa und Katharina. Bei Herrn Dr. H.-P. Vögele möchte ich mich für die sehr kompetente Unterstützung bei technischen Problemen bedanken.

Besonderen Dank gilt meinen Bachelorstudenten Alana Schlieper und Hendrik Kattner für die fruchtbare Zusammenarbeit im Rahmen der Dithiobenzoat- und Trithiocarbonat-vermittelten Polymerisationen. Bei Johannes Barth möchte ich mich für die Einführung in die ESR-Spektroskopie und die aufschlussreichen Diskussionen bedanken. Annika und Oliver Ries danke ich für die zahlreichen Hilfestellungen bei synthetischen Fragen und der Auswertung von NMR- und Massenspektren. Für die Unterstützung bei Computerproblemen jeder Art bedanke ich mich bei Bastian Ebeling. Für das Korrekturlesen dieser Arbeit möchte ich mich bei Hendrik Schröder, Joachim Morick, Nils Wittenberg und Nicolai Sörensen bedanken.

Mein herzlicher Dank gilt meiner gesamten Familie dafür, dass sie mich in all meinen Entscheidungen unterstützt und gefördert hat. Insbesondere danke ich meinen Eltern für ihre materielle und vor allem auch moralische Unterstützung. Meinen Schwestern danke ich für die erlebnisreichen Wochenenden in Berlin, Leipzig, Köln und Bonn, die immer eine willkommene Abwechslung zur Promotion darstellten.

Weiterhin möchte ich mich bei meinen Freunden und WG-Mitbewohnern für die interessante Zeit im und neben dem Studium bedanken. Stellvertretend möchte ich

Dany, Jo, Steffi, Annika, Olli, Christina, Julia, Anke, Anne, Eva und Anja nennen, denen ich eine schöne und erlebnisreiche Zeit verdanke.

Para terminar agradezco a mi marido Alejandro, con todo mi cariño, las experiencias inolvidables de los últimos años y los que todavía vienen. Porque siempre me relajas, me haces sonreír y me recuerdas las cosas importantes de la vida. ¡Quérote moito!

# Lebenslauf

## **persönliche Daten**

geboren am 15. März 1983 in Berlin, Deutsch, verheiratet

## **Schulbildung**

- 09/1989 - 06/1995 Grundschule in Berlin und Teltow
- 08/1995 - 06/2003 Weinberg-Gymnasium Kleinmachnow, Abschluss: Abitur (1,3)
- 10/2000 - 06/2001 Austauschjahr und Besuch der Olive Branch High School in Olive Branch, Mississippi, USA

## **Studium**

- 10/2003 - 01/2009 Studium der Chemie an der Georg-August Universität Göttingen
- 09/2006 - 07/2007 Forschungspraktikum und Studium der Chemie an der Universidad de A Coruña, Galicien, Spanien
- 03/2008 - 09/2008 Diplomarbeit an der Georg-August-Universität Göttingen, Institut für Physikalische Chemie im Arbeitskreis von Prof. Dr. Michael Buback, Titel der Diplomarbeit: *Mechanismus und Kinetik von RAFT-Polymerisationen bis zu hohem Druck*
- seit 04/2008 wissenschaftliche Mitarbeiterin am Institut für Physikalische Chemie der Universität Göttingen
- 01/2009 Diplomprüfungen im Fach Chemie, Note: 1,2
- seit 03/2009 Promotionsstudium an der Georg-August-Universität Göttingen unter der Anleitung von Prof. Dr. Michael Buback